HPC 67-28

MONSANTO/WASHINGTON UNIVERSITY
ARPA ASSOCIATION

HIGH PERFORMANCE COMPOSITES
SECOND ANNUAL PROJECT REVIEW
AND
TECHNICAL REPORT

1 MAY 1966 - 30 APRIL 1967

PROGRAM MANAGER
JOHN D. CALFEE

MONSANTO RESEARCH CORPORATION
A SUBSIDIARY OF MONSANTO COMPANY

800 N. LINDBERGH BOULEVARD ST. LOUIS, MISSOURI 63166

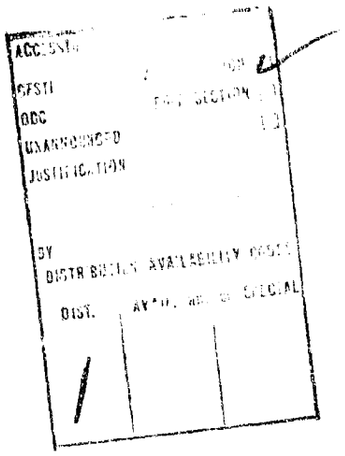

NOTICES

When Government drawings, specifications, or other data are used for any purpose other than in connection with a definitely related Government procurment operation, the United States Government thereby incurs no responsibiliy nor any obligation whatsoever; and the fact that the Government may have formulated, furnished, or in any way supplied the said drawings, specifications, or other data, is not to be regarded by implication or otherwise as in any manner licensing the holder or any other person or corporation, or conveying any rights or permission to manufacture, use, or sell any patented invention that may in any way be related thereto.

HPC 67-28

Monsanto Company/Washington University

ARPA Association

High Performance Composites

SECOND ANNUAL PROJECT REVIEW AND TECHNICAL REPORT

1 May 1966 - 30 April 1967

Program Manager
John D. Calfee, Monsanto Company

Monsanto Company/Washington University
St. Louis, Missouri

FOREWORD

The Advanced Research Projects Agency has advanced the concept that an effective technique for developing a new field of technology in materials research is to couple an industrial laboratory with its counterpart in a university in order to create an environment which will generate a well balanced center of excellence in the chosen field. General goals and expectations for materials research in an industry-university coupling program, along with specific plans and objectives for the Monsanto/Washington University program, were presented and discussed at a symposium (1) held 10 November 1965 in St. Louis, Missouri. The Monsanto/Washington University ARPA program in "High Performance Composites" is designed to test the coupling concept.

This second annual report is an overall review of the Monsanto/Washington University ARPA Association and its activities for the second year. The report is a compilation of papers covering programs conducted by the Association. About two-thirds of the papers were presented orally at the Annual Review Meeting held 12 July 1967 in St. Louis, Mo. The report emphasizes the three areas of prime concern: research, education, and communication. This project is sponsored by the Advanced Research Projects Agency, Department of Defense through a contract with the Office of Naval Research, N00014-67-C-0218 (formerly N00014-66-C-0045), ARPA order no. 873, entitled "Development of High Performance Composites."

The prime contractor is Monsanto Research Corporation. The Program Manager is Dr. John D. Calfee, Monsanto Company, Central Research Department, St. Louis, Missouri, phone 314-Oxford 4-4721.

The Contract period is 30 June 1965 to 30 April 1969. The amount of the contract is $4,009,000.

John D. Calfee
Program Manager
July 12, 1967

(1) High Performance Composites: Transactions of a symposium sponsored by Monsanto Company and Washington University ARPA research project, Washington University, St. Louis, Missouri November 10, 1965.

ABSTRACT

The purpose of the Monsanto/Washington University ARPA program "High Performance Composites," is to demonstrate through accomplishments in research, education, and communication that university-industry coupling is an effective system for doing advanced materials research. This report is an accounting for the second year of the project.

In Mechanics, the finite-element method was used to calculate the longitudinal stiffness of short fiber composites; the instability of parallel edge cracks determined from the energy concept and the strength and inherent crack size obtained from the stability calculations; Young's modulus calculated for randomly oriented fibrous composites; a mathematical approach proposed for calculating stress fields around interior cracks; and invariant properties of a laminated composite derived from the transformation equations of the anisotropic moduli.

In the Physics and Chemistry Section, the electron scanning microscope provided insight into fracture mechanics; composites were improved by incorporating a flexible layer around the fiber; polyacrylic acid reacted with ZnO to produce a high modulus, temperature-resistant matrix; data obtained indicating silane couplers decrease water diffusion at the interface; a decrease in fracture toughness associated with a change in crack propagation mechanism; and the viscosity of aggregate suspensions described by the Mooney equation.

In Fabrication and Processing, techniques were developed for whisker fiber classification; strands of well-oriented whisker fibers made and fabricated into high performance composites; x-ray diffraction techniques applied to measuring fiber orientation, property maps developed for short fiber composites; short boron fibers encapsulated to make a pre-preg molding compound in bead form; fiber-matrix dry mix molding explored; and data obtained relating matrix properties to fatigue characteristics.

In education, a graduate program in materials science was put into effect by the university; two one-semester seminar courses conducted for the Association students and scientists; and a summer workshop in mechanics organized.

In communication, the second annual symposium on high performance composites was held; publication of a new journal, Journal of Composite Materials, begun; and five papers published.

TABLE OF CONTENTS

Table of Contents (Continued)

V. FABRICATION AND PROCESSING

I. SUMMARY (J. D. Calfee)

The overall objective of the Monsanto Company/Washington University ARPA Association is to create a nationally recognized center of excellence for high performance composites by coupling the capabilities of Monsanto Company and Washington University to:

1. Make significant research advances in the science of high performance composites,
2. Apply research information generated to the development of new composite materials having value to government and industry,
3. Train students in the field of advanced materials science,
4. Serve as a center of communications for scientific information on composite materials.

The Association is now two years old. This report covers work conducted during the second year of the project, places the work in perspective relative to short and long term goals, and relates individual researches to basic problems involved in developing a new area in the field of high performance composites. The format of the report is to discuss Association accomplishments and problems: a) coupling, communication, and education in a general treatment, and b) research through presentation of technical papers.

Association research is concerned primarily with high performance composites reinforced with discontinuous fibers of controlled morphology. Orientation of the research is such that the science and technology developed will yield fabrication techniques, engineering analyses for elemental shapes, and performance data applicable to meeting significant aerospace needs in materials, parts, and structures. The research is organized around three disciplines: mechanics, physics and chemistry, and fabrication and processing. The structure of the research and utilization of special skills within the disciplines are designed to provide, in fact demand, university-industry coupling at every level.

In line with the "Center of Excellence" concept, the work must be of such creativity, quality, and depth that it is suitable for publication in the most demanding professional journals. Accordingly work is presented in papers to be submitted for publication or, in order to provide early reporting and/or greater detail, to be edited later by the authors for publication.

II. ORGANIZATION-EDUCATION-COMMUNICATION-COUPLING (J. M. McKelvey)

During the first two years of its existence, the ARPA sponsored M/WU Association has made considerable progress toward its objective of becoming a major center of research and education dedicated to the advancement of the technology of high-performance composite structural materials. An organization structure which integrates the academic and industrial personnel into a coherent research community has evolved, as well as an internal structure within the university which has accommodated itself to both the research and educational objectives of the Association. Both are described in this paper.

In addition, significant progress has been made in the graduate level academic program in materials science and engineering. Its current status is reviewed. The mechanisms established for the dissemination of scientific information are also described.

Organization

During the past two years we have been particularly concerned with devising an organizational framework for the Association that would enable a true research community to develop. It is clearly recognized that, if the Association should become compartmentalized into an academic section concerned with "basic" research and an industry section concerned with "applications", the coupling experiment, as we understand it, would have to be considered a failure.

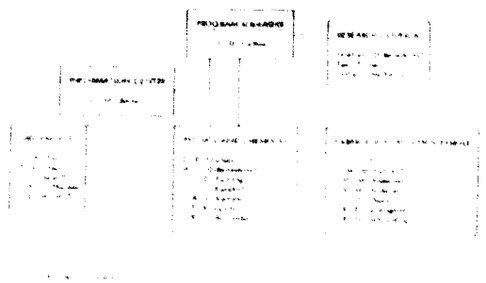

Figure 1 The Monsanto/Washington University Association Organization and Principal Research Staff (July 1, 1967)

Figure 1 shows the organization and principal research staff of the Association. Note that the research is divided into three disciplinary areas: mechanics (stress analysis, fracture mechanics, and testing), physics and chemistry (strong emphasis on interfacial problems), and fabrication and processing. The responsibility for planning the research strategy for each of these disciplinary areas is in the hands of two-man committees, with each committee having one member from the university and the other from the company. These six individuals constitute the Research Council of the Association. The Research Council meets every three to four weeks under the chairmanship of John Collins, Program Manager, and functions as a policy planning and advisory board. It is concerned

primarily with research policies but may review other matters concerning the operation of the Association.

In general, we have found this organizational structure works effectively. It is our judgment that the Association, having passed through the initial and difficult formative stages, is now functioning as a coherent organization.

The Materials Research Laboratory

In August of 1966, and in large part because of the M/WU ARPA Association, Washington University established the Materials Research Laboratory (MRL) as a division of the School of Engineering and Applied Science, with Dr. Stephen W. Tsai as director. The function of MRL is to manage contract research in the field of structural materials. It is intended that the research activities of MRL be of such a nature that they complement the academic programs of the School of Engineering and Applied Science.

The Laboratory, under Dr. Tsai, manages the Washington University portion of the ARPA contract and hence forms a primary interface between Washington University and the Monsanto Company. The Laboratory has its own full-time professional staff plus a number of regular faculty members on a part-time basis. It is the primary research base for graduate students working on composite materials.

Because of severe space problems at Washington University which will not be alleviated for about two years (when the new engineering building will be completed) the ARPA Association staff of MRL occupies laboratory and office space at three different locations. The staff has about 2500 square feet of laboratory and office space within the engineering complex on the main campus, rents 1260 square feet of office space on Lindbergh Boulevard near the Monsanto Company, and occupies a module in the Monsanto Research Center.

Graduate Program in Materials Science and Engineering

As described in last year's Annual Report, the ARPA contract was a significant factor in the Washington University decision to establish research and graduate degree programs in the field of materials science and engineering. The establishment of this new activity has become a part of the general focusing of the engineering school's sights on graduate research and education, in addition to its long established tradition of undergraduate engineering education

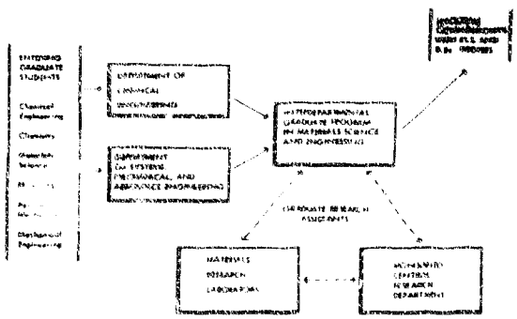

Figure 2 Materials Science and Engineering Program at Washington University and its Relation to the Monsanto/ Washington University ARPA Association

Fig. 2 shows the organizational framework and relationship to the M/WU ARPA Association.

The program is headed by Professor A. T. DiBenedetto who was recruited by Washington University specifically for this purpose. The program has as its objective the training of materials technologists who are broadly educated, but with depth in at least one area of specialization. Our key areas of strength at the present time are polymer science and micromechanics. Participating in this program next year in the capacity of Affiliate Professors will be three Monsanto scientists. A listing of faculty and students is given below:

GRADUATE DEGREE PROGRAM IN MATERIALS SCIENCE AND ENGINEERING
WASHINGTON UNIVERSITY

Faculty

Name	Title	Department	Field
DiBenedetto*	Assoc. Prof.	Chem. Engr.	Chem. Engr.
Bagley	Professor	Chem. Engr.	Phys. Chem.
Gulbransen	Professor	S. M. A.	Metallurgy
McKelvey	Professor	Chem. Engr.	Chem. Engr.
Tsai	Professor	S. M. A.	Mechanics
Kardos	Asst. Prof.	Chem. Engr.	Polymer Phys.
Chen	Affiliate Prof.	S. M. A.	Mechanics
Nielsen	Affiliate Prof.	Chem. Engr.	Phys. Chem.
Sonnino	Affiliate Prof.	S. M. A.	Metallurgy

* Program director

Graduate Students

Name	Previous Degree	Candidate for
Droste	M. S. (U. of Wis.) 1966, Ch. E.	D. Sc.
Wambach	B. S. (U. of Wis.) 1965, Ch. E.	D. Sc.
Trachte	B. S. (U. of Wis.) 1966, Ch. E.	D. Sc.
Kaas	B. S. (U. of Wis.) 1966, Ch. E.	D. Sc.
McDonnell	B. S. (Col. Mines) 1964, Pet. Engr.	M. S.
Ho (Tentative)	M. S. (W. Va. U.) 1961, M. E.	D. Sc.
Lin	M. S. (V. P. I.) 1966, Ch. E.	D. Sc.
Dhingra	M. S. (W. U.) 1966, Met. Engr.	D. Sc.
Chatterjee	M. S. (I. I. T.) 1964, Met. Engr.	D. Sc.

Degrees Granted

Name	Advisor	Degree	Present Location
J. Joseph	Kardos	M. S.	Diamond Alkali Co.
D. Ludwig	McKelvey	M. S.	Monsanto Co.

Information on the graduate study program in materials science and engineering has been given wide circulation. The reproduction of the cover of a bulletin is seen in Figure 3. During the fall of 1967, a vigorous off-campus program for recruitment of strong graduate students will be undertaken.

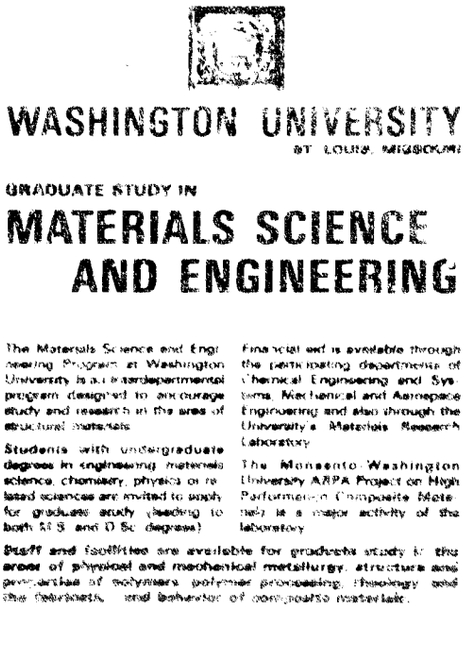

WASHINGTON UNIVERSITY
ST. LOUIS, MISSOURI

GRADUATE STUDY IN
MATERIALS SCIENCE AND ENGINEERING

The Materials Science and Engineering Program at Washington University is an interdepartmental program designed to encourage study and research in the area of structural materials.

Students with undergraduate degrees in engineering, materials science, chemistry, physics or related sciences are invited to apply for graduate study (leading to both M.S. and D.Sc. degrees).

Staff and facilities are available for graduate study in the areas of physical and mechanical metallurgy, structure and properties of polymers, polymer processing, rheology and flow behavior, and behavior of composite materials.

Financial aid is available through the participating departments of Chemical Engineering and Systems, Mechanical and Aerospace Engineering and also through the University's Materials Research Laboratory.

The Monsanto-Washington University ARPA Project on High Performance Composite Materials is a major activity of the laboratory.

Figure 3

Dissemination of Scientific Information

As has been mentioned previously, the M/WU Association considers that one of its key functions is to serve as a center for the dissemination of scientific information about composite materials. There are four ways in which the Association is meeting this responsibility: (1) it publishes the scientific quarterly, Journal of Composite Materials, (2) it conducts an annual symposium on some aspect of high performance composite materials, (3) it offers informal courses and seminars on topics pertaining to composite materials, and (4) it actively

encourages its own research staff to publish significant results in the open scientific literature as soon as it is practicable. These activities are described in more detail below:

1. The Journal of Composite Materials:

The Journal of Composite Materials is intended to be an inter-disciplinary journal-of-record for the publication of original research and review articles pertaining to the science and technology of composite materials.

The first issue of JCM appeared in January 1967. The 1967 volume, consisting of four issues, will total about 400 pages. As of June 1, 1967 there were 550 paid subscribers. The initial costs of establishing JCM are being borne by Monsanto and Washington University, outside of the ARPA contract. It is anticipated that JCM will be financially self-sustaining in about two years. Figure 4 shows the members of the editorial advisory board established for JCM while Figure 5 shows the Table of Contents for the second issue and illustrates the nature and scope of the articles appearing in JCM.

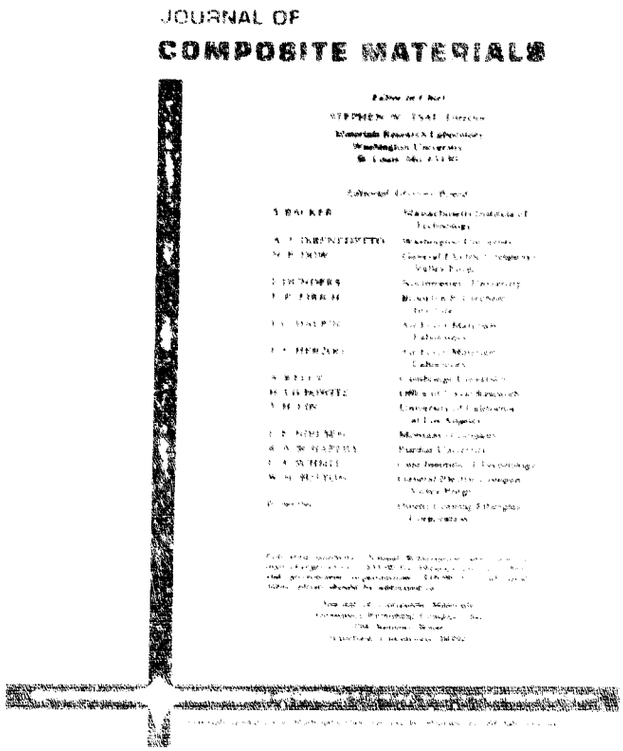
JOURNAL OF
COMPOSITE MATERIALS

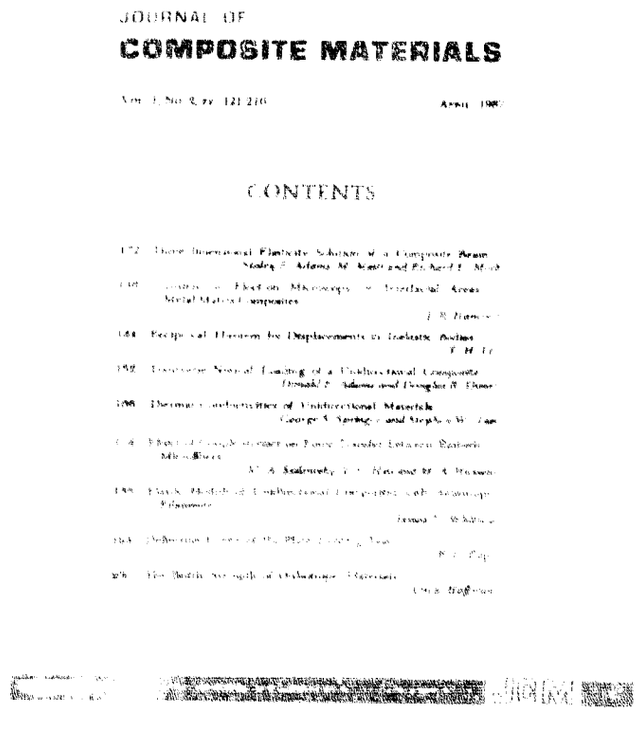
JOURNAL OF
COMPOSITE MATERIALS

CONTENTS

2. Annual Symposium on Composite Materials

The second annual symposium, "Basic Strengthening Mechanisms in High Performance Composites", was held October 20-21, 1966 and attracted a national audience of about 200 scientists and engineers. The third annual symposium on composite materials will be held at Washington University on October 26-27, 1967. As shown in Figure 6, its theme will be the design and fabrication of high performance composite materials.

CALL FOR PAPERS

3rd Annual Symposium on High Performance Composites

Sponsored by

ARPA Monsanto/Washington University Association

to be held at

Washington University, St. Louis, Missouri

October 26-27, 1967

The theme of the symposium will be research on the design and fabrication of high performance composites. Papers dealing with the mechanics, chemistry, and morphology of high performance composites which determine design and performance parameters are being solicited, as are papers on techniques for fabricating shapes and test specimens for property measurements and new tests. Papers will be judged from the standpoint of scientific substance and relevance to composite materials. A five-hundred word abstract should be submitted to:

Stephen W. Tsai

Materials Research Laboratory
Washington University
St. Louis, Missouri 63130

before August 1, 1967. The author is urged to submit complete manuscript to review for publication in Journal of Composite Materials and/or presentation at the symposium can be carried out simultaneously. Format of the manuscript [illegible] this Journal.

Figure 6

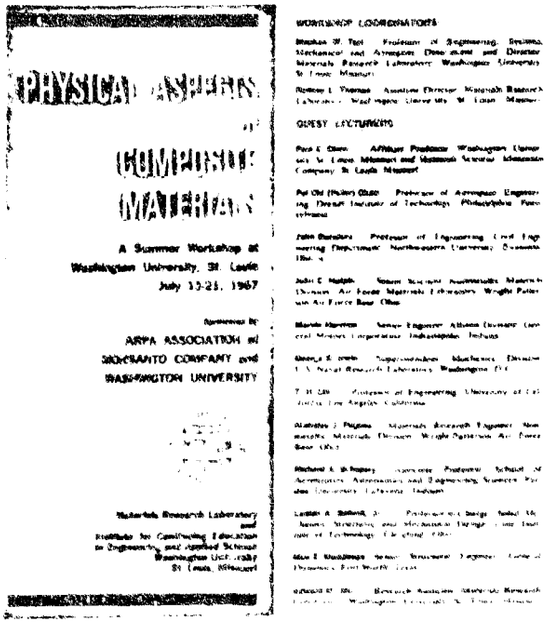
PHYSICAL ASPECTS
OF
COMPOSITE
MATERIALS

A Summer Workshop at
Washington University, St. Louis
July 13-21, 1967

Sponsored by
ARPA ASSOCIATION of
MONSANTO COMPANY and
WASHINGTON UNIVERSITY

Materials Research Laboratory
and
Institute for Continuing Education
in Engineering and Applied Science
Washington University
St. Louis, Missouri

WORKSHOP COORDINATORS

GUEST LECTURERS

Figure 7

3. Informal courses and Seminars:

This summer the M/W U Association will offer from July 13 to 21, a workshop on the "Physical Aspects of Composite Materials". Lectures will be given by a number of outstanding experts, as shown in Figure 7. The maximum number of attendees that can be accommodated is 50. Preregistration indicates that capacity attendance will be attained. The Association Research Council has under consideration the request that the workshop be repeated next summer at Berkeley, California under joint sponsorship with the University of California.

4. Publications

The following papers have been published by the Association:

1) Chen, P. E. "Stress fields around parallel edge cracks in a tensile specimen." J. of Composite Materials 1, #1, January 1967.

2) Fairing, J. D. "Examination of fracture surfaces by scanning electron microscopy." Note to the editor, Journal of Composite Materials 1, #2, April 1967.

3) Tolbert, T. L. "Matrix studies in the Monsanto/Washington University ARPA project." U. S. AF Mat'ls. Lab. Advanced Composite Hardware, 1966.

4) Tsai, S. W. "A review of strength theories of composite materials." U. S. AF Mat'ls. Lab. Advanced Composite Hardware, 1966.

5) Tsai, S. W. "An advancing technology." J. of Composite Materials 1, #1, January 1967.

These have been submitted for publication:

1) Anderson, R. M. "Some major factors controlling torsional fatigue life of fiber reinforced plastic composites."

2) Kenyon, A. S. and Duffey, H. J. "Properties of a particulate filled polymer."

3) Nielsen, L. E. and Chen, P. E. " Young's modulus of randomly oriented fiber-filled composites."

4) Tsai, S. W. and Chen, P. E. "Longitudinal stiffness of discontinuous fiber composites."

As research stands at time of preparation of this report, 8 papers will be submitted during the next 4 months and approximately 10 papers the following 8 months.

Coupling

I shall now speculate about the long-term significance of the coupling concept. My frame of reference is that of the university, but I will comment briefly on its significance for corporations dealing in advanced technologies.

Two years ago I was convinced that a compelling argument could be made for coupling from the engineering educator's point of view. This argument has been made and I will only briefly review it here. To appreciate it one must understand what is happening today in engineering education. In brief, engineering education is rapidly becoming graduate education, as shown in Figure 8. By

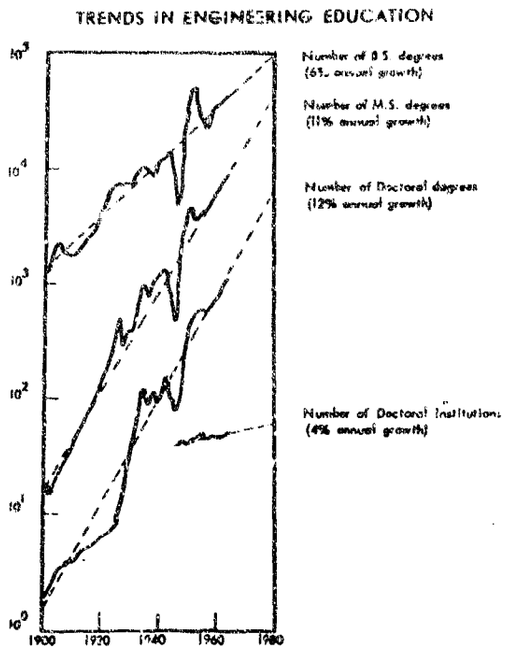

Figure 8

1980 the production of graduate degrees in engineering may reach 50,000 compared to 8,000 or 9,000 in 1960.

Many of these graduate students and their professors will be involved in laboratory research of some kind or another. There is potential here for an educational disaster. If these graduate students and their professors choose to try to imitate the "pure" research being done next door in the departments of natural science, the country will find itself with a generation of "engineers" who are not problem oriented and who could have erroneous ideas as to the function and role of engineering and its relationship to technology.

The ARPA coupling programs can have a very direct and beneficial effect on this problem. By coupling graduate research to the demands of modern technology, engineers have a much better chance of emerging from graduate schools as first class technologists.

In conclusion, the ARPA sponsored M/WU association has committed itself to becoming a "center of excellence" in the new and important field of composite materials technology. It expects to make contributions on three fronts: education, research, and the dissemination of scientific information. I have reviewed some of our accomplishments in the education and communications area. To recapitulate briefly, we are dedicated to producing materials technologists, broadly educated, but with depth in at least one area of specialization, whose education and graduate experience will orient them toward pressing technological problems.

III. MECHANICS (S. W. Tsai and P. E. Chen)

Although high performance composite materials have been of interest for over 10 years, research in the mechanics of composites was initiated only in the last five years. A number of earlier works were intended to describe the mechanical behavior of fiber-reinforced composites, an example of which is the netting analysis pioneered by Young in the U. S., and Cox and Gordon in England. Netting analysis may be interpreted as a special case of the continuum model, but in the process of simplification some basic principles of mechanics are violated. Netting analysis cannot simultaneously satisfy equilibrium, compatibility, and the constitutive equations. It is formulated with the assumption that only the filaments carry load and the matrix is ineffective, which contradicts the physical reality. However, some researchers still find it difficult to discard the theory, because a theoretically sound approach like that of continuum mechanics, requires considerably more mathematical discipline. In our ARPA program, we are trying to project the importance of mechanics in the research of composite materials to a level not yet generally accepted in the field. The underlying philosophy is that mechanics represents an essential discipline in the design and understanding of composites. It follows that engineering data and material characterization must be properly coordinated with the needs of the designer. In the Monsanto/Washington University ARPA program, mechanics is recognized as one of the three basic disciplines. Attempts are made to insure that our graduate students in the Materials Science and Engineering Program have a basic understanding and a working knowledge of the mechanics principles.

The mechanics research in composite materials is intended to achieve the following objectives:

1. To establish the structural performance of composites. Composites belong to a class of materials basically different from ordinary structural materials because of their anisotropic and heterogeneous

properties. Advanced methodology in testing will be developed so that the structural performance of the composites can be better understood. New engineering data will be generated so that such materials can be better designed.

2. To establish analytically and verify experimentally the contribution of the constituent materials to the gross behavior of the composite. Critical factors which must be investigated include the mechanical and geometrical properties of the constituents and the strength of the interface (including a narrow zone which may exist at the interface). The irregular shapes and the random packing of the reinforcing phase and voids in the matrix will also be investigated. The results of this investigation may be used as guidelines for materials design, i.e., the selection of compatible constitutent materials, their geometric shapes, and the controlled interface.
3. To establish a basic mathematical model from which the reliability of composites can be established. In this area of investigation, environmental effects due to cyclic and impact loadings, corrosive atmosphere, and creep will be included. The basic approach will rely on nonlinear viscoelastic theories and fracture mechanics.
4. To translate the results of research into the design criteria of materials which can be used to meet aerospace needs.

Reviewing the work in the Mechanics Section, Drs. S. W. Tsai and P. E. Chen are using the finite-element method to study the stress distribution in composites reinforced by short unidirectional fibers and subjected to longitudinal load. The effects of stiffness ratio, volume fractions of the constituents, and the fiber aspect ratio on the longitudinal composite stiffness are calculated. Comparisons with experimental results have indicated that this method is more accurate than the shear lag analysis. Since a reliable theoretical model can be used to make the parametric study much more efficiently than the experimental

approach, it can be used to eliminate unnecessary laboratory work and optimize the use of the constituent materials.

Dr. Chen has calculated the stress fields around parallel edge cracks in a tensile specimen from the equilibrium and compatibility conditions, and determined the instability of such cracks from the energy concept, based on the Griffith-Orowan theory. From the stability calculation, the strength and inherent crack size of the material can be obtained. On the other hand, it can also be used to calculate the modulus of elasticity or effective surface energy when the other parameters are known.

For many structural applications, the random orientation of the fibers may be desirable since in the plane of the sheet the elastic modulus is the same in all directions. The Young's modulus of fiber-filled composites in which the fibers are randomly oriented in a plane has been calculated by Drs. Nielsen and Chen using equations based on the classical theory of elasticity. For fibers with moduli much greater than that of the matrix, randomly oriented fibers give moduli much smaller than the moduli measured on composites containing fibers all aligned parallel to the direction of the applied tensile stress. One has thus traded great stiffness in one direction for much less stiffness in all directions in going from oriented fibers to a random distribution of fibers.

Using Michell's continuity equations for the single-valuedness of rotations and displacements, and extending Prager's method for calculating the plane elastic strains in doubly-connected regions, Dr. Chen has proposed a mathematical approach for solving the stress fields around interior cracks. Though the computer program and the example presented are that of a single interior crack, the method is applicable for the more general case of multiple interior cracks. A comparison between the theoretical and experimental results is included. The mathematical model will be used to study the interaction among interior micro-cracks, which is vital to the understanding of the strength of composites.

Invariant properties of a laminated composite have been derived by Drs. S. W. Tsai and N. J. Pagano (AFML) from the transformation equations of the anisotropic moduli. These properties may be considered intrinsic because they are independent of the orientations and thicknesses of the constituent layers. These properties are useful for comparing the performance of composite materials with that of homogeneous and isotropic materials, and can also serve as a basis for design optimization.

Currently the Mechanics Section is using the continuum mechanics approach to expand the study of factors affecting the stiffness and strength of discontinuous fiber composites; statistically analyzing the effect of irregular fiber spacings on the transverse stiffness of composites; continuing the calculations of stress fields around interacting cracks and inclusions; and coordinating and translating research results into the language of the design engineer.

Future projects will include variable interface, fracture of composites under combined loading, reliability and fatigue behavior, testing of elemental shapes, and structural evaluation of metallic composites. Mr. Rodney L. Thomas, Drs. Edward M. Wu and Ori Ishai will join the staff of the Mechanics Section this summer.

LONGITUDINAL STIFFNESS OF DISCONTINUOUS FIBER COMPOSITES

(S. W. Tsai and P. E. Chen)

The stress and deformation of composites reinforced with discontinuous fibers have been studied using shear lag analysis, which is based on the strength-of-materials theory. Since this analysis has been extensively reported[1,2,3] and experimentally verified[1,4], it would seem unnecessary to challenge its validity. The success of the shear lag analysis may be fortuitous because the basic theory may not be accurate in analyzing complicated geometry and material variations which exist in discontinuous composites. The shear lag analysis does not always satisfy the basic mechanics principles like compatibility or equilibrium. It also ignores interaction among fibers. However, a substantial amount of knowledge

on composite materials is explicitly and implicitly deduced from the shear lag analysis, examples of which include the load-transfer and reinforcing mechanisms, the concepts of critical aspect ratio and critical fiber volume, the role of the interface and the matrix, the rule-of-mixtures relations, and so on. A more accurate method than the shear lag analysis will improve the understanding of composite materials.

Our method is based on the finite-element technique, which is a numerical approach based on the fundamental concepts of equilibrium and compatibility, for determining stresses and deformations in complex structures. It is particularly suited to the treatment of problems of composite materials because multiphase materials can be handled in a straight-forward fashion. A discontinuous fiber composite is represented in Figure 1. The usual assumptions of plane elasticity are used. Perfect interfacial bonding is assumed unless otherwise indicated. Other assumptions include the idealized packing arrangement of the fibers, and that both constituents are homogeneous, isotropic and linearly elastic. Uniform loading is applied along the axes of the fibers. The present study is restricted to the effects of stiffness ratio E_f/E_m, aspect ratio L/D, and fiber volume fraction V_f. For the sake of completeness, the basic theory of the finite-element method is outlined in the next section.

Theory

The finite-element method[5-9] has been known to stress analysts for more than a decade in its applications to the analysis of large complex structures. The validity of this method has been repeatedly verified by experiments[10, 11]

The method is based on the direct stiffness concept which considers the structure as an assemblage of idealized elastic elements assumed to be joined together at discrete nodes. By adding together at each node the stiffness coefficients of adjacent elements a stiffness matrix for the structure is obtained. This stiffness matrix relates the external forces acting on the nodes to the displacements of the nodes.

$$\{F\} = [K]\{\delta\} \qquad (1)$$

By inverting the stiffness matrix one obtains an influence matrix which gives the nodal displacements as a function of the external forces or loads acting on the structure.

$$\{\delta\} = [K]^{-1} \{F\} \tag{2}$$

Using the same strain pattern for the elastic element that was assumed for deriving its stiffness coefficients, one can derive a matrix of stress coefficients which gives the stresses in the element as a function of its nodal displacements.

$$\{\sigma_n\} = [S_n] \{\delta_n\} \tag{3}$$

Therefore, once equation (2) has been solved for the nodal displacements, the stresses in the n-th element are given by equation (3), where $[S_n]$ is the stiffness matrix for the element and δ_n are its nodal displacements.

Analysis of the Fundamental Region

The idealized fiber packing is shown in Figure 1. In order to facilitate the computation of the effective stiffness and the distribution of stresses and deformation in the composite, the symmetry and compatibility requirements of a

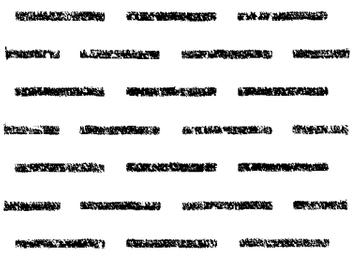

Figure 1 Idealized Discontinuous Fiber Composite.

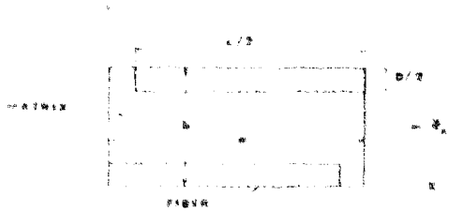

Figure 2 Fundamental Region.

fundamental region as shown in Figure 2 are used. It is assumed that under uniform normal stress applied at infinity, the deformed rectangular fundamental region remains rectangular. The symmetry requirements take into consideration

the interaction among fibers, which is very essential in the study of practical composite materials. The procedure for analyzing this fundamental region by superposition follows that of Reference 12 and is subsequently described.

Since symmetry conditions of the fundamental region require a displacement boundary formulation, superposition of the finite-element solutions must be employed. The object is to solve a typical problem shown as Problem 3 in Figure 3 where arbitrary normal loadings $\bar{\sigma}_{x3}$ and $\bar{\sigma}_{y3}$ at infinity are given. It is desired to obtain the distribution of stress and strain in the fundamental region. One straight-forward method is to solve Problems 1 and 2, shown also in Figure 3, and by superposition Problem 3 is solved.

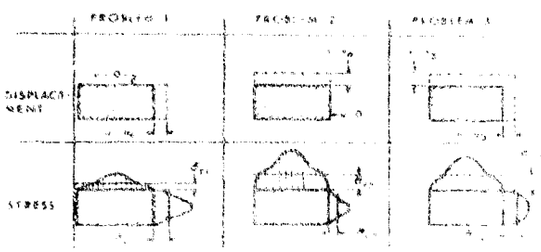

Figure 3 Superposition of Finite-Element Solutions.

The boundary conditions and results for these problems are:

Problem 1

$u = u_o$ at $x = a$

$u = 0$ at $x = 0$

$v = 0$ at $y = 0, b$

$\tau_{xy} = 0$ throughout the boundary.

The results obtained are u_1, v_1, σ_{x1}, σ_{y1}, τ_{xy1}, $\bar{\sigma}_{x_1}$, and $\bar{\sigma}_{y1}$.

Problem 2

$u = 0$ at $x = 0, a$

$v = 0$ at $y = 0$

$v = v_o$ at $y = b$

$\tau_{xy} = 0$ throughout the boundary.

The results obtained are u_2, v_2, σ_{x2}, σ_{y2}, τ_{xy2}, $\bar{\sigma}_{x2}$, and $\bar{\sigma}_{y2}$.

Assuming that each fundamental region is quasi-homogeneous and orthotropic, the effective stiffness of the region must satisfy the generalized Hooke's law:

$$\bar{\sigma}_x = Q_{11}\,\bar{\varepsilon}_x + Q_{12}\,\bar{\varepsilon}_y$$

$$\bar{\sigma}_y = Q_{21}\,\bar{\varepsilon}_x + Q_{22}\,\bar{\varepsilon}_y$$

where $Q_{ij} = C_{ij} - \dfrac{C_{i3}\,C_{j3}}{C_{33}}$ (see Reference 13).

Thus from Problem 1,

$$\bar{\varepsilon}_x = u_o/a, \quad \bar{\varepsilon}_y = 0$$

$$Q_{11} = a\,\bar{\sigma}_{x1}/u_o$$

$$Q_{21} = a\,\bar{\sigma}_{y1}/u_o .$$

From Problem 2,

$$\bar{\varepsilon}_x = 0, \quad \bar{\varepsilon}_y = v_o/b$$

$$Q_{12} = b\,\bar{\sigma}_{x2}/v_o$$

$$Q_{22} = b\,\bar{\sigma}_{y2}/v_o .$$

The compliance S_{ij} can be obtained by matrix inversion with the results:

$$S_{11} = b\,\bar{\sigma}_{y2}/(v_o\lambda)$$

$$S_{21} = a\,\bar{\sigma}_{x1}/(u_o\lambda)$$

$$S_{12} = -b\,\bar{\sigma}_{x2}/(v_o\lambda)$$

$$S_{21} = -a\,\bar{\sigma}_{y1}/(u_o\lambda)$$

where $\lambda = [\bar{\sigma}_{x1}\,\bar{\sigma}_{y2} - \bar{\sigma}_{y1}\,\bar{\sigma}_{x2}] \;/\; [(u_o/a)(v_o/b)]$.

The following engineering constants can be computed:

$$E_{11} = 1/S_{11}$$

$$E_{22} = 1/S_{22}$$

$$\nu_{12} = -S_{12}/S_{11}$$

$$\nu_{21} = -S_{21}/S_{22} .$$

If arbitrary average stresses $\bar{\sigma}_{x3}$ and $\bar{\sigma}_{y3}$ are imposed on the fundamental region,

$$\bar{\epsilon}_{x3} = S_{11}\,\bar{\sigma}_{x3} + S_{12}\,\bar{\sigma}_{y3}$$

$$\bar{\epsilon}_{y3} = S_{21}\,\bar{\sigma}_{x3} + S_{22}\,\bar{\sigma}_{y3} .$$

The displacements u_3 at $x = a$ and v_3 at $y = b$ are:

$$u_3 = a\,\bar{\epsilon}_{x3}$$

$$v_3 = b\,\bar{\epsilon}_{y3} .$$

Substituting these into the previous equations and after rearranging:

$$m = u_3/u_0 = [\bar{\sigma}_{y2}\,\bar{\sigma}_{x3} - \bar{\sigma}_{x2}\,\bar{\sigma}_{y3}] / \lambda'$$

$$n = v_3/v_0 = [-\bar{\sigma}_{y1}\,\bar{\sigma}_{x3} + \bar{\sigma}_{x1}\,\bar{\sigma}_{y3}] / \lambda'$$

$$\text{where } \lambda' = \bar{\sigma}_{x1}\,\bar{\sigma}_{y2} - \bar{\sigma}_{y1}\,\bar{\sigma}_{x2} .$$

Once m and n are known, where subscripts $_1$ and $_2$ refer to the average stresses obtained from Problems 1 and 2, and subscript $_3$ refers to the imposed stresses at infinity, then the resulting displacements and stresses at each point of the fundamental region can be obtained by superposition of the results of Problems 1 and 2:

$$u = mu_1 + nu_2$$

$$v = mv_1 + nv_2$$

$$\sigma_x = m\,\sigma_{x1} + n\,\sigma_{x2}$$

$$\sigma_y = m\,\sigma_{y1} + n\,\sigma_{y2}$$

$$\tau_{xy} = m\,\tau_{xy1} + n\,\tau_{xy2} .$$

Problem 3 may involve several combinations of the normal loadings at infinity, e.g., uniaxial loading along the x- or y-axis, biaxial loading, etc.

Results

The theoretical results of the finite-element method are shown in the following figures, with detailed discussions in the next section.

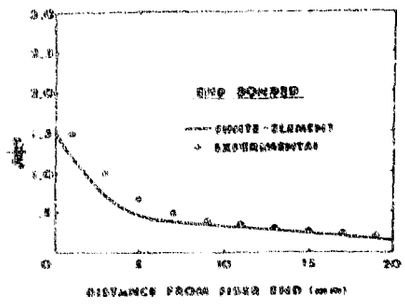

Figure 4 Comparison of Experimental Results With Theoretical Curve for Interfacial Shear.

Figure 4 shows the comparison between Tyson's and Davis' experimental results shown as circles[2,3] and the corresponding curve calculated by the finite-element method for the distribution of shearing stress at the fiber-matrix interface parallel to the interface. The results are for an araldite matrix with an aluminum fiber, and correspond to the case of "fiber end bonded to the matrix."

Figure 5 shows the comparison between the results of the shear lag analysis[3] and the corresponding results of the finite-element method for the interfacial shear. The results are also for araldite matrix with an aluminum fiber, but end adhesion is assumed to be broken.

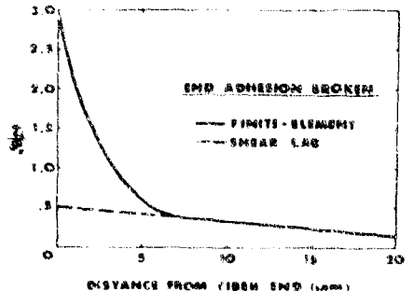

Figure 5 Comparison of Results From Shear Lag Analysis and Finite-Element Method for Interfacial Shear.

It should also be pointed out that the fiber end adhesion must be assumed to be broken in the shear lag analysis, whereas the finite-element method can be used to compute the stresses and deformations for both the "fiber end bonded" and "fiber end adhesion broken" cases.

Figure 6 shows the stiffness utilization factor[14] as a function of aspect ratio for different stiffness ratios and fiber volume fractions. Utilization factor is defined as the ratio of the longitudinal stiffness of a discontinuous fiber composite and that of a continuous fiber composite with the same stiffness ratio and fiber volume. Four stiffness ratios, viz., 1, 6, 20 and 120, are shown. They may represent homogeneous material, boron-aluminum, glass-epoxy and boron-epoxy

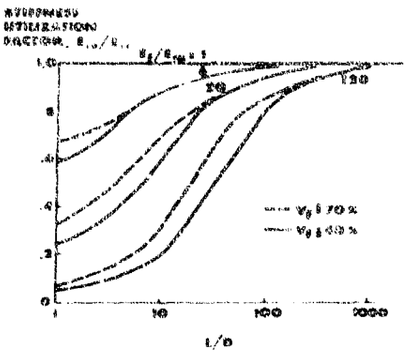

Figure 6 Stiffness Utilization Factor as a Function of Aspect Ratio, Stiffness Ratio, and Fiber Volume Fraction.

composites, respectively. Two fiber volume fractions, approximately 40 percent and 70 percent, are included. The calculation here is based on perfect interfacial bond, including the ends. This assumption is believed to be more realistic for the determination of the composite stiffness. It may be pointed out that the results recently reported by Foye[15] for boron-epoxy composite, and aspect ratio up to 4 agree well with the present theoretical prediction.

Figure 7 is a plot of fiber volume fraction versus the longitudinal stiffness of boron-epoxy composites with various aspect ratios. Limited data of discontinuous boron-epoxy composites are also shown in various symbols corresponding to different aspect ratios indicated on the figure. The data were obtained in the Monsanto/Washington University program. Recent measurements by Kane[14] for L/D = 150 are also shown.

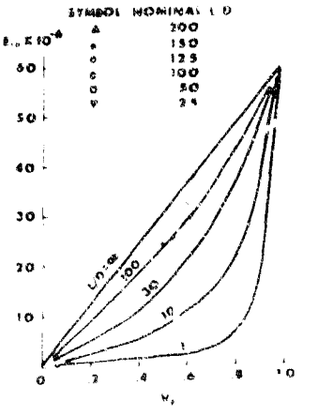

Figure 7 Fiber Volume Fraction Versus Longitudinal Stiffness of Boron-Epoxy Composites With Various Aspect Ratios - Theory Versus Experiment.

Figure 8 shows the comparison between the results of stiffness calculations from the shear lag analysis, which is represented by Equation (5.4) on page 124 in Reference 2, and the corresponding results from the finite-element method for $E_f/E_m = 6$ and 120, and $V_f = 40$ percent. The β value used in the above mentioned equation is calculated for the planar model (3), but the difference between the stiffness computed from this model and that from the cylindrical model

becomes relatively immaterial for high [$\beta \ell$] values. Significant difference is seen for low aspect ratios. As the stiffness ratio and/or aspect ratio increases, the difference between the results from the two methods is reduced.

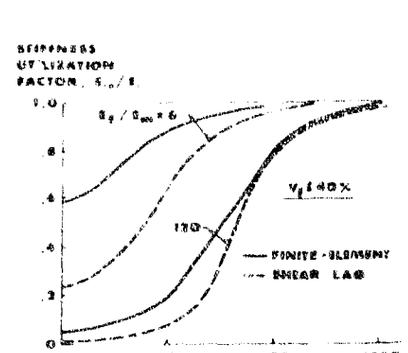

Figure 8 Comparison Between the Results of Stiffness and Calculations From the Shear Lag Analysis and Finite-Element Method for E_f/E_m = 6 and 120, and $V_f \doteq 40$ percent.

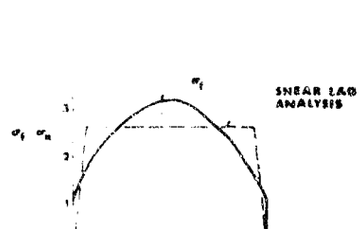

Figure 9 Longitudinal Stress Variation Along a Fiber.

In Figure 9, the normal stress in the fiber, σ_f, is shown as a solid line. This case corresponds to a stiffness ratio of 120 (a typical boron-epoxy composite), aspect ratio of 20 and fiber volume of 40 percent. The Poisson's ratios for both the fiber and matrix are 0.3. Shown as a dashed line is the normal stress profile computed from the shear lag analysis, with the plateau representing the fiber stress derived from the rule-of-mixtures equation, that

$$\sigma_f = E_f \bar{\sigma}_x / [V_f E_f + V_m E_m] . \qquad (4)$$

Figure 10 shows the utilization factor of longitudinal strength as a function of fiber aspect ratio for the case of $E_f/E_m = 3$ (a typical tungsten-copper composite), and $V_f = 50$ percent. The curves represent the results of the shear lag analysis from Dow, and Kelly and Tyson as reported by W. H. Sutton in Chapter 9 of Reference 17. The dots represent data reported by Kelly and

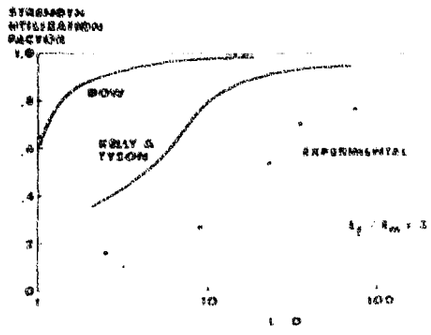

Figure 10 Strength Utilization Factor Versus Aspect Ratio.

Tyson[21]. The strength utilization factor is defined as the strength ratio of the discontinuous to the continuous fiber composites.

Discussion

The results of the finite-element method compare closely with the photoelastic model of single inclusion by Tyson and Davis[3], as shown in Figure 4. Figure 5 shows the comparison of interfacial shear stress between the present method and the shear lag analysis, both of which correspond to the end broken case. Our results show a maximum shear stress six times as large as that by the shear lag analysis. This will be a significant consideration in the understanding of the load-transfer mechanism and the strength of a discontinuous fiber composites.

The utilization factor for the longitudinal stiffness as a function of stiffness ratio, fiber volume fraction and the aspect ratio is shown in Figure 6. The present method of computation is based on the theory of elasticity, as opposed to the strength-of-materials approach of the shear lag analysis. The principal difference is that the interaction among fibers is taken into account in our method. This is important because most composites of interest contain large fiber volume fractions and interaction among fibers must be considered. Comparison of the analytical prediction with available experimental results of boron-epoxy composites are shown in Figure 7. The agreement, with the exception of one point, is amazingly close.

In Figure 8, the results of the shear lag analysis are compared with the finite-element method in terms of the utilization factor of the longitudinal stiffness. The difference between the two methods for high aspect ratios is

relatively small. This, however, is not sufficient to justify the validity of the shear lag analysis. A similar situation exists in the computation of the transverse stiffness of a unidirectional composite. It is known that numerous strength-of-materials approaches agree reasonably well with elasticity solutions. An acceptable explanation may be that the gross elastic moduli of composites are not significantly affected by the local stress distribution. Figure 9 shows the difference between the average fiber stress computed from the two methods. The stress profile does not show abrupt changes from which critical fiber aspect ratio can be defined. Secondly, the peak fiber stress can exceed the maximum level permitted by the shear lag analysis, Equation (4). Figure 5 also shows a significant difference in the predicted interfacial shear stress. The important point is that the shear lag analysis cannot be used for the determination of the local stress distribution.

We believe that the understanding of the behavior of discontinuous fiber composites should be interpreted in the light of more exact methods than the shear lag analysis. From the stress distribution in the fiber, the matrix, and at the interface, the mechanism of load transfer and composite strength may be explained. Although this work is still in progress, we have sufficient information to show that the strength of discontinuous fiber composites is not necessarily governed by the average fiber stress. Using fiber failure as the basis of strength calculation, the shear lag analysis would predict the results shown in Figure 10. Note that experimental data[21] are significantly different from either prediction of the aspect ratio by orders of magnitudes. Thus, the concept of critical aspect ratio and load-transfer mechanisms, and strength of composites should be reexamined.

Conclusions

Based on our results, the following conclusions may be stated:

1. The shear lag analysis does not provide reliable information on the stress distribution in discontinuous fiber composites. The strength of materials theory cannot be extended to solve problems involving multiple inclusions.

2. Critical aspect ratios should be defined in terms of utilization factors for stiffness, strength, and other possible criteria.
3. The role of fibers in a composite is to increase the stiffness and/or the strength of the composite. For light-weight materials, the stiffening aspect is often more important than the strengthening aspect Discontinuous fiber composites seem to have high utilization factors for the longitudinal stiffness, but relatively lower utilization factors for strength. A strong matrix and a strong interfacial bond are both necessary to fully utilize the high strength of the fibers.

Acknowledgment

The computer program used for carrying out the finite-element calculations was written by Professor E. L. Wilson of the University of California at Berkeley whose generosity is gratefully acknowledged. The assistance of Miss Barbara Krueger is greatly appreciated.

Nomenclature

a, b	=	Length and width of the fundamental region.
E_f	=	Young's modulus of the fibers.
E_m	=	Young's modulus of the matrix.
E_{LC}	=	Effective longitudinal modulus calculated from the rule-of-mixtures equation for continuous fiber composite.
E_{LD}	=	Effective longitudinal modulus calculated by the finite-element method for discontinuous fiber composite.
D	=	Diameter of fiber.
L	=	Length of fiber.
L/D	=	Aspect ratio of fiber.
u, v	=	Displacements in x- and y-directions.
V_f	=	Volume fraction of the fibers.
x, y	=	Rectangular coordinates.
σ_x, σ_y	=	Normal stresses in x- and y-directions.
$\bar{\sigma}_x$, $\bar{\sigma}_y$	=	Average σ_x and σ_y (applied at infinity).

ϵ_x, ϵ_y = Normal strains in x- and y-directions.

γ_{xy} = Shearing stress in xy-plane parallel to x- or y-axis.

τ_i = Shearing stress at the fiber-matrix interface parallel to the interface.

$\{F\}$ = Force vector.

$[K]$ = Stiffness matrix.

$\{\sigma_n\}$ = Stress vector for the n-th element.

$\{\delta\}$ = Displacement vector.

$[S_n]$ = Stiffness matrix for the n-th element.

$\{\delta_n\}$ = Displacement vector for the n-th element.

References

1. Holliday, L., Ed. Composite Materials, Elsevier (1966).

2. Kelly, A. Strong Solids, Clarendon, Oxford (1966).

3. Tyson, W. R. and G. J. Davis. "A photoelastic study of the shear stresses associated with the transfer of stress during fiber reinforcement," British J. Applied Physics, 16, 199 (1965).

4. McDanels, D. L., R. W. Jech and J. W. Weeton. "Stress-strain behavior of tungsten-fiber-reinforced copper composites," NASA TN D-1881 (1963).

5. Turner, M. J., R. W. Clough, H. C. Martin and L. J. Topp. "Stiffness and deflection analysis of complex structures," J. Aeronautical Sciences, 23, 805 (1956).

6. Clough, R. W. "The finite element method in plane stress analysis," NSF Report, Research Grant G-7337 (1960).

7. Martin, H. C. "Plane elasticity problems and the direct stiffness method," The Trend in Engineering, University of Washington (1961) p. 5.

8. Martin, H. C. "Truss analysis by stiffness considerations," J. Engineering Mechanics, 82, 1082 (October 1956).

9. Turner, M. J., E. H. Dill, H. C. Martin and R. J. Melosh. "Large deflections of structures subjected to heating and external loads," J. Aero/Space Sciences, 27, 96 (1960).

10. Eggwertz, S. and B. R. Noton. "Stress and deflection measurements on a multicell cantilever box beam with 30° sweep," The Aeronautical Research Institute of Sweden, Report 53, Stockholm (1954).

11. Eggwertz, S. "Calculation of stresses in a swept multicell cantilever box beam with ribs perpendicular to the spars and comparison with test results," The Aeronautical Research Institute of Sweden, Report 54, Stockholm (1954).

12. Tsai, S. W., D. F. Adams and D. R. Doner. "Effect of constituent material properties on the strength of fiber-reinforced composite materials," AFML-TR-66-190 (1966).

13. Tsai, S. W. "Mechanics of composite materials," AFML-TR-66-194, Part II, 51 (1966).

14. Kane, J. L. "Oriented noncontinuous boron composites," J. Composite Materials, 1, 42 (1967).

15. Foye, R. L. "Structural composites," North American Aviation/Columbus Division Quarterly Progress Report No. 2 for Contract No. AF33(615)-5150 (1966).

16. Weeton, J. W. and R. A. Signorelli. "Fiber-metal composite materials," NASA TN D-3530 (1966).

17. Am. Soc. Metals, Fiber Composite Materials, A.S.M. (1965).

18. Rosen, B. W., N. F. Dow and Z. Hashin. "Mechanical properties of fibrous composites," NASA CR-31 (1964).

19. Dow, N. F. "Study of stresses near a discontinuity in a filament-reinforced composite metal," General Electric Report R63SD61 (1963).

20. Cox, H. L. "The elasticity and strength of paper and other fibrous materials," British J. Applied Physics, 3, 72 (1952).

21. Kelly, A. and W. R. Tyson. "Tensile properties of fiber-reinforced metals: copper/tungsten and copper/molybdenum," J. Mech. Phys. Solids, 13, 329 (1965).

ON THE INSTABILITY OF PARALLEL EDGE CRACKS (P. E. Chen)

A numerical approach is proposed in this paper for determining the instability of parallel edge cracks in a tensile specimen. These cracks are likely to develop from two free surfaces or edges in the matrix of a composite material which may lead to the ultimate failure of the composite. The free surfaces or edges are intended to simulate the initial interfacial defect or bond failure of neighboring inclusions in a composite.

From the stability calculation, the strength and inherent crack size of the material can be readily obtained. On the other hand, it can also be used to calculate the modulus of elasticity or effective surface energy when the other parameters are known.

The mathematical model for the stress fields is based on the biharmonic equation for the stress function with appropriate boundary conditions. Isotropy, homogeneity, linearity, as well as plane state of stress are assumed. Photoelastic experiments had been conducted on CR-39 specimens under uniaxial tension. The details of the experiments and the comparison between theoretical and experimental results were reported in a previous paper[1].

Mathematical Model

The tensile specimen under consideration is shown in Figure 1 where the coordinate axes are chosen such that the x-axis coincides with one of the free edges of the specimen, and the half-domain on the right of the y-axis coincides with that on the left after being rotated 180° about the center of the domain. The specimen is loaded at the ends by uniformly distributed tension σ_o. It is assumed that the cracks are perpendicular to the free edges, the crack geometry is that of a slit, the spacing between the two surfaces of a crack is small but not zero, and the crack surfaces are free of both normal and shearing stresses. The length of each crack and the spacing between the cracks are arbitrary.

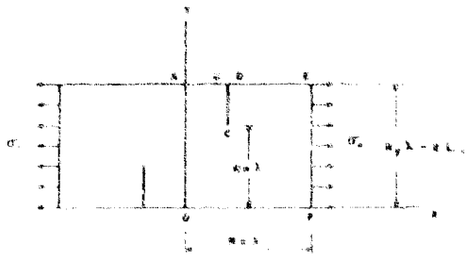

Figure 1 Tensile Specimen.

By introducing a stress function Φ one can write the biharmonic equation

$$\nabla^2 \nabla^2 \Phi = 0 \tag{1}$$

which satisfies both the equilibrium and compatibility equations. In terms of the stress function, the boundary conditions can be expressed as

$$\frac{\partial \Phi}{\partial x} = \text{zero everywhere on the boundary,} \tag{2}$$

$$\frac{\partial \Phi}{\partial y} = \gamma_o (y - L_o) \text{ on EF,} \tag{3}$$

$$= \sigma_o L_o \text{ on ABCDE,} \tag{4}$$

$$= -\sigma_o L_o \text{ on OF,} \tag{5}$$

and also that along EF

$$\Phi = \frac{\sigma_o}{2} (y^2 - 2L_o y + L_o^2), \tag{6}$$

along AB, DE and OF

$$\Phi = \frac{1}{2} \sigma_o L_o^2, \tag{7}$$

and along CB and CD

$$\Phi = \sigma_o L_o y - \frac{3}{2} \sigma_o L_o^2. \tag{8}$$

The finite-difference method is used to calculate the distribution of the stress function Φ in the domain. The stress components are then calculated from the values of Φ.

Energy Calculation

According to the Griffith theory of brittle fracture[2], a crack will become unstable when the elastic energy release due to an incremental crack growth outweighs the demand for surface energy for the same crack growth. For a linear elastic system, the elastic energy release is $-W_e$ with W_e being the decrease in strain energy due to the formation of cracks. The surface energy W_s is defined as the energy gain due to the creation of new crack surfaces having a surface tension T_s.

The Griffith theory can also be applied to brittle-like fracture involving plastic deformation. Orowan[4] has shown that when plastic deformation is concentrated in a region whose thickness is small compared to the length of a crack, the work of plastic deformation may be treated as a contribution to the effective surface energy of the crack. Thus, one can simply add a plastic work factor P to the surface tension T_s, and uses $\gamma = P + T_s$ as the effective surface energy per unit area.

From the Griffith theory the point of instability can be calculated from the following equation:

$$\frac{\partial}{\partial c}(-W_e + W_s) = 0 \tag{9}$$

where W_s will be defined in the Griffith-Orowan sense. The above energy balance equation is illustrated schematically in Figure 2.

Applying the Griffith-Orowan theory to the parallel edge cracks, W_s will be defined as the effective surface energy gained by creating the new surfaces of both cracks, W_e the strain energy increase of the entire domain, and c the total length of both cracks.

For plane state of stress, the strain energy per unit volume V_o can be calculated from

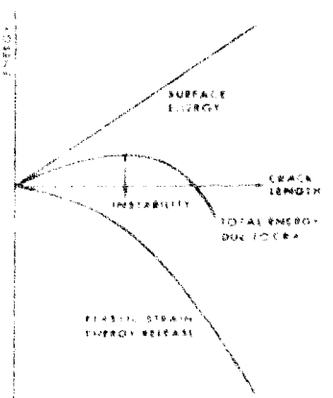

Figure 2 Energy Balance of Crack.

$$V_o = \frac{1}{2E}(\sigma_x^2 + \sigma_y^2) - \frac{\nu}{E}\sigma_x\sigma_y + \frac{1}{2G}\tau_{xy}^2 \tag{10}$$

Assuming unit thickness, the total strain energy of a deformed elastic body is

$$\iint V_o \, dx\,dy \tag{11}$$

where the double integration is to be extended over the entire domain.

In order to evaluate the Young's modulus E or the effective surface energy per unit area Y, the following equation may be used:

$$T = K (2Y/c)^{1/2} \qquad (12)$$

where T is the critical tensile stress, and K is a dimensionless factor determined by the details of the model and the applied load.

Results

A computer program was written to carry out the calculations of the mathematical model and the elastic strain energy.

The program has been used to calculate the normal stresses and the shearing stresses in the entire domain for various crack lengths and spacings. The results of several typical cases are included here to illustrate the effects of spacing and overlap.

Figures 3, 4 and 5 show the distributions of σ_x/σ_o around the cracks for crack spacing = w/4, and crack lengths ranging from 7w/16 to 11w/16 with w being the width of the specimen.

Figures 6 through 9 show the distributions of σ_x/σ_o across the net section through the crack tip for various crack spacings, and crack lengths ranging from w/2 to 11w/16.

Figure 10 shows the variation of σ_x/σ_o versus spacing between cracks at various points along the net section for crack length = 11w/16.

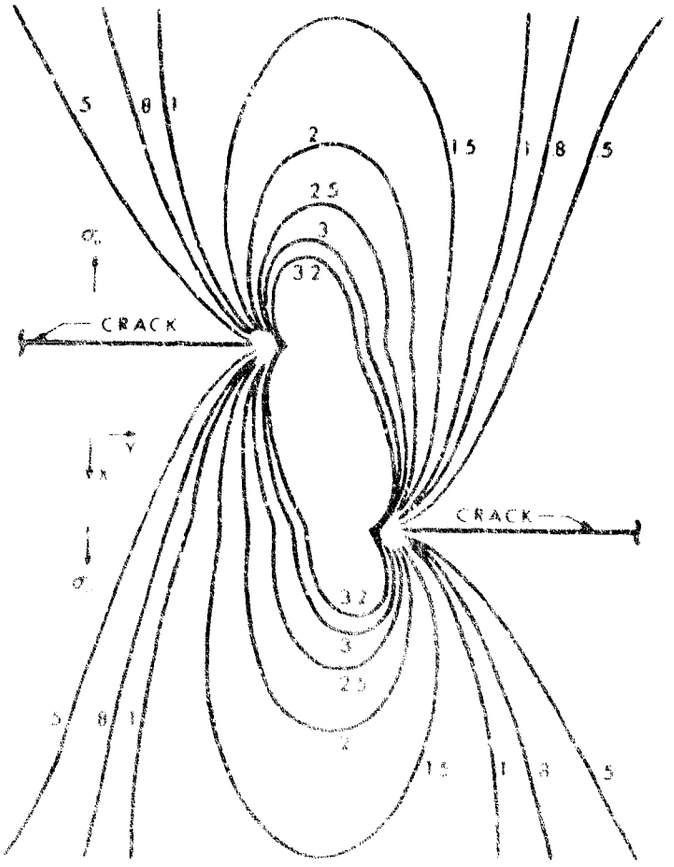

Figure 3 Distribution of σ_x/σ_o Around Cracks for crack length = 7w/16 and crack spacing = w/4 (w = specimen width).

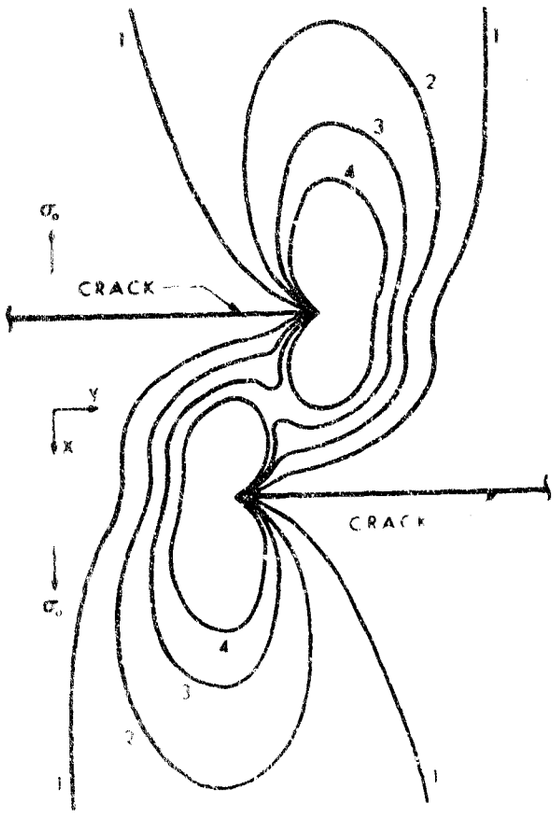

Figure 4 Distribution of σ_x/σ_o Around Cracks for Crack Length = 9w/16 and Crack Spacing = w/4 (w = Specimen Width).

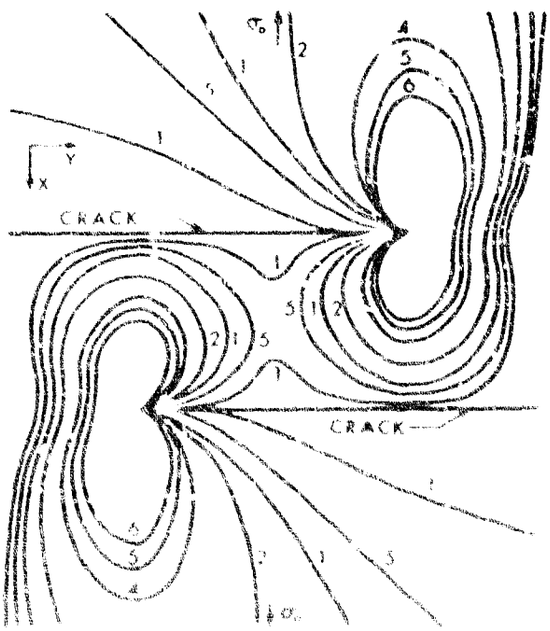

Figure 5 Distribution of σ_x/σ_o Around Cracks for Crack Length = 11w/16 and Crack Spacing = w/4 (w = Specimen Width).

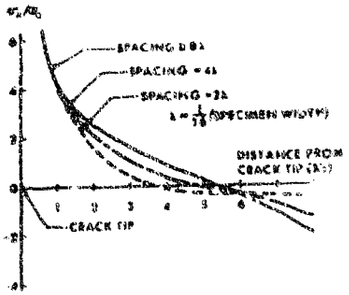

Figure 6 Distribution of σ_x/σ_o Across the Net Section for Crack Length = w/2 and Various Crack Spacings (w = Specimen Width).

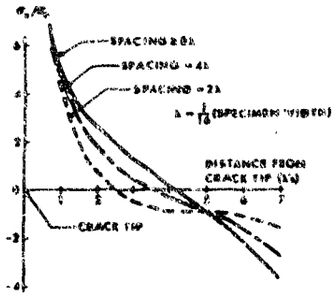

Figure 7 Distribution of σ_x/σ_o Across the Net Section for Crack Length = 9w/16 and Various Crack Spacings (w = Specimen Width).

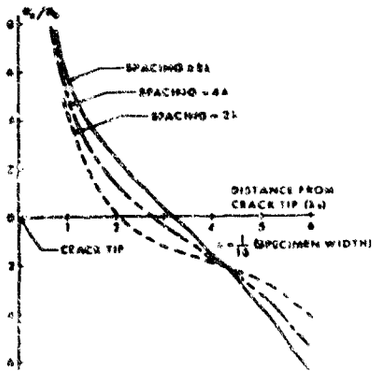

Figure 8 Distribution of σ_x/σ_o Across the Net Section for Crack Length = 5w/8 and Various Crack Spacings (w = Specimen Width).

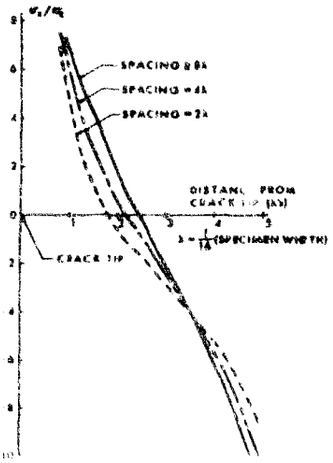

Figure 9 Distribution of σ_x/σ_o Across the Net Section for Crack Length = 11w/16 and Various Crack Spacings (w = Specimen Width).

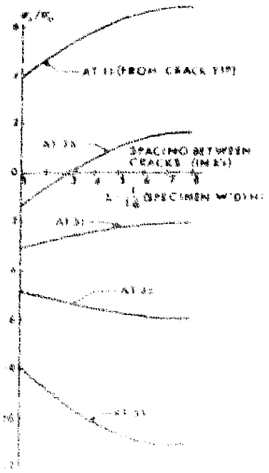

Figure 10 Variation of σ_x/σ_o Versus Spacing Between Cracks at Various Points Along the Net Section for Crack Length = 11w/16 (w = Specimen Width) (Refer to Figure 9).

Figures 11 through 14 show the comparisons between the theoretical and the experimental results for the dependence of tensile strength on crack-size in polymethyl methacrylate (PMMA) and polystyrene (PS) samples. The

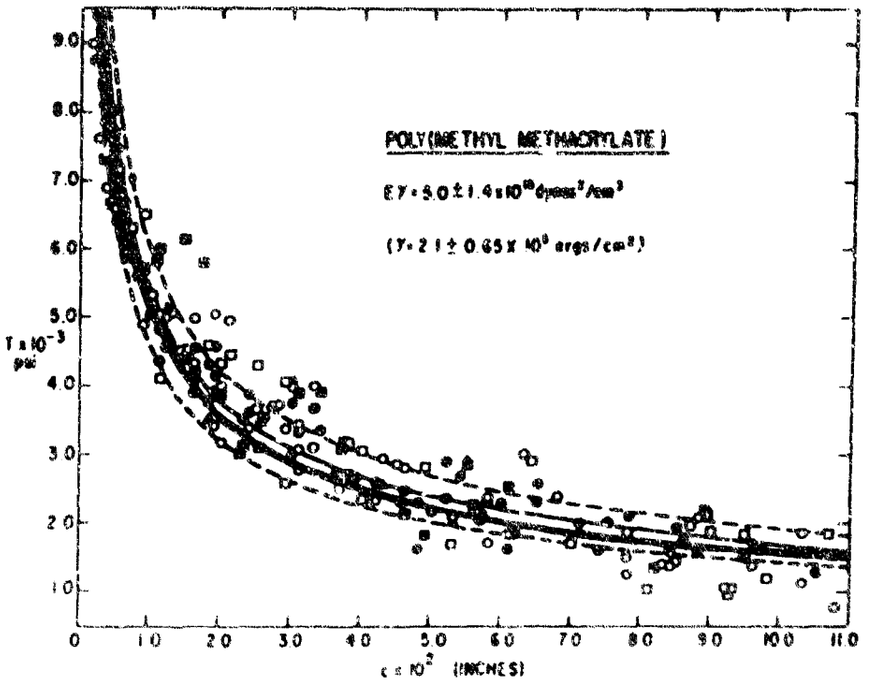

Figure 11 The Dependence of Tensile Strength on Crack-Size in PMMA Samples. (Theoretical results are shown as the curve in boldface. Experimental data were obtained from various sample cross sections and extension rates as reported by J. P. Berry.)

experimental data are as reported by Berry[5]. In the theoretical work, the Young's modulus and the effective surface energy per unit area for PMMA are assumed to be 4×10^5 psi and 1.5 in-lbs/in^2 respectively, and that the same for PS are assumed to be 2.8×10^5 psi and 13 in-lbs/in^2 respectively.

Discussion

The results of our calculations have shown that the stress fields around the cracks remain practically unchanged when the crack spacing increases from $w/2$, provided that the cracks are far enough from the loading edges to avoid their local disturbance. It is shown in Figure 10 that the values of σ_x/σ_0 at

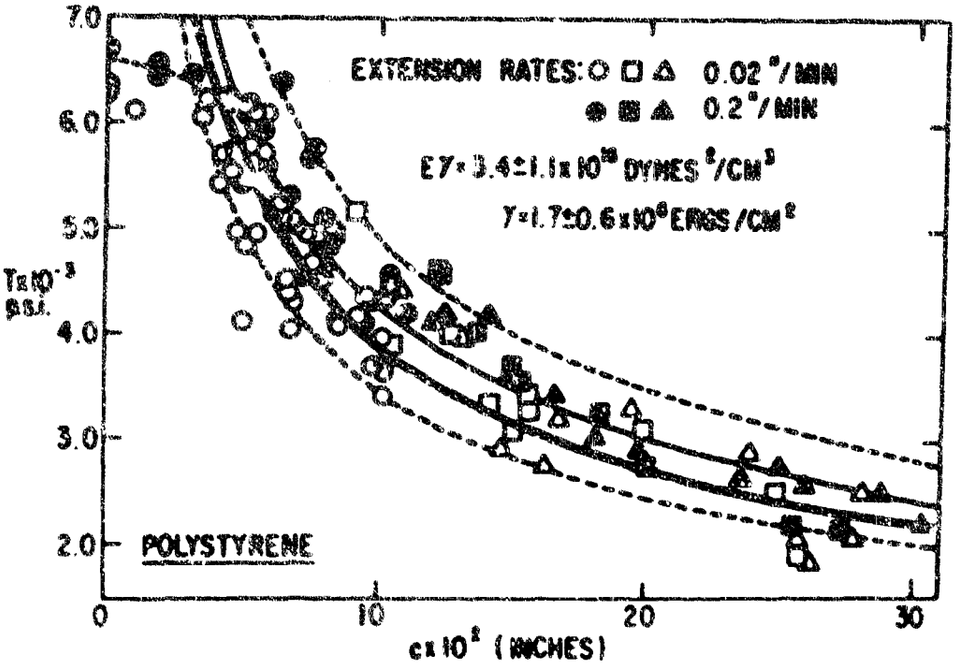

Figure 12 The Dependence of Tensile Strength on Crack Size in PS Samples. (Theoretical results are shown as the curve in boldface. Experimental data were obtained from various sample cross sections and extention rates as reported by J. P. Berry.)

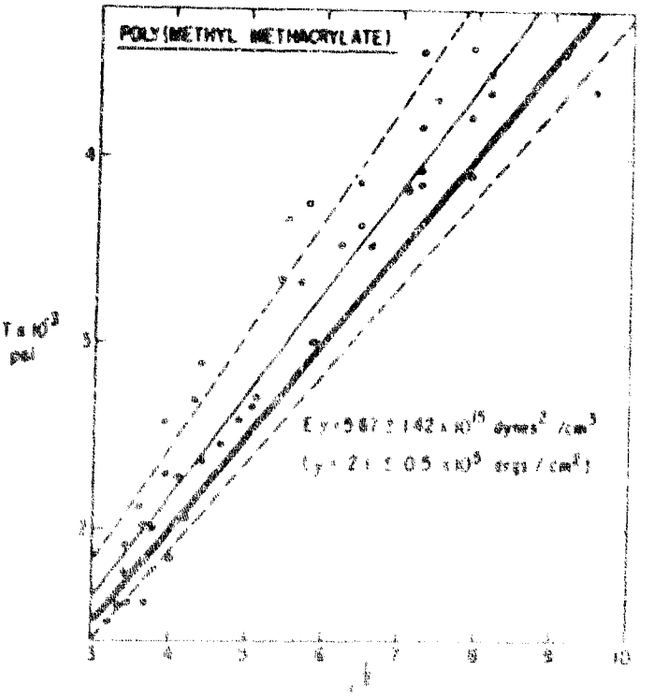

Figure 13 The Dependence of Tensile Strength of PMMA Samples on Crack Size. (Theoretical results are shown as the curve in boldface. Experimental data are as reported by J. P. Berry.)

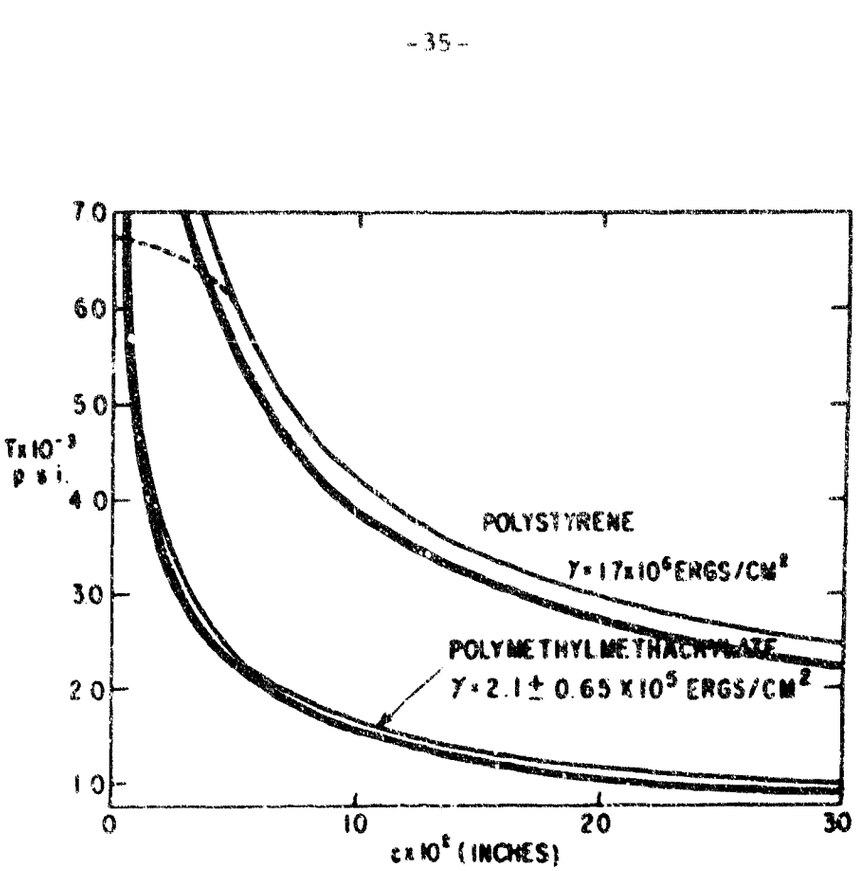

Figure 14 The Dependence of Tensile Strength on Crack-Size in PS and PMMA Samples. (Theoretical results are shown as the curves in boldface. Experimental curves are as reported by J. P. Berry.)

various points along the net section approach certain asymptotic values when crack spacing becomes equal to or greater than w/2. Interaction between the cracks occurs when the spacing becomes smaller than this value. As shown in Figures 6 through 9, the distribution of σ_x/σ_o across the net section through the crack tip varies as the spacing decreases. This variation must be accompanied by the change in stress concentration at the crack tip because of equilibrium considerations. However, the elastic strain energy of the system does not change appreciably with the crack spacing.

Although a direct comparison between our theoretical results for the strength-crack size relationship for the edge cracks and the corresponding experimental data is not possible because of the lack of such data, they seem to follow closely the experimental results for the single interior crack as reported by Berry. Our results also indicate consistently that the strength-

crack size curve for the edge cracks is generally lower than the same for the single interior crack, which have been quite often treated alike.

Perhaps, it should also be pointed out that the Griffith-Irwin theory[6] for the single interior crack neglects the effect of transverse stresses on the strain energy release rate, while our calculation includes the effect of longitudinal, transverse, as well as shearing stresses. The lowering of the strength-crack size curve for the edge cracks may be partly due to different crack morphology and to the increase in strain energy thus calculated. This seems to indicate that the edge cracks are more detrimental than the compatible interior crack in a tensile specimen.

For a tensile specimen as described in this paper, the increase in overlap between cracks is accompanied by the reduction in net section through the crack tip and the increase in the moment at the net section. Consequently, the interaction between the cracks is at least partially compensated by the change in the stress field due to such reasons. It must then be pointed out that the situation here is somewhat different from that for the interior crack in an infinite matrix.

Our calculations also indicate that the elastic model, without directly considering the plastic enclave in the stress field calculation but including its effect in the effective surface energy as proposed by Orowan, seems to be able to predict fairly well the strength-crack size behavior under the previously described limitations.

Acknowledgments

Thanks are due Dr. Lawrence E. Nielsen, Senior Scientist, Monsanto Company, for his valuable contributions and interest. The author also wishes to thank Dr. M. L. Williams for his suggestions concerning the extension of our work on the stress fields around parallel edge cracks to fracture mechanics applications. The assistance of Miss Barbara Krueger is greatly appreciated.

Nomenclature

x, y - Rectangular coordinates.

h - Finite-difference mesh size in both x- and y-directions.

b_0 - Half-width of the specimen.

N_x = Number of divisions in the finite-difference network in the half-length of the specimen.

N_y = Number of divisions in the finite-difference network in the width of the specimen.

N_n = Number of divisions in the finite-difference network in the net section.

ϕ = Stress function.

σ_x, σ_y = Normal components of stress parallel to x- and y-axes.

τ_{xy} = Shearing stress in xy-plane parallel to x- or y-axis.

σ_o = Uniformly distributed tension at the ends of the specimen.

∇^2 = Laplacian operator $\frac{\partial^2}{\partial x^2} + \frac{\partial^2}{\partial y^2}$.

W_e = Increase in strain energy.

W_s = Effective surface energy as defined by Orowan.

P = Plastic work per unit area.

T_s = Surface tension per unit area.

γ = Effective surface energy per unit area.

c = Total length of cracks.

V_o = Strain energy per unit volume.

E = Young's modulus.

G = Shear modulus.

ν = Poisson's ratio.

T = Tensile strength.

K = Coefficient for tensile strength.

w = Width of the specimen.

References

1. Chen, P. S. "Stress fields around parallel edge cracks," J. Composite Materials, 1, 82 (1967).

2. Griffith, A. A. "The phenomenon of rupture and flow in solids," Phil. Trans. Roy. Soc. London, A221 163 (1920).

3. Love, A. E. H. A Treatise on the Mathematical Theory of Elasticity, Oxford (1926), p. 173.

4. Orowan, E. "Fundamentals of brittle behavior in metals," Proceedings of the Symposium on Fatigue and Fracture of Metals, Wiley (1950), p. 139.

5. Berry, J. P. "Brittle behavior of polymeric solids," Fracture Processes in Polymeric Solids, Wiley (1964), p. 155.

6. Irwin, G. R. "Fracture mechanics," Proceedings of the First Symposium on Naval Structural Mechanics, Pergamon Press, New York, N. Y. (1960), p. 557.

7. Inglis, C. E. "Stresses in a plate due to the presence of cracks and sharp corners," Transactions of Royal Institution of Naval Architects, London, 60, 219 (1913).

8. Bowie, O. L. "Rectangular tensile sheet with symmetric edge cracks," J. Applied Mechanics, 31, 208 (1964).

9. Stimpson, L. D. and D. M. Eaton. "The extent of elasto-plastic yielding at the crack point of an externally notched plane stress tensile specimen," AD 266 347 (1961).

10. Sneddon, I. N. "Crack problems in the mathematical theory of elasticity," AD 256 458 (1961).

11. Swedlow, J. L. and M. L. Williams. "A review of recent investigations into fracture initiation at GALCIT," AD 610 078 (1964).

12. Bowie, O. L. and D. M. Neal. "Single edge cracks in rectangular tensile sheet," AD 603 855.

13. Wells, A. A. and D. Post. "The dynamic stress distribution surrounding a running crack - a photoelastic analysis," Proceedings of the Society for Experimental Stress Analysis, 16, 69 (1958).

14. Post, D. "Photoelastic stress analysis for an edge crack in a tensile field," Proceedings of the Society for Experimental Stress Analysis, 12, 99 (1954).

15. Dixon, J. R. "Stress distribution around edge slits in a plate loaded in tension," Journal of the Royal Aeronautical Society, 66, 320 (1962).

16. Timoshenko, S. and J. N. Goodier. Theory of Elasticity, McGraw-Hill, New York, N. Y. (1951).

17. Allen, D. N. de G. Relaxation Methods, McGraw-Hill. New York, N. Y. (1954).

18. Nielsen, L. E. Mechanical Properties of Polymers, Reinhold, New York, N. Y. (1962).

STRESS FIELD AROUND INTERIOR CRACK (P. E. Chen)

Using Michell's[1, 5, 9] continuity equations for the single-valuedness of rotations and displacements, and extending Prager's[2] method for calculating the plane elastic strains in doubly-connected domains, a mathematical approach is proposed for solving the problem of stress fields around interior cracks.

Based on the general approach, a computer program has been written to calculate the stress field around single interior crack in a tensile specimen. Photoelastic experiments have been conducted on CR-39 allyl diglycol carbonate specimens under uniaxial tension. The theoretical and experimental results are compared.

It is assumed that (1) the materials is isotropic, homogeneous and obeys Hooke's law, (2) the strains are infinitesimal, (3) the body forces are negligible, (4) the specimen is in a plane state of stress or strain, and (5) the cracks penetrate through the thickness of the specimen.

Theory

The domain under consideration is shown in Figure 1. Instead of having a simply-connected region as in the case of edge cracks[3], we now have a multiply-connected region.

If we let n denote the direction of the outward normal of the boundary of the region, s the direction of the tangent, X and Y the components of the resultant surface force per unit area, γ the angle between the x-axis and the outward normal, σ_x and σ_y the normal stresses, τ_{xy} the shearing stress, as illustrated in Figure 2, then from equilibrium we have

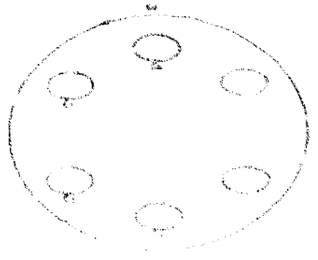

Figure 1 A Multiply-Connected Region.

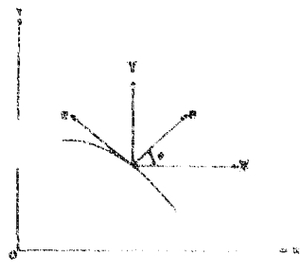

Figure 2 The Surface Forces on the Boundary.

$$X = \sigma_x \cos \Psi + \tau_{xy} \sin \Psi \tag{1A}$$

$$Y = \sigma_y \sin \Psi + \tau_{xy} \cos \Psi . \tag{1B}$$

In terms of the stress function Φ, the above equations can be expressed as

$$X = \frac{\partial^2 \Phi}{\partial y^2} \frac{\partial y}{\partial s} + \frac{\partial^2 \Phi}{\partial x \partial y} \frac{\partial x}{\partial s}$$

$$= \frac{\partial}{\partial s} \left(\frac{\partial \Phi}{\partial y} \right) \tag{2A}$$

$$Y = - \frac{\partial^2 \Phi}{\partial x^2} \frac{\partial x}{\partial s} - \frac{\partial^2 \Phi}{\partial x \partial y} \frac{\partial y}{\partial s}$$

$$= - \frac{\partial}{\partial s} \left(\frac{\partial \Phi}{\partial x} \right) . \tag{2B}$$

Upon integration, one obtains

$$\frac{\partial \Phi}{\partial n} = A \cos \Psi + B \sin \Psi + \alpha \cos \Psi + \beta \sin \Psi , \tag{3}$$

Hence

$$\Phi = \int_0^s (B \cos \Psi + A \sin \Psi) \, ds + \alpha x \quad \beta y + \gamma \tag{4}$$

where

$$A = \int_0^s Y \, ds , \qquad B = \int_0^s X \, ds , \tag{5}$$

α, β and γ are the constants of integration which for a simply connected region can be chosen arbitrarily. If the region is multiply-connected, these constants can still be chosen arbitrarily for the external boundary but their values on the internal boundaries are restricted by additional boundary conditions. To ensure

simple-valuedness of rotations and displacements, the following continuity equations must be satisfied for each internal boundary:

$$\oint_i \frac{\partial}{\partial s} (\nabla^2 \phi)\, ds = 0 \tag{6}$$

$$\oint_i \left[y \frac{\partial}{\partial n} (\nabla^2 \phi) - x \frac{\partial}{\partial s} (\nabla^2 \phi) \right] ds = 0 \tag{7}$$

$$\oint_i \left[y \frac{\partial}{\partial s} (\nabla^2 \phi) + x \frac{\partial}{\partial n} (\nabla^2 \phi) \right] ds = 0 \tag{8}$$

where

$\oint_i$ is the line integral over the i th internal boundary,

∇^2 is the Laplacian operator,

and i varies from 1 through N, assuming that there are N internal boundaries.

Equation (6) represents the rotation condition, and equations (7) and (8) the displacement conditions. These equations can be derived by the variational method, utilizing the principle of minimum energy and Green's theorem for the plane.

Let ϕ_0, ϕ_{11}, ϕ_{12}, ϕ_{13}, ... ϕ_{N1}, ϕ_{N2}, ϕ_{N3} be the biharmonic functions defined by the following boundary conditions:

(1) ϕ_0 and $\partial\phi_0/\partial n$ have the prescribed boundary values on the loaded boundary curve C_0 and vanish on the other boundary curves C_1, C_2, C_3, ... C_N;

(2) $\phi_{11} = \partial\phi_{11}/\partial n = 0$ on C_0, C_2, C_3, ... C_N, $\phi_{11} = x$ and $\partial\phi_{11}/\partial n = n_{11}$ on C_1;

(3) $\phi_{12} = \partial\phi_{12}/\partial n = 0$ on C_0, C_2, C_3, ... C_N, $\phi_{12} = y$ and $\partial\phi_{12}/\partial n = n_{12}$ on C_1;

(4) $\phi_{13} = \partial\phi_{13}/\partial n = 0$ on C_0, C_2, C_3, ... C_N, $\phi_{13} = 1$ and $\partial\phi_{13}/\partial n = 0$ on C_1;

(5) $\phi_{21} = \partial\phi_{21}/\partial n = 0$ on C_0, C_1, C_3, ... C_N, $\phi_{21} = x$ and $\partial\phi_{21}/\partial n = n_{21}$ on C_2;

(6) $\Phi_{22} = \partial\Phi_{22}/\partial n = 0$ on C_o, C_1, C_3, ..., $C_{N'}$

$\Phi_{22} = y$ and $\partial\Phi_{22}/\partial n = n_{22}$ on C_2;

(7) $\Phi_{23} = \partial\Phi_{23}/\partial n = 0$ on C_o, C_1, C_3, ..., $C_{N'}$

$\Phi_{23} = 1$ and $\partial\Phi_{23}/\partial n = 0$ on C_2;

etc.

where the n_{ij}'s are the normal derivatives of the Φ_{ij}'s to be calculated from equation (3).

Substituting

$$\Phi = \Phi_o + \sum_{i=1}^{N} (\alpha_i \Phi_{i1} + \beta_i \Phi_{i2} + \gamma_i \Phi_{i3}) \qquad (9)$$

into equations (6), (7) and (8), we obtain a set of 3N simultaneous linear equations from which the coefficients α_i's, β_i's and γ_i's can be determined. Symmetry and other conditions can be utilized to simplify the solution.

An Example

Applying the above theory, a computer program has been written to calculate the stress field around an interior crack in a tensile specimen for various crack lengths. As shown in Figure 3, the crack is assumed to be perpendicular to the applied stress σ_o, and the reference frame is chosen such that both the crack and the domain are symmetrical with respect to the coordinate axes. Due to twofold symmetry, the coefficients α_i and β_i become zero, and the displacement conditions (7) and (8) are automatically satisfied. Hence the stress function can be expressed as

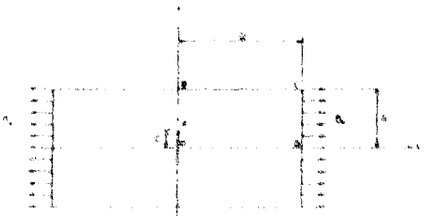

Figure 3 Single Interior Crack in a Tensile Specimen.

$$\Phi = \Phi_o + \gamma_1 \Phi_{11} \quad \text{or} \quad \Phi_o + \gamma \Phi_1 \qquad (10)$$

In the above equation, Φ_o is the biharmonic function defined by the following boundary conditions:

along CD

$$\Phi_o = \frac{1}{2}\sigma_o y^2, \qquad \frac{\partial \Phi_o}{\partial x} = 0, \tag{11}$$

along BC

$$\Phi_o = \frac{1}{2}\sigma_o a^2, \qquad \frac{\partial \Phi_o}{\partial y} = \sigma_o a, \tag{12}$$

along OA

$$\Phi_o = 0, \qquad \frac{\partial \Phi_o}{\partial x} = 0, \tag{13}$$

and at A

$$\Phi_o = 0, \qquad \frac{\partial \Phi_o}{\partial y} = 0, \tag{14}$$

Φ_1 is the biharmonic function defined by the following boundary conditions:

along CD

$$\Phi_1 = 0, \qquad \frac{\partial \Phi_1}{\partial x} = 0, \tag{15}$$

along BC

$$\Phi_1 = 0, \qquad \frac{\partial \Phi_1}{\partial y} = 0, \tag{16}$$

along OA

$$\Phi_1 = 1, \qquad \frac{\partial \Phi_1}{\partial x} = 0, \tag{17}$$

and at A

$$\Phi_1 = 1, \qquad \frac{\partial \Phi_1}{\partial y} = 0, \tag{18}$$

while the coefficient γ is to be determined from

$$\oint_{\Phi_1} \frac{\partial}{\partial n} \left[\nabla^2 (\Phi_o + \gamma \Phi_1) \right] ds = 0$$

or

$$\int_o^c \frac{\partial}{\partial x} (\nabla^2 \Phi_o)\, dy + \gamma \int_o^c \frac{\partial}{\partial x} (\nabla^2 \Phi_1)\, dy = 0. \tag{19}$$

The relaxation method[4] is used to calculate the biharmonic functions Φ_o and Φ_1 based on the boundary conditions as given by equations (11) through (18). The stress function Φ is evaluated from equation (10), using the value of γ calculated from equation (19). The stresses can then be computed from their basic relations with the stress function.

The results of a typical case are included here for illustrative purposes. In this case, the width of the specimen is divided into 32 equal divisions with the length of each division equal to λ. The length of the specimen is equal to 32 λ, and the length of the crack 8 λ. Stress contours, representing various σ_x/σ_o ratios are given in Figure 4.

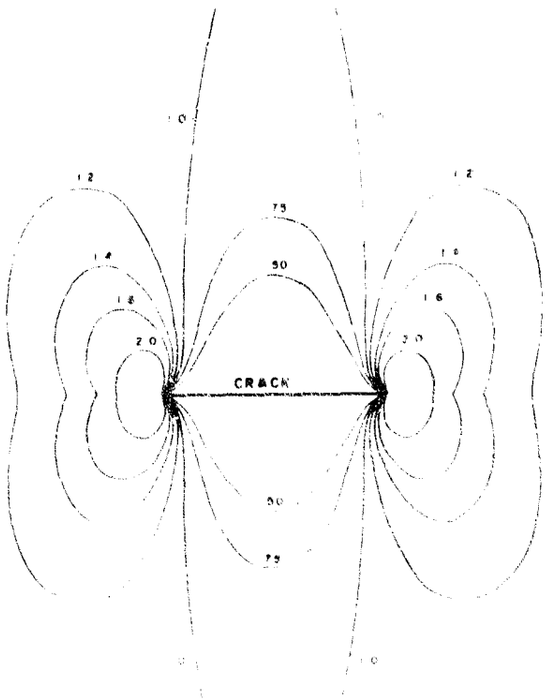

Figure 4 σ_x/σ_o Distribution of the Typical Case.

Experiment

The stress fields around interior cracks have also been studied experimentally using the photoelasticity techniques. Black and white pictures of the isochromatic fringe patterns for the difference between the principal stresses are taken from a monochromatic light source. Kodak Panatomic-X 35 mm films are used on Leica camera with f-8 lens opening and 10-second time exposure. The tensile specimens are cut from 1/4" thick CR-39 plates made by the Homalite Corporation in Wilmington, Delaware. Each specimen is 8.9" long and 2.5" wide. The narrow portion of the specimen is 6.3" long and has a nominal width of 1.5" which increases to 2.5" at the ends through 0.5" radius fillets. The cracks are introduced by a 0.020" wire saw. The calibration is based on the tension method. The photoelastic constant of the specimen material is 88 lbs. per in. per fringe. Tests are performed at room temperature. Tensile loads are applied to the specimens by gradually adding weights to a hanger suspended at the free end of a cantilever beam which is supported by a hinge at the other end and attached to the lower end of the specimen at a distance from the

hinge support equal to one-third of the span length. In order to achieve more uniform load distribution, the tensile specimen is suspended at the top from the loading frame and attached at the bottom to the cantilever beam through two pairs of steel clamping plates. Two 3/8" shoulder bolts with washers and nuts are used at each end to connect the specimen to the clamping plates.

An Example

This corresponds to the example mentioned previously for the theoretical approach. The width of the specimen is 1.490", and the length of the crack is 0.373". A picture of the isochromatic fringe pattern, as shown in Figure 5, was taken under applied stress σ_o equal to 90 lbs. per in., thus the first fringe represents $\sigma_1-\sigma_2 \doteq \sigma_o$.

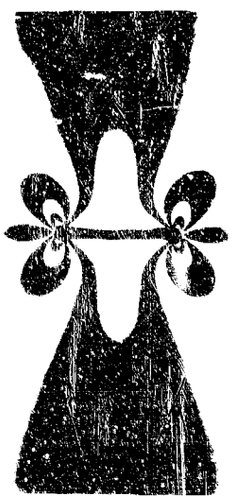

Figure 5 $\sigma_1-\sigma_2$ Distribution of the Typical Case.

Comparison

The theoretical and experimental results for $(\sigma_1-\sigma_2)/\sigma_o$ distribution along the net section adjacent to the crack tip of the typical case are shown in Figure 6 where point A is at the crack tip. The agreement is good.

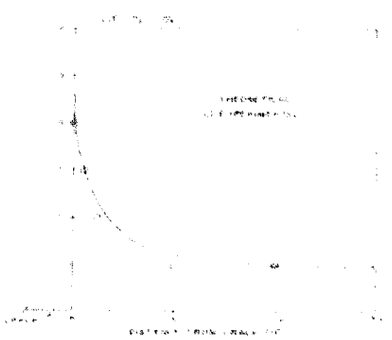

Figure 6 $(\sigma_1-\sigma_2)/\sigma_o$ Distribution Along the Net Section Adjacent to the Crack Tip of the Typical Case.

Acknowledgments

Thanks are due Dr. Lawrence E. Nielsen, Senior Scientist, Monsanto Company, for his valuable contributions and interest. The assistance of Miss Barbara Krueger is greatly appreciated.

Nomenclature

x, y	=	Rectangular coordinates.
X, Y	=	x- and y-components of the resultant surface force per unit area.
ϕ	=	Stress function.
σ_x, σ_y	=	Normal components of stress parallel to x- and y-axis.
τ_{xy}	=	Shearing stress in xy-plane parallel to x- or y-axis.
n	=	Direction of the outward normal at the boundary of the region.
s	=	Direction of the tangent at the boundary of the region.
Ψ	=	Angle between the x-axis and the outward normal.
∇^2	=	$\frac{\partial^2}{\partial x^2} + \frac{\partial^2}{\partial y^2}$
σ_o	=	Uniformly distributed tension at the ends of the specimen.
σ_1, σ_2	=	Principal stresses.

References

1. Michell, J. H. "On the direct determination of stress in an elastic solid, with application to the theory of plates," Proceedings of London Mathematical Society, 31, 100-146 (1899).

2. Prager, W. "On plane elastic strain in doubly-connected domains," Quarterly Journal of Applied Mathematics, III, 377-380 (1946).

3. Chen, P. E. "Stress fields around edge cracks," AD 481 654.

4. Allen, D. N. de G. Relaxation Methods, McGraw-Hill, New York, N. Y. (1954).

5. Sneddon, I. N. "Crack problems in the mathematical theory of elasticity," AD 256 458 (1961).

6. Williams, L. L. and M. L. Williams, "A review of recent investigations into fracture initiation at GALCIT," AD 610 078 (1964).

7. Irwin, G. R., "Fracture mechanics," Proceedings of the First Symposium on Naval Structural Mechanics, Pergamon Press, New York, N. Y., p. 557-594 (1960).

8. Timoshenko, S. and J. N. Goodier, Theory of Elasticity, McGraw-Hill, New York, N. Y. (1951).

9. Redshaw, S. C. and K. R. Rushton, "An electrical analogue solution for the stresses near a crack or hole in a flat plate," Journal of the Mechanics and Physics of Solids, 8, 173-186 (1960).

YOUNG'S MODULUS OF RANDOMLY ORIENTED FIBER-FILLED COMPOSITES

(L. E. Nielsen and P. E. Chen)

The theory of the longitudinal and transverse Young's modulus of oriented or aligned fiber-filled composites is fairly well worked out[1, 2, 3]. Likewise, the mathematical theory of the elastic modulus of an oriented fiber-filled composite as a function of the angle between the fibers and the direction of the applied tensile load has been derived[2, 4, 5, 6]. Apparently, however, no one has gone one step farther and calculated the Young's modulus from basic elastic constants of the constituents for the case where the fibers are oriented at random in a plane. The equations derived by Horio and Onogi[7] for fibrous materials such as paper are not exact and are only good approximations when the anisotropy is small compared to the results often found in fiber-filled composites. For many applications, the random orientation of the fibers may be desirable since in the plane of the sheet the elastic modulus is the same in all directions. A computer program making use of the classical theory of elasticity was used to calculate the expected dependence of Young's modulus on the amount of long fibers in the composite and the ratio of the moduli of the fiber phase to that of the matrix phase. The fibers need not be infinitely long but only long enough to be above the critical length where modulus becomes nearly independent of length.

From classical elasticity theory, the angular dependence of Young's modulus for long fibers all aligned in one direction is[2, 4, 5]:

$$\frac{E_\theta}{E_m} = \cos^4\theta + \frac{E_{\parallel}}{E_{\perp}}\sin^4\theta + \left(\frac{E_{\parallel}}{G} - 2\nu_{12}\right)\cos^2\theta\sin^2\theta \qquad (1)$$

E_θ is Young's modulus measured at any angle θ between the longitudinal axis of the aligned fibers and the direction of the applied load.

$E_{\parallel}$ is Young's modulus of a fiber-filled composite in the direction parallel to the aligned fibers, i.e., $\theta = 0°$.

$E_{\perp}$ is Young's modulus of a fiber-filled composite measured in the direction perpendicular to the fibers, i.e., $\theta = 90°$.

G is the shear modulus of the composite with respect to the direction parallel and perpendicular to the fibers.

ν_{12} is the major Poisson's ratio of the composite.

The quantities $E_{\parallel}$, $E_{\perp}$, G, and ν_{12} can be experimentally determined values, or they can be estimated from such as the following theoretical equations assuming perfect adhesion between the fibers and the matrix[1, 3]:

$$E_{\parallel} \doteq E_1 \Phi_1 + E_2 \Phi_2 \tag{2}$$

$$E_{\perp} \doteq 2[1 - \nu_2 + (\nu_2 - \nu_1)\Phi_1]\left[\frac{M_2(2M_1 + G_1) - G_1(M_2 - M_1)\Phi_1}{(2M_1 + G_1) + 2(M_2 - M_1)\Phi_1}\right] \tag{3}$$

$$G \doteq G_1 \frac{2G_2 - (G_2 - G_1)\Phi_1}{2G_1 + (G_2 - G_1)\Phi_1} \tag{4}$$

$$\nu_{12} \doteq \frac{M_2 \nu_2 (2M_1 + G_1)\Phi_2 + M_1 \nu_1 (2M_2 + G_1)\Phi_1}{M_2(2M_1 + G_1) - G_1(M_2 - M_1)\Phi_1} \tag{5}$$

where

$$M_1 = \frac{E_1}{2(1-\nu_1)} \quad \text{and} \quad M_2 = \frac{E_2}{2(1-\nu_2)} .$$

Φ_1 and Φ_2 are the volume fractions of matrix and fibers, respectively. The M's are areal moduli, the G's are shear moduli, and the ν's are Poisson's ratios; the subscripts 1 and 2 always refer to the matrix phase and the fibers, respectively.

The value of the modulus for the case of randomly oriented fibers can be found by averaging the value of the modulus E_θ given in equation (1) over all values of the angle θ. Thus,

$$\langle E_{\theta} \rangle = \frac{\int_0^{\pi/2} E_\theta \, d\theta}{\int_0^{\pi/2} d\theta} \tag{6}$$

$\langle E_\theta \rangle$ is the Young's modulus for the case of random orientation of fibers in a plane.

Equation (6) was solved by computer for a number of values of fiber concentration Φ_2 and modulus ratio E_2/E_1. The values of $E_{||}$ were calculated from equation (2). The values of $E_\perp$ and G were calculated by equations (3) and (4). Typical values for polymers were used, i.e., $G = 1 \times 10^{10}$ dynes/cm^2, $E_1 = 2.70 \times 10^{10}$ dynes/cm^2, and $\nu_{12} = 0.35$. Figures 1, 2 and 3 give some of the

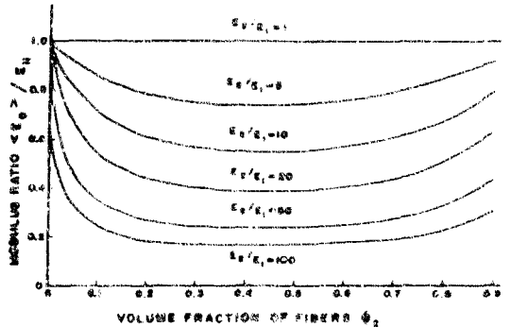

Figure 1 Ratio of the Randomly Oriented Fiber Composite Young's Modulus of the Parallel Oriented Modulus, i.e., $\langle E_\theta \rangle / E_{||}$, as a Function of the Volume Fraction of Fibers in the Composite for Different Values of E_2/E_1.

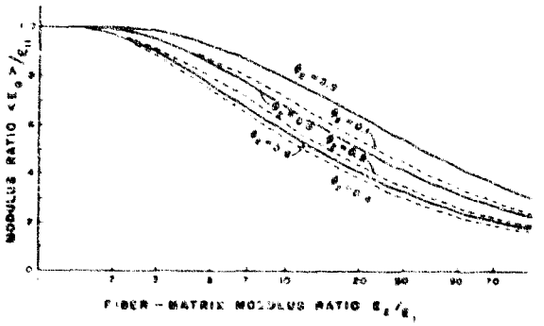

Figure 2 Modulus Ratio $\langle E_\theta \rangle / E_{||}$ as a Function of the Fiber-Matrix Young's Modulus Ratio E_2/E_1 for Different Values of the Volume Fraction of Fibers.

results in terms of $\langle E_\theta \rangle / E_{||}$ and F, where F is a fiber efficiency factor relative

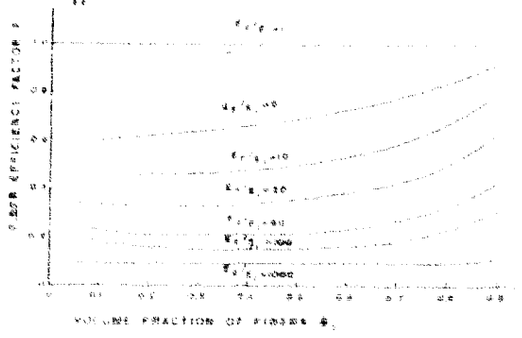

Figure 3 Fiber Efficiency Factor F as a Function of the Volume Fraction of Fibers for Different Values of E_2/E_1.

to oriented fibers as defined by the following equation:

$$\langle E_\theta \rangle = E_1 \phi_1 + F E_2 \phi_2 . \tag{7}$$

The figures show that the fiber efficiency factor F is a slowly varying function of ϕ_2 as well as a function of E_2/E_1. For most composites of practical interest, F varies from about 0.15 to 0.60 and $\langle E_\theta \rangle / E_{\parallel}$ varies from about 0.15 to 0.70. Especially for very stiff fibers, i.e., values of E_2/E_1 greater than 5, the random case gives a much smaller modulus than $E_{\parallel}$ for the oriented fiber case. This is illustrated in Figure 4. One has traded great stiffness in one direction for much less stiffness in all directions in going from oriented fibers to a random distribution of fibers.

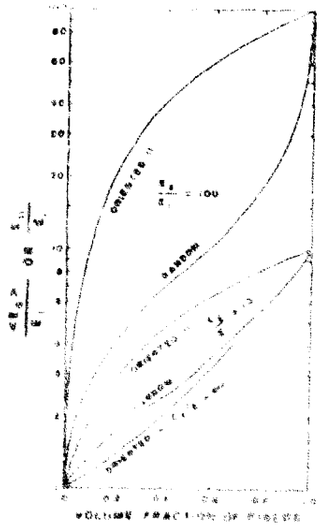

Figure 4 The parallel oriented and randomly oriented fiber composite moduli relative to the matrix modulus as a function of volume fraction of fibers. Two values of fiber-matrix modulus ratio E_2/E_1 are considered -- 10 and 100. The lowest curve gives the Young's modulus of an oriented fiber composite measured in the direction perpendicular to the direction of the fiber length for the case where $E_2/E_1 = \infty$.

Horio and Onogi[7] used equation (6) rather than equation (1) for the angular dependence of Young's modulus:

$$E_\theta = \frac{E_{\parallel} E_{\perp}}{E_{\parallel} \sin^2 \theta + E_{\perp} \cos^2 \theta} \tag{8}$$

This equation gives results which are good at low degrees of anisotropy, i.e., when $E_{\parallel}$ is not much greater than $E_{\perp}$. However, this equation does not take into account shearing effects. Changes in the angle θ and change in shape of the test specimen when a tensile load is applied [illegible] at angles other than 0°

and 90° to the fibers. Also, it is assumed that $E_{\parallel}$ and $E_{\perp}$ are experimentally determined values rather than calculated from the constituent properties. Equation (8) predicts that:

$$\frac{\langle E_\theta \rangle}{E_{\parallel}} = \left(\frac{E_{\perp}}{E_{\parallel}}\right)^{1/2} \tag{9}$$

rather than the much more complicated results derived from equation (1). As a first approximation, equation (9) gives a good estimate of $\langle E_\theta \rangle / E_{\parallel}$; the error is roughly 5 percent for $E_2/E_1 = 4$, 12 percent for $E_2/E_1 = 10$, and 25 percent for $E_2/E_1 = 100$.

For a quasi-isotropic laminate which consists of three or more layers of unidirectional fiber-filled systems oriented at equal angles between the principal directions of adjacent layers, the $\langle E_\theta \rangle$ value as calculated by the method presented in this paper is in good agreement with the result obtained from the equations given by Fischer[8] as validated by the experimental data of the Forest Products Laboratory[9].

References

1. Hermans, J. J. (submitted for publication to Proc. Amsterdam Acad.).

2. Shaffer, B. W. "Material properties of reinforced plastics." Trans. SPE, 4, 267-276 (1964).

3. Tsai, S. W. "Structural behavior of composite materials," NASA CR-71 (1964).

4. Tsai, S. W. Paper presented at Sixth Annual Symposium of Filament Structure Technology, Albuquerque, New Mexico (1965).

5. Hoff, N. J. Engineering Laminates. A. G. H. Dietz, Ed., Chapter 1, p. 15, John Wiley and Sons (1949).

6. Cox, H. L. "The elasticity and strength of paper and other fibrous materials," British Journal of Applied Physics, 3, 72 (1952).

7. Hirao, M. and S. Ogata. Journal of Applied Physics, 22, 971 (1951).

8. Fischer, L. "Optimization of orthotropic laminates," ASME Journal of Engineering for Industry, WA/RP-5 (1966).

9. Werren, F. and C. B. Norris, "Mechanical properties of a laminate designed to be isotropic," FPL 1841 (1959).

INVARIANT PROPERTIES OF COMPOSITE MATERIALS* (S. W. Tsai and N. J. Pagano - AFML)

The superior performance of composite materials over light-weight metals has been well publicized in recent years. Composites have been claimed to possess improvements in stiffness and in strength of several fold over ordinary materials. The claim, however, is based on either the properties of the fibers alone or the longitudinal properties of a unidirectional composite against those of the metals. Since composites are normally used in laminated forms which consist of layers of a unidirectional composite, a more realistic measure of the performance of the composites than that based on the fiber or longitudinal properties is needed.

In this work, the transformation properties of unidirectional and laminated composites are derived using multiple angles, instead of the classical relations using powers of sines and cosines. The effect of lamina orientation is then examined. It is shown that the invariant properties of both the unidirectional and laminated composites have the same components, and can be used as an effective measure of the performance of the composites. Simple formulas for these invariant properties are derived, from which the performance of composites, irrespective of the lamina orientation, can be determined from the properties of the consitutents. This work should be of value to system analysts who must evaluate the performance of composites, to structural designers who must establish a rational design procedure, and to materials engineers who may need guidance in the selection and fabrication of composite materials.

---

* This publication was prepared in cooperation with the Nonmetallic Materials Division, Air Force Materials Laboratory, Wright-Patterson AFB.

The elastic moduli of laminated composites have been reported by many investigators in recent years, examples of which include Reissner and Stavsky[1], Dong, et al.[2], and Tsai[3,4]. The usual assumptions in all these studies are:

(a) All layers are in a state of plane stress, relative to the x-y or 1-2 plane, that

$$\sigma_3 = \sigma_4 = \sigma_5 = 0 \tag{1}$$

(b) All layers are bonded together and the strain components in the 1-2 plane are linear functions of z,

$$\epsilon_i = \epsilon_i^o + zk_i \tag{2}$$

where i = 1, 2 refers to the normal components, and i = 6, the engineering shear strain component.

(c) All layers obey the generalized Hooke's law,

$$\sigma_i = C_{ij}\,\epsilon_j \tag{3}$$

With these assumptions, the constitutive equation for a laminated composite can be derived. The stress-strain relation for the assumed plane stress condition including the thermal effect for each layer is

$$\sigma_i = Q_{ij}\,\epsilon_j - Q_{ij}\,\alpha_j\,T \tag{4}$$

where $$Q_{ij} = C_{ij} - \frac{C_{i3}\,C_{j3}}{C_{33}}$$ = reduced stiffness matrix. (5)

α_i = anisotropic thermal expansion matrix

T = temperature increase from a reference (stress-free) temperature.

Stress resultants (N_i) and stress couples (M_i) can be defined as:

$$(N_i, M_i) = \int_{-h/2}^{h/2} \sigma_i\,(1, z)\,dz \tag{6}$$

Substituting Equations (2) and (4) into (6) renders

$$\bar{N}_i = N_i + N_i^T = A_{ij}\,\epsilon_j^\circ + B_{ij}\,k_j$$
$$\bar{M}_i = M_i + M_i^T = B_{ij}\,\epsilon_j^\circ + D_{ij}\,k_j \tag{7}$$

where

$$[N_i^T,\ M_i^T] = \int_{-h/2}^{h/2} Q_{ij}\,\alpha_j\,[1,\ z]\,dz \tag{8}$$

$$[A_{ij},\ B_{ij},\ D_{ij}] = \int_{-h/2}^{h/2} Q_{ij}\,[1,\ z,\ z^2]\,dz \tag{9}$$

The brackets above and for the remaining part of this paper are symbolic rather than operational; the equality applies to the corresponding terms in the bracket. The limits of integration are from -h/2 to h/2, and will remain the same in this paper unless otherwise specified.

The constitutive equations of laminated composites are given by Equations (7), and the material coefficients are expressed by the A, B, and D matrices. Our present work is concerned with the nature of the Q, A, B, and D matrices.

Transformation of Q_{ij}

We would like to establish the transformation property of the reduced stiffness matrix Q_{ij}. This can be done by use of Equation (5) and the transformation equations for C_{ij} tabulated by Hearmon[5], and Tsai[4]. A typical example is as follows:

$$
\begin{aligned}
Q_{11}' &= C_{11}' - \frac{C_{13}'^2}{C_{33}'} \\
&= m^4 C_{11} + 2m^2n^2C_{12} + n^4C_{22} + 4m^2n^2C_{66} \\
&\quad + 4m^3nC_{16} + 4mn^3C_{26} - \frac{1}{C_{33}}(m^2C_{13} + n^2C_{23} + 2mnC_{36})^2 \\
&= m^4\left(C_{11} - \frac{C_{13}^2}{C_{33}}\right) + 2m^2n^2\left(C_{12} - \frac{C_{13}C_{23}}{C_{33}}\right) \\
&\quad + n^4\left(C_{22} - \frac{C_{23}^2}{C_{33}}\right) + 4m^2n^2\left(C_{66} - \frac{C_{36}^2}{C_{33}}\right) \\
&\quad + 4m^3n\left(C_{16} - \frac{C_{13}C_{63}}{C_{33}}\right) + 4mn^3\left(C_{26} - \frac{C_{23}C_{63}}{C_{33}}\right) \\
&= m^4 Q_{11} + 2m^2n^2 Q_{12} + n^4Q_{22} + 4m^2n^2 Q_{66} \\
&\quad + 4m^3n Q_{16} + 4mn^3 Q_{26}
\end{aligned}
\tag{10}
$$

The transformation of the other components of Q_{ij} can also be shown. The transformation is a rotation through an angle θ about the 3-axis, for which $C_{33} = C_{33}'$ = invariant, and $m = \cos\theta$ and $n = \sin\theta$. It is assumed that a plane of symmetry exists in the 1-2 plane. Based on the result of Equation (10) and similar results for the other components of Q_{ij}, we conclude that Q_{ij} transforms the same as C_{ij}. Having established the transformation property, we can apply the usual material symmetries like orthotropy, isotropy, etc., and invariants of the transformation.

For our present study, it is more convenient to express the transformation equations in terms of multiple angles than the conventional powers of sines and cosines. The following trigonometric identities shown by Cox[4] can be used:

$$
\begin{aligned}
m^4 &= (3 + 4\cos 2\theta + \cos 4\theta)/8 \\
m^3 n &= (2\sin 2\theta + \sin 4\theta)/8 \\
m^2 n^2 &= (1 - \cos 4\theta)/8 \\
mn^3 &= (2\sin 2\theta - \sin 4\theta)/8 \\
n^4 &= (3 - 4\cos\theta + \cos 4\theta)/8
\end{aligned}
\tag{11}
$$

By direct substitution of Equation (1) into the conventional transformation equations, a new form of transformation equations for Q_{ij} (and C_{ij}) can be derived with the results shown in Table I.

Table I Transformation Equations of Q_{ij}

	Constant	cos 2θ	sin 2θ	cos 4θ	sin 4θ
Q_{11}'	U_1	U_2	$2U_6$	U_3	U_7
Q_{22}'	U_1	$-U_2$	$-2U_6$	U_3	U_7
Q_{12}'	U_4	0	0	$-U_3$	$-U_7$
Q_{66}'	U_5	0	0	$-U_3$	$-U_7$
$2Q_{16}'$	0	$2U_6$	$-U_2$	$2U_7$	$-2U_3$
$2Q_{26}'$	0	$2U_6$	$-U_2$	$-2U_7$	$2U_3$

where
$$
\begin{aligned}
U_1 &= (3Q_{11} + 3Q_{22} + 2Q_{12} + 4Q_{66})/8 \\
U_2 &= (Q_{11} - Q_{22})/2 \\
U_3 &= (Q_{11} + Q_{22} - 2Q_{12} - 4Q_{66})/8 \\
U_4 &= (Q_{11} + Q_{22} + 6Q_{12} - 4Q_{66})/8 \\
U_5 &= (Q_{11} + Q_{22} - 2Q_{12} + 4Q_{66})/8 \\
U_6 &= (Q_{16} + Q_{26})/2 \\
U_7 &= (Q_{16} - Q_{26})/2
\end{aligned}
\tag{12}
$$

From Table I and Equation (12), the following two invariants can be established by observation:

$$
\begin{aligned}
I_1 &= Q_{11}' + Q_{22}' + 2Q_{12}' \\
&= 2(U_1 + U_4) \\
&= Q_{11} + Q_{22} + 2Q_{12} \\
I_2 &= Q_{66}' - Q_{12}' \\
&= U_5 - U_4 \\
&= Q_{66} - Q_{12}
\end{aligned}
\tag{13}
$$

By combining Equations (12) and (13), we can show that among the U's:

$$
\begin{aligned}
U_1 &= (3I_1 + 4I_2)/8 \\
U_4 &= (I_1 - 4I_2)/8 \\
U_5 &= (I_1 + 4I_2)/8
\end{aligned}
\tag{14}
$$

are invariant as expected because they are the constant terms in Table I. But only two of them are independent because

$$U_5 = (U_1 - U_4)/2 \tag{15}$$

U_2, U_3, U_6, and U_7, on the other hand, are not invariant.

If Q_{ij} is orthotropic,

$$Q_{16} = Q_{26} = 0$$

from Equation (12), we see that

$$U_6 = U_7 = 0 .$$

If Q_{ij} is isotropic,

$$\begin{aligned} Q_{11} &= Q_{22} \\ Q_{66} &= (Q_{11} - Q_{12})/2 \\ Q_{16} &= Q_{26} = 0 . \end{aligned} \tag{16}$$

From Equation (12), we see that

$$\begin{aligned} U_1 &= Q_{11} \\ U_4 &= Q_{12} \\ U_5 &= (Q_{11} - Q_{12})/2 = Q_{66} \\ U_2 &= U_3 = U_6 = U_7 = 0 . \end{aligned} \tag{17}$$

The components of Q_{ij} can be expressed in terms of engineering constants if and only if Q_{ij} is orthotropic:

$$\begin{aligned} Q_{11} &= E_{11} / (1 - \nu_{12}\nu_{21}) \\ Q_{22} &= E_{22} / (1 - \nu_{12}\nu_{21}) \\ Q_{12} &= \nu_{12} Q_{22} = \nu_{21} Q_{11} \\ Q_{66} &= G_{12} \end{aligned} \tag{18}$$

We have shown in this section the transformation equations of Q_{ij} in terms of multiple angles, and the meaning of the coefficients U_i.

Transformation of A, B, D Matrices

If a laminated composite consists of constituent layers of the same orthotropic material ($U_6 = U_7 = 0$) with arbitrary lamina orientations and thicknesses, the elastic moduli of the laminated composite A_{ij}, B_{ij} and D_{ij} from Equation (9) can be expressed, for example:

$$[A_{11}, B_{11}, D_{11}] = \int Q_{11} [1, z, z^2] \, dz \tag{19}$$

Since Q_{11} is a function z, i.e., it varies from layer to layer because of the varying lamina orientations. From Table I [where Q_{11} in Equation (19) is actually Q_{11}']:

$$Q_{11}' = U_1 + U_2 \cos 2\theta + U_3 \cos 4\theta \tag{20}$$

The transformation of Q_{11} consists of one constant plus two cyclic terms. If the same material is used in a laminated composite, say, boron-epoxy composite, U_1, U_2 and U_3 remain constant for all the layers. Equation (19) can be expanded, in terms of multiple angles, as follows:

$$\begin{aligned} [A_{11}, B_{11}, D_{11}] &= \int (U_1 [1, z, z^2] + U_2 \cos 2\theta [1, z, z^2] \\ &\quad + U_3 \cos 4\theta [1, z, z^2]) \, dz \\ &= U_1 [h, 0, h^3/12] + U_2 \int \cos 2\theta [1, z, z^2] \, dz \\ &\quad + U_3 \int \cos 4\theta [1, z, z^2] \, dz \end{aligned} \tag{21}$$

The same derivation can be applied to the other components of A_{ij}, B_{ij} and D_{ij}, and the final relations are summarized in Table II.

Table II A, B, D Matrices in terms of Lamina Properties

	$V_{0[A,B,D]}$	$V_{1[A,B,D]}$	$V_{2[A,B,D]}$	$V_{3[A,B,D]}$	$V_{4[A,B,D]}$
$[A_{11}, B_{11}, D_{11}]$	U_1	U_2	0	U_3	0
$[A_{22}, B_{22}, D_{22}]$	U_1	$-U_2$	0	U_3	0
$[A_{12}, B_{12}, D_{12}]$	U_4	0	0	$-U_3$	0
$[A_{66}, B_{66}, D_{66}]$	U_5	0	0	$-U_3$	0
$2[A_{16}, B_{16}, D_{16}]$	0	0	$-U_2$	0	$-2U_3$
$2[A_{26}, B_{26}, D_{26}]$	0	0	$-U_2$	0	$2U_3$

where the U_i are the same as those in Equation (13), and the $V_{i[A,B,D]}$ are defined as follow :

$$V_{0[A,B,D]} = [h,\ 0,\ h^3/12] \tag{22}$$

$$V_{1[A,B,D]} = \int \cos 2\theta\ [1,\ z,\ z^2]\ dz$$

$$V_{2[A,B,D]} = \int \sin 2\theta\ [1,\ z,\ z^2]\ dz$$

$$V_{3[A,B,D]} = \int \cos 4\theta\ [1,\ z,\ z^2]\ dz \tag{23}$$

$$V_{4[A,B,D]} = \int \sin 4\theta\ [1,\ z,\ z^2]\ dz$$

If the constituent layers are homogeneous, the integrals above can be replace by the following summations:

$$V_{iA} = \sum_{k=1}^{n} W_k (h_{k+1} - h_k)$$

$$V_{iB} = \frac{1}{2} \sum_{k=1}^{n} W_k (h_{k+1}^2 - h_k^2) \qquad (24)$$

$$V_{iD} = \frac{1}{3} \sum_{k=1}^{n} W_k (h_{k+1}^3 - h_k^3)$$

when $i = 1, \quad W_k = \cos 2\theta_k$

$= 2, \quad = \sin 2\theta_k$

$= 3, \quad = \cos 4\theta_k$

$= 4, \quad = \sin 4\theta_k$

where k is the index of summation and n, the number of layers. Table II is not a transformation relation as in Table I, although the appearance is very similar. Table II is an expression of Equation (9) in terms of multiple angles and is valid for a laminated composite consisting of layers of the same material, otherwise the U_i's cannot be taken out of the integral signs. The purpose of expressing A_{ij}, B_{ij}, and D_{ij} in this format is to aid the understanding of laminated composites which may not be as apparent by use of Equation (9). The derivation for the case of an anisotropic material (U_6, $U_7 \neq 0$) can be carried out in a similar fashion.

The transformation equations of A_{ij}, B_{ij} and D_{ij} can be derived by using the expressions in Table II. For example, the transformed A_{11}, i.e., A_{11}^1, can be obtained by rotating the entire laminated composite through an angle ϕ. This is accomplished by substituting $(\theta - \phi)$ for θ_k. Thus

$$A_{11}^1 = U_1 h + U_2 \int \cos 2(\theta - \phi)\, dz + U_3 \int \cos 4(\theta - \phi)\, dz \qquad (25)$$

Since Φ is constant for the entire laminated composite, thus, independent of z:

$$\begin{aligned} A_{11}' &= U_1 h + U_2 \cos 2\Phi \int \cos 2\theta\, dz + U_2 \sin 2\Phi \int \sin 2\theta\, dz \\ &\quad + U_3 \cos 4\Phi \int \cos 4\theta\, dz + U_3 \sin 4\Phi \int \sin 4\theta\, dz \\ &= U_1 h + U_2 V_{1A} \cos 2\Phi + U_2 V_{2A} \sin 2\Phi \\ &\quad + U_3 V_{3A} \cos 4\Phi + U_3 V_{4A} \sin 2\Phi \end{aligned} \tag{26}$$

where $V_{1A}, \ldots V_{4A}$ represent the integrals defined in Equation (23) or the summations in (24), and the subscript A signifies that a component of A_{ij} is being evaluated. Similar results can be obtained for the other components of A_{ij}'. The final transformation equations for A_{ij} can be shown in tabular form:

Table III Transformation Equations of A_{ij}

	Constant	$\cos 2\Phi$	$\sin 2\Phi$	$\cos 4\Phi$	$\sin 4\Phi$
A_{11}'	$U_1 V_{0A}$	$U_2 V_{1A}$	$U_2 V_{2A}$	$U_3 V_{3A}$	$U_3 V_{4A}$
A_{22}'	$U_1 V_{0A}$	$-U_2 V_{1A}$	$-U_2 V_{2A}$	$U_3 V_{3A}$	$U_3 V_{4A}$
A_{12}'	$U_4 V_{0A}$	0	0	$-U_3 V_{3A}$	$-U_3 V_{4A}$
A_{66}'	$U_5 V_{0A}$	0	0	$-U_3 V_{3A}$	$-U_3 V_{4A}$
$2A_{16}'$	0	$U_2 V_{2A}$	$-U_2 V_{1A}$	$2U_3 V_{4A}$	$-2U_3 V_{3A}$
$2A_{26}'$	0	$U_2 V_{2A}$	$-U_2 V_{1A}$	$-2U_3 V_{4A}$	$2U_3 V_{3A}$

The transformation equations for B_{ij} and D_{ij} are the same as those shown in Table III except the V_{iA} must be replaced by V_{iB} and V_{iD}, respectively, where i = 0, 1, 2, 3, 4. Comparing Tables I and III, in conjunction with Table II, the corresponding transformation relations are identical. U_6 and U_7 do not appear in Table III because we are investigating the case of Q_{ij} being orthotropic. Thus A_{ij} transforms the same as Q_{ij}. Similarly, it can be shown that B_{ij} and D_{ij} also transforms like Q_{ij}. The transformation is needed for establishing the material symmetries like orthotropy, isotropy, etc., and the invariants of this transformation. From Tables II and III and Equation (14), the following invariants exist:

$$P_1 = A_{11} + A_{22} + 2A_{12} = L_1 h = (Q_{11} + Q_{22} + 2Q_{12})\, h$$

$$P_2 = A_{66} - A_{12} = L_2 h = (Q_{66} - Q_{12})\, h \tag{27}$$

Similarly, invariants for B_{ij} and D_{ij} are:

$$P_3 = B_{11} + B_{22} + 2B_{12} = 0$$

$$P_4 = B_{66} - B_{12} = 0$$

$$P_5 = D_{11} + D_{22} + 2D_{12} = L_1 h^3/12 = P_1 h^2/12 \tag{28}$$

$$P_6 = D_{66} - D_{12} = L_2 h^3/12 = P_2 h^2/12$$

There are several features of the invariants above.

(a) The invariants for the A and D matrices are the same as those for the Q matrix except for correction factors involving the thickness h.

(b) The invariants of the A, B and D matrices impose definite limits on the variability of their components. If A_{11} and A_{22} are selected to meet certain loading requirements, we no longer have any freedom in specifying A_{12} and A_{66} because of invariants P_1 and P_2. A similar statement can be made about the D matrix.

(c) When $B_{11} + B_{22} = 0$, which occurs in a cross-ply composite[3] we know immediately from invariants P_3 and P_4 that

$$B_{12} = B_{66} = 0.$$

Thus, in a lamina optimization procedure of a given material, say, a boron-epoxy composite, the range of variability of the elastic properties is predetermined. As shown in Table II, each of the six independent components of the A, B, D matrices is governed by a constant term, which is not affected by lamina orientation, and variable terms expressed by $V_{i[A, B, D]}$ in Equations (23) and (24).

Special Properties of Laminated Composites

We will examine a number of special laminated composites and hope to shed light on the nature of $V_{i[A, B, D]}$, in this section. Since the limits of integration are $\pm h/2$, integration of an odd function (antisymmetric function with respect to $z = 0$) will be zero; that of an even function, not zero. Let us examine the following cases:

(a) If θ is an odd function of z, which may be represented by a 2-layer angle-ply with $\pm \theta$ orientation shown in Figure 1a, the following integrands are odd:

$$\cos p\theta\,[z] \qquad \sin p\theta\,[1, z^2]\ .$$

The following integrands are even:

$$\cos p\theta\,[1, z^2] \qquad \sin p\theta\,[z]$$

where $p = 2$ or 4.

Thus, the following integrals among those in Equation (23) vanish:

$$V_{1B} = V_{3B} = V_{2A} = V_{2D} = V_{4A} = V_{4D} = 0\ . \tag{29}$$

From Table II:

$$\begin{aligned} A_{16} &= A_{26} = 0 \\ B_{11} &= B_{22} = B_{12} = B_{66} = 0 \\ D_{16} &= D_{26} = 0 \end{aligned} \tag{30}$$

Hence, A_{ij} and D_{ij} are orthotropic.

(b) If θ is an even function of z, which is known as a symmetric laminate and may be represented by Figure 1b, the following integrands are odd:

$$\cos p\theta\ [z] \qquad \sin p\theta\ [z]$$

The following integrands are even:

$$\cos p\theta\ [1,\ z^2] \qquad \sin p\theta\ [1,\ z^2]$$

Thus, the following integrals among those in Equation (23) vanish:

$$V_{1B} = V_{2B} = V_{3B} = V_{4B} = 0 \tag{31}$$

From Table II:

$$B_{ij} = 0 \tag{32}$$

which means that there is no coupling between bending and extension in the laminated composite. And A_{ij} and D_{ij} are, in general, anisotropic.

(c) Let θ be a random function of z, i.e., layers are randomly oriented, as shown in Figure 1c, and defined $\bar{V}_i$ as the average value:

$$\bar{V}_i = \frac{1}{\pi} \int_{-\pi/2}^{\pi/2} V_i \, d\theta$$

$$= \frac{1}{\pi} \int_{-\pi/2}^{\pi/2} \int_{-h/2}^{h/2} \begin{pmatrix} \cos p\theta \\ \sin p\theta \end{pmatrix} [1,\ z,\ z^2]\ dz\ d\theta \tag{33}$$

where p is even. We have dropped the second subscript in $V_{i[A,\,B,\,D]}$ since it is immaterial here. Interchanging the order of integration, we get

$$\bar{V}_i = \frac{1}{\pi} \int_{-h/2}^{h/2} \int_{-\pi/2}^{\pi/2} \begin{pmatrix} \cos p\theta \\ \sin p\theta \end{pmatrix} d\theta\ [1,\ z,\ z^2]\ dz \tag{34}$$

$$= 0$$

Thus, for random orientation of the constituent layers, all the $\bar{V}_i$ with the exception of the constant terms in Table II will vanish. The laminated composite becomes isotropic, since

$$A_{11} = A_{22} = U_1 h$$

$$A_{12} = U_4 h \qquad (35)$$

$$A_{66} = U_5 h$$

$$A_{16} = A_{26} = 0$$

and from the above and Equation (15)

$$A_{11} - A_{12} = 2A_{66} \qquad (36)$$

which satisfies the condition of isotropy of A_{ij}. The isotropy of A_{ij} only implies that the moduli of a laminated composite are isotropic. The stress distribution, however, is not the same as that in a homogeneous, isotropic body. Similarly it can be shown that

$$B_{ij} = 0$$
$$D_{ij} = A_{ij} h^2/12 \qquad (37)$$

Thus D_{ij} is also isotropic. The laminated composite satisfies the condition of homogeneity as well, although the stress distribution is different from that in a homogeneous material.

(d) If a laminated composite has n equal layers ($n > 2$) and the orientation of layers are at increment of π/n, the integral V_{1A} may be expressed as

$$V_{1A} = (\cos 2\pi/n + \cos 4\pi/n + \ldots \cos 2\pi)\, h/n \qquad (38)$$

From Pierce's table (4th Edition), formula (639):

$$\cos x + \cos 2x \ldots + \cos nx = \frac{\sin (n + \frac{1}{2}) x}{2 \sin \frac{1}{2} x} - \frac{1}{2} \qquad (39)$$

For $x = 2\pi/n$

$$V_{1A} = 1/2 - 1/2 = 0$$

Similarly, from Pierce, Formula (637),

$$\sin x + \sin 2x \ldots + \sin n x = \frac{\sin \frac{1+n}{2} x \sin \frac{n}{2} x}{\sin \frac{x}{2}} \qquad (40)$$

For $x = 2\pi/n$

$$V_{3A} = 0$$

Using Equation (39) and (40), we can show for $x = 4\pi/n$:

$$V_{2A} = V_{4A} = 0$$

Since V_{iA} vanish for this type of laminated composite, A_{ij} is isotropic. The same relations as those in Equations (35) and (36) are obtained. This, of course, is the well-known result of the in-plane quasi-isotropic composites where the lamina orientations are: (-60) - 0 - 60, (-90) - (-45) - 0 - 45, etc., shown in Figures 1d and 1e. B_{ij} and D_{ij} can be made quasi-isotropic by more complex stacking sequences than that for A_{ij}.

Finally, the area under the A_{ij}' versus ϕ curve from $\phi = 0$ to $\phi = 2\pi$ can be obtained by the integration of the transformation equations listed in Table III. Since,

$$\int_0^{2\pi} \begin{pmatrix} \cos p\phi \\ \sin p\phi \end{pmatrix} d\phi = 0 \qquad (41)$$

where p is even, only the constant terms remain. Thus the areas under the A_{ij}' are constant and the average numerical values are the isotropic constants in Equation (35) for the randomly oriented lamina composites and those quasi-isotropic laminates described in the previous subsection. This leads to the conclusion that the invariant properties of constants U_1 and U_5, U_4 being dependent on U_1 and U_5, may constitute a measure of the performance of an orthotropic material. Lamina orientation variations only change the shape of the A_{ij}' curve

as ϕ varies but the area under the curve remains constant. We can also conclude that the area under the $B^{\prime}_{ij}$ curve is zero and that under $D^{\prime}_{ij}$, constant.

Invariant Properties

We have shown that the elastic properties of a unidirectional composite are strongly influenced by two independent invariants,

$$U_1 = (3Q_{11} + 3Q_{22} + 2Q_{12} + 4Q_{66})/8 \tag{42}$$

$$U_5 = (Q_{11} + Q_{22} - 2Q_{12} + 4Q_{66})/8 \tag{43}$$

For laminated composites, the same invariants exist, except that corrections for thickness of h and $h^3/12$ must be applied for the A and D matrices, respectively. The invariants for B_{ij} are identically zero, as shown in Equation (28).

If the material is isotropic, the resulting relations shown in Equation (17) are:

$$U_1 = Q_{11}, \qquad U_5 = Q_{66} \tag{44}$$

Because U_1 and U_5 reduce to the stiffness and shear rigidity of an isotropic material, we shall designate U_1 and U_5 defined in Equations (42) and (43) as the isotropic stiffness and isotropic shear rigidity, respectively. These isotropic properties, which are specific combinations of orthotropic properties, represent a realistic measure of the stiffness capability of composite materials, which can be compared directly with isotropic materials. This measure of stiffness is different from the common practice of comparing the longitudinal stiffness Q_{11} with isotropic materials. Although Q_{11} for many modern composites can be several times higher than light-weight metals on the weight basis, this is not a fair comparison because the weakness of most composites in transverse stiffness and shear rigidity is ignored.

In addition to a realistic basis of comparison with isotropic materials, the proposed use of invariant or isotropic properties may lead to a better understanding of the variability of lamina optimization of composite materials. If we start initially with a unidirectional composite, for which

$$A_{ij} = Q_{ij} h$$

any change in fiber orientation of some layers within the same composite will change A_{ij} according to Table II. These changes are governed by the integrals V_1, V_2, V_3 and V_4, while V_0, being the isotropic constants, remains invariant. The V's dictate the magnitude of the variability in the elastic properties of a laminated composite and the variation oscillates above or below the isotropic constants. Since the absolute value of sine and cosine functions are bounded between 0 and 1, the variability of the V's are also bounded.

The concept of invariant properties may simplify lamina optimization process. Structural optimization should begin with the isotropic constants. They should represent the minimum stiffness of composite materials. Any lamina design that falls below the performance of that based on isotropic constants should be automatically rejected.

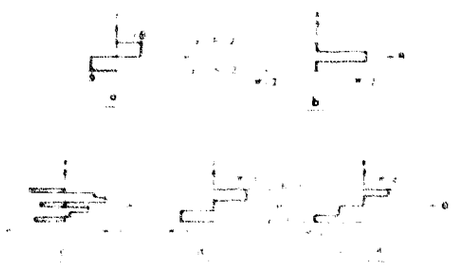

Figure 1 Examples of Lamina Orientations

Figure 2 shows the transformation relations of A_{11} for various boron-epoxy composites, using the following data:

$$\begin{aligned} Q_{11} &= 40 \times 10^6 \text{ psi} \\ Q_{22} &= 4 \times 10^6 \text{ psi} \\ Q_{12} &= 1.0 \times 10^6 \text{ psi} \\ Q_{66} &= 1.5 \times 10^6 \text{ psi} \end{aligned} \qquad (45)$$

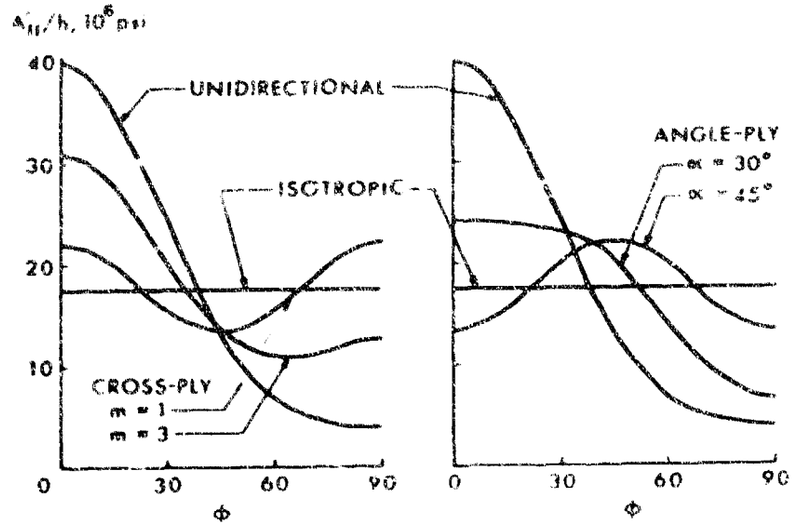

Figure 2 A'_{ij}/h for Various Boron-Epoxy Laminated Composites

The unidirectional and isotropic composites are shown in both diagrams. On the left diagram, two cross-ply composites with cross-ply ratio m equal to 1 and 3 are also shown. Cross-ply ratio is the ratio of the thickness of the 0° to 90° layers. On the right diagram, two angle-ply composites with helical angle α equal to 30° and 45°. Angle-ply composites consist of equal numbers of layers oriented $+\alpha$ and $-\alpha$. These diagrams illustrate that the areas under all the A'_{11} curves are the same. If a cross-ply with m = 1 is combined with an angle-ply with α = 45°, the resulting composite is isotropic. This agrees with the conclusion of the previous section and is shown in Figure 1e. All the cross-ply composites have the same value at Φ = 45°. This can be shown from the transformation equation. Finally, it can be seen when the number of lamina orientations increases, the resulting laminated composite will very rapidly approach the isotropic state. It appears to be a more effective method for the lamina optimization program to begin from the isotropic laminate than to begin with the unidirectional composites.

It may be useful to determine approximately the numerical values for the invariant properties represented by Equations (42) and (43). We will define

$$U_1 = \overline{E}, \qquad U_5 = \overline{G} \tag{46}$$

For highly orthotropic composites like glass-epoxy and boron-epoxy composites

$$Q_{11} \tilde{=} E_{11}, \qquad Q_{22} \tilde{=} E_{22} \tag{47}$$

because the minor Poisson's ratio ν_{21} is usually less than 0.1. If ν_{12} is .3, $1 - \nu_{12}\,\nu_{21} > .97$. The approximation of Equation (47) introduces an error less than 3 percent. From elasticity solutions by Adams and Doner on longitudinal shear[7] and transverse loading[8] of a unidirectional composite,

$$Q_{66}/G_m = G_{12}/G_m = F_1\,(G_f/G_m,\ \nu_f) \tag{48}$$

$$Q_{22}/E_m = E_{22}/E_m = F_2\,(E_f/E_m,\ \nu_f) \tag{49}$$

functional relations F_1 and F_2 are approximately the same which can be shown by comparing Figure 5 of (7) with Figure 4 of (8). For a fiber volume of 70 percent or less, the error introduced by letting

$$F_1 = F_2 \tag{50}$$

is 10 percent or less. Since

$$G_m = E_m/2\,(1 + \nu_m) \tag{51}$$

we obtain, for $\nu_m = 0.33$, from Equations (48) and (49)

$$Q_{66} = G_{12} = E_{22}/2.66 \tag{52}$$

Hence, if we substitute

$$\begin{aligned} Q_{11} &= E_{11}, \quad Q_{22} = E_{22} \\ Q_{12} &= \nu_{12}\,Q_{22} = .25\,E_{22} \\ Q_{66} &= G_{12} = E_{22}/2.66 \end{aligned} \tag{53}$$

into Equations (42) and (43), we obtain approximately:

$$\text{Isotropic Stiffness} = \overline{E} = \frac{3}{8} E_{11} + \frac{5}{8} E_{22} \tag{54}$$

$$\text{Isotropic Shear Rigidity} = \overline{G} = \frac{1}{8} E_{11} + \frac{1}{4} E_{22} \tag{55}$$

These approximate equations are simple to use and give reasonable values to represent the invariant properties. For boron-epoxy composites,

$$\begin{aligned} E_{11} &= 40 \times 10^6 \text{ psi} \\ E_{22} &= 4 \times 10^6 \text{ psi} \\ \nu_{12} &= .25 \\ G_{12} &= 1.5 \times 10^6 \text{ psi} \end{aligned} \tag{56}$$

A comparison of the laminated composites analysis[3] with the approximate relations above are:

	$\overline{E}$	$\overline{G}$
Method of Reference 3	16×10^6 psi	5.9×10^6 psi
Approx. (Eq. 54 and 55)	17.5×10^6 psi	6.0×10^6 psi
Error	8%	1%

Cox[5] derived isotropic constants for randomly oriented fiberous composites as

$$\overline{E} = E_{11}/3, \qquad \overline{G} = E_{11}/8 \tag{57}$$

These values are lower than those of Equations (54) and (55). Loewenstein[9] also showed the 3/8 factor for in-plane random orientation (the transverse stiffness is taken to be zero). Bishop[10] also derived a theory which has results similar to that reported by Loewenstein[9]. Both References 9 and 10 may be considered as having

$$Q_{22} = Q_{12} = Q_{66} = 0 \tag{58}$$

The conditions implied by this equation, however, are not reasonable for modern fiber-reinforced composites. The transverse and shear moduli are significant quantities in determining the elastic behavior of composite materials.

An approximate estimate of the performance of fiber-reinforced composite is shown in terms of invariant properties in Figure 3. The normalized $\overline{E}$ and $\overline{G}$ are derived from Equation (54):

$$\overline{E}/E_m = \frac{3}{8}\left(E_{11}/E_m\right) + \frac{5}{8}\left(E_{22}/E_m\right) \tag{59}$$

$$= \frac{3}{8}\left[(1-v_f) + v_f E_f/E_m\right] + \frac{5}{8} F_2$$

where, the rule-of-mixtures equations is used:

$$E_{11} = (1-v_f)E_m + v_f E_f \tag{60}$$

and F_2 is expressed in Equation (49), the numerical values of which are obtained from Reference 8. From Equation (55),

$$\overline{G}/G_m = \frac{2.66}{8}\left[(1-v_f) + v_f E_f/E_m\right] + \frac{5.32}{8} F_2 \tag{61}$$

where Equation (51) is used with $v_m = 0.33$. Comparing Equations (59) and (61), we notice that for E_f/E_m of values between 6 and 120,

$$\overline{E}/E_m \cong \overline{G}/G_m \tag{62}$$

Figure 3 shows the normalized $\overline{E}$ and $\overline{G}$ for fiber-reinforced composites with $v_f = 70$ and 40 percent. For convenience, absolute units for $\overline{E}$ are also shown for boron-aluminum, glass-epoxy, and boron-epoxy composites. Figure 3 represents the minimum capabilities of the composite materials; the advantage of designed anisotropy to meet a specific loading condition has not been claimed.

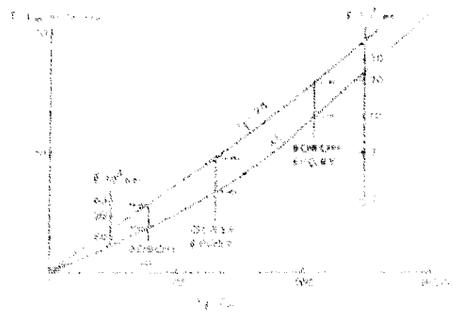

Figure 3 Isotropic Constants of Fiber-Reinforced Composites

Summary

We have shown that the transformation equations of tensors can be expressed in multiple angles instead of the usual powers of sines and cosines. In the multiple angle representation, the transformation properties consist of invariant terms, which correspond to the isotropic constants, and cyclic terms, which control the variation and directionality of properties due to anisotropy. The transformation equations for two-dimensional layers (Q_{ij}) and the laminated composites A_{ij}, B_{ij} and D_{ij} can be readily derived.

The elastic properties of laminated composites as functions of lamina orientation is shown in Table II. The components of A_{ij}, B_{ij} and D_{ij} are governed by invariant terms, plus variable terms in terms of integrals V_i. It is proposed that isotropic properties for anisotropic materials be used as a measure of the minimum stiffness capability. They may be considered intrinsic properties of the material because they are independent of the lamina orientations and can thus represent the capability of a given anisotropic material in all forms of lamination including the unidirectional case. Direct comparisons of the stiffness represented by $\overline{E}$ and $\overline{G}$ with isotropic materials appear to be more realistic than the use of the longitudinal stiffness of unidirectional composites. Approximate expressions for these isotropic constants are shown in Equations (54) and (55), and their numerical results, in Figure 5. The results may be helpful in systems application of composite materials. The relative merits of controllable variables like E_f/E_m and v_f can be determined directly from Figure 5 which should be of value to materials engineers.

Finally, the basis of lamina optimization may be more easily carried out and better understood by the multiple-angle relations than the conventional treatment. The degree of variability can be determined from the values of the integrals V_i. If anisotropy is to be beneficial for a given loading condition, the performance of the composite should in all cases exceed that of the isotropic laminate. Thus optimization should begin with the isotropic constants. The isotropic constants, the integrals V_i and the invariants U_i should be considered as additional constraints

to lamina optimization procedures. For practical design, the numberof lamina orientations in a laminated composite may be kept to, say, no more than 4 orientations. The variation of the properties may be more effectively controlled through the lamina thickness than the orientation. The reduction in lamina orientations may introduce immediate simplification in structural analysis, design procedures and automated fabrication techniques of laminated composites. The present concept may lead to an optimum design based on strain energy from which desired anisotropy in a composite material may be determined. A similar approach to the problem of strength seems possible.

Nomenclature

A_{ij}, B_{ij}, D_{ij}	Elastic constants of laminated composites, Equation (19).
C_{ij}	Elastic stiffness matrix of 3-dimensional bodies.
Q_{ij}	Reduced stiffness matrix for bodies under plane stress.
I_1, I_2	Invariants of Q_{ij}.
$U_1, \ldots U_7$	Coefficients of transformation equations in Table I, defined by Equation (14).
V_0	Isotropic constants for A_{ij}, B_{ij} and D_{ij} defined by Equation (22).
$V_1, \ldots V_4$	Integrals defined by Equation (23).
N_i	Stress resultants.
M_i	Stress couples.
k_i	Components of curvature.
m	$\sin^2\theta$, or cross-ply ratio which is the ratio between the thickness of 0° and 90° layers in a cross-ply composite.
n	$\sin\theta$, or number of layers in Equations (38) to (40).
h	Total thickness of laminated composites.
E	Young's modulus.
G	Shear modulus.

T	Temperature.
v	Volume fractions.
α_i	Thermal expansion coefficients.
ϵ_i	Strain components.
σ_i	Stress components.
ν	Poisson's ratio.
θ, ϕ	Angles of rotation.
subscript f	Pertaining to fibers.
subscript m	Pertaining to matrix.
bar	Average quantities or isotropic constants.
prime	Transformed component.

References

1. Reissner, E. and Y. Stavsky. "Bending and stretching of certain types of heterogeneous aeolotropic elastic plates," J. Appl. Mech., 28, 402 (1961).

2. Dong, S. B., K. S. Pister and R. L. Taylor, "On the theory of laminated anisotropic shells and plates," J. Aero. Sci., 28, 969 (1962).

3. Tsai, S. W. "Strength characteristics of composite materials," NASA report CR-224 (1965).

4. Tsai, S. W. "Introduction to mechanics of composite materials, Part II - Theoretical aspects," Air Force Materials Laboratory Report, AFML-TR-66-149 (1966).

5. Hearmon, R. F. S. An Introduction of Applied Anisotropic Elasticity, Oxford (1961).

6. Cox, H. L. "The elasticity and strength of paper and other fibrous materials," Brit. J. Appl. Phys., 3, 72 (1952).

7. Adams, D. F. and D. R. Doner, "Longitudinal shear loading of a unidirectional composite," J. Comp. Mat., 1, [illegible] (1967).

8. Adams, D. F. and D. R. Doner, "Transverse [illegible] loading of a unidirectional composite," J. Comp. Mat., 1, [illegible] (1967).

9. Loewenstein, K. L. "Glass sytems," Chapter V, Composite Materials, L. Holliday, Ed., Elsevier (1966).

10. Bishop, P. H. H. "An improved method for predicting mechanical properties of fibre composite materials," Royal Aircrafts Establishment, RAE Technical Report No. 66245 (1966).

IV. PHYSICS AND CHEMISTRY (L. E. Nielsen and A. T. DiBenedetto)

The major effort of the Physics and Chemistry group has been directed toward developing an understanding of the effects of interaction between a filler and an organic matrix on the mechanical behavior and environmental stability of composite materials. Our primary objectives may be listed as follows:

1. To discover the mode and extent of interaction between phases and to determine the effects of interaction on physical properties.
2. To examine the mechanism and quantify the variables for crack propagation and catastrophic failure.
3. To examine the effects of voids and other structural defects on the properties.
4. To investigate the environmental stability of composites.
5. To determine the effects of filler aggregation, shape and orientation on the properties of filled systems.

Investigations made to date have been on "prototype" organic resins and glass fillers. However, with appropriate fabrication and measurement techniques developed and basic concepts confirmed, emphasis will be shifted to the study of the properties of composites with boron, graphite, and whisker reinforcement.

Fatigue, Fracture and Mechanical Behavior

Considerable effort has gone into developing composites that exhibit improved mechanical response and into developing an understanding of fracture phenomena in composites.

Many of our projects in fracture are relying heavily on the use of the electron scanning microscope to elucidate some of the details of the fracture process. Throughout this report you will see many examples of the usefulness of this tool. In this section, Mr. J. L. Fatring presents a review paper summarizing the use of the electron scanning microscope and its pertinence to fracture mechanics.

A great deal of progress has been made in understanding the behavior of thick elastic interface composites. Drs. A. S. Kenyon and R. J. Slocombe have developed techniques for applying silane coupling agents, flexible innerlayer resins and rigid outlayer resin coatings to glass beads and chopped glass fibers. Experimental data show that improved physical properties are directly related to improved adhesion and presence of the flexible innerlayer. Electron scanning microscopy techniques are used to show the improved adhesion between phases due to specific coupling agents and to show the changes in fracture mechanism caused by this adhesion.

The polyelectrolyte work conducted by Drs. L. E. Nielsen and J. E. Fields has been an attempt to produce a high modulus, high temperature-resistant matrix by forming ionically bonded metal salts with an organic polymer. The primary emphasis has been on reacting polyacrylic acid with a zinc oxide powder and filling the resulting matrix with aluminum flake, iron flake, lead powder and boron filaments. Composite shear moduli up to $1.5 - 1.7 \times 10^6$ psi at 300° C, compression strengths approaching 60,000 psi, and thermal expansion coefficients of roughly 1/5 to 1/10 of normal organic polymers (in the range of some metals) are attainable. Application of this work to the fabrication of useful shapes is discussed in the Fabrication Section.

The fracture characteristics of edge-notched composite sheets have been investigated by Messrs. A. D. Wambach and K. L. Trachte. They have shown that at low loadings the fracture toughness of a particulate reinforced composite material may be significantly lowered by an improvement in adhesion between phases. Electron microscopy is used to show that this decrease in fracture toughness is associated with a change in the mechanism of crack propagation in the composite.

Recognizing the extreme importance of water permeation in composites to the mechanical behavior, Dr. E. Peyser has been concerned with improving and applying the tritium-based technique (reported last year) for accurately measuring relative rates of diffusion of water through an epoxy resin and along

a glass-epoxy interface. In the absence of detectable cracks and voids, it appears that in contrast to work reported by others, silane treatments decrease the rate of diffusion of water along the interface.

Peyser's work emphasizes again the need for accurate measurement of the defect content in composites. Some recent results (premature for coverage by a paper in this report) of the Washington University group lead us to believe that the measurement of internal pressure above the glass transition temperature of the polymer is a very sensitive means of detecting voids in the concentration range of 0.10% void content and less. This may be a very simple and very reliable way of detecting structural soundness of thermoplastics, B-staged resins, and lightly crosslinked structures.

Interactions, Aggregates and Networks

Dr. T. B. Lewis has studied the effects of inter-particle forces and particle size on the mechanical properties of composites. The initial work was conducted on a system of Aroclor (chlorinated biphenyl) filled with glass beads. Measurements were made on dispersed systems, in which filler particle interactions were negligible, on agglomerated systems, in which there were weak cohesive forces between particles in an agglomerate, and on aggregated systems, in which there were strong cohesive forces between particles in an aggregate. He found that spheres of uniform size, distributions of sphere sizes and aggregates of sintered spheres can be described by the Mooney equation for the viscosity of suspensions. He also found that suspensions of aggregates become non-Newtonian at lower volume fractions than do suspensions of uniform spheres, and that agglomerates held together by weak forces act more like uniform dispersed spheres than they do like strong aggregates.

This is the first time that the effects of strong aggregates have been clearly shown. The work is continuing in order to measure the elastic moduli of similar rigid filled systems to determine if the ratio of viscosities is equal to the ratio of moduli. This will be followed by the measurement of elastic moduli for discontinuous fibrous systems with a similar range of inter-particle forces.

In a closely related project, D. Droste has been studying the effects of filler-matrix interactions on the thermodynamic and mechanical properties of filled thermoplastics. An increase in glass transition temperature with increasing filler concentration for phenoxy-attapulgite composites and Epon 1031-attapulgite composites indicates a change in the polymer matrix because of the presence of the filler.

Torsion pendulum data on the phenoxy-attapulgite composites confirm the shift in glass transitions observed by differential thermal analysis. Changes in the loss moduli and damping capacities with increasing filler concentration over the whole temperature range studied indicate that the filler particles are influencing the rheologic properties of the polymer phase.

Mr. J. R. Joseph has completed his Master's thesis entitled, "The Growth, Morphology and Reinforcement Potential of Low Molecular Weight Crystals in Amorphous Polymeric Media." A rigid amorphous polymer (styrene-acrylonitrile copolymer) and low molecular weight compounds (acetanilide and anthracene) soluble in the polymer at fabrication temperature and crystallizing out of the viscous melt at lower temperatures was employed as a prototype system. In general, Joseph has shown that in-situ growth of low molecular weight crystals in polymers is a feasible technique for fabricating composite materials as long as certain compatibility requirements are satisfied. Since the morphology of the precipitated phase is strongly dependent on crystallization rate and temperature, this technique may also be a powerful tool for studying the effects of filler shape and orientation on the properties of composites.

Future Emphasis

Summarizing, the Physics and Chemistry group is interested in the interaction of constituent materials on the microscopic and submicroscopic scale. The mechanisms of deformation and fracture in composites, the nature of the interface, and the characterization of the constituent materials are some of the important problems.

What we do in the future depends to a great extent on the outcome of our present projects. Based on what we know now, however, the following problems will be considered.

1. An effort will be made to study the relation of mechanical properties to the morphology of the filler. Work on spheres and fibers will be extended to flakes, mats, interlocking networks and complex dendritic shapes.
2. Work will be expanded in trying to relate the interfacial studies to problems in fracture mechanics. Our ability to do a wide variety of fractography experiments will be utilized to its maximum on a wide variety of composite systems.
3. Environmental stability and material reliability will be investigated to a greater extent. The effects of water and oil environments are of special concern in organic matrix composites.
4. In the near future we will probably want to investigate transport properties. It is very likely that the detailed nature of the interaction between phases and the presence of voids and other structural defects affect volume resistivity, thermal conductivity and the dielectric character of a composite. The use of these and other transport properties may possibly be valuable for non-destructively evaluating the soundness of a material.

FRACTOGRAPHY OF COMPOSITE MATERIALS WITH THE SCANNING ELECTRON MICROSCOPE (J. D. Fairing and W. J. Renaudette)

A vital part of any investigation of fracture mechanics in metals is the study of fracture surfaces with the electron transmission microscope[1,2]. It is difficult to find any literature on the subject that is not replete with excellent micrographs. Such is not the case in the field of composite materials. Fractographs of composites are seldom published for the simple reason that it has been virtually impossible to take meaningful pictures by existing techniques.

The exceedingly irregular topography of composite fracture surfaces restricts the use of the optical microscope with its inherent shallow depth of field to magnifications below 100, a value far too low for most studies. Although conventional electron transmission microscopes have the required depth of field

they cannot be used to examine a fracture surface directly without replication. Satisfactory replication is generally restricted to composites containing particulate fillers only as the tendency for composites reinforced with fibers is to yield fracture surfaces resembling a porcupine's back.

To study composite fracture surfaces successfully an instrument is required that will permit direct examination of the sample, without replication, at magnifications from less than 200 to well over 20,000 times, and that will provide a large depth of field at all magnifications. The varied nature of the surfaces encountered requires the examination of relatively large areas to avoid bias. Furthermore, it is desirable to be able to look at the surface from various angles. As a consequence of the required large depth of field, object planes will not be separated. Steroscopic viewing is required to avoid misinterpretation.

The Scanning Electron Microscope described by Smith[3] and Oatley[4, 5] satisfies the requirements for the study of composite materials fractography. In this instrument a beam of 20,000 volt electrons is focused to a spot 70 to 100 Å in diameter on the sample surface and is scanned over the surface in a raster of 1,000 to 2,500 lines. This primary beam causes the sample to emit secondary electrons with an average energy of 6 e.v., which are collected, amplified, and used to modulate a cathode ray tube scanning in synchronization with the primary beam. The ratio of the length of the scanning line on the CRT to that on the sample surface determines the magnification. The variation in the number of secondary electrons collected is a function of surface contour; as a consequence, the displayed image resembles the optical appearance of the surface.

The collected secondary current (s) may be expressed, to a first approximation, by equation (1)

$$s = \frac{K}{\alpha + \beta \sin \theta} \qquad (1)$$

where θ is the angle between the primary beam and the surface and "constants" K, α, and β are complex functions of the primary beam current and energy, sample secondary emission ratio, work function, average atomic number,

collector voltage and geometry, and other parameters. The relative change in collected secondary current with change in surface angle, and therefore, the change in brightness of the image on the CRT (that is, the image forming process) is given by equation (2).

$$\frac{\delta s}{s} = \frac{-\beta \operatorname{Cot} \theta}{\alpha + \beta \sin \theta} \delta\theta \qquad (2)$$

By making reasonable assumptions about the relative values of α and β (e.g. $\alpha \ll \beta$) equations (1) and (2) may be reduced to the simplified approximations given by Smith[3].

$$s = K \operatorname{Cosec} \theta$$

$$\frac{\delta s}{s} = -\operatorname{Cot} \theta \, \delta\theta \quad \text{for} \quad 20° \leq \theta \leq 40°$$

Although the image displayed by the scanning microscope closely resembles an optical one, there are points of difference, the most important being the appearance of a sharp edge. If an edge or a thin part of the sample is oriented to the electron beam and to the collector in such a way as to enable secondary electrons to emerge from both sides of the edge, excessive brightness will result and all detail will be lost in this bright area. It is this "edge effect" that causes the white line around many of the fibers in the pictures shown.

If the sample surface is not a conductor an electrical charge may accumulate resulting in loss of detail in mild cases, or complete obliteration of the image in severe ones. To obviate this, non-conducting surfaces are coated with a thin (200 to 400 Å) layer of vacuum deposited metal. Chromium has been used to coat all samples illustrated in this report; however, an alloy of 60% gold - 40% palladium has been employed successfully. The charging phenomenon is not clearly understood. We have, for example, found some apparently non-conducting areas in which charging was not evident. Studies are being conducted to clarify this point.

The applicability of the scanning electron microscope to composite fractography can be demonstrated readily by a comparison with an optical microscope. Figure 1 is an optical micrograph of a discontinuous glass fiber reinforced epoxy resin fracture surface, while Figure 2 is the same surface (but not necessarily

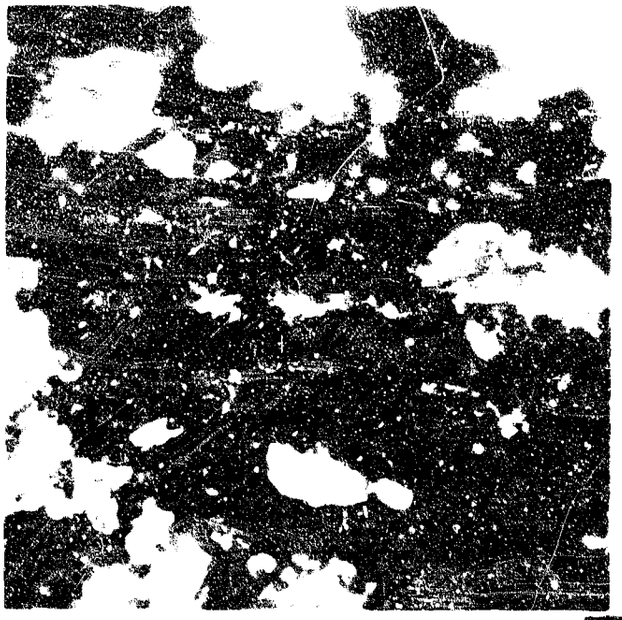

Figure 1 Optical Micrograph of Tensile Fracture Surface of Discontinuous Glass Fiber Reinforced Epoxy Resin, 175 X.

Figure 2 Tensile Fracture Surface of Discontinuous Glass Fiber Reinforced Epoxy Resin. Fibers had been Treated with a Parting Agent (SC-87) to Prevent Adhesion, 205 X.

the identical area) as photographed with the scanning microscope. The benefit accruing from the enormous depth of field is apparent. In this, as in all scanning micrographs presented in this report, the surface was inclined at 45° to the line of view.

Studies have been made of tensile fracture surfaces of epoxy matrix composites reinforced with beads (glass), discontinuous fibers (glass, boron, carbon, silicon carbide, and asbestos), and, to a limited extent, continuous fibers (glass, boron, and carbon). Since only limited observations have been made of continuous filament reinforcements, this report will cover discontinuous fibers and beads only.

Fracture surfaces show widely varying morphologies. However, there are present specific features which can be correlated with physical properties of composites and which indicate failure modes. A preliminary discussion of these features has been published[6].

In the majority of systems studied failure occurred at (or indistinguishably near) the matrix-reinforcement interface over a significant portion of the fracture surface. Such interfacial failure is indicative of poor bonding of the resin to the reinforcement and is characterized by a fracture surface containing large numbers of exposed denuded fibers as is shown in Figures 2 and 3. Concurrent with this is

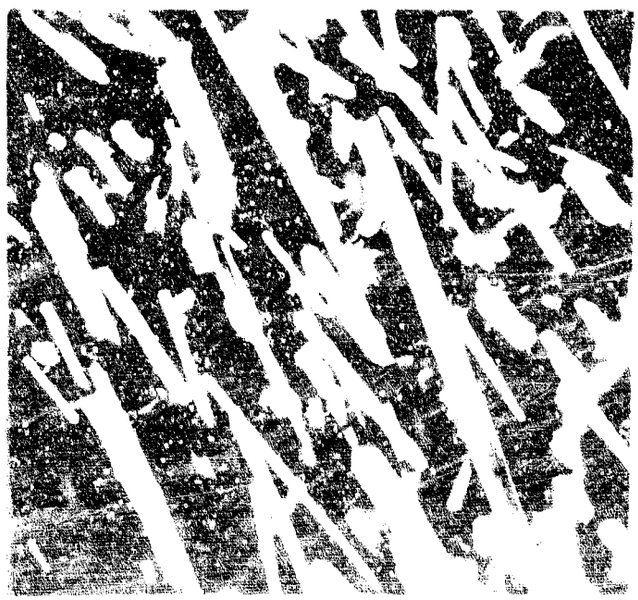

Figure 1. Tensile Fracture Surface of an Epoxy Resin Reinforced with Untreated Silicon Carbide Whiskers, 1,840 X.

the presence of clear "mold" marks in the matrix from which fibers have been removed without crossing cohesive matrix failure. These "molds" reproduce, in detail, the topography of the fiber surfaces: glass produces smooth molds (Figure 4), while boron, carbon, and silicon carbide leave the characteristic structure of their surfaces imprinted in the matrix.

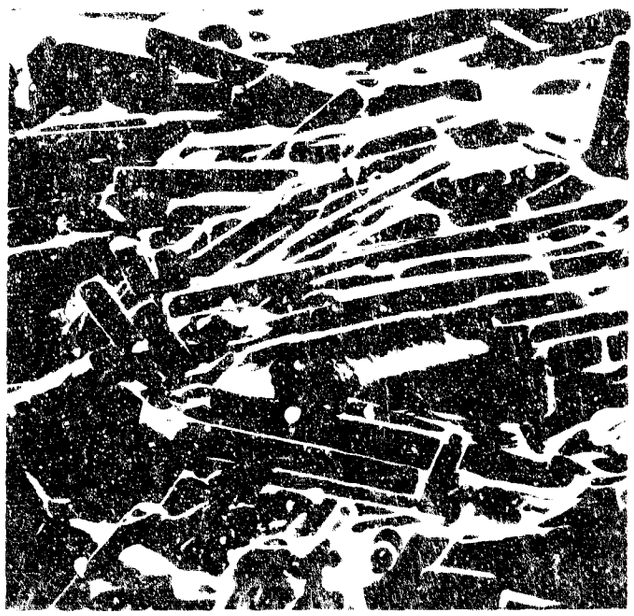

Figure 4 Tensile Fracture Surface of Discontinuous Glass Fiber Reinforced Epoxy Resin. Fibers had been Treated with a Parting Agent (SC-87) to Insure Poor Adhesion. Note Mold Marks Where Fibers have been Removed, 460 X.

The region at the intersection of fibers with the polymer fracture surface exhibits two distinctive features in composites lacking good adhesion: cracks between matrix and filler extending from the primary fracture surface along the interface between partially exposed filler and matrix, but not from this surface into the resin, and the absence of any deviation of the matrix fracture surface at its intersection with reinforcing fibers or molds. Figure 5 illustrates both of these points.

A strong bond between resin and reinforcement is indicated by the absence of extensive interfacial failures and by the rough surface displayed by even little retracted fiber, as shown in Figure 6; exposed portions of fibers are short and often have matrix adhering to them. Fractured fibers are rarely evident in such specimens, and there is frequently evidence of "wetting out" in the

Figure 5 Tensile Fracture Surface of an SC-87 Treated Discontinuous Glass Fiber Reinforced Epoxy Resin. Note Interfacial Crack Between Fiber and Resin, 2,000 X.

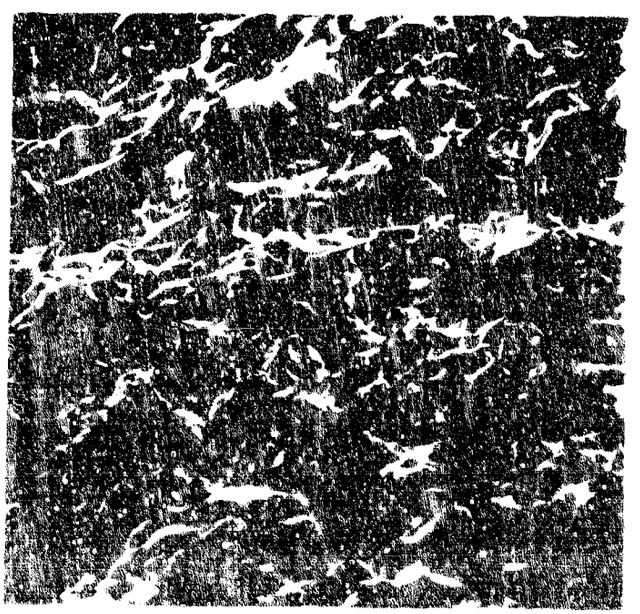

Figure 6 Tensile Fracture Surface of a Discontinuous Glass Fiber Reinforced Epoxy Resin Composite having Good Adhesion. The Fibers have been Coated with a Flexible Interlayer, 180 X.

matrix surrounding the fiber as illustrated in Figures 7, 8, 9 and 10. The width of this zone, as well as the frequency of its occurrance appears to increase with increasing bond strength and is clearly defined only in those systems characterized by good adhesion.

Figure 7 Tensile Fracture Surface of an Epoxy Composite Reinforced with Discontinuous Glass Fibers Coated with a Flexible Interlayer. Note Fractured Fiber and Zone of Influence in Matrix, 1,800 X.

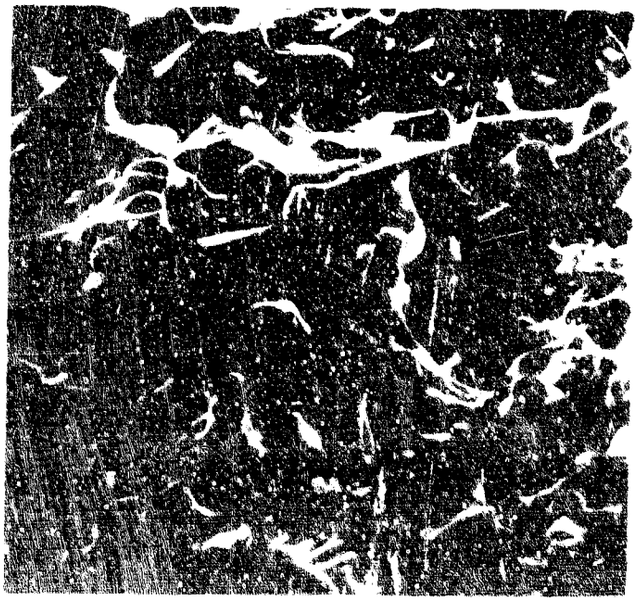

Figure 8 At Least Five Zones of Influence can be Seen in this Tensile Fracture Surface of an Epoxy Composite Containing Discontinuous Glass Fibers Coated with a Flexible Interlayer, 450 X.

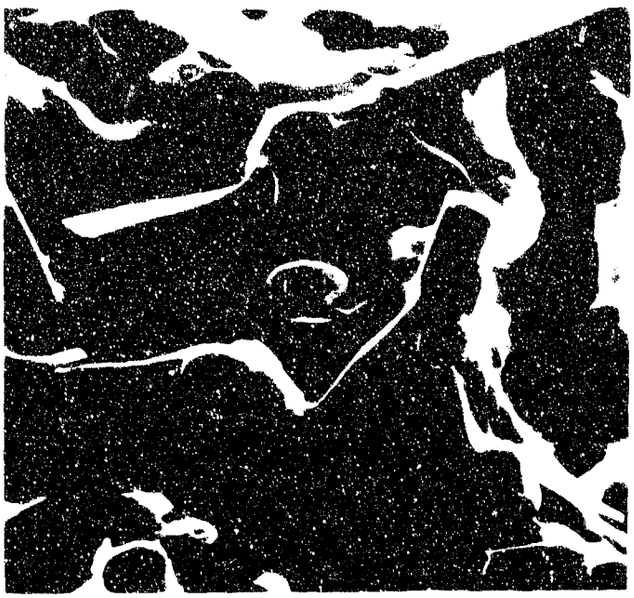

Figure 9 An Enclarged View of Figure 8, 900 X.

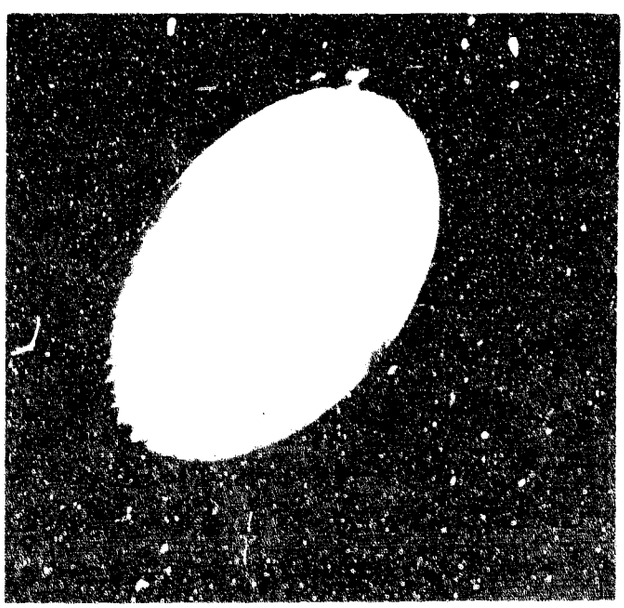

Figure 10 A Narrow Zone of Influence. The Fibers had been Treated with Y-1032, 1,000 X.

The strong interaction between reinforcement and matrix in a well bonded system causes the fracture to be displaced away from the reinforcing elements without exposing them, as demonstrated by Kenyon and Slocombe[7] for beads, or to intersect them at acute angles to their surface as depicted in Figures 11 and 12. Finally, the fracture surfaces of such samples exhibit many large and small secondary fractures or cracks in the matrix which are not seen when a weak interfacial bond exists.

Seldom, if ever, does any single surface display criteria of only good or only poor bonding; some indications of both types can be found, although one type generally predominates. Furthermore, not all listed characteristics will necessarily be seen on any given surface. The final interpretation must be based upon a consideration of all of the features present.

and undoubtedly only some of the significant characteristics of the surface have been defined.

This work is continuing on characterizing fracture surface morphology of composites and correlating it with physical properties and types of induced failure. Its objective is the stablishment of the failure mechanisms of composite materials by scanning electron fractography, similar to that done for metals by electron transmission fractography.

Acknowledgments

Appreciation is expressed to Dr. A. S. Kenyon for supplying most of the composites reported here, and to Drs. Kenyon and Nielsen for advice and encouragement throughout this study.

A Cambridge "Stereoscan" Scanning Electron Microscope, Mark II, manufactured by Cambridge Instrument Company, Ltd., Cambridge, England, and distributed by Engis Equipment Company, Morton Grove, Illinois, was used for this investigation.

Figure 11 Tensile Fracture Surface of an Epoxy Composite Containing Untreated Discontinuous Glass Fibers, 1,800 X.

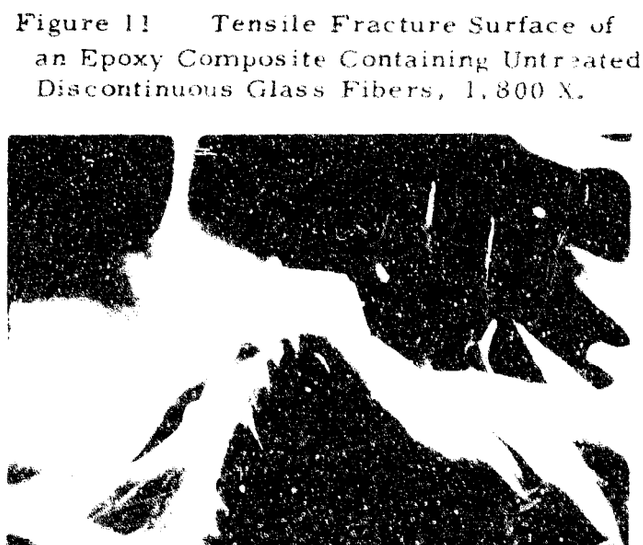

Figure 12 Tensile Fracture Surface of an Epoxy Composite Reinforced with Discontinuous Glass Fibers Coated with a Flexible Interlayer, 1,250 X.

References

1. Beachem, C. D. "The interpretation of electron microscope fractographs," U. S. Naval Research Laboratory, Report 6360 (1966).

2. Phillips, A., V. Karling and B. V. Whiteson. "Electron fractography handbook," ML-TDR-64-416 (1965).

3. Smith, K. C. A. in "Encyclopedia of electron microscopy," Reinhold, New York, N. Y. (1961) p. 241.

4. Oatley, C. W., W. C. Nixon and R. F. W. Pease. Advances in Electronics and Electron Physics, 21, 181 (1965).

5. Oatley, C. W. Sci. Prog., Oxford, 54 483 (1966).

6. Fairing, J. D. J. Comp. Mat., 1, 208 (1967).

7. Kenyon, A. S. and R. J. Slocombe, This report p. 92.

COMPOSITES WITH FLEXIBLE INNERLAYERS (A. S. Kenyon and R. J. Slocombe)

In this work primary significance is attached to the thin layer of matrix resin which surrounds the reinforcing agent in organic matrix composite systems. If it has a suitable structure, this innerlayer of resin is viewed as being in position to promote stress distribution, improve adhesion and reduce voids at the interface. A preferred ordering of molecular structure is also possible through the operation of forces at the interface when the innerlayer is deposited. These views on stress distribution are supported by the preliminary studies of Kenyon[1], and by theoretical considerations by Matonis and Small[2] and Gaonkar[3]. Factors related to adhesion and interfacial voids have been surveyed by Zisman[4] and some aspects of the orientation of polymer molecules at interfaces summarized by Stromberg and Kline[5] and by Kipling[6]. From a synthesis viewpoint, molecular species may be developed in a resin innerlayer that do not exist in the bulk matrix resin. Consequently, the performance of composites with "good" innerlayers may be found to exceed that predicted by a "rule of mixtures" that treats the matrix as a homogeneous domain in terms of the bulk properties of the resin.

In recognition of these possibilities, initial experimentation has been directed to exploration of relationships between synthesis variables and to obtain positive indications of performance potentials. Basically, the synthesis procedures were designed to allow control of the thickness and composition of innerlayers produced on chopped glass fibers. Operating procedures were designed and carried out as individual steps in the following sequence:

1. Preparation of outerlayer protomatrix resin.
2. Preparation of silane-treated fibers.
3. Adding innerlayer to silane-treated fibers.
4. Adding outerlayer protomatrix resin to innerlayer-coated fibers and working up the granular epoxy prepreg product.
5. Molding and curing the prepreg product into test specimens.

Background studies for carrying out steps 1 and 4 were described previously by Slocombe[7].

Prior to their incorporation in the prepreg form of a composite, the resin compounds were partially reacted to produce a relatively stable solution (protomatrix resin solution). The solvent used for the reaction of the epoxide and amine components was formulated to meet the solubility requirements and to provide a hydrogen donor to catalyze their reaction. In its final form, the solution of protomatrix resin was produced with 50% solids in acetone. In addition to solubility requirements, acetone was selected primarily for the stability it affords the protomatrix resin. The stage of the chemical reaction during the formation and storage of the protomatrix resin solution was followed by dual titrations. The analytical procedure of Durbetaki[8] was used to determine the total oxirane oxygen content plus the amine content. A corresponding sample was titrated with perchloric acid to determine just the amine content, and the oxirane content was subsequently determined by difference.

For the silane treatment of discontinuous fibers, the procedure was adapted from a standardized method[9]. The conditions used for adding the innerlayer to the silane-treated fibers were selected in consideration of the need for a reactive

solvent and the solution volume required to produce a slurry of individually dispersed glass fibers. Maximum cure was the prime consideration recognized in selecting the curing conditions.

To obtain more specific information on adhesion and fracture behavior, experiments were subsequently carried out using glass beads which provided an untreated glass surface of known geometry. Various silane couplers were used with and without innerlayer in a matrix resin.

Preparation of Outerlayer Protomatrix Resin

The following description applies specifically to the preparation of protomatrix solution No. 35 (PMS-35). However, it must be regarded as an example typical of numerous runs.

Solution-A was prepared by dissolving 75.0 g. methylenedianiline in a solution of 817.5 g. methanol and 114.0 g. water. Solution-B was prepared by dissolving 249.0 g. Epon-826 in 355.0 g. xylene. The A-point analytical specimens were taken from a mixture prepared at room temperature using 33.3 g. solution-A and 20.0 g. solution-B. To produce the protomatrix resin, a tared one-neck three-liter flask fitted with a reflux condenser attached through a Y-adapter was charged with 966.2 g. solution-A. The solution was heated with a Glas-Col mantle and stirred with a magnet-driven bar. At the reflux point, 579.8 g. solution-B was added quickly from a dropping funnel at the Y-adapter. The funnel was immediately replaced with a thermometer and to maintain a solution temperature of 68°, refluxing quickly restored as heating continued. After 10 minutes, the B-point analytical specimens were taken and the flask was transferred to a Rinco rotary evaporator to remove the solvents under reduced pressure. A water bath at 50° was used to heat the flask and solvent removal was completed in an hour. The methanol rapidly vaporized and the solution became milky, as it passed through a period of partial miscibility. The temperature inside the flask was judged by feel to be in the range of 25° to 30°C. Toward the end of the solvent-removal period, the product became a very thick, clear, amber-colored syrup. At this time, the C-point analytical specimens were taken,

The flask was weighed to determine the amount of syrup remaining, and a material balance was made assuming that the only resin components lost from the reactor were those in the analytical specimens. This calculation showed that the syrup contained 0.942 g. resin components per gram of syrup, and consequently, the 324 g. of product contained 305 g. resin components and 19 g. residual solvent which was assumed to be xylene. By subtraction, it was calculated that 286 g. acetone should be added to give a solution with 50% solids. The D-point analytical specimens were taken after the dilution was made. The solution was sealed in pint bottles for future use with one bottle put in a refrigerator for cold-storage testing. Solids determinations were made on the solution by drying 0.3 g. samples dispersed in small pans of sand in a vacuum oven. The test showed 49.89 and 49.97% solids.

Analysis of Protomatrix Resin

The A- and B-point analytical specimens each consisted of two 10 ml. samples, and the C- and D-point specimens each consisted of two 1 g. samples. For each analytical point in the procedure, one of the specimens was titrated with 0.5 N. hydrobromic acid in glacial acetic acid, and the other specimen was titrated with 0.1 N. perchloric acid in glacial acetic acid. Both of the reagent solutions were handled in automatic burettes to minimize contamination and evaporation losses. They were standardized on the same day the analyses were made using certified acidimetric standard grade of potassium acid phthalate. The titrations were made in 125 ml. flasks with magnet-driven, Teflon-coated stirring bars. Before titrating, each specimen was diluted with 50 ml. glacial acetic acid and 5 or 6 drops of indicator added (0.1% solution of crystal violet in glacial acetic acid).

Analytical data from the protomatrix resin synthesis, PMS-25, are given in Table I, and storage data on this same protomatrix solution are given in Table II.

TABLE I

ANALYTICAL DATA ON PROTOMATRIX SYNTHESIS PMS-35

Analysis Point	Sample Size	Hydrobromic Acid m.eq./g.	Perchloric Acid m.eq./g.	Oxirane Oxygen m.eq./g.	Oxirane Amine Ratio
A	10 ml.	11.22	4.32	3.58	1.81
B	10 ml.	3.62	1.09	2.62	1.66
C	1 g.	4.88	2.09	2.73	1.61
D	1 g.	2.62	1.14	1.48	1.30

TABLE II

PROTOMATRIX SOLUTION STORAGE DATA
PMS-35 AT 5° AND 25°C

Solution Age Days	Hydrobromic Acid m.eq./g.		Perchloric Acid m.eq./g.		Oxirane Oxygen m.eq./g.		Oxirane Amine Ratio	
	25°	5°	25°	5°	25°	5°	25°	5°
0	2.62	2.62	1.14	1.14	1.48	1.48	1.30	1.30
5	2.43	2.57	1.08	1.16	1.35	1.41	1.25	1.22
12	2.29	2.53	0.96	1.14	1.31	1.39	1.24	1.22
26	1.96	2.50	0.81	1.14	1.21	1.36	1.17	1.16

Silane Treatment of Fibers

A 3-liter flask was fitted with a stirrer, electric heating mantle, reflux condenser and thermometer, and charged with 30 g. 1/32" chopped fiber glass and 2500 ml. acetone. After stirring 10 minutes for washing, the acetone was removed by suction with a filter stick, and replaced by a solution of 0.09 g. γ-aminopropyltriethoxysilane in 2500 ml. water. The slurry was stirred gently to avoid balling the fibers, heated to 70°, and held at this temperature for 10 minutes. After the water was removed by the filter stick, the fibers were washed twice with one-liter portions of acetone.

Deposition of Innerlayer Resin on Fibers

A quantity of innerlayer solvent was prepared by mixing 3200 ml. methanol, 1200 ml. acetone and 600 ml. water. The innerlayer resin solution was prepared by mixing 115 g. Epon-815 and 135 g. EM-207 with 2,250 ml. of the innerlayer solvent. The remainder of the innerlayer solvent was used to rinse 50 g. of acetone-washed 1/32" chopped glass fibers in the silane treating assembly.

Innerlayer solution was then added and heated while stirring gently. At about 40°, 28.75 g. triethylenetetramine was added and heating continued for a specified period after reaching the reflux temperature, 64°. The innerlayer solution was then removed by suction with a filter stick and the fibers rinsed twice by swirling gently with a liter of acetone.

Deposition of Outerlayer Resin on Fibers

An acetone slurry containing 30 g. of 1/32" chopped glass fibers from previous steps was transferred to a one-liter tared beaker and most of the acetone removed by decantation, leaving about 100 to 120 g. to keep the fibers wet. The protomatrix solution was weighed by difference from a closed bottle and added dropwise while gently mixing with a lifting motion to avoid balling the fibers. The prepreg was precipitated in granular form by adding half of this mixture in small portions with a spoon to each of two four-liter beakers equipped with a motor-driven paddle stirrer and containing three liters of 0.17% PDR-14 solution at 0°-5° C. The product was washed six times with about 3500 ml. ice-cold water to harden the resin and subsequently spread out on a fine-mesh sieve over absorbent paper to drain water from the porous granules. The product was dried on Teflon trays in vacuum ovens for about 16 hours at room temperature. When 60 g. of protomatrix solution was used, the yield of dry prepreg was about 50 g. Samples showed 50-55% ash content (fiber) upon ignition.

Molding and Curing the Prepreg

Moldings were made by charging 23 g. of freshly dried prepreg in a positive pressure mold with a 2 x 6" cavity. Appreciable care and prepacking was necessary to achieve a uniform distribution in the mold which had been previously coated with a fluorocarbon release agent (MS-136 supplied by Miller-Stephenson Chemical Company, Inc.). Mold temperatures were measured with a thermocouple located in a small hole in the side of the mold. Pressures inside the mold were 1500 psi from 25° to 110°, 2600 psi to 130°, and 5000 psi to an upper temperature range of 140° to 150° which was held for 15 minutes. Whenever the oozing of resin was noted during molding, no further increase in pressure was

made. The maximum pressure was maintained on the mold while it was cooled to below 60°. Moldings were cured by heating for 3 hours at 150° followed by 3 hours at 80°. An unc.itical test gave better strength using this curing sequence than when reve.sed. Two 3/4 x 6" strips were cut from each molding, and these strips were routed to give specimens for tensile testing in an Instron machine with an extensometer to obtain stress-strain data given in Table III. The epoxy resin (Epon-815) and flexibilizer (EM-207) were used in the ratios shown in this table.

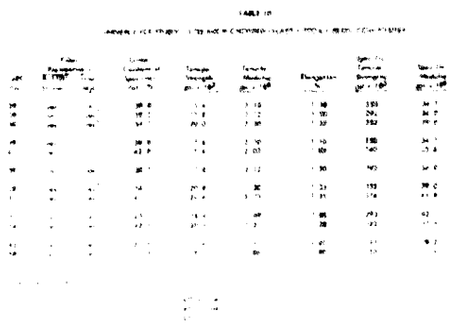

Glass Beads With Couplers and Innerlayers

Microbeads (Cataphote Corporation Type 4000) having an average size of 0.001" and ranging from 0.0005" to 0.0015" were surface treated by stirring in 1% solutions of various silanes, (Table IV) in a ratio of 1 ml. per gram of beads at room temperature for 30 minutes. The beads were removed from the solutions and dried and cured by baking at 140° for an hour. Some of the treatments yielded agglomerated beads. However, they were readily dispersed in the matrix resin mixture or the innerlayer solution. For these tests, the matrix resin mixture was Epon 815 and triethylenetetramine in a ratio of 7/1. In those examples having an innerlayer (Table IV) 100 g. of the silane-treated beads were coated by stirring in a refluxing solution of the following composition: 6.25 g. Epon 815, 6.25 g. EM-207 and 250 ml. innerlayer solvent mixture (7.6% water, 67.2% methanol, 25.2% acetone). After one hour, 1.8 g. triethylenetetramine was added, and the refluxing was continued for two hours longer. The coated beads

TABLE IV

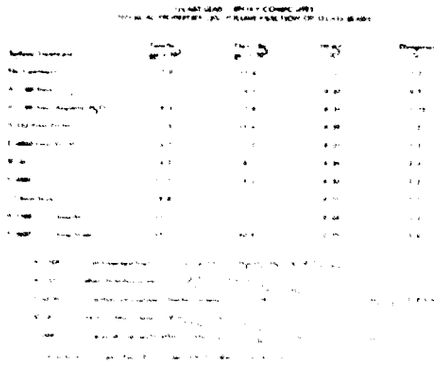

were separated from the solution by filtration on a Buchner funnel, dried for 15 hours at 70°, and then dispersed in the matrix resin mixture.

Raw Materials

Epon 815 and 826 are commercially available resin components consisting largely of bis-phenol-A-diglycidyl ether. Epon 815 contains some monofunctional epoxy diluent. Both materials were obtained from Shell Chemical Company. p, p'Methylenedianiline was obtained as a purified grade from Dow Chemical Company. EM-207 is a low molecular weight polyester obtained from Thiokol Chemical Corporation. These resin components were analyzed by titrating with hydrobromic acid by the precedure used for analysing the protomatrix solution. The gram-equivalent weights were as follows: 183 g. for Epon 826, 187 g. for Epon 815, 99.50 g. for methylenedianiline, and 6×10^5 for EM-207. Theoretical gram-equivalent weights are 170.2 g. for bis-phenol-A-diglycidyl ether and 99.64 g. for methylenedianiline. A-1100 is a commercial grade of γ-amino-propyltriethoxysilane obtained from Union Carbide Corporation. A technical grade of triethylenetetramine was used as obtained from Fisher Scientific Company. PDR-14 is a copolymer of acrylic acid and 2-ethylhexylacrylate in a 96/4 weight ratio obtained from Monsanto Company. Analytical reagent grades of acetone and methanol were used as obtained from Mallinckrodt Chemical Works. The fiber glass, obtained as a 20-end roving from Ferro Corporation was designated Type 1014 and had been treated with a silane coupler and coated with epoxy resins by the producer. Strands of the roving were laid together and sandwiched between cellophane tape for chopping into 1/32" lengths with a guillotine-type chopper. The shredded tape was removed by sieving. The fiber diameter was measured with a microscope and found to be 9 microns.

Discussion

The results presented in this paper should be regarded as having more of the character of exploratory findings rather than a definitive study because the number of variables involved in carrying out a thoroughly systematic investigation is beyond the scope of this initial effort.

From a working viewpoint, the innerlayer is regarded as the matrix resin that immediately surrounds the reinforcement and has structural and property characteristics significantly different from those of the major portion of resin in the matrix. Basically, the synthesis procedures were designed to allow control of factors related to the thickness and composition of the innerlayer so that test specimens could be produced for appraising the potential of flexible innerlayers in discontinuous fiber systems.

The constitution of freshly prepared protomatrix solution has been deduced largely from consideration of initial and final values of the oxirane/amine (Table I) and the known stoichiometry of the resin components. Under the conditions provided, it is expected that the first reaction product between the diamine and diepoxide should yield dimer-A and that the subsequent reaction of this dimer would probably be either trimer-B or trimer-C as shown schematically in Figure 1. To satisfy the requirements imposed by the initial oxirane/amine ratio of 1.8 and the final ratio of 1.3 as shown in Table I, the composition of the protomatrix solution at this stage should consist largely of dimer-A, trimer-B and unreacted diepoxide monomer with small amounts of trimer-C and higher oligomers.

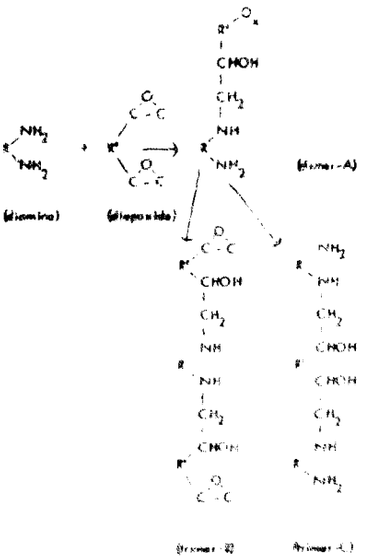

Figure 1 Protomatrix Resin Synthesis.

Storage data on protomatrix solutions (Table II) show significant differences not only in the rate at which the changes occur, but also in the kind of changes. When stored at 25°, the analyses showed equivalent decreases in both the oxirane oxygen and the amine function. The net effect appeared as an increase in the oxirane/amine ratio since the excess of oxirane was proportionately increased by this

reaction. From this, it was inferred that the epoxy-amine reaction had produced macromolecules in which the amine groups were inaccessible to the acidic reagents in acetic acid. In contrast, when the protomatrix solution was stored at 5°, the titratable amine content was essentially constant throughout the test period, and the decrease in oxirane content was markedly slower. The net effect of the changes at 5° appeared as a slow decrease in the oxirane/amine ratio, and from this it was inferred that the epoxy-amine reaction had produced molecular species in which the amine groups remained accessible to titration in acetic acid. These interpretations suggest that different network structures can be produced by controlling the solution storage temperature, and thereby it may be possible to produce resins with improved properties. All of the test specimens reported herein were made from protomatrix solutions stored at room temperature. No correlation was observed between the age and properties of resin specimens prepared from protomatrix solutions which had been stored at room temperature for various time periods.

Table III gives the physical properties of composites made by molding prepregs of 1/32" chopped glass fibers with and without flexible innerlayers in a rigid outer matrix resin. Improved tensile strength, modulus and elongation were found for the composites containing the innerlayer. All samples in this series were molded under the same conditions so that the orientation of the fibers should be comparable.

Nielsen and Chen[10] have derived a relation for Young's modulus of randomly oriented fiber filled composites in which the modulus values are a function of the ratio of the moduli of the filler to matrix and the volume fractions of the components. In the case of glass-epoxy system, the ratio E_2/E_1 is approximately 30, and the ratio of the modulus at random angle to the modulus when all fibers are oriented parallel to the direction of stress is $\frac{\langle E_\theta \rangle}{E_{11}} = 0.33$.

From the equation,

$$\langle E_\theta \rangle = E_1 \Phi_1 + F E_2 \Phi_2$$

where F is the fiber efficiency factor, the values for a calculated modulus and fiber factor can be determined. Table V shows the calculated values compared

with the experimental. In three of the four cases, the calculated values for the modulus and fiber factor is lower than the observed values. In the case where the fiber manufacturer's surface treatment was destroyed by heat cleaning, the calculated and observed values agree.

TABLE V

GLASS FIBER - EPOXY COMPOSITES

Polymer	δ_2	$E_{(obs)}$	$(E)_{cal}$	F_{obs}	F_{cal}
GEC 45 No Innerlayer	42.8	2.03	1.78	.36	.30
GEC 40R 1:1 Innerlayer	39.9	2.25	1.66	.42	.30
GEC 37 1:2 Innerlayer	43.1	2.69	1.79	.47	.30
GEC 52 No Innerlayer Heat Cleaned	32.5	1.32	1.34	.32	.325

As a consequence of the compression molding operation, the short fibers did show partial alignment in planes parallel to the platens of the mold. Even with this very limited orientation, the observed modulus values were higher than expected and also higher than predicted for specimens with a high degree of planar orientation. Further work may show that these higher values can be attributed to better adhesion and improved stress distribution at the interfaces.

An examination of innerlayer-coated fibers by phase contrast microscopy showed rounded deposits of resin on the fiber ends, whereas fibers free of innerlayer have sharp edges which could cause high stress concentrations. The reduction of fiber end-effects by an innerlayer coating could contribute significantly to improved performance of the composites. As subsequently confirmed with beads, improved adhesion of the matrix resin to the fibers by the use of flexible innerlayers could contribute to improved composite performance by the following:

1. Reduction of flaws at the interface.
2. Alteration of the stress distribution and stress transfer.
3. Modification of the resin in the vicinity of the interface through preferred orientation of the molecules.

With regard to this latter point, the use of a flexible innerlayer allows the zone of influence resulting from preferential adsorption[11] to be extended into the matrix resin.

For detailed study of adhesion and fracture behavior, glass beads were selected for use as the filler since they present surfaces with known geometry and known composition and thereby reduce the number of variables encountered in fiber systems.

Kenyon and Duffey[12] studied the physical properties of a glass bead filled polymer at filler loadings up to 50 volume fraction. They showed composite containing beads treated with γ-glycidoxypropyltriethoxysilane had greater elongation than predicted, based upon no alteration of the base resin, and cited this as evidence of a change in the resin by preferential adsorption. In this study the effects of surface treatments were established by using different silanes as coupling agents.

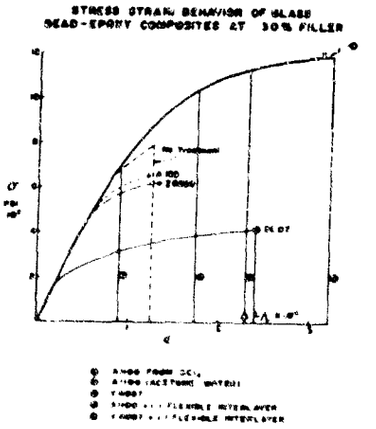

Figure 2

In Figure 2, the stress-strain characteristics are related to the molecular structure of silane surface treating agents. The principal curve in this figure is governed by the properties of the base resin, and those curves that branch off at the lower stress levels are interpreted as indicating debonding at the glass-resin interface. Those silanes which do not provide a functional group for reaction with the matrix components show this branching from the principal curve. This behavior is illustrated by methylchloro, phenyl and methacryloxy silanes (SC-87, A153 and Z6030 respectively). Untreated glass surfaces show stronger interaction with the matrix resin than glass surfaces treated with the foregoing agents.

Aminopropyl and glycidoxy silanes provide functional groups that can react with the matrix resin, and composites made from beads treated with these agents allowed significantly higher levels of stress and strain to be attained. The glycidoxy silane appeared to be more effective as a coupler, and from this it is inferred to be more reactive with the matrix resin. The influence of the solvent used in depositing the silane is illustrated by systems 1 and 2 in Figure 2

in which carbon tetrachloride was found to be a less effective solvent than the acetone-water system. These results are in accord with Wong[13] who reported poorer properties on composites when glass fibers were treated with amino silane deposited from chlorinated solvents.

The highest levels of stress and strain were shown by specimens having a flexible innerlayer added to the beads with the aminopropyl or glycidoxy silane couplers. In these systems, the improved adhesion allows stresses to develop that cause some bead fracture when flaws or voids exist in the beads, Figure 3.

Figure 3 Tensile Fracture Surface Y-4087 Surface Treatment plus 1:1 Flexible Innerlayer Showing Bead Fracture, 1910 X.

Since no evidence of bead fracture was observed for coupling agents giving adhesion less than obtained with glycidoxypropyl silane, it is inferred that better stress transfer is obtained with improved adhesion.

The principal curve in Figure 2 shows that the initial modulus of all samples is equivalent. The bead treatments and test data for all samples is summarized in Table IV. The measured moduli of these samples agrees with calculated values based on a modified Kerner equation[14] for a 30 volume fraction loading. The degree of adhesion does not alter the initial modulus because the filler is subject to a clamping action of the resin due to its shrinkage.

Figure 4 shows that innerlayers are effective in improving tensile strengths of composites over a range of 0 to 50% filler loadings.

The effectiveness of silane couplers on adhesion is shown by the electron scanning photomicrographs, Figures 5, 6, 7 and 8. Tensile fracture surfaces of specimens summarized in Table IV and Figure 4 are shown in these views. Typical debonding shown in Figure 5 is characteristic of results obtained with methylchloro, phenyl and methacryloxy silanes. Improved bonding is reflected by the appearance of resin adhering to the filler surface as the fracture occurs farther into the matrix. This behavior is illustrated photographically in Figures 6, 7 and 8 where the improvement in adhesion parallels the improvement in strength shown in Figure 4.

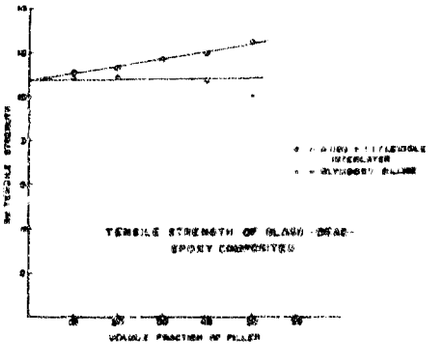

Figure 4

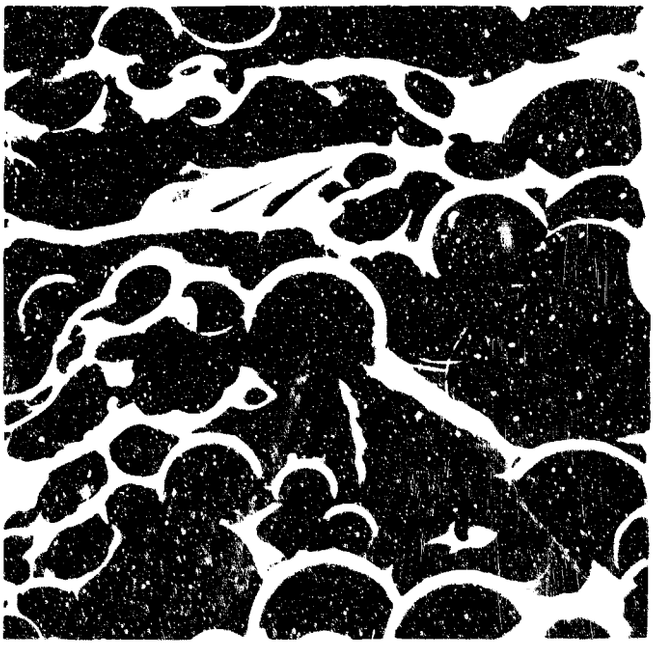

Figure 5 Tensile Fracture Surface Glass Beads Treated with Parting Agent (SC-87), 950 X.

These results illustrate the importance and practicability of a concept that uses flexible innerlayers with silane couplers to produce composites with superior performance.

Conclusions

Techniques for sequentially applying silane coupling agents, flexible innerlayer resins, and rigid outerlayer resin coatings to glass beads and chopped glass fibers have been demonstrated.

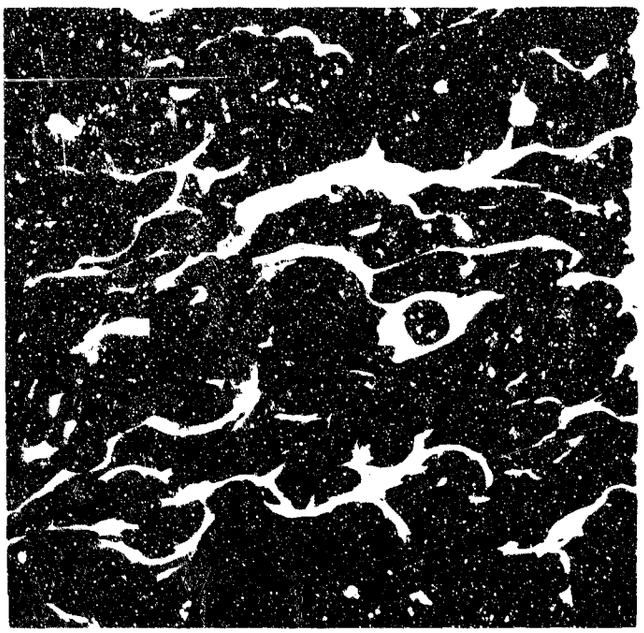

Figure 6 Tensile Fracture Surface Glass Beads Treated with Amino Silane (A-1100), 540 X.

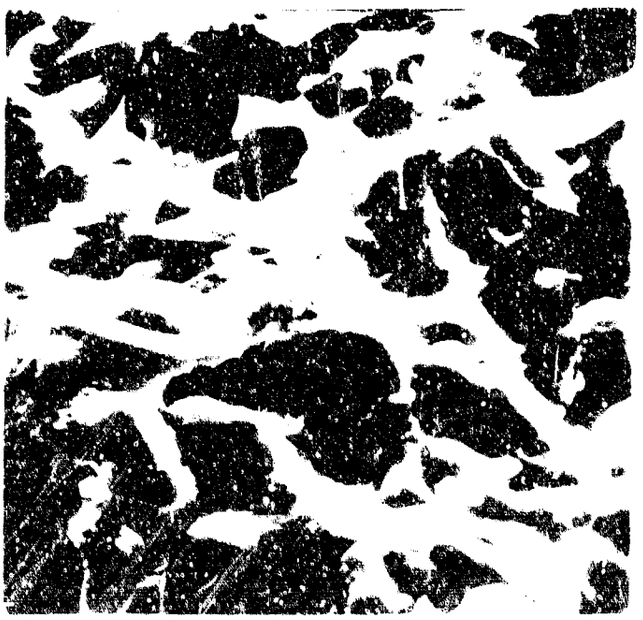

Figure 7 Tensile Fracture Surface Glass Beads Treated with Glycidoxy Silane (Y-4087), 1100 X.

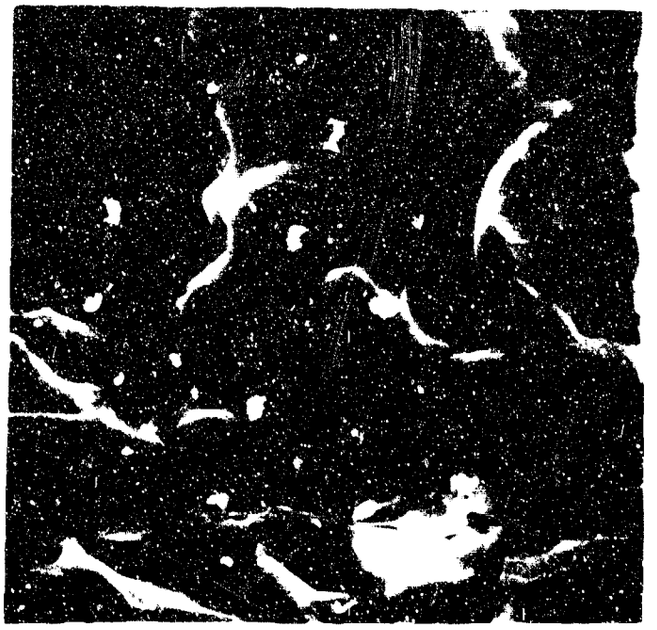

Figure 8 Tensile Fracture Surface Y-4087 Surface Treatment Plus 1:1 Flexible Innerlayer, 985 X.

Prepregs made from discontinuous fibers have been shown to give molded specimens with physical property improvement attributed to a flexible innerlayer with good adhesion.

Improved adhesion was shown to be at least partially responsible for greater strength provided by composites made with flexible innerlayers. With improved adhesion, better stress transfer is also feasible.

The contributions of silane coupling agents and flexible innerlayers have been shown to be mutually complementary in achieving high tensile properties.

Future Work

Utilize sequential deposition techniques to synthesize innerlayers of resin with known structure. Controlling the surface chemistry will allow the building of known structures and thickness.

Correlate the structure and properties of the innerlayer of resin with performance characteristics of their composites.

Quantify the contribution of resin components to the performance of composites through studies with continuous glass filaments that will allow controlled orientation of the reinforcement.

Acknowledgment

The many helpful discussions with Dr. L. E. Nielsen and J. D. Fairing is gratefully acknowledged. Mr. Fairing is also responsible for the electron scanning photomicrographs which so clearly shows the surface treating effects. We also express our appreciation for the assistance of A. L. Schmidt and G. D. Muehl who carried out laboratory experiments and testing. The efforts of D. C. Morris are acknowledged for his help in providing the chopped fiber glass.

Rеferences

1. Kenyon, A. S. AD 487 208, p. 22 (1966).

2. Matonis, V. A. and N. C. Small. "A macroscopic analysis of materials containing layered spherical inclusions," Thesis - University of Connecticut (1967).

3. Gaonkar, G. H. "Plane stress fields due to isolated and multirows of inclusions in an elastic continuum," Dissertation - Washington University (1967).

4. Zisman, W. A. Ind. Eng. Chem., 57, 26 (1965).

5. Stromberg, R. R. and G. M. Kline. Modern Plastics, 38, 123 and 241 (1961).

6. Kipling, J. J. "Adsorption from solutions of non-electrolytes," Academic Press, London, New York, N. Y. (1965).

7. Slocombe, R. J. AD 487 208, p. 61 (1966).

8. Durbetaki, A. J. Anal. Chem., 28, 2000 (1956).

9. Andersen, H. M. Private communication.

10. Nielsen, L. E. and P. E. Chen. "Young's modulus of randomly oriented fiber-filled composites," Submitted for publication.

11. Erickson, P. W., A. Volpe and E. R. Cooper. 19th Annual Conference, SPI, Section 21A, 1 (1964).

12. Kenyon, A. S. and H. J. Duffey. Polymer Eng. and Sci. - in press.

13. Wong, R. Private communication.

14. Nielsen, L. E. "Mechanical properties of polymers," Reinhold Publishing Company (1962) p. 135.

DYNAMIC MECHANICAL PROPERTIES OF SOME POLYMERIC ACID ZINC SALTS (J. E. Fields and L. E. Nielsen)

Mechanical properties of a range of rigid polyelectrolyte type polymers have been reported[1]. Polyelectrolytes such as the metallic salts of polymeric acids were shown to have moduli values several times greater than those of the common thermoplastic materials. Since preformed salts of such polyacids do not measurably soften below their decomposition temperatures, specimens were fabricated by in situ reaction of mixed polyacid and metal oxide powders in a mold at high temperatures (over 200° C) and high pressure (5-10, 000 psi). Such techniques may easily lead to variable property results, partly due to non-uniform degree of reaction as molding conditions may vary.

In this work, the degree of reaction was followed by X-ray techniques so that the composition of the molded specimens could be estimated. With this information, answers were obtained to such questions as: (a) how dependent is modulus upon degree of reaction? (b) how much increase, over classical filler action, is obtained by ionic bonding through salt formation? and (c) what is the effect of excess (over theory) metal oxide when charged as additional filler?

Materials and Techniques

The polyelectrolyte system used was a 94/6 (by weight) copolymer of acrylic acid and 2-ethylhexyl acrylate, a product of Monsanto Company, designated as PDR-14. The polyacid had a glass transition (Tg) of 130° C with the onset of decomposition at 300° C, as determined by a Perkin Elmer Differential Scanning Calorimeter. The density of molded specimens of PDR-14 (by buoyancy) was determined as 1.3589. Predried PDR-14 (110° C, 48 hours, vacuum) with a loss on drying at 110° C of 0.3% was used throughout.

Various zinc PDR-14 salts were prepared in situ from intimately mixed ry powders of PDR-14 and ZnO by positive pressure molding techniques[1]. he powders were mixed in a Spex "wiggle-bug" for ten minutes in a me tal ixing jar. Molding c nditions, varying from 200-300°C and from 5-10, 000 si, for the various materials are given in Table III, Appendix. Strip specimens, .377 by 4.00 inches with thicknesses varying from 0.020 to 0.035 inches were repared for dynamic mechanical testing.

Dynamic mechanical properties, shear modulus, damping, and glass transi- on (Tg) were measured on a recording torsion pendulum[2]. The Tg was easured as the maximum in the mechanical damping peak at about 1 c/s. The eory and discussion of dynamic mechanical testing is presented by Nielsen[3].

The extent of reaction of molded specimens was determined by measuring e intensity of unreacted zinc oxide crystal peaks in X-ray goniometer tracings hich were standardized by mixed but unreacted powders of known composition. n all cases the p oportionality between the (100) (002) (101) lines for ZnO emained constant and the estimated error was plus or minus 2%.

Infrared analyses of KBr pellets containing samples identical with those used or X-ray analysis were made in order to correlate metal oxide disappearance ith carboxyl carbonyl disappearance.

esults and Discussion

In any reacted system the possibility exists that five species may be present varying amounts depending upon the course of reaction as schematically shown Figure 1. ese are (a) pendent half-salt, b) in-chain di-salt from either adjacent or on-adjacent carboxyls, (c) cross-chain i-salt, (d) unreacted polyacid, and (e) nreacted ZnO. A system containing the rst four of these species exists as an ntertangled network of the species present nd not as a mixture of the various species.

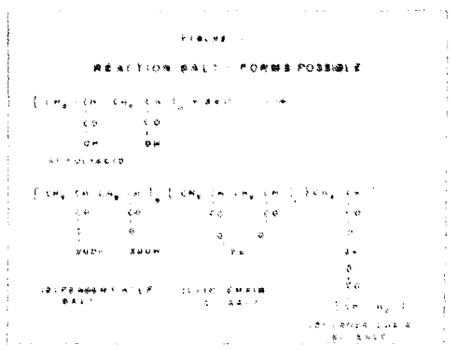

However, each specie will have its own influence on the total properties, whether modulus, damping, or Tg. Thus, di-salt forms (b) and (c) will contribute more to stiffening than the half-salt (a) due to greater restrictions on rotation. However, the half-salt (a) will contribute more, unit-wise, than (b) or (c) from a simple filler standpoint because of its higher metal content. From a bond strength standpoint, the [-O-Zn-O-] ionic-type bonds of the di-salt (b) or (c) are considered stronger than the [-O-Zn-OH] bonds of the half-salt and, again would contribute more to stiffness due to a smaller tendency for interchange between reaction sites. The greater interchange tendency of the half-salt (a) would result in lower modulus increases, higher damping, and lower Tg levels. In a partially reacted system there is no way of knowing which specie may act as the continuous or discontinuous phase. However, one can assume that any unreacted ZnO will act as filler to all other species in relation to the volume fraction of that phase present.

A series of zinc polyacrylate (PDR-14) salts were prepared using from 25 to 200 percent of the stoichiometric amount of zinc oxide as shown in Table I together with the determined extent of reaction and the mechanical properties of the molded products. Typical dynamic mechanical results are illustrated in Figures 2 and 3. Infrared analyses of KBr pellets containing samples identical with those used for X-ray analysis were made for samples 1 through 5 in order to correlate metal oxide disappearance with carboxyl carbonyl disappearance. As metal reacted approached 100% of the stoichiometric theory complete disappearance of the carboxyl carbonyl also was noted. No other interpretation of the complex spectra was attempted.

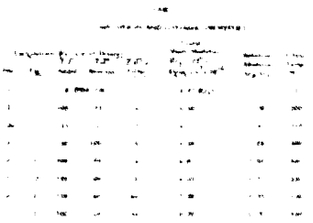

Whereas most common rigid organic polymers have a shear modulus of about 1×10^{10} dyne/cm^2, the free polyacid modulus was found to be 2.37×10^{10}, probably due to its highly hydrogen bonded structure. As more and more metal

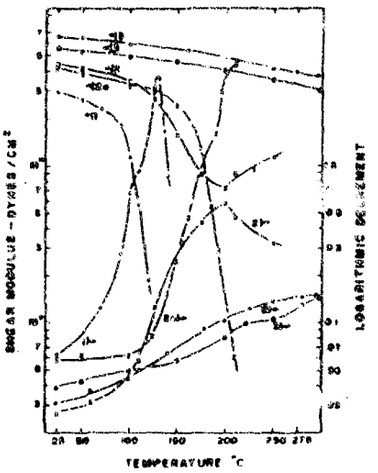

Figure 2 Dynamic Mechanical Properties

(1) PDR-14 Polyacid
(2) 100% theory ZnO, 94% reacted
(2a) 25% theory ZnO, 100% reacted
(3) 50% theory ZnO, 100% reacted
(5) 100% theory ZnO, 100% reacted

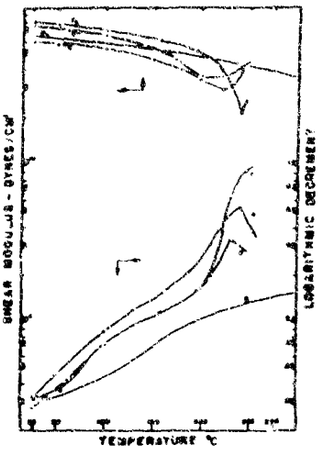

Figure 3 Dynamic Mechanical Properties

(4) 100% theory ZnO, 94% reacted
(5) 100% theory ZnO, 100% reacted
(6) 150% theory ZnO, 86% reacted
(7) 200% theory ZnO, 146% reacted

salt was incorporated through reaction with ZnO a steady increase in the modulus was noted as expected due to formation of strong ionic-type bonds. Further, the Tg was increased with greater amounts of salt formation until 100% of theory salt formation was reached where no Tg was noted, at least up to 300°C. At this point, Sample 5, both ZnO and carboxyl were absent by analysis, and the modulus of 6.55 can be considered as the modulus of the di-salt forms. Whereas over-theory ZnO additions further increased the 25°C modulus, the Tg appeared to drop below that attained by adding (and reacting) only the theoretical amount. This effect on Tg will be discussed later.

For products containing up to 100% theory ZnO, incomplete reaction (Figure 2, curve 2; Figure 3, curve 4) leads to complex product mixtures, containing reacted zinc salts, unreacted portions of polyacid, and unreacted ZnO acting as filler. Such compositional heterogeneity, evident from the specimen opacity, results in high and broad mechanical damping areas and lower modulii at high temperatures.

The sharp discontinuities observed over 200° C are not characteristic of the polymer but are probably due to continuation of incomplete reactions of half-salt forms, polyacid, and unreacted ZnO as suggested by Fitzgerald and Nielsen[1]. Such further reaction cannot occur until the Tg of the system is reached. For example, with Sample 2, further reaction became evident at over 200° C. This point corresponds to the Tg (about 210° C) for Sample 2a wherein only 25% theory ZnO was added. In this case complete reaction of ZnO precluded further reaction and the product contained only di-salt and polyacid species. The complete modulus and damping curves for 2a resembled those of the unreacted polyacid (curve 1) except for a much higher 25° C modulus and a displacement of the curves to higher temperatures by about 70-80° C. Complete reaction of the ZnO (Figure 2, curves 3, 5), whether at the 50 or 100% theory level, leads to more tightly crosslinked systems through cross-chain di-salt formation. These products yield modulus curves which are relatively insensitive to high temperatures and are low damping.

The modulus improvement due to ionic-type bonding through salt formation relative to the classic filler effect was calculated assuming no reaction of the ZnO. Results are given in Table II and illustrated in Figure 4. For comparison,

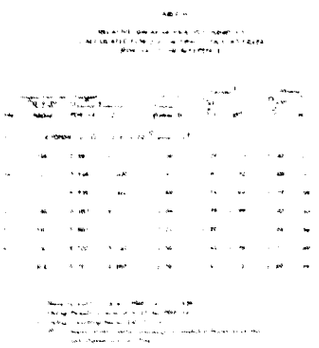

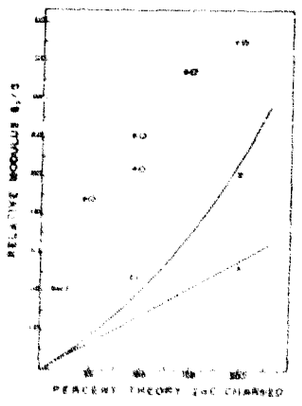

Figure 4 Relative Shear Modulus at 25° C, Found vs. Calculated as Filler. (A) Theory for Kerner. (B) Theory for Mooney. The numbers 2-7 refer to experimental points from Table I.

the reinforcing action of spherical filler particles was calculated by three theories, Kerner[4], Guth-Smallwood[5,6] and Mooney[7]. These relationships are given in the Appendix. A comprehensive comparison of the merits of these and other theories of filler action is given by Nielsen[8]. Only the Kerner and Mooney comparisons are shown since at the ZnO levels employed, below 0.2 volume fraction, the Guth-Smallwood and Mooney relations give substantially equivalent results.

A substantial improvement ratio (increase in modulus found over that calculated only as filler) is noted in all cases from 25 through 200% theory ZnO added. This increase in modulus, due to ionic bonding vs. filler effect, was found to be 60-80% greater as calculated by the Kerner relation and from 40-60% greater as calculated by either the Guth-Smallwood or Mooney relations.

The modulus curves (Figure 3, curves 6, 7) for added excesses over theory of ZnO relate quite well with the degree of reaction found, Table I. Although the 25°C modulus continues to increase, the results at higher temperatures are more revealing. With 150% theory charged (curve 6) the product analyzed as 86% of a theory reacted with a remainder of 64% of a theory ZnO acting as filler. Thus, curve 6 is similar in shape to curve 4 in Figure 3 obtained for 94% of a theory reacted but with a lower level of unreacted filler. At the 200% theory ZnO charged level a lowering of the improvement ratio is noted in Table II. Analysis of the product indicated 146% theory ZnO consumed with 54% theory remaining as filler. To obtain over-theory reacted zinc one must introduce a new salt specie, the pendent half-salt form, $-C(=O)-O-Zn-OH$. As mentioned previously this salt-form may be expected to increase the modulus at 25°C somewhat, but to have a definite T_g at elevated temperatures barring further reaction. Curve 7 in Figure 3 illustrates this prediction with precipitous lowering of the modulus over 150°C and a very high damping effect. Since 46% ZnO reaction over theory implies the splitting of an identical portion of a theoretical di-salt, then the salt portion of Sample 7 must contain 92% of a theory as pendent half-salt and only 8% of theory as di-salt. The corresponding unit volume fractions are 0.43

pendent and 0.37 di-salts. Thus the dominating effect on mechanical properties comes from the pendent half-salt, which would not be expected to exhibit high temperature modulus stability.

One can estimate a modulus (G_x) for the pendent half-salt form as 7.08×10^{10} dyne/cm^2. This was done by distributing unreacted ZnO, on a volume basis, between the half- and di-salt species and, using the Mooney relation with 6.55 for the modulus of the di-salt specie, calculating a modulus for the filled di-salt specie. Then, using the rule of mixtures and the modulus found for Sample 7, one can obtain a modulus for the filled half-salt specie. From this, G_x is obtained, again from the Mooney relation. G_x, 7.08, for the half-salt specie is higher than G_2 found (6.55) for the di-salt because of its higher metal content. However, the improvement ratio for the pure half-salt-form (over theoretical filler action) is lower than that for the corresponding di-salt because of weaker and more mobile salt linkages. At a volume fraction of 0.209 ZnO, equivalent to pure half-salt, the improvement ratio was only 1.14 contrasted with the higher improvement ratio of 1.56 found for the di-salt using the Mooney relation. This smaller improvement ratio accounts for the lower trend noted for relative moduli found for Sample 7 where major amounts of pendent half-salt are present.

The almost identical broad and high damping curves for Samples 6 and 7 (Figure 3) below 200°C, again indicating compositional heterogeneity, suggest the presence of pendent half-salts in the 150% theory ZnO sample. The same suggestion also applies to Samples 2 and 4 where less than complete reaction was observed. The short stress relaxation times reported[1] for monovalent sodium salt of similar polyacids, compared with much longer stress relaxation times for divalent barium salts, may likewise be evident in the case of pendent half-salt forms compared with more heat stable di-salt forms.

Summary

In the *in situ* formation of polyacid metal salts by compression molding polyacid and metal oxide powder mixtures, it has been shown that only complete reaction of oxide will lead to temperature insensitive high-modulus low-damping

products. Incomplete reaction, for whatever cause - low temperature, low pressure, poor mold venting, or excess metal oxide, results in products which are high damping and have poor modulus-temperature characteristics. This effect may be due to pendent half-salts of the form, $-\overset{O}{\overset{\|}{C}}-O-Zn-OH$. Such a salt-form must be assumed to be present where over-theory excesses of ZnO were used and where more than theory zinc was found to be reacted.

The increase in modulus due to ionic bonding, from whatever salt form may be present over that expected from classical filler action alone, ranges from 40-80% depending upon the theory chosen to calculate filler action. Any unreacted metal oxide appears to act as classical filler in the polyelectrolyte salt matrix. For the theoretical di-salt form, modulus values of 6 to 7 times those for normal organic rigid polymers were obtained.

Acknowledgment

The authors acknowledge the assistance of Mr. D. M. Hemmerly for sample preparation and property determination.

Appendix

The Kerner relation[4] is:

$$G_o = G_1 \left[\frac{\frac{\Phi_F G_F}{(7-5\nu_1) G_1 + (8-10\nu_1) G_F} + \frac{\Phi_P}{15(1-\nu_1)}}{\frac{\Phi_F G_1}{(7-5\nu_1) G_1 + (8-10\nu_1) G_F} + \frac{\Phi_P}{15(1-\nu_1)}} \right]$$

where G_o is the shear modulus of the two-phase system and G_1 and G_F are the shear moduli of the polymer or continuous phase and of the filler or discontinuous phase, respectively. The volume fraction of the polymer is Φ_P and that of the filler is Φ_F. Poisson's ratio of the material in the continuous phase is ν_1.

For rigid fillers which have moduli much greater than that of the polymer, Kerner's equation may be simplified at low volume fractions of filler to:

$$G_o = G_1 \left[1 + \frac{\Phi_F}{\Phi_P} \left\{ \frac{15(1-\nu_1)}{8-10\nu_1} \right\} \right]$$

For calculations, ν_1 of the polyacid was used as 0.35 and that for any salt-form as 0.30.

The Guth-Smallwood relation[5,6] is:

$$G_o = G_1 \left(1 + 2.5\, \phi_F + 14.1\, \phi_F^2\right)$$

The Mooney equation (7) is:

$$\ln \frac{G_o}{G_1} = \frac{2.5\, \phi_F}{1 - S\, \phi_F}$$

For calculations, the packing factor S was taken as 1.4, see Reference 8.

The various molding conditions for the reported samples are summarized in Table III, below:

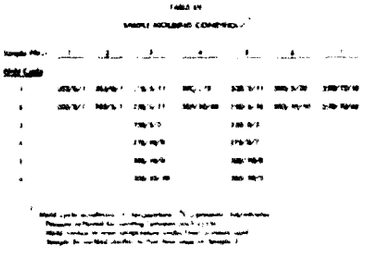

References

1. Fitzgerald, W. E. and L. E. Nielsen. Proc. Roy. Soc., 282A, 137 (1964).

2. Nielsen, L. E. Rev. Sci. Instr. 22, 690 (1951).

3. Nielsen, L. E. "Mechanical properties of polymers," Reinhold Publishing Company (1962).

4. Kerner, E. H. Proc. Phys. Soc., 69B, 808 (1956).

5. Guth, E. J. Appl. Phys., 16, 20 (1945).

6. Smallwood, H. M. J. Appl. Phys., 15, 758 (1944).

7. Mooney, M. J. Colloid Sci., 6, 162 (1951).

8. Nielsen, L. E. J. Composite Materials, 1, 100 (1967).

PROPERTIES OF STRONG ACID POLYACID SALTS: PHOSPHORYLATED POLYVINYL ALCOHOL AND POLYSTYRENE SULFONIC ACID

(J. E. Fields and J. R. Ripley)

The dynamic mechanical properties of zinc polyacrylate as a function of degree of salt formation has been reported[1]. For this carboxy polyacid, the shear modulus increase due to ionic bonding as the di-salt, over that expected from classical filler action, ranged from 40-80% depending upon the theory chosen to calculate filler action. Only complete reaction as the di-salt, at 300°C and 10,000 psi results in low damping products with "temperature insensitive" high modulus. Excesses of metal oxide over theory were shown to lead to pendent half-salt forms which exhibit high damping and have temperature sensitive shear moduli. The half-salt gives smaller moduli increases, over filler action, and unreacted metal oxide appears to act as classical filler in an intertangled complex polyelectrolyte salt matrix. The di-salt modulus was 6-7 times higher than moduli for normal organic rigid polymers.

In this work, *in situ* reaction of mixed polyacid and metal oxide powders was extended to polyacids of higher acid strength than polyacrylic acid to determine the effect of ionic bond strength on shear modulus increase. Two polyacids were examined briefly, (a) polyvinylphosphoric (PVP) and (b) polystyrene sulfonic (HSPS). The comparative acid strengths of the polyacids were:

	pKa	K
Polyvinylphosphoric	3.50	3.1×10^{-4}
Polystyrene sulfonic	3.33	4.7×10^{-4}
Polyacrylic (COOH)	6.15	6.4×10^{-7}

All titrated as monobasic acids. The second available acid group of PVP was too weak to give an endpoint but had an approximate pKa at 8.00 or a K of 1×10^{-8}.

As before the degree of reaction (salt formation) was followed by X-ray techniques so that the composition of molded specimens could be estimated and a proper estimate of modulus increase due to ionic bonding could be made.

Materials and Techniques

The two polyvinylphosphate samples reported upon herein were prepared by phosphorylation of polyvinyl alcohol with urea and phosphoric acid by the method of Daul and Reid[2,3]. A total of 27 preparations were made to identify reaction parameters, but only two are reported upon. For 627434, low molecular weight PVOH (Elvanol 70-05) (98.5% hydrolyzed) was used and for 627437, high molecular weight PVOH (Elvanol 71-24) (98.5% hydrolyzed) was used. In each case the ratio of H_3PO_4/urea/PVOH was 1: 1: 1 with a curing time of 3 hours at 110° C followed by 20 min. at 150° C for 627434 and 30 min. at 150° C for 627437. Products were isolated by solution in water, digestion with HCl, dialysis to remove urea and salts, cation exchanged through Amberlite IR-120H, and vacuum freeze drying. Product analyses were:

	M. W.	% P	% N	Phosphoric Groups Mole %	Mol. Wt. Per Phosphoric Group
627434	L	13.25	1.00	29.0	233
627437	H	15.13	0.61	35.7	205

Modulus vs. temperature data for molded specimens of these materials indicated the presence of water in spite of storage in a desiccator and density (by buoyancy) measurements were not reproducible. Therefore densities were calculated for 627434 as 1.46 and for 627437 as 1.50 and these values were used in subsequent calculations relative to zinc salt compositions.

The small nitrogen content left after ion-exchange may either represent approximately one NH_4^+ salt per 10 phosphate units or 1 carbamate substituent per 10 phosphate units arising from the decomposition of urea at 150° C.

Free HSPS was prepared from crude ammonium salt having about one SO_3/styrene with a base molecular weight of polystyrene of 50,000. This was repeatedly digested with HCl, dialysed, and ion-exchanged with Amberlite IR-120H and then vacuum freeze dried. By analysis: S = 15.72%, N = 1.27%, C = 50.90%, H = 4.90%. These analyses calculate as 0.9 SO_3H groups per styrene with 1 out of 5

remaining as the ammonium salt. Attempted moldings, reported herein, were made on this material. A sample of free acid (no salt) was prepared by sulfonation of polystyrene with SO_3-dichlorodiethyl ether complex following a procedure of Baer[4] but no moldings have as yet been attempted.

Various salts of the polyacids were prepared, as before, by in situ positive pressure molding techniques on intimately mixed dry (?) powders of polyacid and metal oxide. The powders were mixed in a Spex "wiggle-bug" for 10 minutes in a metal mixing jar. Molding conditions for the PVP-metal oxides were 100-150°C at 5-10, 000 psi due to low decomposition points for the PVP samples (approximately 180°C). The polystyrene sulfonic acid was molded at 300-325°C at 10-15, 000 psi. Strip specimens, 0. 377 by 4. 00 inches with thicknesses varying from 0. 020 to 0. 035 inches were prepared for dynamic mechanical testing. The dynamic mechanical properties - shear modulus, and damping, were measured on a recording torsion pendulum. True glass transitions (Tg) were not measured since damping peaks and modulus fluctuations appeared to reflect water removal or interaction of various salt species.

The extent of reaction in molded specimens was determined by measuring the intensity of unreacted metal oxide cyrstal peaks in X-ray goniometer tracings which were standardized by mixed but unreacted powders of known composition. For ZnO the proportionality between the (100) (101) lines remained constant and were used to estimate intensity. The estimated error was plus or minus 2%.

Results and Discussion

Due to the di-acid character of the phosphoric acid group and to the possibility of chelated structures with residual hydroxyl (from PVOH) groups, the possible number of species existing in the PVP salt-form system is greater than in the corresponding acrylic system. This is schematically indicated in Figure 1. These salt forms are in addition to unreacted polyacid and metal oxide. A system containing these species exists as an intertangled network of the species present and not as a mixture of the various species. However each specie will have its own influence upon the total properties, modulus, damping, Tg, etc. Thus

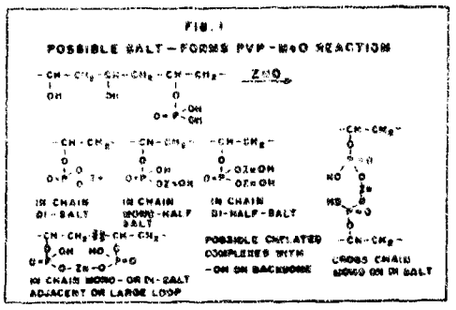

cross-chain or large-loop salt forms will contribute more to stiffening than in-chain salt forms due to greater restrictions on rotation. From a simple filler viewpoint di-salt forms will contribute more, unit-wise, than half-salts because of higher metal content per unit. From a bond-strength standpoint di-salts should interchange less readily than half-salts. However, due to the different acid strengths of the $P\begin{smallmatrix}OH\\OH\end{smallmatrix}$ group there may be a considerable tendency to interchange at elevated temperatures thus resulting in lower modulus, higher damping and lower Tg levels.

In a partially reacted system there is no way of knowing which specie may act as the continuous or discontinuous phase. Nevertheless, one can assume that any unreacted metal oxide will act as filler to all other species in relation to the volume fraction of that phase present. Because of the complexity of the situation, reacted metal oxide has been considered as di-salt (in accordance with the general equation in Appendix I) for purposes of modulus calculations.

A series of ZnO and PbO in situ molded PVP products were prepared using 100 and 200% of the stoichiometric metal oxide theory as indicated in Table I. The extent of reaction by X-ray, where obtained, the molding conditions, and the shear modulus found at 25°C, are also given.

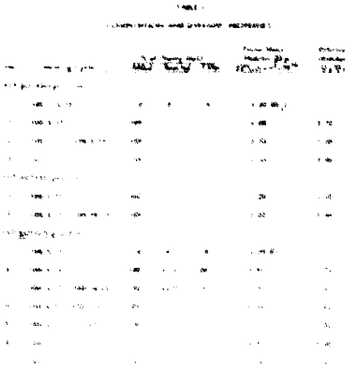

Relative modulus G_2/G_1 values are plotted in Figures 2, 3, 4 for the three systems against the theoretical reinforcing action of spherical filler particles as calculated by three theories: Kerner, Guth-Smallwood, and Mooney, using the relations in Appendix I of reference 1.

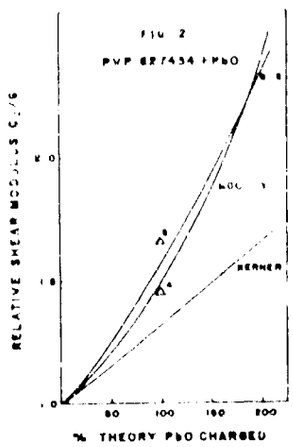
FIG 2
PVP 627434 + PbO
RELATIVE SHEAR MODULUS G'/G
MOONEY
KERNER
50
100
150
200
% THEORY PbO CHARGED

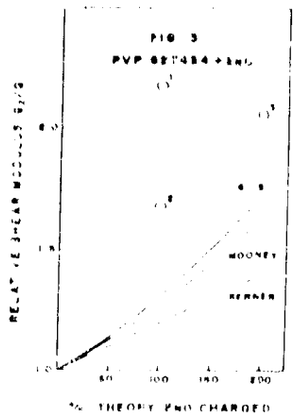
FIG 3
MOONEY
KERNER
% THEORY ZnO CHARGED

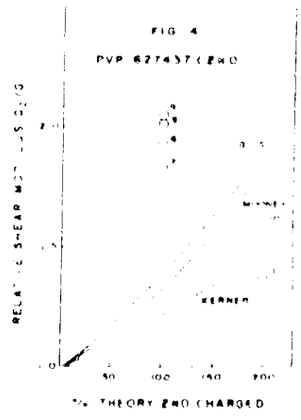
FIG 4
PVP 627437 + ZnO
KERNER
% THEORY ZnO CHARGED

Improvement ratios (IR) (increase in modulus found over that calculated only as filler) are listed in Table II.

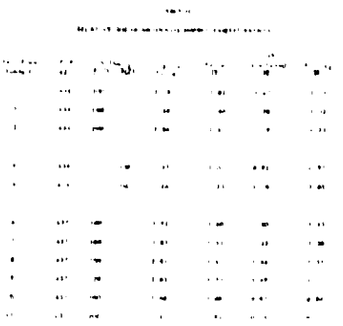

From Figure 2, it is apparent that the PbO merely exhibited filler action at the molding conditions used. For the low molecular weight PVP, Figure 3, the improvement due to ionic bonding over filler action was 65-82% for 100% theory ZnO moldings at 100°C. At 150°C molding or for 200% theory ZnO the improvement dropped to 25-47%. For the high molecular weight PVP, Figure 4, at 100% theory ZnO, the improvement over filler action ranged from 40-70% regardless of molding temperature with 150° being better than 100°C. Pressure, 5-10,000 psi variation, gave only minor differences in modulus. Again, for 200% theory ZnO, modulus was lower and would appear to be determined by filler action. However, about 77% of a theory ZnO was found reacted (by X-ray) so that one must conclude that excess ZnO favored in-chain half salts which are free to rotate and thus do not greatly improve modulus.

When it is realized that the PVP was only 29-36 mole % converted to the phosphate and that the phosphate was only 40-75% converted to the salt it becomes of interest to calculate (1) a possible modulus for the completely converted phosphate di-salt, and (2) an organic weight/Zn/modulus ratio for the PVP system in comparison to the zinc polyacrylate system. These values will give one some idea of the possible effect of acid strength variation upon modulus.

Modulus calculations for the completely converted phosphate di-salt (at the 35.7 phosphate level) were made as described in Appendix I and are summarized in Table III. The results indicate that the product species distribution is different depending upon the molding conditions and that higher pressures and temperatures act to give lower-modulus species distributions. This probably reflects the greater variety of species available due to di-acid character of the phosphate and increased bond interchange reactions with increased temperature.

TABLE III

CALCULATED MODULUS OF COMPLETE PVP DI-SALT
(PVP - 35.7% Phosphate) (100% Theory ZnO)

Molding Cycle °C/Kpsi/min.	100/5/ 5	100/5/15 100/10/15	100/5/15 150/5/15
Shear Modulus Calc. dynes/cm^2 x 10^{10}	9.36	8.21	7.04

A comparison of the PVP Zn salt system with the polyacrylic (PDR-14) Zn salt system was made on the basis of calculated modulus obtainable vs. an organic/metal weight ratio in order to further observe the possible effect of acid strength (ionic bond strength). This is shown in Table IV. The data indicate that even at an organic/Zn ratio 50% higher for PVP than for the carboxylate and for PVP only 35.7% phosphorylated, moduli are obtained which are substantially higher than for the polycarboxy acid. This appears to reflect the increased ionic character of the salt bonds due to higher acid strengths of the PVP polyacid.

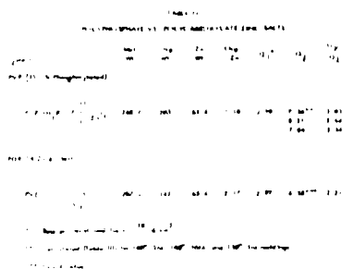

Dynamic modulus and damping vs. temperature curves are illustrated in Figure 5 representative of the PVP (627437) (35.7% phosphate) plus ZnO system on which X-ray data were obtained (see Table I). The banded area contains the four curves 6, 7, 8, 9 for 100% theory ZnO at either 100° or 150°C and 5 or 10,000 psi. The shapes are equivalent and the broad damping

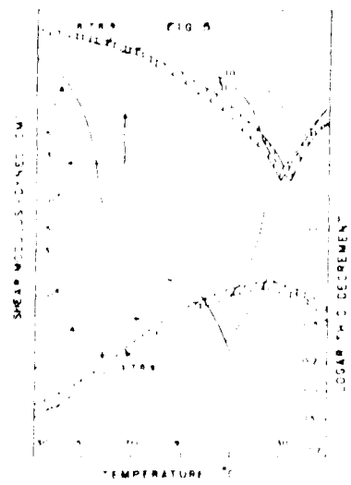

character is evidence for specie mixtures and water which appeared to foam out at about 130°C. The discontinuity at 130° probably represents stiffening due to loss of water or specie reaction or both.

Curves 10 and 11 are for 200% theory ZnO and are different in shape from the 100% ZnO curves. Flatter modulus vs. temperature is noted through 110° but the loss above 110° is more rapid. Again the discontinuity occurs between 120-140°. Samples heated above 150° exhibited severe decomposition, swelling, and irregular behavior both with modulus and damping.

Curves (A) for the base PVP polyacid indicates the presence of substantial amounts of water which seems to be driven off in two steps at about 55° and 90°C.

Moldings of PVP-ZnO were immersed in boiling water for 10-15 minutes without evidence of swelling or softening. No quantitative studies were made. However, this observation should be qualitatively compared with Zn polystyrene sulfonate (see below).

Positive pressure moldings were attempted with mixed powders of HSPS (containing about 20% of the groups as NH_4^+ salt) and various oxides including ZnO, PbO, BaO, and CaO at 100% theory level. No reaction or fusion of any powder was noted at 200°C and 10,000 psi. With BaO and CaO only partial (less than 10% fusion) was obtained at 300°C and 10,000 psi. However, with ZnO at 300-325°C and 10-15,000 psi (pressure applied at room temperature and held throughout heating time) complete fusion was obtained, yielding a very brittle light amber and almost transparent specimen. The extreme brittle character prevented obtaining samples for torsion pendulum testing.

X-ray analysis of the product showed complete absence of unreacted ZnO. A half inch piece of this Zn salt was boiled in water for 10-15 minutes with resultant swelling to 25-50 times the original volume. The swollen "blob", dried in air over night, returned to its original dimensions and hardness.

Conclusions and Recommendations for Future Work

I. Phosphorylated PVOH Polyacids

Plus Points

1. Strong acid results in higher modulus metal salts due to stronger ionic bonding as compared with polycarboxy acids (PDR-14) even at phosphorylation levels of only 35 mole % and organic to Zn ratios 50% higher than in the carboxy series.
2. For 100% phosphorylation one might estimate modulus values approaching 2 times that for carboxy salts.
3. Salts may be water insensitive if complete reaction was obtained.

Negative Points

1. Complete phosphorylation of PVOH is very difficult and would require considerable study.
2. PVP polyacids are extremely hygroscopic.
3. PVP polyacid salts are not heat stable. Decomposition of the C-O-P bond sets in above 150°C.
4. Dibasic character of PVP polyacids leads to a large variety of salt species which may have a greater tendency to interchange at higher temperatures if incompletely reacted.

Recommendations

1. Further work, if any, on phosphorus acids should be done on polyvinylphosphonic acid with a more stable C-P bond. Unfortunately, it is difficult to prepare high molecular weight polymers of this type.

II. Polystyrene Sulfonic Acid

Plus Points

1. Salts and acid have high heat stability.
2. Salts may be prepared, *in situ*, by molding certain metal oxides and polyacid mixed powders.
3. Modulus values of salts can be expected to be much higher than carboxy acid salts due to stronger ionic bonding resulting from higher acid strength.

4. Monobasic character of the polyacid would lead to fewer salt species with higher stability.

Negative Points:

1. HSPS is extremely hygroscopic, absorbing about 1 mole H_2O per SO_3H (or about 10% wt.) in 12 minutes at room temperature.
2. ZnSPS is extremely water sensitive. In fact, Baer[4] reports only the Al or Ba salts to be water insoluble (no quantitative data). Present studies confirm this on a wide variety of salts.

Recommendations

1. Further work is indicated using NH_4^+ free HSPS (on hand) with aluminum salts to form possible water insoluble products.
2. Since vinyl sulfonic acid can be prepared and polymerized, such polyacids should be studied.
3. Sulfonation of PVOH to form polyvinylsulfate types should be studied, however, decomposition problems may parallel these of PVP above and completeness of reaction will again be difficult.

References

1. Fields, J. E. and L. E. Nielsen. "Dynamic mechanical properties of some polymeric acid zinc salts," This report p. 109.

2. Daul, G. C., J. D. Reid and R. M. Reinhardt. Ind. Eng. Chem., 46, No. 5, 1042 (1954).

3. Daul, G. C. and J. D. Reid. U.S. 2,609,360 (1952).

4. Baer, M. "Preparation of water soluble sulfonated polystyrene," Monsanto proprietary report.

Appendix I

Modulus Calculations

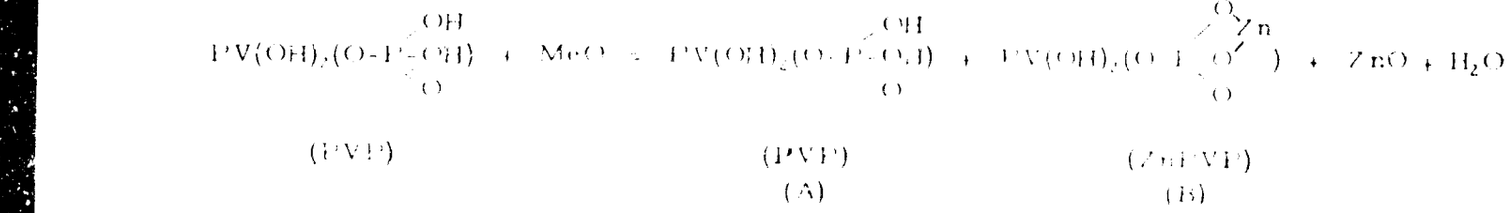

(PVP) (PVP) (A) (ZnPVP) (B)

Based on X-ray analysis the product mixture from 1 mole of PVP is considered to consist of 0. X moles di-salt (B), 1-0. X moles unreacted PVP (A), 1-0. X moles unreacted MeO as filler and 0. X moles water. The unreacted MeO filler and water of reaction were distributed between A and B in proportion to their respective volume fractions, ΦA and ΦB. These volume fractions were calculated from X-ray analysis and from calculated densities for the appropriate phosphorylated products.

PVP Preparation	627434	627437
Mol. Wt. PVOH	Low	High
Mole % Phosphorylation	29.0	35.7
Mol. Wt. per P atom	233	205
Calc. Density PVP	1.46	1.50
Mol. Wt. Di-Zinc Salt	296.4	268.4
Calc. Density Di-Zinc Salt	1.96	2.01

The MeO used was either ZnO (d = 5.47, m. wt. = 81.4) or PbO (d = 9.0, m. wt. = 223.2).

Since no product with 100% reaction was achieved the objective of the calculations was to calculate a modulus of the complete metal salt from a knowledge of the product mixture composition. The reaction and calculation steps for ZnO include:

1. $PVP + ZnO = \underset{(A)}{PVP} + \underset{(B)}{PVPZn} + \underset{(filler)}{ZnO} + H_2O$
2. Add H_2O back into (A) and (B) in relation to ΦA and ΦB where $\Phi A + \Phi B = 1$.
3. Add ZnO filler (f) into (A) and (B) in relation to ΦA and ΦB to obtain filled species fA and fB where $\Phi fA + \Phi fB = 1$.

On a volume basis (v = volume):

	System 1		System 2	
	↓		↓	
Products →	vA	+	vB	and $\Phi A + \Phi B = 1$
	+		+	
	vf_A		vf_B	
	∥		∥	
Sample 3 →	vfA	+	vfB	v Total System (TS)

Therefore in:

System 1 - $vA + vf_a = vfA$ and $\Phi A + \Phi f_a = 1$

System 2 - $vB + vf_b = vfB$ and $\Phi B + \Phi f_b = 1$

System 3 - $vfA + vfB = vTS$ and $\Phi fA + \Phi fB = 1$

For System 1: Knowing G_A, ΦA and Φf_a, calculate the modulus for the filled A system (G_{fA}) by the Mooney equation.

For System 3: From the calculated G_{fA} and knowing ΦfA, ΦfB, and G_{TS} (determined by experiment), calculate the modulus for the filled B system by either the law of mixtures:

$$G_{TS} = (\Phi fA)(G_{fA}) + (\Phi fB)(G_{fB})$$

or by the long-form Kerner equation where it is assumed that the cross-chain di-salt B is the continuous phase with a Poisson's ratio of 0.3. The modulus calculated by Kerner results in answers 5-15% higher than by the law of mixtures probably due to specie interaction since System 3 is not a true mixture of species.

For System 2: From the calculated G_{fB} (by Kerner) and knowing ΦB and Φf_b, calculate the modulus of the metal phosphate ad di-salt (G_B) by the Mooney relation.

The calculated values so derived for three molding cycles used with PVP (627-137) plus 100% theory ZnO are given below,

Molding Cycle: °C/Kpsi/min.	100/5/15	100/5/15 100/10/15	100/5/15 150/5/15
% ZnO reacted, wt. or mole	41.4	43.9	77.3
ΦA (PVP unreacted)	0.586	0.561	0.227
ΦB (PVP Zn Salt)	0.414	0.439	0.773
In System 1:			
G_A (PVP found)(x 10^{10} d/cm^2)	3.1	3.1	3.1
$\Phi A + H_2O$	.9425	.9448	.9776
Φf	.0575	.0552	.0224
G_{fA} (calc. by Mooney)	3.62	3.60	3.28

Molding Cycle: °C/Kpsi/min.	100/5/15	100/5/15 100/10/15	100/5/15 150/5/15
In System 3: (By Kerner)			
G_{TS} (found)	5.98	5.67	6.24
G_{fA} (calc. above)	3.62	3.60	3.28
ΦfA	.59	.56	.23
ΦfB	.41	.44	.77
G_{fB} (calc. by Kerner)	10.94	9.53	7.46
In System 2:			
G_{fB} (calc. above)	10.94	9.53	7.46
$\Phi B + H_2O$	.9424	.9451	.9776
Φf_b	.0576	.0549	.0224
G_B (PVP Zn Salt)	9.36	8.21	7.04

Similar calculations were not made on the 627437 system plus 200% theory ZnO since the modulus increase was similar to that required by filler action (see Figure 4). However, X-ray analysis indicated about 76-77% of a theory ZnO reacted, and the excess ZnO thus appeared to promote formation of only in-chain type half-salts which would not increase modulus because of rotational freedom. Further, such calculations were not made on the low molecular weight PVP (627434) system due to the absence of X-ray data.

PROPERTIES OF ZINC POLYACRYLATE AND ITS COMPOSITES

(L. E. Nielsen and D. M. Hemmerly)

Work has continued on measuring the mechanical properties of zinc polyacrylate and composites made by using this polyelectrolyte as the matrix material. The matrix material gave compressive strengths of 54,000 psi (maximum) and 47,000 psi (average). A composite containing 40 volume percent iron flake gave a compressive strength of 43,000 psi while one containing 20 volume percent aluminum flake gave a strength of 20,500 psi. Because these were first attempts and because too small a number of samples were made to get good statistical averages, it is believed that considerably higher values are achievable with the metal-filled composites.

Typical shear modulus data are:

Material	Vol. % Loading	Shear Modulus (psi) 25° C	300° C
Zn Polyacrylate (ZP)	--	950, 000	520, 000
ZP + Al powder	40	1, 370, 000	870, 000
ZP + Iron flake	40	1, 380, 000	870, 000
ZP + Cu powder	20	1, 270, 000	870, 000
ZP + Zn powder	20	920, 000	580, 000
ZP + boron fibers 1/8" (randomly oriented)	20	1, 530, 000	1, 530, 000

The more generally measured Young's modulus should be about 2.7 times as great as these values for shear moduli. The value for the composite filled with randomly oriented boron fibers is slightly less than the value predicted by the theory of Nielsen and Chen. It is also worth noting that the modulus values for the metal powder filled composites are less than what might be expected from some theories. This is because the modulus of the matrix is so high itself that it is beginning to approach the modulus of the fillers.

Attempts have been made to measure tensile strengths, but the present equipment is not adequate for such tests on brittle specimens. The zinc polyacrylate matrix material appears to have a tensile strength of about 10, 000 psi or higher. Metal powder filled composites have experimental values of 3500 to 5000 psi, but these values are believed to actually be much too low for the tensile strength.

Coefficients of thermal expansion are very small for polyelectrolytes compared to normal polymers; in fact the values are in the same range as common metals. The following table gives data on polyelectrolytes and on polystyrene:

Material	Volume Percent	Coef. Expansion/°C
Polyacrylic acid	--	5.52×10^{-5}
Zinc polyacrylate (ZP)	--	1.44×10^{-5}
ZP + Iron flake	40	1.46×10^{-5}
ZP + Aluminum flake	40	2.14×10^{-5}
Polystyrene	--	8.1×10^{-5}

FRACTURE TOUGHNESS OF GLASS FILLED POLYPHENYLENE OXIDE COMPOSITES (A. Wambach, K. Trachte and A. DiBenedetto)

In the design of any load bearing structure, the choice of the material must be influenced by its ability to resist fracture. The ability to resist fracture can be measured by a property called fracture toughness. It is related to the energy required for a crack to propagate through a material.

Fracture toughness testing permits an evaluation of the stress level or strain energy required to cause fracture. The fracture toughness depends on the adhesion between the matrix and the reinforcing phase, the degrees of dispersion of the reinforcement, and the properties of the constituent phases. The sensitivity of fracture toughness to subtle changes in structure gives it value as a measure of the performance and efficiency of a composite.

In this study, the fracture toughness has been determined using double edge-notched tensile specimens. All fracture surfaces have been carefully examined by using optical, electron scanning and electron microscopy. Standard micro tensile tests have also been used in order to determine tensile modulus and yield strength.

Preliminary data of polyphenylene oxide (PPO) filled with untreated glass beads at volume fractions of .05, .10, and .15 indicate an increase in fracture toughness with filler concentration. By treating the beads with A-1100 silane at a volume fraction of .10, a significant decrease of about 60 percent in toughness is observed while at the same time the tensile modulus is unaffected and the ultimate strength is increased only 4 percent. Thus, by increasing the volume

fraction of glass beads having no adhesion to the polymer, the energy required to propagate a crack increases; by adding an effective coupling agent, these energy requirements drop. Fractographic evidence of improved adhesion is shown for the beads treated with A-1100 silane coupling agent. A tentative mechanism for crack propagation is postulated from the existing evidence.

Theory

Consider an unstressed sheet with a crack at one edge. As a stress is applied perpendicular to the axis of the crack, the two surfaces of the crack separate. Stress immediately concentrates around the tip of the crack, causing the strain in this region to become very large. Very little average stress is required to cause plastic flow in the region very near the crack tip. As this strain increases, the sharp tip becomes relatively blunt. At a critical value of strain, the material finds it less difficult to fracture than to deform further. Griffith[1] and Orowan[2] have discussed this concept from an energetic point of view. It is postulated that a crack will propagate when the decrease in elastic strain energy is at least equal to the energy required to create a new crack surface. The release of elastic strain energy is the only source of energy to the fracture process zone. This implies that all fracture energy (i. e., the plastic work, crazing, generation of heat, and creation of new surfaces) must be obtained from release of elastic strain energy.

Griffith and Orowan use Inglis'[3] elastic analysis in order to calculate the elastic strain energy around an included crack. The Griffith criterion for crack instability is that the net energy change in the solid is negative as the crack length increases (i. e. $d\Gamma/da < 0$).

For a continuous sheet with an included crack, subjected to a uniform, uniaxial stress, the critical gross stress for plane strain is[2]:

$$\sigma_c = \left(\frac{2 E \gamma}{\pi a (1-\nu^2)}\right)^{1/2}$$

where γ is the total energy required to create 1 cm^2 of fracture surface, (a) is the half length of the included crack at instability, ν is the Poisson ratio and E is the tensile modulus.

Experimental results[4] show that the energy γ is roughly equal to the thermodynamic surface energy for a brittle solid such as glass, but it several orders of magnitude greater than the surface energy for metals and plastics.

The Griffith-Orowan theory has not been used extensively for semi-brittle materials such as high strength steels, aluminums, and most polymers. One of its limitations appears to be its inability to modify the elastic strain energy for the inelastic deformation in the vicinity of the crack tip.

Irwin[5] realized this possible shortcoming and has offered a related approach which permits a calculation of the size of the plastic zone in front of the crack tip. From this theory one can calculate the energy and stress level required for the crack movement to change from a slow stable growth to a rapid, catastrophic propagation. A material property called the strain energy release rate, $\mathcal{G}_{Ic}$, characterizes this condition. The strain energy release rate includes all contributions to the energy dissipated as the crack advances, including those which are not related directly to that required for the formation of new surface area. For the edge notched sheets shown in Figure 1, Irwin has shown that the fracture toughness is characterized by the following equations[6]:

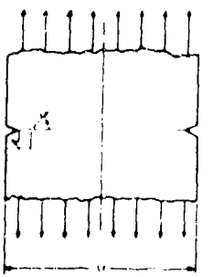

Figure 1 Double Edge-Notched Sheets are Used for Fracture Toughness.

$$K_{Ic} = \sigma W^{1/2} (\tan u + 0.1 \sin 2u)^{1/2}$$

$$u = \frac{\pi a}{W} + \frac{K_{Ic}^2}{2 W \sigma_y^2}$$

$$\mathcal{G}_{Ic} = \frac{K_{Ic}^2 (1-\nu^2)}{E} \quad \text{(plane-strain)}$$

where K_{Ic} and $\mathcal{G}_{Ic}$ are the stress intensity parameter and strain energy release rate and are material properties of the composite. The quantity σ is the gross-section tensile stress, σ_y is the yield strength of the composite, and (a) is the

crack size at the onset of catastrophic failure. All of these are measurable properties of the composite. The size of the plastic zone around the crack tip is characterized by the length r_y:

$$r_y = \frac{K_{Ic}^2}{2\pi\sigma_y^2}$$

This "plastic zone size" is often very small in the systems we have been studying but it is felt that it maybe an important parameter for characterizing the dissipative processes in the vicinity of the crack tip.

It can be shown that the strain energy release rate is related to the energy parameter of the Griffith-Orowan theory by:

$$\mathcal{G}_{Ic} = 2\gamma$$

Experimental Results

The double edge-notched tensile specimen, shown in Figure 2, was used for toughness testing. The geometry of the specimen conforms to the dimensions recommended by Irwin[6].

The samples are notched with a custom designed, carbide-tipped flycutter used on a milling machine. The notch dimensions are:

Depth - 0.200 ± 0.001 inches

Width - 0.100 ± 0.003 inches

Included angle of tip - 45°

Root radius of tip - < 0.0008 inches.

The notched root radius can be of extreme importance and is a subject of great discussion in literature on the fracture toughness of metals[7]. There is essentially no data that can be used to determine the importance of root radius in notched plastics, however.

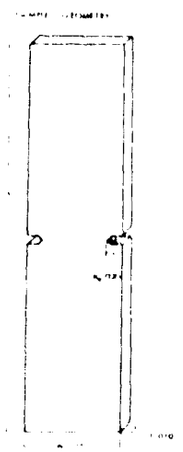

Figure 2

Under the test conditions we have been using, cracks grow slowly from the notch tip before rapid propagation. It is thought that as long as the rapid propagation is preceeded by slow crack growth, the notch root radius at the onset of catastrophic failure is probably small enough so that the fracture toughness is relatively insensitive to the initial machined notch radius.

With the notch radius being effectively zero, another major consideration is whether the machining seriously affects the properties near the notch. Fortunately PPO is birefringent which allows the observation of the disruptance near the crack tip by polarized light. When the polymer is strained nonuniformly, colored birefringent rings are created showing the disturbed regions. After machining the notches in the unfilled PPO, only slight disturbance was noticed. The measured disturbance region extended less than .002 inches. If the notch was further extended with a razor blade, bright rings were apparent with the disturbed region extending to about .010 inches from the tip. Since the plastic zone, r_y, was determined to be about .030 inches, it was assumed that the disturbance due to machining was negligible. The filled polymers were rather opaque and it was difficult to measure the region of disturbance due to machining with polarized light. However, since the calculated r_y is about .070 inches, again the disturbance is assumed negligible. It should also be pointed out that the slow crack growth region extends an average distance of .020 inches which would appear to insure that the machining effects were negligible.

The specimens are mounted in the specimen holders shown in Figure 3. The centerline of the specimen is within $\pm$ 0.001 inches of the loading axis. In order to improve on the pin loading suggested by Irwin (and used exclusively for testing of metals), the specimens are glued to the specimen holders with Eastman 910 adhesive. The specimen holders are then pin loaded. It is felt that loading via the adhesive joint permits a more uniform load than afforded by pin loading.

After allowing the adhesive to set (at least 2 hours) the samples are mounted on the Instron in an environmental chamber. The information needed for analysis

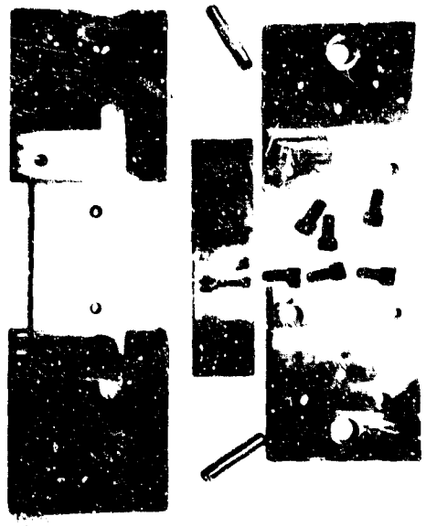

Figure 3 Mounting of Tension Specimen.

can then be determined from the chart record and specimen halves. The fracture toughness test analysis sheet (Figure 4) outlines the calculation procedure.

Figure 4 Fracture Toughness Test Calculation Sheet

Date

Sample No.

Cross Head Speed — Chart Speed

Temperature

σ_y = Yield Stress

E = Tensile Modulus

F_ℓ = Fracture Load — Elongation at Break

Side Crack Started From

Sample Dimensions

Notch Radius - Side 1: — Side 2:

W = Width

T = Thickness

A_E = Width x Thickness

a_0 = Machined Half Crack Length

a = Measured Half Crack Length

Calculations

σ_n = Gross Section Stress = $\frac{F_\ell}{A_g}$

$\frac{\pi a}{W}$ =

$(\frac{\sigma_n}{\sigma_y})^2$ =

$K_{Ic} = \sigma_n (q_2 W)^{1/2}$ = where q_2 =

$r_y = K_{Ic}^2 / 2\pi \sigma_y^2$ =

$\mathcal{G}_{Ic} = (K_{Ic}^2 / E)(1-\nu^2)$ =

$\gamma = \frac{1}{2} \mathcal{G}_{Ic}$ =

Fracture toughness tests have been made for pure PPO over a range of thicknesses of .03 to .20 inches, pure PPO over a range of crosshead rates of .05 cm/min to 5 cm/min, PPO filled with untreated glass microbeads (diameter = 1-30 microns) at filler concentrations of 5, 10 and 15 percent by volume, and PPO filled with A-1100 silane treated glass microbeads. In addition, the fracture toughness for PMMA was determined as a check with published data. The tests of pure PPO over a range of thicknesses were carried out at room temperature; all others were completed in the environmental chamber at 68 ± 0.2°F. The data is summarized in Table I.

The calculated γ-fracture toughness of Plexiglas II UVA (PMMA) was 2.02×10^5 ergs/cm^2. This value agrees well with a published value of $2.1 \pm 0.85 \times 10^5$ ergs/cm^2[4]. The calculated plastic zone for PMMA is only .0036 cm. Because of its small size, the plastic zone correction factor is negligible and any good purely elastic analysis is sufficient.

The study of pure PPO over a range of thicknesses from .03 to .20 inches was made to determine the state of stress during testing. The results are shown in Figure 5 and indicate that K_{Ic} is independent of thickness over the range studied. We feel that we are well within the plane strain region for thicknesses greater than 0.05 inches. Figure 6 shows the relative plastic zone size as a function of thickness. For an accurate fracture mechanics analysis, the plastic zone size should be smaller than the sample thickness. A sample thickness of 0.1 inch is considered to be suitable for our testing conditions.

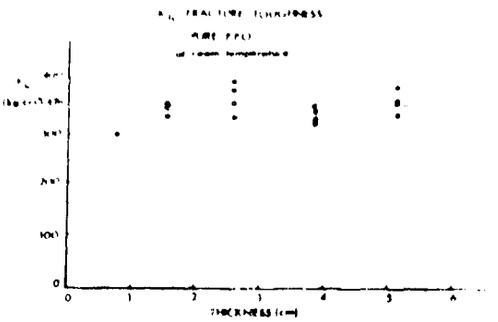

Figure 5

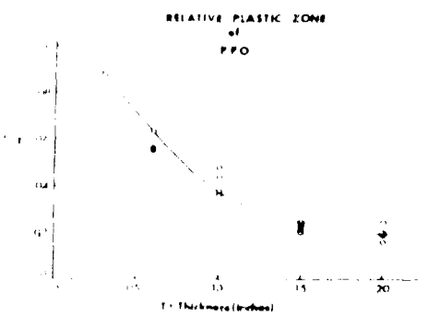

Figure 6

Since elongation at break and tensile strength are known to depend on the viscoelastic properties of a material, the strain rate dependence of fracture toughness was investigated. Pure PPO was tested on an Instron over the range of crosshead speeds of .05 to .5 cm/min. Although the crosshead speeds available include up to 50 cm/min, the recording pen response time limited the useful range to 5 cm/min. The data shown in Figure 7 indicates no significant change for fracture toughness due to crosshead rate. Although fracture toughness probably does vary with strain rate, there is no significant effect due to the relatively small range studied. There appears to be little value in varying the crosshead rate as a parameter for future studies on this system using the Instron tester.

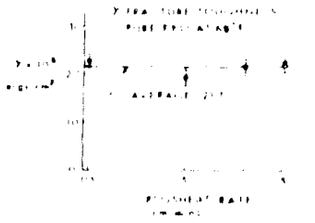

Figure 7

Preliminary tests of the PPO filled with untreated glass beads indicate that crosshead rates of about 0.1 centimeters per minute permit extensive yielding before fracture. This yielding is caused by the specimen breaking at a net stress near its yield point and thus does not permit proper analysis. This difficulty was overcome by increasing the crosshead rate to 2 cm/min at which all subsequent tests were carried out.

Both K_{Ic} and γ-fracture toughness of the untreated glass bead composites increase linearly with volume fraction of filler up to about 15% loading (Figures 8 and 9). An additional point at 20% loading indicates that the fracture toughness

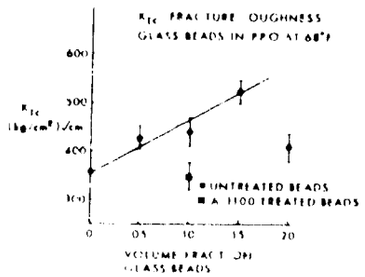

Figure 8

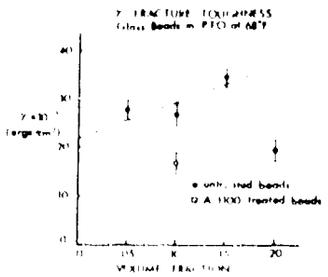

Figure 9

may reach a maximum in the range 15-20%. Although this type of behavior is reasonable, it is not yet certain whether the decrease is associated only with the fabrication process (the 20% specimens were made from a different batch of raw materials than the other concentrations).

Fractographic evidence indicates that there is probably little or no adhesion between the untreated beads and the polymer. When there is no adhesion between phases one may consider that each bead acts as a void in the solid. From the data, it seems that a low concentration of such voids causes an increase in fracture toughness. Treatment of the beads with A 1100 silane coupling agent significantly decreases the fracture toughness of the composite when compared to the same concentration of untreated beads. The γ-fracture toughness is even lower than that of the pure matrix. Fractographic evidence shows that the treated beads have a greater degree of adhesion to the polymer matrix. Thus, it follows that improving the integrity of the system (i.e., removing the voids) seems to decrease fracture toughness.

A complete understanding of this behavior is not available at this time. However, it does appear that the increased energy requirements for the system with the untreated beads is related to additional physical disturbance (plastic flow, secondary cracks and crazing) at and beneath the fracture surface. By improving the adhesion, this disturbance is restricted to the fracture surface and thus the fracture process requires less energy. As the concentration of beads (or voids) increases there is a greater chance of agglomeration and coalescence of voids which at high concentrations should lead to a decrease in fracture toughness. (In the limit of no matrix, no energy is required to separate the beads.)

The fact that at 10 percent by volume of glass beads in PPO the γ-fracture toughness was decreased by 60% due to treatment with A-1100 is interesting considering that the ultimate strength increased only four percent and the elastic modulus remained constant. It appears that fracture toughness testing may be a valuable tool in determining the relative adhesion between the matrix and filler for many composite systems.

Yield stress and tensile modulus, required to calculate K_{Ic} and $\mathcal{G}_{Ic}$, are determined by the use of microtensile samples. The samples are milled from the 1 1/4 by 5 inch molded bars to the specifications of ASTM test D 1708[3].

The yield stress is a relatively difficult property to determine. A thermoplastic is viscoelastic which infers that there will be some flow at any stress level. The object of determining a yield stress is to determine the stress at which general plastic flow beings to occur. This level should be indicated by a noticeable change in slope in the stress-strain curve. It was very difficult to differentiate this from the inherent slippage of the sample in the Instron's wedge-action grips. It was felt that an offset stress had little merit due to the unknown slippage. The best alternative was to choose a crosshead rate that permitted the material to exhibit a ductile yield (i.e. the stress-strain curve has a maximum). The ultimate stress was then a good reproducible measure of the stress required for yielding. For the convenience of testing, 0.2 cm/min was

chosen as the crosshead rate for all samples. Only the PMMA samples failed to show this kind of yielding and required that an approximate 2 percent offset be used.

Figure 10 shows that the ultimate strength of the pure PPO increases about linearly with the logarithm of the crosshead rate. The addition of untreated glass beads to PPO decreases the ultimate strength as shown in Figure 11. The results show little scatter, with the curve showing sharpest decrease in strength in the low concentration range. By treating the beads with A-1100 silane at 10 percent by volume glass beads, the strength was increased by 4 percent over the untreated beads but remained far below that of the unfilled PPO.

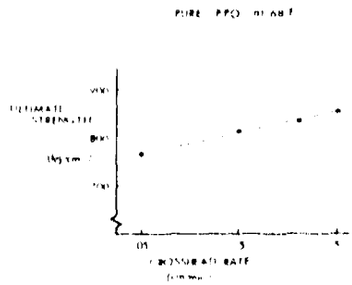

Figure 10

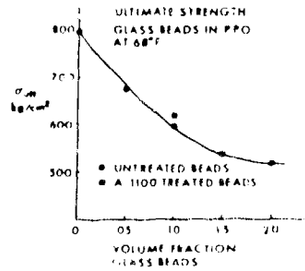

Figure 11

The tensile modulus was determined from microtensile samples and in most cases was checked by one-half inch wide bars. The strain was measured by Instron strain gage extensometers mounted on the samples. The extensometers are quite accurate (within 1/2%) but it was found that extreme care must be taken in placement on the samples. Failure to make triplicate readings may permit a 5 percent error due to misalignment.

Figure 12 shows that the tensile modulus increases with filler concentration. The increase appears to fall within the region predicted by the Kerner[9] and van der Poel[10] equations. Treatment with A-1100 causes no significant change of elastic modulus.

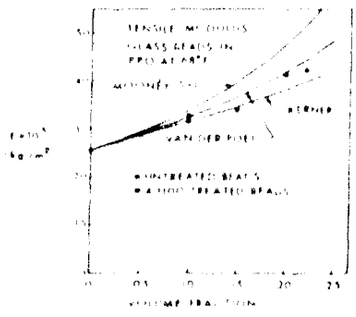

Figure 12

Fractography Studies

The fracture surfaces of pure PPO were examined with the optical microscope (Figure 13) and the electron scanning microscope (Figures 14 and 15).

Direction of Propagation

Figure 13 Parabolas Characteristic in the Fracture Surface of a Glassy Thermoplastic, 240 X.

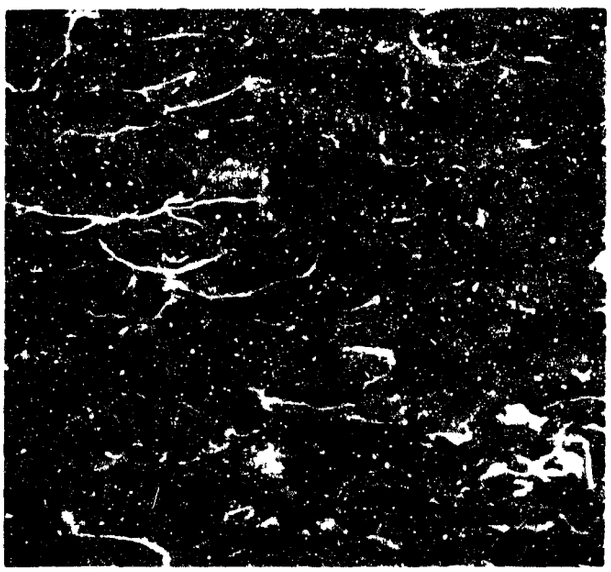

Direction of Crack

Figure 14 Electron Scan Pictures of PPO Surface, 200 X.

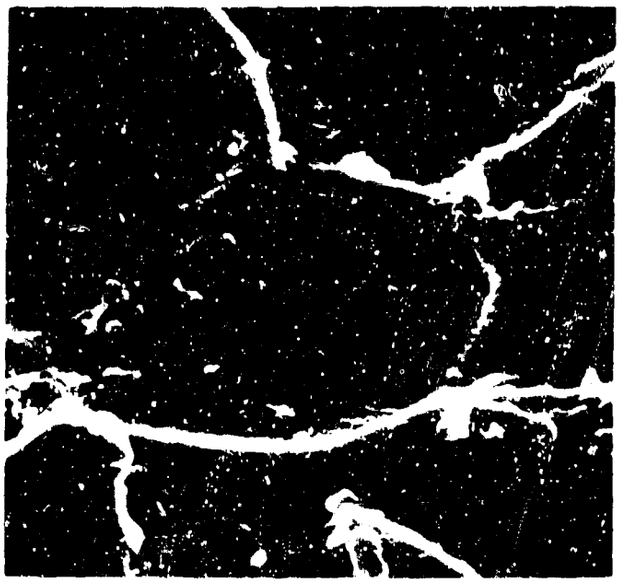

Direction of Crack

Figure 15 Electron Scan Pictures of PFO Surface, 1000 X.

The parabolic character of the crack front and the topology are clearly shown. Figure 16 qualitatively shows the relation between the parabolic front and the interaction of different crack fronts.

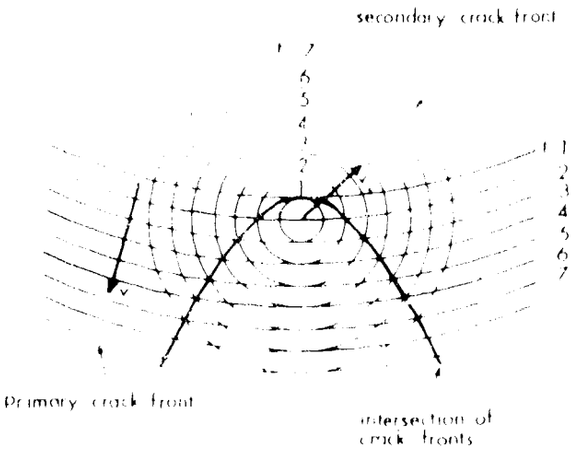

Figure 16 Formation of Characteristic Parabola Glassy Thermoplastic.

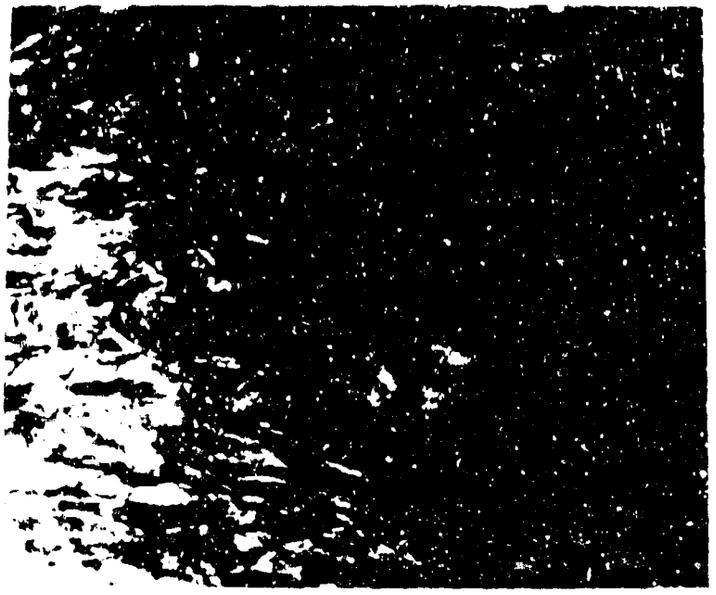

Direction of Propagation

Slow Growth Region

Rapid Propagation Region

Figure 17 Crack Velocity Transition Region in PPO Optical Micrograph, 80 X.

Figure 17 shows a region of the pure PPO fracture surface in which the crack growth goes through a transition from slow growth to rapid propagation. In the slow growth region the surface is nearly featureless. Suddenly, the crack propagates rapidly and the surface shows the characteristic parabolic patterns. A probable explanation of this observation is that during slow growth, the stress level ahead of the crack is not high enough for the flaws to become operative. As the stress level builds up, the flaws become operative and the crack propagates rapidly. Further study will be needed to verify this suggestion.

Optical pictures (Figure 18) of the untreated glass bead filled PPO show grain-like regions which appear to parallel, in some respects, the paraboloids of the unfilled system. Optical photographs of A-1100 treated composites appear identical with those of the untreated. The electron scan pictures (Figures 19 to 22) show obvious improvement of adhesion when A-1100 coupling agent is used. One cannot tell from these pictures whether there is [illegible] orientation in

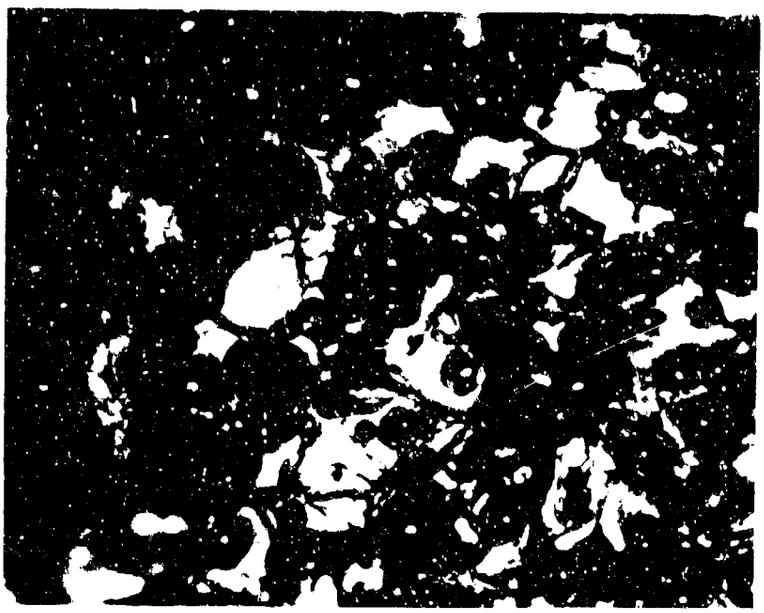

Direction of Crack Propagation

Figure 18 Fracture Surface of a PEO/ Glass Bead Composite (Optical Photograph), 240 X.

Diameter of Micro beads = 1-50 u

Figure 19 Electron Scan Photograph of Untreated Glass Beads (10% by volume) in PEO, 212 X.

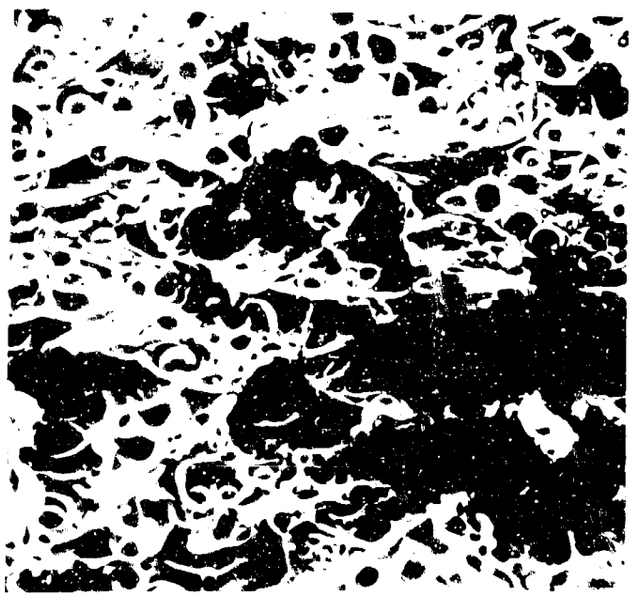

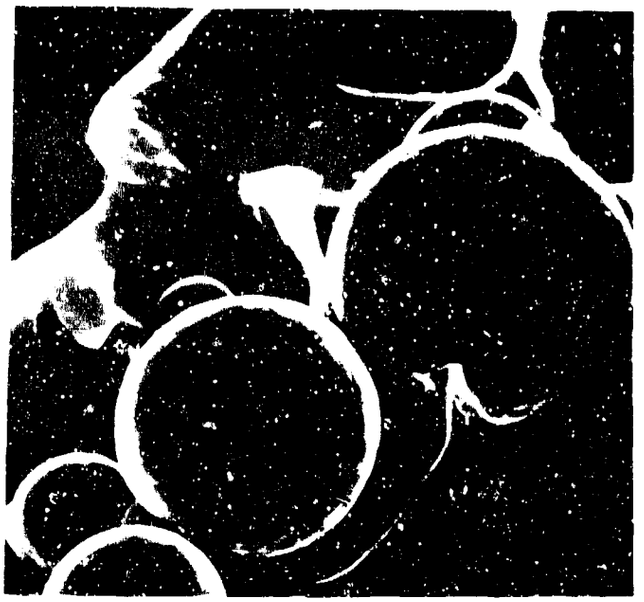

Diameter of Microbeads = 1-30 μ

Figure 20 Electron Scan Photograph of Untreated Glass Beads (10% by volume) in PEO, 1020 X.

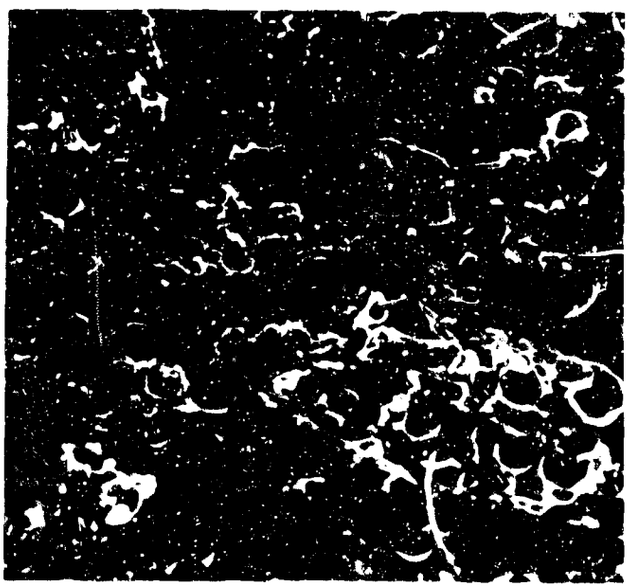

Diameter of Microbeads = 1-30 μ

Figure 21 Electron Scan Photograph of A-1100 Treated Glass Beads (10% by volume) in PEO, 212 X.

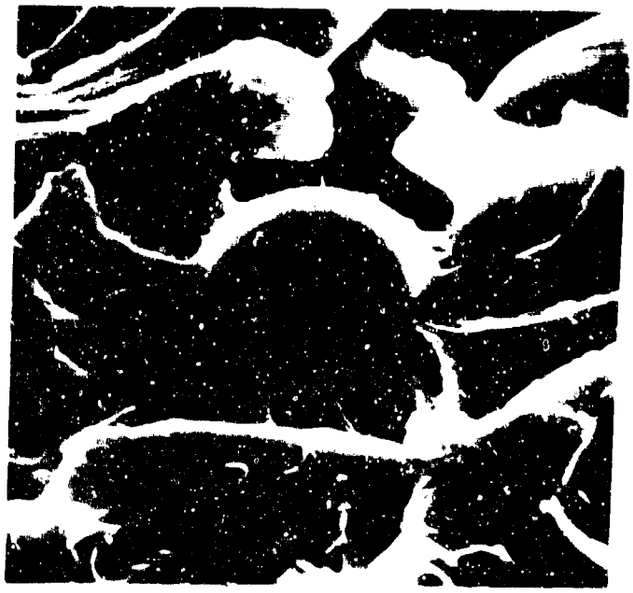

Figure 22 Electron Scan Photograph of A-1100 Treated Beads (10% by volume) in PPO, 1020 X.

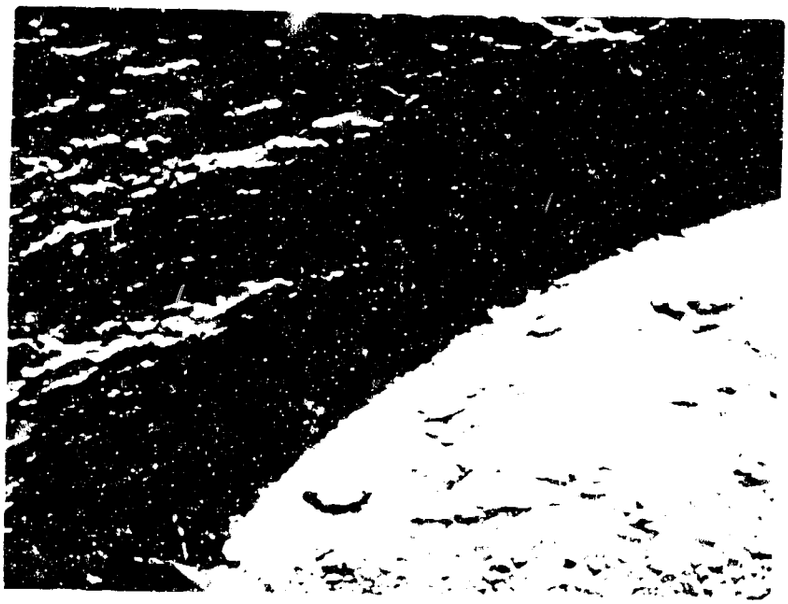

Figure 23 Electron Micrograph of the Interface Between an A-1100 Treated Glass Bead and PPO, 25,000 X.

the surface of the PPO filled with treated versus untreated beads. Figure 23 is an electron microscope photograph which clearly shows the inhibition of flow near the surface of an adhering glass bead.

Acknowledgment

The authors wish to express their thanks to Mr. John D. Fairing for obtaining the fracture surface pictures taken on the electron scanning microscope.

References

1. Griffith, A. A. "The phenomena of rupture and flow in solids," Phil. Trans. Roy. Soc. London, A221, 163 (1920).

2. Orowan, E. "Fundamentals of brittle behavior in metals," Fatigue and Fracture of Metals, 139 (1950).

3. Inglis, C. E. "Stresses in a plate due to the presence of cracks and sharp corners," Trans. Inst. Naval Architects, LV, 219 (1913).

4. Berry, J. P. "Brittle behavior in polymeric solids," Fracture Processes in Polymeric Solids, B. Rosen, ed., Interscience, N. Y. (1964) p. 195.

5. Irwin, G. R. "Analysis of stresses and strains near the end of a crack traversing a plate," ASME Trans. 24, 361 (1957).

6. Irwin, G. R. "Fracture toughness of high-strength sheet materials under conditions appropriate for strom analysis," Naval Research Lab. Report 5486 (1960).

7. Weiss, V. and S. Yakawa. "Critical appraisal of fracture mechanics," ASTM STP 381, 1 (1965).

8. "Plastics-methods of testing," ASTM Standards, Part 27, p. 553 (1965).

9. Kerner, E. H. "The elastic and thermo-elastic properties of composite media," Proc. Phys. Soc., 69B, 808 (1956).

10. van der Poel, C. "On the rheology of concentrated dispersions," Rheologica Acta, 1, 198 (1958).

DIFFUSION OF WATER ALONG THE GLASS-EPOXY INTERFACE (P. Peyser)

It is generally believed that the interfacial region plays a major role in determining the characteristics of composites. Water is frequently troublesome in weakening composites while suitable coupling agents are effective in substantially increasing the wet strength of composites. Hence, a study of the diffusion of water along composite interfaces is of great interest and the elucidation of the mechanism of this diffusion is of vital importance. A few such studies have been undertaken. Laird[1] reported that water diffuses along the glass-epoxy interface 450 times faster than through the epoxy resin. Patrick and Layne[2] reported a substantial diffusion of water through a glass-epoxy system (2.5×10^{-5} g/cm^2/day) with a great deal of the diffusion occurring in microcracks spread throughout the resin and along the interface. Moreover, they found that their coupling agent actually increased the rate of diffusion along the interface. We, however, do not find as great a diffusion of water through our glass-epoxy system and find that the application of coupling agent to the interfacial region sometimes did not hinder and other times helped retard the diffusion of the water. This work is a continuation of the work began by J. Schaeffer[3].

Basic Method

A model glass-epoxy composite was constructed as shown in Figure 1. The permeation of tritiated water from the inside of the cell through the resin and through the resin-glass interface was measured as a function of time. A permeation of 10^{-8} g/cm^2/day was easily detected. Diffusion cells, as shown in Figures 2 and 3 were also constructed, and these cells approximated the condition where only the diffusion occurring through the resin was detected. The difference between these two experiments was a measure of the diffusion of water through the interface alone. The resin shrinks away from the walls of the cylinder when the sample is allowed to cool to room temperature after being

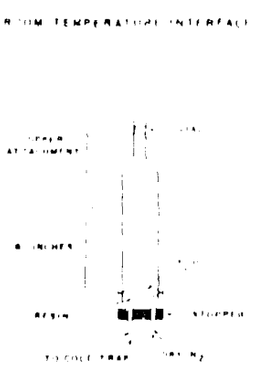

Figure 1

Figure 2

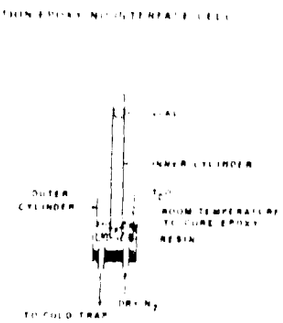

Figure 3

cured at elevated temperatures. A large strain is thereby created at the interface. The effect of this strain upon interfacial diffusion was studied by performing the experiments at various temperatures. Also, in order to increase considerably the interfacial region in a diffusion cell and increase the sensitivity by which interfacial effects could be detected, experiments were performed on epoxy filled sintered discs.

We wish to emphasize that measurements were only made on cells which showed no sign of interfacial crack or failure. In deed, a good many cells were discarded because of visible defects.

Experimental

A variety of different diffusion cells were constructed, each of which has its particular usefulness. The one-cylinder-interface-cell will first be described in detail and then the variations applicable to the other cells will be considered. One cylinder cell: A pyrex glass cylinder of 6 cm diameter was cut smoothly at one end to a length of 6 inches, slightly fire-polished and annealed overnight. The final cleaning of the cylinder was accomplished by refluxing isopropanol onto the fire-polished end of the cylinder and then immersing the cylinder into boiling isopropanol. Kel-F film was wrapped and tied around the fire-polished end of the cylinder to seal one end of the cylinder with a smooth wrinkle free film.

Shell Epon-820 was thoroughly mixed with Shell Curing Agent D in a ratio of 100 parts (by weight) resin to 12.5 parts curing agent. Ten grams of the mixture was poured in and the cylinder placed in an oven to cure at 75°C. The total time of cure, beginning with the mixing of the resin with curing agent, was three hours. To remove air bubbles arising from the mixing process and the initial curing process, a vacuum was pulled on the samples during the first half hour of cure. One sample (D 90) did not receive the vacuum treatment and air bubbles were clearly visible in the cured resin. The Kel-F film was removed after the cure. The top part of the diffusion cell was then attached to the cylinder (see Figure 1). Tritiated water, T_2O, and a Teflon coated magnet were sealed into a breakable glass vial and the outside of the vial washed to remove any traces of radioactivity. For room temperature studies the vial was placed in the diffusion cell and the top of the cell sealed. For higher temperature work, a condenser and a cold trap were attached to the cell as shown in Figure 4. Dry

Figure 4

nitrogen gas was passed over the bottom of the outside of the diffusion cell and then into a cold trap collector. The flow was sufficient to essentially carry over to the trap any diffusing water but slow enough so that in tests a second trap in series with the first did not show any radioactivity. The amount of T_2O in the cold trap was measured by removing (and replacing) the cold trap container, filling it with 15 ml of scintillating solution, and mixing the solution thoroughly with the contents of the trap. The contents of the trap were then poured into a scintillation vial (at least a 99% transfer was achieved) and the sample counted in a Packard Model 574 liquid scintillation spectrometer. Before the vial containing the T_2O was broken in the diffusion cell (with the help of an outside magnet), a blank was run to assure that no radioactivity had accidentally slipped into the system. The vial was then broken and the contents of the cold trap analyzed as a function of the time elapsed beginning from the breaking of the vial.

Temperature Measurements

An outer glass jacket was attached to the diffusion cell as shown in Figure 4 and a heating tape was wrapped about the jacket in the vicinity above and below the epoxy disc. A thermister probe and a thermometer were inserted just below the disc and with the help of a thermister relay, temperature held constant to within ± 1°C. An early run where the temperature control was much poorer (D 91A) is indicated as such in the results. Temperature equilibrium was established before the vial was broken.

Thin Cells: During cure, a Teflon rod of 2.5 cm diameter was inserted into the epoxy resin at a distance of a few milimeters from the Kel-F film. After cure, the rod was pulled away from the resin leaving a circular cavity in the disc. A pyrex cylinder was then attached to the thin part of the epoxy disc by pouring room temperature cure epoxy resin liberally on the outside of this inner cylinder and curing. T_2O was placed inside the inner cylinder.

Two Cylinder Cells: An inner pyrex cylinder of 5.1 cm diameter was partially inserted into the curing disc. The area between the inner and outer cylinders was filled with water and T_2O was placed inside the inner cylinder.

Sintered Glass Cells: A coarse sintered glass tube of disc diameter 1.3 cm was cleaned by first refluxing the tubes overnight with isopropanol in a soxhelet. After drying, the tubes were heated overnight at 450°C in a muffle oven and allowed to cool slowly. The disc was filled with a few drops of epoxy resin which had been curing for 1/2 hour and the rest of the cure continued for the normal 3 hours. The top and bottom of the cell were then attached as is shown in Figure 5.

Coupling Agent: Dow A-1100, γ-aminopropyltriethoxysilane, was applied to some of the cylinders from a 1% solution in isopropanol by adding the coupling agent to the isopropanol used in the reflux cleaning of the cylinders previously described. Application to the sintered discs was from a room temperature 1% solution of A-1100 in acetone which had previously been hydrolyzed overnight with a stoichiometric amount of water[4]. After application, the cylinder and discs were allowed to drain and were heated for one hour at 100°C.

Figure 5

Scintillating Solution and Standardization: 16.9 grams of 2,5-diphenyloxazole and 0.64 gram of 4-methyl-5-phenyloxazolyl-benzene, obtained from the Packard Instrument Company was dissolved in four pints of reagent grade toluene and one pint of reagent grade methanol to produce the scintillating solution. Tritiated water of specific activity of one millicure/gram was obtained from the New England Nuclear Corporation. It was diluted about ten-fold before use. The water was standardized by pipeting 50 λ of the diluted water into a scintillating vial, adding scintillating solution and counting in the scintillation counter. A typical sample gave about 3×10^7 counts per minute per gram of water. A correction was applied to take into account the dead time error of the counter.

Method of Analysis

Assuming Fickian diffusion and neglecting end effects, a measurement of the amount of water which has diffused through a membrane as a function of time allows one to determine the diffusion constant, D, (cm/min^2) and the solubility, C, (g/cm^3) for the system. The product of C x D is known as the permeability constant, P. Most common analysis of the data (time-lag method) involves plotting the amount of water which has diffused through the membrane as a function of time until the steady state has definitely been achieved. Then the slope of the straight line in the steady state region and the intercept of this line extended into the time axis, are simply related to P and C[5]. Howeve., the smallness of the diffusion constant for the system of our measurement and the need to use relatively thick membranes in order to guarantee interfacial contact between resin and glass made analysis by the time-lag method impractical. For example, steady state at room temperature was not achieved after a year for the diffusion of water through the glass-epoxy cells where the thickness of the disc was about 3.5 mm. For short times, a non-exact but highly accurate solution of the Fickian diffusion differential equation, for the boundary conditions of our interest was first given by Rogers, Buritz and Alpert[6] as the following:

$$\ln\left(\frac{dQ}{dt} \cdot t^{1/2}\right) = \ln\left[2AC\left(\frac{D}{\pi}\right)^{1/2}\right] - \frac{L^2}{4Dt} \qquad (1)$$

where Q = amount of water, gm, which has diffused through the membrane.

A = area of membrane, cm^2.

ℓ = length of membrane, cm.

t = time, min.

C = solubility of water in the membrane, gm/cm^3.

(Note: Since the derivation of the above solution is not, to the author's knowledge, clearly stated in the literature, the following brief outlined derivations are presented. One method is to apply the transformation which is found on page 275 of Carslaw and Jaeger[7] to the well known solution of the differential equation which is given on page 47 of Crank[5]. Another method is to make use of the solution given on page 276 of Carslaw and Jaeger[7]. First this solution should be put into diffusion terms by using the one to one correspondence that exist between heat conduction and diffusion. Set $t' = 0$ and make use of the relationship

$$\sum_{-\infty}^{\infty} (\quad) = 2 \sum_{0}^{\infty} (\quad) \quad .$$

Solve for $\frac{dQ}{dt}$ by first differentiating and then integrating, making use of the relationship

$$\frac{dQ}{dt} = -D \left(\frac{\partial C'}{\partial x}\right)_{x = \ell}$$

where C' is the concentration of the diffusing substance at a distance x from the end of the membrane where the diffusion began. The linear form of the solution is obtained by retaining only the first term of the infinite series which is valid for short times.)

Hence a plot of the left side of the equation (1) against the reciprocal of time should give a straight line whose slope is directly related to D and whose intercept is related to the logarithm of $C \times D^{1/2}$. Note, however, that the accuracy in the determination of D is much greater than that of C. The diffusion data was fitted to equation (1) by a least square analysis.*

*The author wishes to thank Dr. Allan Dickerson for his help in analyzing the data by use of the computer.

Results

A typical plot of the diffusion data is shown in Figure 6. As can be seen, a straight line fit of the data, indicating Fickian diffusion is reasonable but the accuracy of the fit is not very good. The values of D and C obtained from such fits should be analyzed taking into consideration the inaccuracy of the fit. As previously mentioned, the value of C so obtained, is especially inaccurate. Despite such inaccuracies, the results clearly indicate that an increased diffusion occurred due to the presence of the interface. Graphically Figure 6 demonstrates this point. The top line represents the best fit for the measured rate of diffusion and the bottom line is what the straight line would be like if diffusion was only through the resin. Diffusion through the resin alone was measured in two ways by use of the thin cells and the two cylinder cells. In both cases, end effects are assumed to be negligible. The two cylinder cell, in particular, closely resembles the interface cells and the resin was subject to identical conditions of cure. The value of C for room temperature was also measured directly by weighing a thin piece of epoxy, which had been soaked in water for a time sufficient to guarantee equilibrium absorbtion of water and then plotted and weighed. The results for room temperature diffusion is shown in Table I. As indicated, interfacial diffusion differed from diffusion through the resin primarily by an increased value of C while the values of D were somewhat lower.

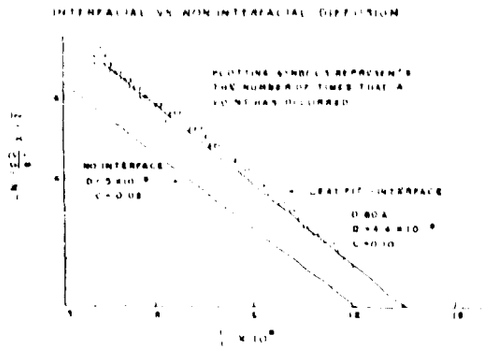

Figure 6

The product of C x D, the permeability constant, was about an order of magnitude too large. It was not expected that interfacial diffusion should show itself by an increased value of C and no increase in D. Such a result might be an artifact arising from fitting innaccurate data to an invalid Fickian model. However, another explanation is possible. Namely, that deterioration of the interface by diffusing water occurs only after water has reached the interfacial region by

TABLE I

[illegible] WATER-EPOXY DIFFUSION

Sample	Type	D x 10^{8}	[illegible]	[illegible]	P x 10^{10}	[illegible]
D 80A	Interface	4.4	[illegible]	0.30	42.0	[illegible]
D 80A	Interface	4.2	[illegible]	[illegible]	9.1	[illegible]
D 84	Interface	1.7	[illegible]	0.12	70.8	[illegible]
D 96	Interface	6.8	0.38	0.01	[illegible]	
D 97	Interface	5	0.31	0.01	[illegible]	
D 90	Interface	4.1	0.31	0.13	51.9	[illegible]
D 91	Thin	(~5)	0.15	0.03	[illegible]	Assumed value 4.0
D 94	Thick	1.9	0.24	0.26	100	Epoxy-fiber complex. Evaporation is probably negligible
D 95	Thick	5.3	0.18	0.05	23.6	
D 89	Thin	2.1	0.06	0.05	10.3	
	Direct Measurement	[illegible]	0.25	0.02	[illegible]	
D 101	Interface Coupling Agent	5.4	0.16	0.04	19.8	
D 102	Interface Coupling Agent	5.6	0.11	0.04	19.2	

diffusion through the resin. Keeping in mind that D is primarily a measure of how quickly the permeating water can be detected and C is a measure of the quantity of water which will permeate through the resin, the above mechanism is plausible. In any event, the amount of water permeating through the interfacial cell was orders of magnitude less than that reported by other researchers. It should be emphasized, however, that extreme care was taken in the construction of the diffusion cell that they not be subject to mechanical or thermal shock. Also any cell which showed even the slightest sign of an interfacial crack was discarded. Hence, the measurements we are reporting are representative of idealized conditions and serve as an indication of what might be expected from superior interfacial bondings.

Increasing the temperature of 50°C and 73°C also increased the value of C (but not D) and hence P by about a factor of 10 as seen in Table II. The high values of C obtained for the two cylinder samples, D 100 and D 103 are no doubt due to experimental error (cracks). The results indicate that releasing the strain at the interface by increasing the temperature, does not decrease the diffusion of water along the interface.

The results of diffusion through the sintered glass cylinder are shown in Table III. These cells had about 100 times the interfacial areas as compared with the interfacial cells previously discussed. Since, however, the sintered discs

TABLE II

TEMPERATURE DEPENDENCE

Sample	Type	$D_0 \times 10^4$	E_{act}	r	$P \times 10^{10}$	Remarks
A. 49°C						
D 98	Interface	9.9	0.34	0.15	105.8	
D 99	Interface	50.2	0.31	0.13	134.2	
D 100	Epoxy Paste	9.3	0.57	0.91		
D 103	Epoxy Paste	32.7	0.3	0.35		
D 156	Interface Coupling Agent	1.1	0.33	0.30	135.6	Made parallel with D 155
D 155	Interface	12.1	0.35	0.38	223	Made parallel with D 156
D 151	Interface Coupling Agent	32.3	0.35	0.30	326.5	
D 150	Interface Coupling Agent	10.5	0.34	0.33	140	
B. 37°C						
D 91A	Interface	45.2	0.34	0.28	1286	Temperature cycled prior to 37°C
D 91B	Interface		0.35		< D 91A	Diffusion began at a faster rate than D 91B and then slowed down and was similar to D 91A
D 104	Epoxy Powder	19.4	0.31	0.306	252	
D 152	Epoxy Powder	63.2	0.32	0.04	243	

TABLE III

SINTERED DISC CELLS

Sample	Diffusion First Detected Days	Remarks
D 157	1	No coupling agent.
D 160	3	No coupling agent.
D 161	6	No coupling agent.
D 162	13	Coupling agent. Diffusion after a month and a half was barely detectable.
D 163	13	

were not characterized, no attempt was made to analytically analyze the diffusion through them. The thickness of the discs was such that diffusion would not have been detected for about 6 months had diffusion occurred only through the resin. It was expected that such cells would be able to magnify small differences previously detected in the one interface cells. Indeed such an effect was found for the cell treated with coupling agent. As shown in Table I and II, the effect of adding coupling agent to the interface of the one interface cells is either to slightly decrease the interfacial diffusion or to have no effect on the diffusion. For the sintered glass discs, however, the effect of applying coupling agent was to dramatically decrease the diffusion. As previously mentioned, these results differ from those of Patrick and Laird. It may be that our results are specific to the coupling agent used and to the method by which it was applied. Indeed, the method of applying coupling agent and its effect on the interfacial bond had not been adequately studied (as reported in the literature). We also observed that when coupling agent was applied, the cells had a greater tendency to break. Our results might be representative of relatively uncracked cells.

There is an indication from the results that there is a tendency of interfacial diffusion to decrease with time. Perhaps a swelling of the resin occurs which tends to seal the interface.

The results are inconclusive for they do not represent a statistical evaluation of interface. Moreover, it is impossible to determine the mechanism of water diffusion from these results. However, the findings tend to emphasize the role which the interface and cracks at the interface play in the diffusion process. In addition they show how entirely different results can be obtained by various researchers. Therefore, unless it becomes possible to adequately control this variable (the cracks) a study and evaluation of other variables would be most difficult.

Conclusions

1. In many cases glass-epoxy systems contain cracks or broken interfaces which allow water to rapidly pass through such composites.

2. In the case of good interfaces, water still appears to go along the interface faster than through the bulk polymer but at a much smaller rate than previously reported.
3. Silane coupling agent A-1100, in the case of good interfaces, either reduces the rate of water transmission through the composite, or it has little effect.

Acknowledgment

Mr. Dave Morotz helped with much of the experimental work.

References

1. Laird, J. A. "Glass surface chemistry for glass-fiber reinforced plastics," Final Report, Navy Contract No. W-0679-C (F. B. M.) (June 1963).
2. Layne, W. S and R. L. Patrick. Government Report, AD 644,219 (1966).
3. Schaefer, J. F. First Annual Project Review and Technical Report, Monsanto/Washington University ARPA Project, AD 487 208 L.
4. Wong, R. Owens-Corning Fiberglass Corporation. Private communication.
5. Crank, J. The Mathematics of Diffusion, Oxford (1964).
6. Rogers, W. A., R. S. Buritz and D. Alpert. J. Appl. Phys., 25, 868 (1954).
7. Carslaw, H. S. and J. C. Jaeger. Conduction of Heat in Solids, 2nd Edition, Oxford (1959).

EFFECTS OF DISPERSION AND AGGREGATION OF FILLER PARTICLES

(F. B. Lewis)

Differences in the measured value of a physical property of a composite material are usually attributed to several factors, one being the degree of dispersion and aggregation of the filler material[1]. This work was initiated to distinguish what effect total dispersion and varying degrees of aggregation have on the rheological properties of a filled system. Viscosity measurements were selected for the work because of the comparisons which can readily be made. The extensive data and theoretical equations for the viscosity of a Newtonian suspension

of uniform spherical particles have been reviewed in recent years[2, 3]. In addition the influence of filler content on the viscosity of a suspension is mathematically analogous to the effect of filler content on the shear modulus of a composite[4, 5, 6].

A totally dispersed system is characterized by negligible inter-particle cohesive forces. An aggregated system has strong cohesive forces between particles, while an agglomerated system would have weak cohesive forces. (Weak and strong cohesive forces are distinguished by the ability and inability, respectively, of ordinary dispersion techniques to break up the cluster.) The inter-particle attractive forces represent the condition of filler particles exhibiting a "stickiness" and not being wetted individually by the matrix phase. It is possible for the extent of agglomeration and/or aggregation to range from doublets or triplets to very complex structures. In these measurements, all experimental parameters and conditions are held constant except for the extent of aggregation of the filler particles. The aggregated systems are characterized by the number of particles per aggregate. The inter-particle forces are of sufficient magnitude that the extent of aggregation is constant, independent of shear rate in the viscosity measurements.

The concentration range for suspensions can best be considered in three segments: infinitely dilute, moderate (to about 0.25 volume fraction filler), and highly concentrated (0.25 to the maximum volumetric packing fraction). Einstein[7] derived the equation for the viscosity of a suspension of non-interacting rigid dispersed spheres at infinite dilution. Most of the theoretical equations in the literature for finite concentrations are based on his result, and usually are presented with supporting data obtained concurrently or with an analysis of several sets of data from the literature. These equations predict essentially the same behavior at moderate concentrations, but very divergent behavior at high concentrations. In all the theories inter-particle interactions are taken into account, implicitly or explicitly, at high concentrations.

Gillespie[8] considered aggregated systems when measuring the viscosity of polystyrene latex suspensions. He observed the extent of aggregation with an optical microscope. By introducing a modification in the equation of Brinkman[9], he could account for the results theoretically. His primary conclusion is that the Einstein coefficient increases as a function of the number of particles per aggregate. His measurements were carried out in the moderate concentration range.

Glass beads in a highly viscous fluid, Aroclor, were selected for the measurements here because the system can serve as a useful model for composite materials. In addition, the spherical shape and surface of glass can be accurately characterized. Viscosities for dispersed and aggregated systems, with concentrations as high as 0.53 volume fraction solids, are shown to fit the Mooney[10] equation over the entire concentration range, if the Einstein coefficient is increased for the aggregated system as suggested by Gillespie[8]. One of the parameters in the Mooney equation, as in most theories for viscosity of moderate and high concentrations is the maximum volumetric packing fraction, Φ_m. Accordingly, measurements of Φ_m were carried out under several conditions.

Experimental

Aroclor[(a)], a chlorinated biphenyl, is a Newtonian fluid with a viscosity of 65 poises and a density of 1.535 gm/cc at 25°C. The glass beads[(b)] were fractionated to obtain a narrow particle size distribution for each size range. The metal which is normally found in glass beads with diameters less than 70 μ was carefully removed. The beads were cleaned in refluxing isopropanol and vacuum dried at 150°C to remove adsorbed water. They were classified in four size ranges as indicated in Table I.

(a) Type 1254, manufactured by Monsanto Co., St. Louis, Mo. 63166

(b) Soda-lime type, obtained from Microbeads Div., Cataphote Corp., Jackson, Mississippi.

TABLE I

PARTICLE SIZE DISTRIBUTION

Average Diameter	Range of Sizes
95 μ	90 - 105 μ
51 μ	45 - 60 μ
24 μ	18 - 32 μ
7 μ	5 - 10 μ

The following technique was developed for making aggregates. Beads of a certain size range were poured into a Vycor vessel containing large glass spheres[a], ten times larger in diameter and of a different composition than the former beads. By vibrating the container with a mechanical generator the small beads settled into the intersitial sites of the larger spheres. The mixture was heated to 635° C, maintained at this temperature for six hours, and allowed to cool slowly. The points of contact of the small spheres fused together, while the larger spheres would not fuse together or to the smaller spheres. The aggregates were separated by passing the mixture through a series of Tyler sieves. A very sharp distribution in the average number of particles per aggregate could be obtained from each of the sieves, as was determined from observations with an optical microscope. An example of the type of distribution that can be obtained is given in Table II for aggregates made from beads of 95 μ average diameter. Photomicrographs of singlets used for the aggregates are shown in Figure 1 for the beads before and after the initial classification by fractionation. Examples of aggregates with an average of 3, 4.5, and 7 particles per aggregate are shown in Figure 2.

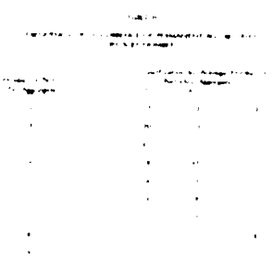

(a) Crown barium type, obtained from Ballotini Div., Potter Bros., Inc. Carlstadt, New Jersey, 07070

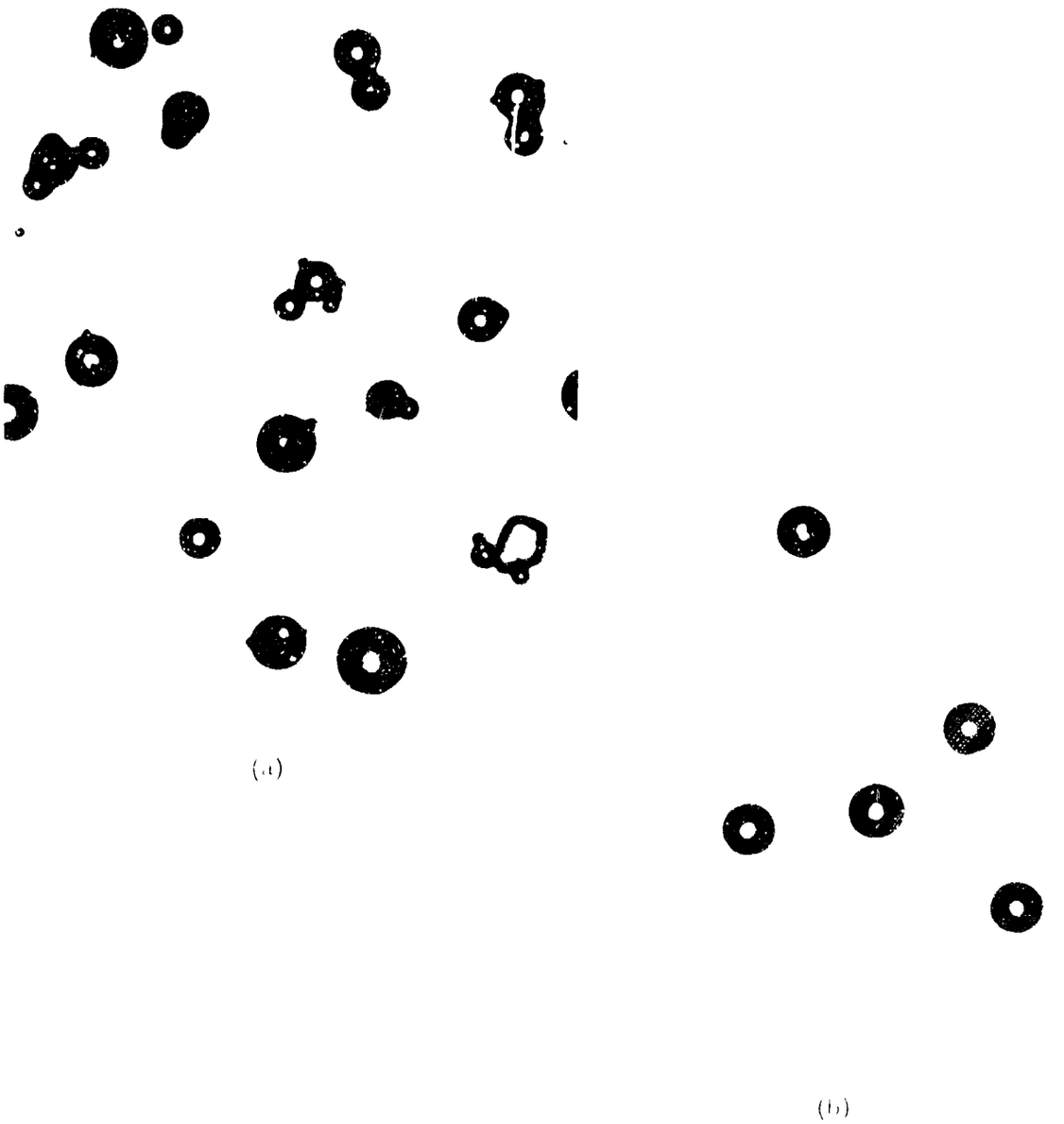

(a)

(b)

Figure 1 — Photomicrographs of Glass Beads Before (1a) and After (1b) Inertial Classification by Sieving. Scale: 100 μ = 0.88 cm.

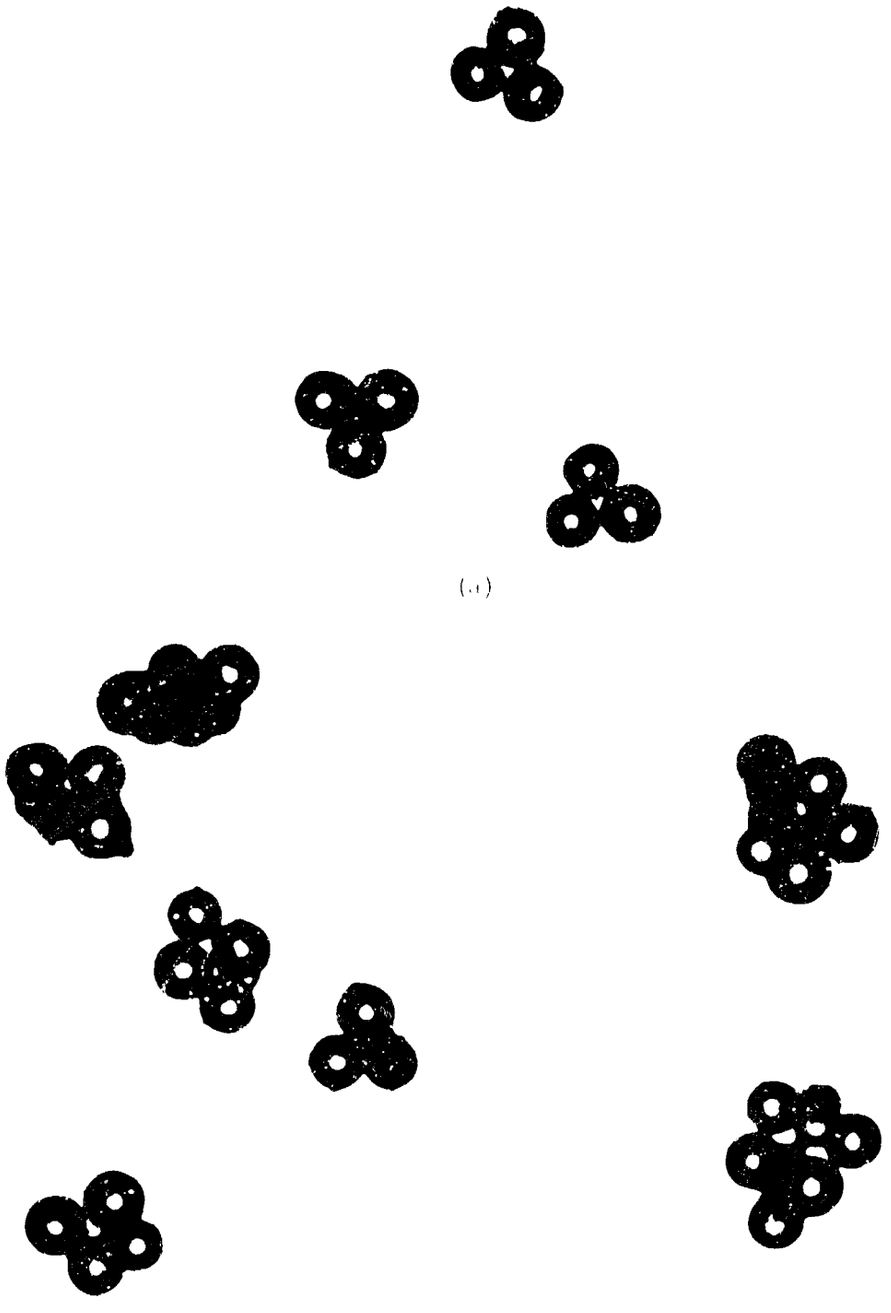

(a)

(b) (c)

Figure 2. Electron micrographs of Aggregates Made from Monodisperse Spheres Showing 8 Particles per Aggregate (2a), 4-5 Particles per Aggregate (2b) and 7 Particles per Aggregate (2c). Scale = 100 nm = 0.88 in.

Homogeneous suspensions of the dispersed and aggregated systems were prepared by introducing the Aroclor into a container with the cleaned beads under vacuum. The density of the beads was 2.38 gm/cc, and for the experiments reported here the settling rate of the beads in Aroclor is negligible compared to the time of the experiment.

Viscosity measurements were obtained at 25°C using a Couette viscometer[a] with a minimum shear rate of 0.3 sec^{-1}. The separation of the inner and outer walls of the viscometer was 0.55 cm. Thus the ratio of the filler particle size to separation distance was much less than unity, and correction factors for such size effects are negligible. Temperature control was maintained by pumping fluid from a bath to a chamber surrounding the viscosity cell. The bath was regulated to within $\pm$ 0.03°C.

Values of the maximum volumetric packing fraction were obtained by centrifuging the homogeneous suspensions and determining the sedimentation volume.

Results

Viscosities as a function of volume concentration, Φ, of filler have been obtained for dispersed systems with average particle sizes of 95 μ, 51 μ, and 24 μ. All of these systems exhibit Newtonian behavior except at the highest concentrations where shear stress starts to become a non-linear function of rate of shear above Φ = 0.45. These results are shown in Figure 3. The reproducibility of measuring viscosity is $\pm$ 1%, except for the highest concentrations which are somewhat less accurate due to the non-linear behavior.

The curve drawn through the data in Figure 3 was calculated from the theoretical equation for relative viscosity, n_r, of Mooney[10],

$$n_r = \exp\left(\frac{k_E \Phi}{1 - s\Phi}\right) \qquad (1)$$

with k_E = 2.5 and s = 1.4. This value of k_E is defined as the Einstein coefficient.

(a) Rotovisco Model by Haake, obtained from Brinkman Instruments, Westbury, New York, 11590.

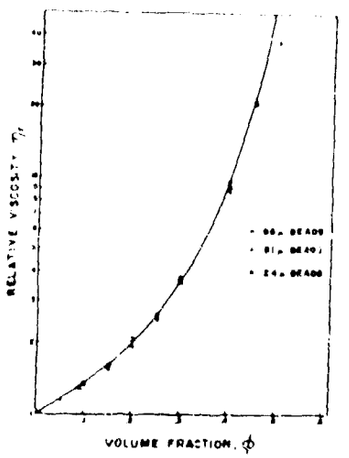

Figure 3 Relative Viscosities of Dispersed Glass Spheres in Aroclor as a Function of Volume Concentration for Three Average Particle Diameters, $\bar{d}$: $\bar{d}$ = 95 μ, ○; $\bar{d}$ = 51 μ, +; and $\bar{d}$ = 24 μ, Δ. The Smooth Curve is a Plot of the Mooney equation:

$$n_r = \exp\left(\frac{2.5\,\Phi}{1-1.4\,\Phi}\right).$$

Aggregates made of the 95 μ spheres were used for the completed viscosity measurements of aggregated systems. The smallest aggregate size selected had an average of three particles per aggregate. For this system a non-linear behavior of shear stress as a function of rate of shear was first detected at a concentration of about Φ = 0.20, although viscosities could be fairly accurately determined for concentrations as high as Φ = 0.37. These results are shown in Figure 4. It can be seen that the slope at the lowest concentrations is greater than the slope for the singlet measurements.

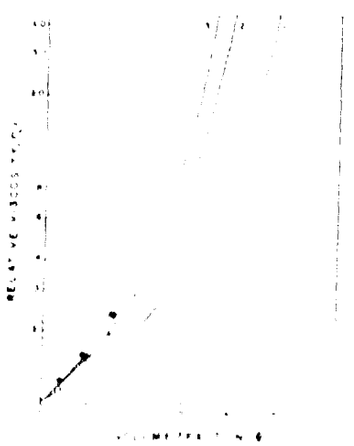

Figure 4 Relative Viscosity of Aggregated Spheres in Aroclor as a Function of Volume Concentration for Two Sizes of Aggregates: 3 Particles per Aggregate, ○, and 4.5 Particles per Aggregate, ①. The Smooth Curves are Plots of the Equation:

$$n_r = \exp\left(\frac{k_E\,\Phi}{1-s\,\Phi}\right),$$

where (1) corresponds to k_E = 2.5 and s = 1.4 (dispersed system); (2) corresponds to k_E = 3.6 and s = 1.6; and (3) corresponds to k_E = 3.8 and s = 1.8.

Viscosity measurements of aggregated systems with a higher average number of particles per aggregate were more difficult to obtain. For aggregates with an average of 4.5 particles per aggregate, the highest concentration that could be used to attain meaningful results was $\Phi = 0.15$, and in this case only a lower limit could be placed on the value of viscosity. However, the viscosities for aggregates of this size provide a measure of the behavior at the lower concentrations.

Values of the maximum volumetric packing fraction were obtained in air, water, and Aroclor, as indicated in Table III and Figure 5.

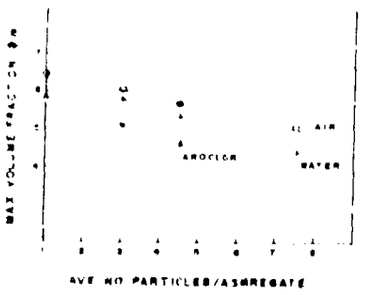

Figure 5 Maximum Volumetric Packing Fraction of Aggregated Glass Beads in Air, (), Water, +, and Aroclor, Δ, Plotted as a Function of the Average Number of Particles per Aggregate. Straight Lines were Drawn Through the Experimental Values. The Value of Φ_m in Aroclor for 1.5 Particles per Aggregate was Obtained by Extrapolation.

Discussion

The results shown in Figures 3 and 4 clearly indicate that the slope of the relative viscosity versus concentration curve at low concentration increases with the extent of aggregation. The Einstein relation for dispersed non-interacting spheres in a suspension reduces at infinite dilution to

$$n_r = 1 + 2.5\,\Phi . \qquad (2)$$

This predicts a slope for the dispersed case of 2.5, and this holds for the data presented here. Gillespie[8] accounted for aggregation by modifying the Einstein coefficient to

$$k_E = \frac{25}{6} - \frac{5}{3\bar{n}} \qquad (3)$$

where $\bar{n}$ is the average number of particles per aggregate. This gives values of k_E equal to 3.6 and 3.8, for aggregates with an average of three and 4.5 particles, respectively.

The value of s in equation (1) was described by Mooney as an experimental parameter, but it is normally identified as the inverse of the maximum volumetric packing fraction. It has been shown[1] that a value of s = 1.4 gives the best fit of several sets of experimental data in the literature. This value of s would predict a value of $\Phi_m = 0.71$. However, the maximum volumetric packing fraction for spheres in air has been determined by a number of workers[11, 12, 13] as ranging from 0.62 to 0.64. Robinson[14] and Landel[15] have measured Φ_m in conjunction with their viscosity data and obtain values in the range 0.60. It is not obvious from Mooney's development[16] that s must be the inverse of Φ_m, and further, the data presented here along with the reference cited above indicate that a value of s = 1.4 does give a very good fit for n_r of dispersed systems. The values of Φ_m for Aroclor listed in Table III were used to determine values of s according to the following expression:

$$s\ (\text{aggregates}) = \frac{\Phi_m(\text{dispersed})}{\Phi_m(\text{aggregates})} \times 1.4 \qquad (4)$$

and are included in Table III.

These values of s along with the values of k_E determined from equation (3) were used in equation (1) to compute the smooth curves of Figure 3. These curves predict a behavior which is slightly greater than the experimental measurements with the three particle aggregates, and slightly less than the results with the 4.5 particle aggregates.

TABLE III

MAXIMUM VOLUMETRIC PACKING FRACTION Φ_m

Average Number of Particles/Aggregate	Air	Water	Aroclor	s (aggregates) from Eq. (4)
1*	.64	.63	.59	1.4
3	.60	.56	.51	1.6
4.5	.57	.54	.47**	1.8
∞	.51	.45		

* Dispersed
** Obtained by Extrapolation

Experimentally one often finds that particles tend to stick together or agglomerate as particle size is decreased. Preliminary viscosity results of dispersed spheres in the range 5-10 μ indicate a similar behavior to that obtained with the larger spheres. If agglomeration did become apparent, similar behavior to that detected for the aggregated systems would be expected.

Presently experiments are being carried out to construct aggregates from smaller sized spheres than the 95 μ beads since the smaller size may eliminate some of the experimental difficulties encountered in the viscosity measurements with the aggregates of the larger sized beads.

It can be concluded from this work that:

1. Viscosity measurements for dispersed spheres in suspension can be predicted over the entire concentration range by the Mooney equation;
2. Particle size effects in dispersed systems for the range (5 μ - 100 μ) are not apparent in the measurements of the relative viscosity.
3. Viscosity measurements for aggregated systems can be predicted by the Mooney equation if the Einstein coefficient is increased according to equation (3) and values of s are calculated from maximum volumetric packing data.

References

1. Nielsen, L. E. J. Composite Materials, 1, 100 (1967).

2. Frisch, H. L. and L. Simha in "Rheology" edited by F. R. Eirich, Vol. 1, Ch. 14 (1956) Academic Press, Inc., New York.

3. Rutgers, I. R. Rheol. Acta., 2, 202 (1962).

4. Lassdel, R. F. and T. L. Smith. ARS Journal, 31, 599 (1961).

5. Hashin, Z. in "Proc. 4th Internat. Cong. Rheology," edited by E. H. Lee, Pt. 3, p. 30-32 (1965) Interscience Pub., Inc., New York.

6. Guth, E. J. Appl. Phys., 16, 20 (1945).

7. Einstein, A. Ann. Physik, 19, 286 (1906); 34, 591 (1911).

8. Gillespie, T. J. Colloid Sci., 18, 32 (1963).

9. Brinkman, H. C. J. Chem. Phys., 20, 571 (1952).

10. Mooney, M. J. Colloid Sci., 6, 162 (1951).

11. Scott, G. D. Nature, 188, 908 (1960).

12. Bernal, J. D. and J. Mason. Nature, 188, 910 (1960).

13. McGeary, R. K. J. Am. Ceram. Soc., 44, 513 (1961).

14. Robinson, J. V. Trans. Soc. Rheology, 1, 15 (1951).

15. Landel, R. F., B. G. Moser and R. J. Bauman in "Proc. 4th Internat. Cong. Rheology," edited by E. H. Lee, Pt. 2, p 663-692 (1965) Interscience Pub. Inc., New York.

POLYMER-FILLER INTERACTIONS IN COMPOSITES (D. Droste and A. T. DiBenedetto)

Considerable effort has gone into studying the nature of filler-coupler-polymer interfaces because of the strong influence interfaces have on the physical properties of composites. Much of this work is on model systems under ideal treating conditions. From such work has come an understanding of the types of bonding possible in various filler-coupler-polymer combinations and a feeling for the conditions required for optimum properties.

In spite of the extensive disagreement in the literature as to actual mechanism of coupling action, several basic conclusions are agreed upon by almost everyone:

1. Structures that contain non-adhering phases behave differently than those with adhering phases.
2. Couplers are used in order to promote a continuous adhesive structure through the phase boundaries.
3. The extent of interaction between phases is a highly specific phenomenon, determined by the nature of the interacting surfaces and, in many cases, the way in which they are brought together.
4. In order to achieve interaction between phases it is necessary for the interacting components to come into molecular contact with one another.

It is generally recognized that when specific components are mixed together in a complicated fabrication process, unexpected events can often occur which place doubt on the nature (or reliability) of the finished composite. Thus, mechanistic laboratory studies on model systems do not always relate to the performance level of a specific composite material.

The main objective of this study is to develop relatively simple physical property measurements on a fabricated composite material, that can be interpreted in terms of the extent of interaction between the constituents of the material. These experiments are not aimed at determining the mechanism of interaction, but rather are designed to quantify the extent of the interaction and to determine what effect the interaction has on the performance of the material.

Our study is based on the assumption that if there is interaction between a filler and a polymer matrix, the molecular properties of the polymer matrix will be affected. The nature of the molecular change will, of course, depend specifically on the type of interaction involved. A chemical reaction between the constituents, for example, can change the chemical constitution and average molecular weight of the polymer phase. A strong adsorption of polymer on the filler surface, on the other hand, may merely change the mobility and flexibility of the polymer chains. In any specific composite system, it is likely that more than one phenomenon may occur that can change the properties of the polymer molecules.

The important point is that the physical properties of the matrix material in the composite are not necessarily the same as those of the pure unfilled material. It follows that if one makes a composite in which a significant fraction of the polymer is in contact with a filler surface and if the polymer strongly interacts with the filler, the degree of interaction (regardless of mechanism) should manifest itself by changes in the thermodynamic and viscoelastic properties of the matrix.

Experimental Program

Two experimental techniques are described in this paper. The glass transition temperatures of composites were measured using a DuPont 900 Differential Thermal Analyzer (DTA). The basic idea is to supply thermal energy to both a sample and an inert reference material. The temperature difference between sample and reference is recorded. When a sudden change in specific heat or

thermal conductivity of the sample occurs (such as that occurring at the glass transition temperature of the polymer), a change in the heating rate between sample and reference occurs, which marks the transition temperature of the material.

Dynamic moduli and damping capacities of the composites were measured using a freely oscillating torsion pendulum[1]. A schematic diagram is shown in Figure 1. The basic idea is to impose a sinusoidal torsional strain on the composite sample by means of an inertia disc and measure the frequency of oscillation and its decrease in amplitude with time. From this data one may calculate storage modulus, loss modulus and damping capacity[2]. Two composite systems have been chosen for study:

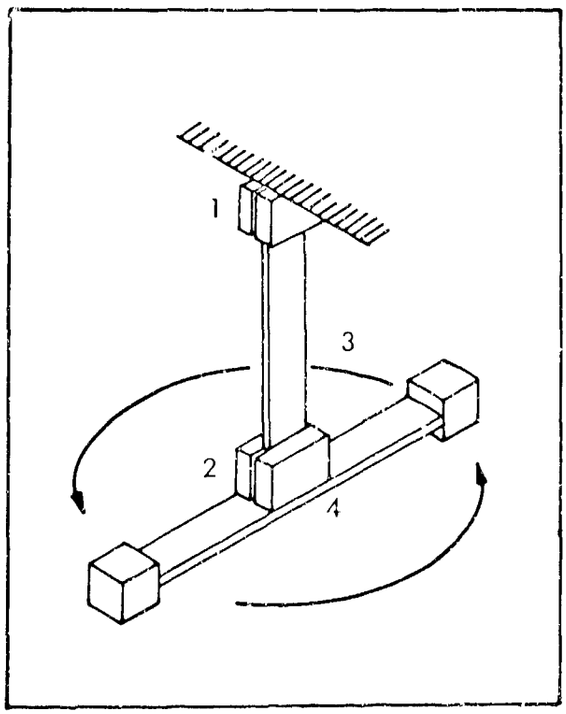

1 Stationary Sample Clamp
2 Movable Sample Clamp
3 Polymer Sample
4 Moment of Inertia Member

Figure 1 The Simplified Functions of the Torsion Pendulum Indicate that this Instrument is Primarily used for Constant Frequency Measurements.

Phenoxy PKHH*, a thermoplastic with a repeating structure of $+O\text{-}C_6H_4\text{-}C\text{-}(CH_3)_2\text{-}C_6H_4\text{-}O\text{-}CH_2\text{-}CH(OH)\text{-}CH_2+$ and a molecular weight of about 31,000, was filled with an attapulgite clay, Attagel 40,** which had a rod-like morphology and an average ultimate particle size of 200 Å diameter and 1 micron in length. The actual BET surface area of the filler is 210 m^2/gm.

---

* Tradename for a phenoxy resin made by Union Carbide Corporation.

** Tradename for a clay filler made by the Attapulgus Clay Products Company.

Epon 1031*, a thermoplastic epoxy monomer with a structure $\{(CH_2 - \underset{\diagdown O \diagup}{CH}-CH_2-O-C_6H_4)_2CH\}_2$ and an average molecular weight of about 700 to 800 (some dimer is present in material), also was filled with Attagel 40 clay.

The phenoxy composite specimens were prepared by dissolving the polymer in a solvent mixture of 40% acetone, 40% toluene and 20% butanol, and slurrying the as-received filler in the solution. After sonification of the slurry, the solvent was slowly evaporated and then the composites were placed in a vacuum oven at 120°C for 100 hours. The resulting powders were then compression molded into 4 x 0.5 x 0.025" bars at 3000 psi and 100-120°C. The Epon 1031 composites were made in a similar manner, but the solvent was acetone.

Experimental Results

Figure 2 shows that the addition of attapulgite to Epon 1031 causes a marked increase in the glass transition temperature of the matrix. This increase is a manifestation of a strong interaction between the two constituents; the matrix material has considerably different properties after the addition of the filler. There are several potential mechanisms that can be used to explain this interaction. One possibility is that the filler surface can act as a catalyst for the polymerization of the monomeric material. An increase in molecular weight could explain the increase in Tg. Another possibility is that a significant portion of the monomer is strongly adsorbed on the filler surface, thereby decreasing the mobility and molecular flexibility of the molecules. Further experimentation is required to distinguish between these or other mechanisms.

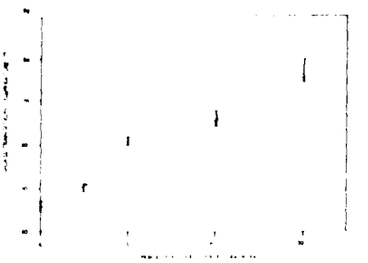

Figure 2 The Presence of the Filler in the Epon 1031-Attagel Composite Results in Major Shifts of the Glass Transition Temperature.

---

* Tradename for an epoxy resin made by Shell Chemical Company.

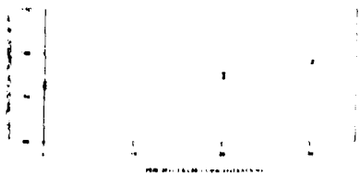

Figure 3 The Glass Transition Temperature of the Phenoxy PKHH-Attagel Composite is Less Affected by the Presence of the Filler.

Figure 3 shows that the addition of attapulgite to the phenoxy resin also causes an increase in the glass transition temperature. In this case the change, and therefore the extent of interaction, is smaller than with the Epon 1031.

The torsion pendulum was used to determine whether these interactions would also manifest themselves in the viscoelastic properties of the matrix. The uncrosslinked Epon 1031 system could not be studied because the low molecular weight material was too brittle for mechanical testing. If work on this system is continued, the matrix material will have to be lightly crosslinked. Figures 4 and 5 show the dynamic test results for the phenoxy-attapulgite composites.

The shear moduli and loss moduli near 100°C show the same shift in the glass transition temperature as was found with the DTA. At the transition temperature of the pure polymer, the onset of rapid viscous flow causes a near-infinite rise in the damping capacity of the material. The addition of twenty percent attapulgite suppresses this peak somewhat but viscous flow again predominates at a temperature that is a few degrees higher than for the pure polymer. At thirty percent filler concentration the damping peak is relatively low and a definite maximum is observed. Thus, the composite is beginning to exhibit some strength above the glass transition temperature. This is the kind of behavior one would expect from a crystalline or lightly crosslinked polymer.

Low temperature peaks at -67°C in the loss moduli and damping capacities are also observed, indicating a secondary glass transition for the polymer. The peak temperatures and the shape of the damping curves appear to be independent of filler concentration. The relative peak heights for the damping curves are also proportional to the volume fraction of filler. Thus, if the damping capacities are compared on a unit volume of polymer basis, the damping curves may be superimposed.

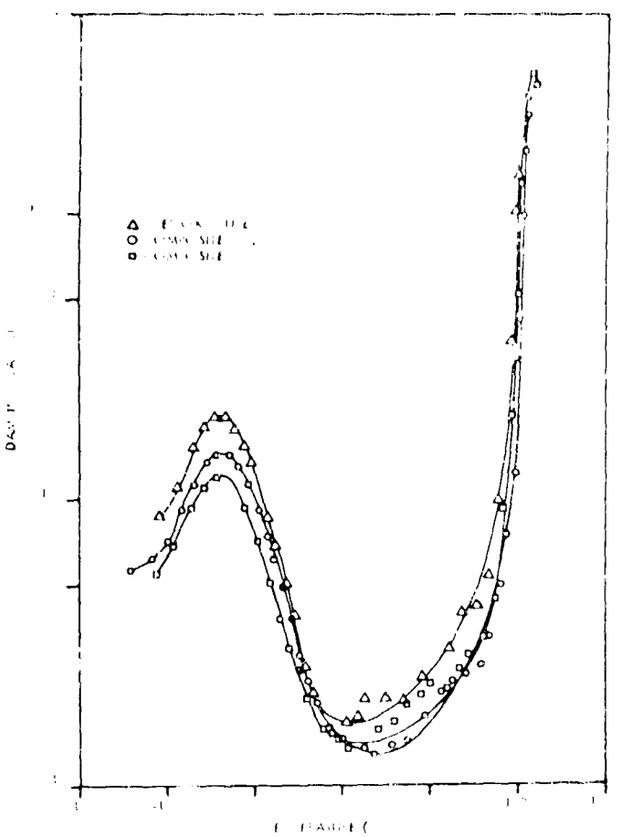

Figure 4 The Damping Capacity of the Phenoxy PKHH-Attagel Composite Indicates that Smaller Side Groups of the Phenoxy Molecule are Less Affected by the Filler than Larger Ones.

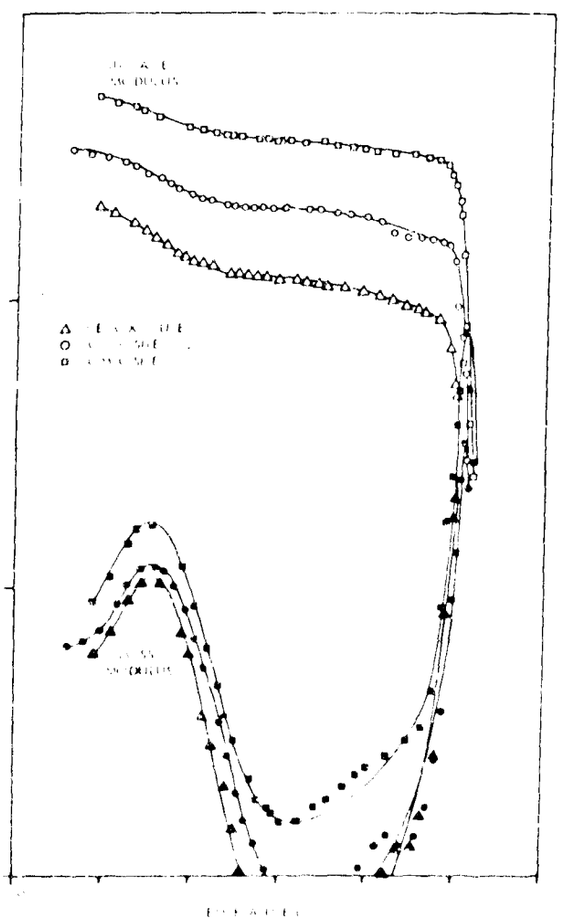

Figure 5 The Storage Modulus and the Loss Modulus of the Phenoxy PKHH-Attagel Composite Show Substantial Increases at Higher Filler Loadings.

These data might be interpreted as follows: The low temperature transition involves specific short segments along the polymer chain. The flexibility and mobility of these short segments are not strongly affected by the presence of filler surface and thus the portion of the relaxation spectrum associated with these motions is not significantly changed by the presence of filler. The higher temperature transition, on the other hand, involves the flexibility and mobility of larger segments of the polymer chains The shift of the glass transition temperature and the decrease in viscous dissipation per unit volume of polymer leads one to believe that the longer range chain flexibility and mobility are inhibited. In other words, the relaxation spectrum in the longer relaxation time region is shifted to still longer times because of the presence of the filler. A physical picture of a polymer chain being adsorbed at a few points along the chain and forming loops back into the bulk of the polymer matrix is consistent with the data. It should be pointed out that this latter description of the polymer morphology at the filler surface is purely hypothetical but is at least consistent with what has previously been reported in the literature on the adsorption of polymers on high energy surfaces.

The data alsc show that the filler increases the shear moduli of the composites. The effective reinforcement in the glassy state is close to that predicted by the van der Poel equation (3). In the higher temperature region around the glass transition point, the storage moduli of the composites decrease with temperature at a faster rate than does the storage modulus of pure phenoxy. This might indicate that the effective reinforcement in the rubbery state is less than in the glassy state, which could be a manifestation of poor adhesion. To investigate this possibility data will be taken in the rubbery region.

Conclusions

The measurement of glass transition temperature, dynamic moduli, and probably any other property which depends primarily on the flexibility and mobility of the polymer molecules, can be used as a quantitative indication of the extent of interaction between a reinforcing filler and a polymer matrix.

Additional experimentation is required to sort out the various mechanisms for these interactions. Work will continue on relating physical properties of composites to the extent of interaction between constituents.

References

1. Nielsen, L. E. Rev. Sci. Inst., 22, 690 (1951).

2. Nielsen, L. E. "Mechanical properties of polymers," Reinhold Publishing Corporation.

3. van der Poel, C. Rheologica Acta., 1, 198 (1958).

THE GROWTH, MORPHOLOGY, AND REINFORCEMENT POTENTIAL OF LOW MOLECULAR WEIGHT CRYSTALS IN AMORPHOUS POLYMERIC MATRICES

(J. R. Joseph, J. L. Kardos and L. E. Nielsen)

In many cases it would be convenient to be able to make composite materials which could be fabricated at high temperatures as homogeneous melts from which a rigid reinforcing phase develops as the system is cooled down to the solid state. A possible way of achieving this goal would be to use mixtures of rigid amorphous polymers and low molecular weight organic compounds, which are soluble in the polymer at high (fabrication) temperatures and which become insoluble and crystallize out of the viscous melt as the temperature is lowered. Thus, the well-known difficulties of processing and fabricating filled systems, especially those containing fibrous fillers, would be avoided. In addition, such techniques offer the possibility of controlling crystal morphology and orientation to a degree not possible with conventional fabrication techniques involving the flow of filled polymer melts.

Mixtures of organic compounds and high polymers offer possible answers to a number of important scientific questions in addition to those mentioned above:

1. What is the mechanism and rate of crystal growth of organic compounds from viscous liquids?
2. What changes in morphology of the crystalline phase are possible?
3. What are the elastic moduli of small organic crystals? Do such crystals offer the possibility of acting as good reinforcing fillers in the same way as single crystal whiskers of inorganic materials?

Two workable systems have been found and their phase diagrams determined. Crystallization kinetics and crystal morphology have been determined under a variety of conditions for crystals grown from very viscous polymer melts. Dynamic mechanical properties of such two-component, two-phase systems have been measured. It appears that the elastic moduli of organic crystals, which are held together by Van der Waal's forces, are about the same as the moduli of organic polymers in the glassy state rather than the higher moduli associated with inorganic single crystals.

Criteria for System Selection

In choosing the polymer matrix and the low molecular weight (LMW) component to be selectively crystallized, the following criteria must be considered:

(a) Transition Temperatures

The melting point, and in most cases the dissolution (fabrication) temperature, of the LMW component must be considerably above the glass transition temperature (T_g) of the polymer matrix for several reasons. First, crystallization cannot occur readily from the glassy state, diffusion being much too slow; second, a wide crystallization temperature range above T_g permits better control over the crystallization morphology; and finally, the higher the melting point is above T_g, the lower will be the polymer viscosity, thus hastening the dissolution process.

Obviously, the dissolution temperature cannot exceed the degradation temperature of either the polymer matrix or the LMW component. The LMW component also must not be volatile at the dissolution temperature.

(b) Solubility

At the fabrication (dissolution) temperature, the two components must be completely miscible. However, the solubility should decrease as the temperature is lowered so that the LMW component can crystallize. Ideally, the LMW component would be 100% soluble slightly above its melting point and insoluble at the T_g of the pure polymer.

(c) Degree of Dissolved Phase Interaction

Any type of chemical reaction between the dissolved components is certainly undesirable, since it would affect the matrix properties in addition to hindering

the subsequent crystallization process. Any other strong interactions which would tend to induce crystallization in the polymer at the dissolution temperature should also be avoided.

Since solubility and chemical interaction data are practically nonexistant for systems of this type, a considerable number of combinations were screened using differential thermal analysis (DTA). Styrene-acrylonitrile copolymer (SAN) was chosen as the matrix because of its good chemical stability, convenient T_g and ability to remain amorphous under all conditions used. The SAN contained 26 weight percent acrylonitrile and had a number average molecular weight of about 60,000. DTA showed a T_g of 100-102° C and a degradation temperature of about 280° C for the pure copolymer. Of several possible LMW compounds (hereafter designated fillers), acetanilide and arthracene, whose physical constants are summarized below, were chosen to combine with SAN giving two model systems which fulfill the above criteria reasonably well.

TABLE I

PHYSICAL CONSTANTS OF THE LOW MOLECULAR WEIGHT COMPOUNDS

Compound	Chemical Formula	Molecular Weight	Melting Temp.	Boiling Temp.	Density 20° C
Acetanilide	$CH_3CONHC_6H_5$	135	113-114° C	307° C	1.21
Anthracene	$C_6H_4(CH)_2C_6H_4$	178	216° C	340° C	1.25

Sample Preparation

A rotating hammer mill was used to grind the SAN pellets, along with dry ice to prevent softening, into a fine (80 mesh) powder. Both the SAN and filler powders were dried overnight at 80° C under a slight vacuum. The filler and polymer powders were weighed out and mixed in proportions calculated from the densities to yield the desired volume fractions.

Two types of specimens were prepared. The first was a test-tube sample containing about 5 grams of powder mixture. The test tubes were heated in an oil bath for 4 hours at 160°C for the acetanilide and at 200°C for the anthracene mixtures. (Anthracene is soluble slightly below its melting point.) Following complete dissolution the samples were quenched in liquid nitrogen to prevent crystallization and give a hard glassy solid solution. The high volume-fraction acetanilide samples were stored in liquid nitrogen since the glass transition temperature of the SAN was depressed below room temperature. At this point the samples were ready for use in determining the phase diagrams and the crystallization kinetics for both systems. The second type of sample was prepared solely for dynamic testing and will be described below.

Phase Diagrams

Phase diagrams of the two model systems were determined for use in guiding subsequent crystallization kinetics experiments. Each phase diagram consists of two curves; the glass transition curve where T_g of the polymer matrix is plotted against the volume fraction filler, and the solubility curve where the crystallization temperature is plotted versus the filler volume fraction still in solution after complete crystallization (equilibrium).

(a) Glass Transition Curve

Seven acetanilide - SAN and five anthracene - SAN test-tube samples were prepared containing various filler volume fractions from 0 up to 0.3 and 0.2 respectively. At higher concentrations it was difficult to avoid crystallization during the quenching step. After quenching, a DTA scan was run on each sample to determine the glass transition temperature.

(b) Solubility Curve

Several sets of test-tube samples containing dissolved volume fractions of 0.3 acetanilide and 0.2 anthracene were prepared. Each set of samples was immersed in an oil bath at a chosen temperature and allowed to crystallize isothermally. After two to three days of isothermal crystallization, the first sample of the set was quenched and its T_g measured with DTA. The remaining

samples were allowed to remain in the bath for one more day after which another sample was quenched and analyzed with DTA. This step was repeated until a constant equilibrium T_g was obtained. The amount of LMW material remaining in solution at the chosen crystallization temperature was determined from the equilibrium T_g value and the glass transition curve. The entire procedure was repeated for a range of crystallization temperatures and a solubility curve constructed for each system.

Bulk Crystallization Kinetics

Two sets of test-tube samples were prepared, one containi , 3 volume fraction acetanilide and the other 0.2 volume fraction anthracene. The following procedure was used to determine the increase in crystallinity as a function of time at constant temperature.

Five samples were simultaneously immersed in a thermostatted oil bath at the desired crystallization temperature. At regular intervals one sample was removed and quenched in liquid nitrogen and its T_g determined with DTA. The volume fractions left in solution after each time interval were determined from the T_g curve, and the difference between these values and the initial volume fraction yielded the crystallized volume fraction or crystallinity.

Specimen Characterization

(a) Electron Microscopy

The morphology of the crystallized phase was studied using electron microscopy. Samples crystallized at various temperatures were quenched in liquid nitrogen and fractured. Platinum-carbon replicas of the fracture surface were then made and examined in the microscope.

(b) Dynamic Mechanical Measurements

Special samples were prepared for dynamic testing. A large excess of powder, mixed as previously described, was poured into a 4" x 3/8" x 1/16" sandwich-type mold. A heating time of one hour at 150°C for acetanilide and 200°C for anthracene was sufficient to dissolve the filler crystals in the polymer. The solution was then molded under 1000 psi to flash out the excess and remove voids. Subsequent

quenching in liquid nitrogen caused severe cracking in the thin specimens making them useless for dynamic testing. However, cold water quenching gave crack-free samples and, at the same time, prevented crystallization.

After molding and quenching, the rectangular beam-shaped specimens were crystallized isothermally in a thermostatted oil bath for several days while still in the mold. Then, following a cold-water quench, each sample was removed from the mold and mounted on a freely oscillating torsion pendulum[1]. Damped oscillation curves were recorded at 1 cycle per second throughout a wide temperature range beginning at 243°K and extending through the transition of each sample.

Phase Diagrams

(a) Glass Transition (T_g) Curves

DTA curves for quenched samples of various anthracene concentrations are shown in Figure 1. A noticeable break in the slope occurs at T_g. As the dissolved filler volume fraction increases, the T_g break shifts to a lower temperature. Similar curves resulted for the acetanilide system.

Figure 1 DTA Scans at 25°C/Min. of the Anthracene-SAN System at Various Volume Fractions (V_f), Showing the Lowering Influence of the Plasticizer on the Glass Transition Temperature.

The effect of dissolved filler on T_g is summarized by the data points in Figures 2 and 3 (T_g curve) for the acetanilide and anthracene systems respectively. The solid lines are the result of fitting the following expression[2] to the data points,

$$T_g = \frac{\alpha_p (1-V_f) T_{gp} + \alpha_f V_f T_{gf}}{c_p (1-V_f) + \alpha_f V_f} \qquad (1)$$

where f and p refer to the filler and pure polymer respectively. V is the volume fraction, and α is the linear expansion coefficient. For SAN, $\alpha_p = 8.1 \times 10^{-5}$

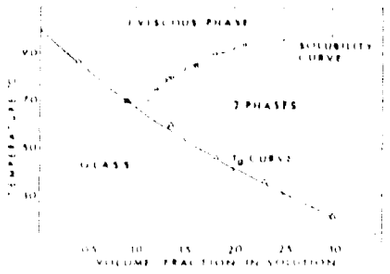

Figure 2 Phase Diagram of the Acetanilide System Showing the T_g Curve and the Solubility Curve.

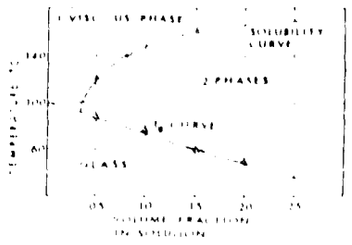

Figure 3 Phase Diagram of the Anthracene System Showing the T_g Curve and the Solubility Curve.

per °C, α_f and T_{gf} are unknown and were adjusted to fit the data points. In the case of acetanilide $\alpha_f = 18 \times 10^{-5}$ per °C and $T_{gf} = -63.5$°C. Both values appear to be reasonable, although no data are available for comparison.

For anthracene, the experimental points fall nearly on a straight line. In terms of equation (1) when $\alpha_f = \alpha_p$, the linear expression $T_g = V_p T_{gp} + V_f T_{gf}$ results. Fitting this equation to the data resulted in a T_{gf} of 44°C for anthracene.

As expected, acetanilide is more efficient in lowering T_g because of its lower glass transition temperature. It is interesting to note that the empirical rule predicting a glass transition temperature at about 2/3 of the melting temperature for unsymmetrical polymers applies to the anthracene, but not to the acetanilide.

(b) Solubility Curve

Figures 2 and 3 also display the equilibrium dissolved volume fraction of filler as a function of temperature. The curves for both systems flatten out while still below the melting point of the pure filler, indicating a marked degree of solid solubility in the concentration range studied.

The intersection of the solubility curve with the T_g curve represents the temperature at which maximum crystallization can occur (90°C for the anthracene and 68°C for the acetanilide). Above this optimum temperature, the crystallization is limited by a thermodynamic solubility equilibrium; while below the

optimum, the glassy state is the crystallization barrier. The latter was checked by measuring T_g after complete crystallization at low temperatures. In all cases T_g was found to be equal to the crystallization temperature.

Figures 2 and 3 thus serve as phase diagrams which mark the boundaries between three states. Above the two curves, the system is one viscous liquid phase. Between the curves, the system is made up of two phases, a crystalline phase and a viscous liquid phase. Below the T_g curve, the polymeric matrix is in the glassy state containing dissolved filler, although filler crystals may also be present depending on the prior thermal history.

Crystallization Kinetics

A primary concern in the fabrication of selectively crystallized composites is the rate at which the filler crystals are formed. Kinetic data also are helpful in the interpretation of crystal morphologies. In Figures 4 and 5 the sample

Figure 4 Progression of Isothermal Crystallization of Acetanilide in SAN at Various Temperatures. The initial Volume Fraction in Solution is 0.30.

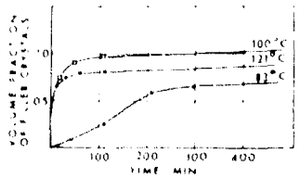

Figure 5 Progression of Isothermal Crystallization of Anthracene in SAN at Various Temperatures. The initial Volume Fraction in Solution is 0.15.

crystallinity (volume fraction crystallized filler) has been plotted against time at several different crystallization temperatures for both systems. In the acetanilide system (Figure 4) the initial volume fraction in solution was 0.30, while the initial dissolved fraction was 0.15 for the anthracene (Figure 5).

In both systems the crystallization rate, as evidenced by the initial slope of the curves, increases to a maximum and then decreases as the crystallization temperature is decreased. At first glance this suggests that the familiar competition between nucleation control (positive temperature coefficient) and diffusion control (negative temperature coefficient) is taking place, resulting in a maximum.

However, when the crystallinity was plotted against the square root of time, a straight line resulted for all temperatures. This would imply that the crystal growth was diffusion-controlled at all temperatures if one assumes that the crystals grew unidirectionally with a constant concentration gradient. Electron micrographs showed that all the crystals did not grow unidirectionally; consequently, additional growth rate studies using hot-stage optical microscopy will be necessary to establish the limits of the diffusion controlled regime. As one might expect, the maximum crystallization rate and the maximum yield of crystals occur at nearly the same temperature.

Comparison of the two systems shows that anthracene crystallized considerably faster than acetanilide. This is expected since the thermodynamic driving force (T eq. - T cryst.) for the anthracene was larger than that of the acetanilide in the temperature ranges investigated.

Filler Crystal Morphology

Electron micrographs of fracture-surface replicas from various composite samples are shown in Figures 6 - 11. They clearly reveal well-formed, low molecular weight crystals with a large variety of sizes and shapes. In general, the bumpy polymer fracture surface is easily distinguished from the smooth crystal surfaces. The well-defined morphology of each sample depends on the heat treatment and crystallization temperature.

(a) Acetanilide - SAN System

Fracture surfaces from acetanilide composites crystallized at 90, 75, and 60°C were examined. In all three cases the initial dissolved filler volume fraction was 0.30. The final volume fraction of filler crystals (V_f) was determined from the phase diagram under complete crystallization conditions.

At 90°C (Figure 6), large crystals have grown in an elongated rectangular shape whose ends often exhibit sharp crystallographic angles. The measurable aspect ratios vary from 2 to 10, with the length being about 20-50 microns and the width 5-20 microns. The shadow lengths and overlapping of crystals suggest a thickness which is considerably smaller than the width. The dark fibrous

Figure 6 Fracture surface of an acetanilide - SAN composite crystallized at 90°C. Note the apparently intact crystal-matrix interface. V_f 0.12; 8000X.

material visible on the left end of the crystal in Figure 6 is polymer which adhered to the crystal edge during fracture and then subsequently adhered to the replica. The bright ridge which runs the length of the crystal is more likely a wrinkle in the replica film and not a feature of the crystal itself. From the drawn appearance of the polymer the fracture was probably ductile in the matrix, while the faint fracture rings on the crystal surface indicate a brittle fracture through the filler. One important observation is that the crystal-matrix interface appears to be intact, indicating that adhesion is relatively good at the interface.

Crystals grown at 75°C (Figure 7) have about the same aspect ratio as those grown at 90°C, but are smaller and more numerous. The occasional dark lines stretching across the crystal from the edges are polymer threads which were drawn out during fracture.

At 60°C (Figure 8), the crystal morphology is considerably different from that of the previous samples. The crystals are long, thin and highly branched. The dendritic bundles appear to have been nucleated at one point from which they grew in all directions. Figure 9 shows a mixture of the two morphologies which resulted from a slow-cooling crystallization. The larger, more perfect crystals were formed at the higher temperatures, followed by dendritic growth which, in some cases, nucleated on the already-grown large crystals.

The replica observations were confirmed by observing actual fracture surfaces with scanning electron microscopy. The advantage of the replica technique lies in its higher resolution which allows more details to be seen at the interface.

(b) Anthracene - SAN System

Instead of two distinct morphologies this system exhibits three different types of crystals grown from an initially dissolved filler volume fraction of 0.20. At a crystallization temperature of 121°C (Figure 10), polygonal-shaped crystals have grown which measure between 1 and 2 microns across. Figure 10 illustrates a rather rare case where the fracture has propagated through the polymer matrix to the interface and then up over the crystal along the interface. The left edge of the crystal is protruding from the matrix, as evidenced by the bright shadow, and the majority of the crystal lies embedded in the matrix.

Figure 7 Fracture surface of an acetanilide - SAN composite crystallized at 75°C. The crystals are smaller and more numerous than in the previous figure. V_f 0.18; 8,000X.

Figure 8 Fracture surface of an acetanilide - SAN composite crystallized at 60°C. The crystals have a highly dendritic morphology. 2400X.

Figure 9 Fracture surface of an acetanilide - SAN composite crystallized by slowly cooling to 60°C. Both large perfect crystals, dendritic bundles and combinations of the two are present. V_f 0.17; 12,000X.

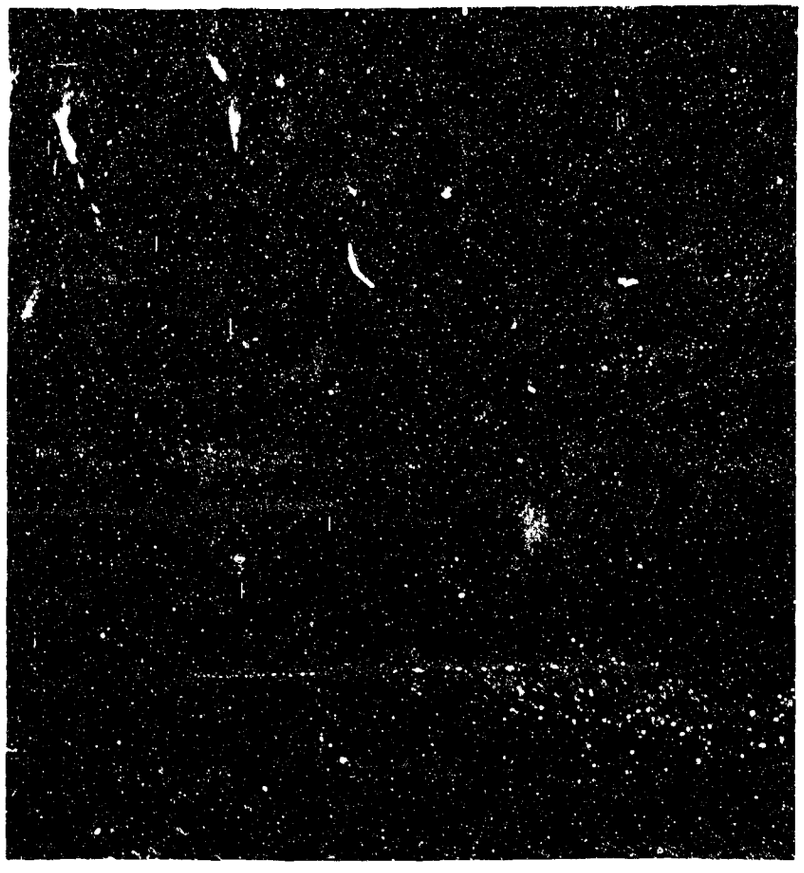

Figure 10 Fracture surface of an anthracene - SAN composite crystallized at 121°C. The left edge of the crystal is protruding slightly indicating fracture up over the crystal along the interface. $V_f = 0.10$; 52,000X.

At 100°C dendritic bundles, very similar to the acetanilide dendrites, were the predominant morphology. However, at 83°C long thin rods appeared which grew with random distribution and orientation. One of these is shown at high magnification in Figure 11. The rods have aspect ratios from 6 to 30 with lengths up to 3 microns and widths of 0.05 to 0.1 micron. The rod surfaces appear to be striated in the long direction. Although the reason for the striations is not known, they could be due to fracture along the length of the rod or they might be the faces of a reasonably perfect single crystal fiber of anthracene.

For both systems the filler crystals are larger and more perfectly shaped at the higher crystallization temperatures. As the temperature decreases, the crystals become smaller and more numerous. At still lower temperatures, both systems exhibit dendritic growth, in agreement with general crystallizations theory. However, the needle-like anthracene crystals differentiate the two systems. Moreover, there seems to be no obvious reason for dendritic growth to be replaced by needle growth at still lower temperatures. Further work is presently aimed at determining why and under what conditions the needles are formed.

Mechanical Properties

The elastic modulus of a polymer filled with infinitely rigid spherical particles should be at least as great as that predicted by the limiting Kerner equation[3]:

$$\frac{G_o}{G_1} = 1 + \frac{15\,(1-V_1)}{8-10\,V_1}\,\frac{\Phi_2}{\Phi_1} \qquad (2)$$

G_o and G_1 are the shear moduli of the filled system and the unfilled polymer, respectively. The volume fractions of polymer and filler are given by Φ_1 and Φ_2 while the Poisson's ratio of the polymer is V_1. Particles of other shapes generally increase the modulus even more than what is observed with spherical particles. If the modulus of the filler is not infinite but is comparable in magnitude to that of the matrix, the composite modulus is less, and the more general form of the Kerner equation must be used for spheres[4].

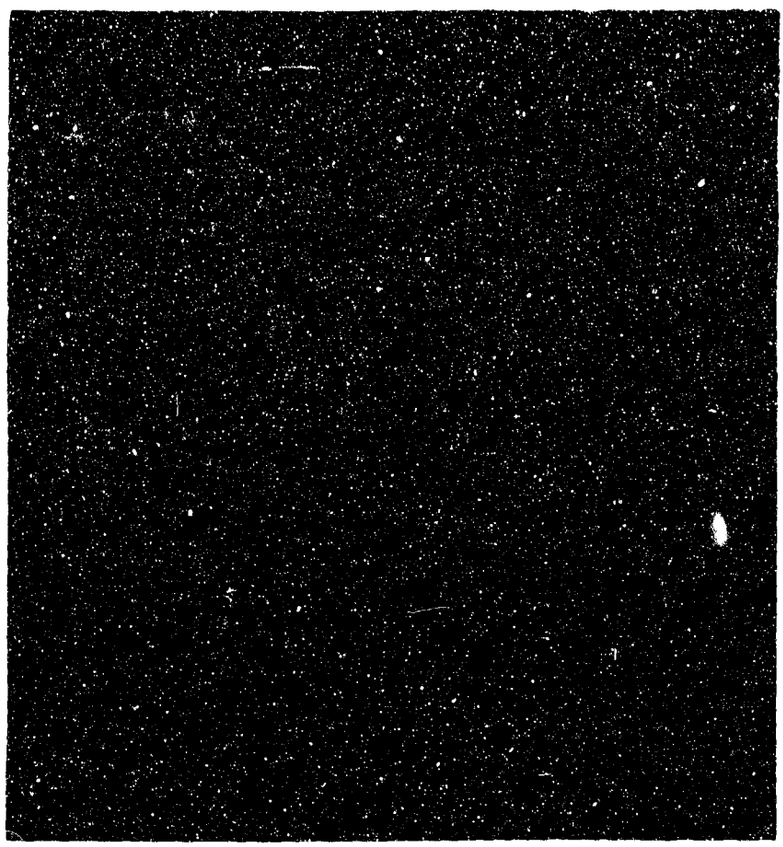

Figure 11 Fracture surface of an anthracene - SAN composite crystallized at 83°C. The small needle-shaped crystals appear to be striated along their length. V_f = 0.08; 39,200X.

$$\frac{G_o}{G_1} = \frac{\dfrac{G_2 \Phi_2}{(7-5V_1)G_1 + (8-10V_1)G_2} + \dfrac{\Phi_1}{15(1-V_1)}}{\dfrac{G_1 \Phi_2}{(7-5V_1)G_1 + (8-10V_1)G_2} + \dfrac{\Phi_1}{15(1-V_1)}} \qquad (3)$$

where G_2 is the shear modulus of the filler phase. In both of these equations it is assumed that there is good adhesion between the two phases.

Figures 12 and 13 show dynamic mechanical data measured on some of the

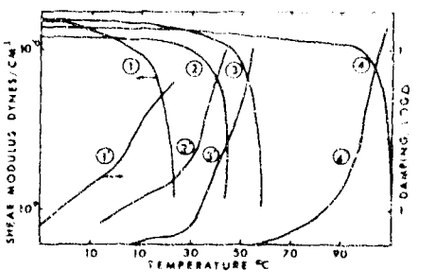

Figure 12 Variation of the Shear Modulus and Damping for Samples of Various Crystal Volume Fractions of Acetanilide. Primed Curves - Damping; Unprimed Curves - Modulus: 1-V_f = 0.30, Non-Crystallized; 2-V_f = 0.18; 3-V_f = 0.38; 4-Pure SAN.

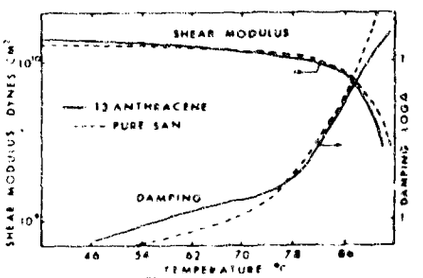

Figure 13 Variation of the Shear Modulus and Damping With Temperature for a 0.13 Crystal Volume Fraction Anthracene Sample and a Pure SAN Sample. The Pure SAN Curves have been Shifted 16°C to the Left for Comparison Purposes.

SAN - acetanilide and SAN - anthracene systems. Dissolved acetanilide and anthracene plasticize the polymer, but if the curves are shifted on the temperature scale an amount equal to the difference in T_g between the filled and unfilled polymers, the shear modulus curves are essentially all superimposable. However, there is little indication that the organic crystals have increased the elastic modulus. The crystallized systems contained crystal volume fractions of 0.18 and 0.38 in the case of acetanilide and 0.13 in the case of anthracene. If the shear moduli of the crystals were much greater (say 10 times or more) than that of the SAN polymer, the shear moduli should have increased at least 48 and 133 percent in the case of acetanilide and over 32 percent in the case of anthracene. The experimental results show no such increase. Since the electron microscope studies seem to

indicate good adhesion between the phases, it can be assumed that the moduli of the organic crystals are approximately the same as that of SAN polymer in the glassy state.

However, if the filler phase is not spherical in shape but fibers or needles oriented perpendicular to the specimen faces as electron microscope pictures tend to indicate, then the shear modulus G_L should be equal to or greater than what the following equation predicts[5]:

$$\frac{G_L}{G_1} = \frac{2G_2 - (G_2 - G_1)\,\Phi_1}{2G_1 + (G_2 - G_1)\,\Phi_1} \qquad (4)$$

In this special case of oriented fibers, the shear modulus is less than what it would be if the filler particles were spheres. If the fibers have high moduli compared to the polymer, the shear moduli should have increased at least 44 and 123 percent in the case of acetanilide and 30 percent in the case of anthracene as filler. Even after the SAN curve is shifted so as to compare the data at the same $(T_g - T)$ values, the observed increase in modulus is only 9 percent for the anthracene case at 38°C. For the acetanilide case containing 0.38 volume fraction of crystals, the experimental increase in shear modulus is 15 percent at -30°C and 22 percent at 10°C. The modulus of the material containing 18 volume percent acetanilide is actually less than that of pure SAN even after the curves are shifted horizontally to compare at equal values of $(T_g - T)$. The error in the absolute value of the experimental moduli is estimated to be about 5 percent. Thus, even after picking the modulus data that show the greatest reinforcing action, it can be shown that the shear moduli of the crystals must be less than twice that of the SAN polymer[4, 6]. Additional evidence that the elastic moduli of organic crystals is about 10^{10} dynes/cm^2 is found in recent measurements on polymer crystals; the elastic moduli in directions perpendicular to the polymer chains are essentially the same as the moduli of polymers in the glassy state[7, 8].

Elastic modulus measurements are not common on single crystals of organic materials. Many measurements, however, are available on materials which have strong bonding forces such as metals and ionic inorganic crystals where it is

found that the moduli are ten to one hundred times as great as the moduli of polymers in the glassy state. Molecules in organic crystals and glassy polymers are both held together by the same type of weak Van der Waal's forces, so it is not surprising that they both appear to have approximately the same moduli. Thus, it is concluded that high modulus polymers cannot be appreciably reinforced or stiffened by organic crystals. However, organic crystals might be very good reinforcing materials for rubbers and low modulus polymers.

References

1. Nielsen, L. E. Rev. Sci. Instr., 22, 690 (1951).

2. Buche, F. Physical properties of polymers, Interscience, Wiley, New York, p. 117 (1962).

3. Nielsen, L. E. Mechanical properties of polymers, Reinhold, New York (1962).

4. Kerner, E. H. Proc. Phys. Soc., London, 69B, 808 (1956).

5. Tsai, S. W. NASA CR-71 (July 1964).

6. van der Poel, C. Rheol. Acta., 1, 198 (1958).

7. Sakurada, I., T. Ito and K. Nakamae, Bull. Inst. Chem. Res., Kyoto Univ., 42, 77 (1964).

8. Sakurada, I., T. Ito and K. Nakamae, J. Poly. Sci. (Symposia) 15C, 75 (1966).

V. FABRICATION AND PROCESSING (J. M. McKelvey and T. L. Tolbert)

The role of Fabrication and Processing Section can be summed up as one of demonstrating, through application of Association research, the fabrication and performance of new, practical, high performance, composite structural materials. In line with the charter to develop a new area, the major emphasis is on the development of discontinuous fiber composites which have high performance properties and can be readily fabricated. Initial performance goals have been defined here, as elsewhere in the Association, in terms of surpassing the specific properties of aluminum.

The work divides naturally into three areas: composite fabrication and evaluation, process research, and technical support. Work in the fabrication and evaluation area has been aimed at (a) evolution of new technology for the fabrication of discontinuous fiber composites, (b) establishing experimentally practicable levels of composites performance as determined by fiber morphology, loading, and fiber/matrix modulus ratio and (c) testing experimental samples and providing performance standards.

Process research has been concerned primarily with the refinement and improvement of processes found by Association research for incorporating discontinuous fibers in matrices to produce prepregs and/or finished composites. This work has provided specimens for evaluation and mechanics studies, as well as the base for process engineering investigations.

Technical support has been provided to the entire M/WU Association by (a) providing a supply of fibrous materials of known quality (whiskers and chopped continuous filaments) by carrying out filament chopping, fiber and whisker cleaning and classification, and fiber characterization operations, (b) fabricating and molding test coupons and elemental shapes, and (c) performing mechanical and environmental tests.

Whisker fibers (silicon carbide and silicon nitride) and short chopped fibers (boron and carbon) have received primary attention. Each type offers utility in preparing and effectively reinforcing complex shapes which cannot be fabricated satisfactorily from continuous filament or fabric. Glass fiber has been employed as a prototype fiber when its use was considered technically sound and effective in reducing the cost of research materials.

Work has been restricted largely to the use of epoxy resins as matrices; studies employing higher performance resins are being initiated, however. Preliminary experiments with polyelectrolyte resins developed in the Chemistry and Physics Section have shown particular promise. Scouting studies with metal matrices will be initiated shortly.

Efforts in the major processing and fabrication programs are summarized in the following paragraphs.

Cutting, Clean-up, and Classification of Short Fibers

Preparation, clean-up and classification of short fibers and whiskers is now routine. Methods have been established by Messrs. R. E. Lavengood and D. C. Morris for cutting filament to size on a rotary or guillotine chopper. The fiber is then cleaned and sorted using a vibrationally fed trough device in which controlled amounts are collimated and carried over a series of increasingly large collection slots. Whiskers are too small to be handled in this way.

A technique has been developed by Mr. J. D. Fairing for removal of the large amounts of debris in "as received" whisker material and sorting of the whiskers to size. It is based on water jet break-up of clumps and wet screening of the resulting slurry. DS-grade silicon carbide whiskers from Carborundum Company yields about 30% of reasonably good quality whiskers in this process. Qualitative observations indicate there is little breakage or loss of the better fibers. Nominal aspect ratios of the classified material run from 50-60 for the better whiskers to 20-40 for the poorer grades.

Fiber and Whisker Characterization

Dr. R. C. Schierding has established procedures and developed techniques for characterizing fibers and whiskers for size, condition, and orientation. Characterization for number and volume average length and diameter is based on standard cumulative photocounting techniques. Condition, extent of overgrowth or other preparative imperfections, and degree of processing damage are determined by optical and electron scanning microscopy. Fiber orientation in prepregs and composites is measured by an X-ray diffraction technique developed from metallographic practice. Measurements have been automated using a full circle goniometer.

Composite Evaluation and Testing

An expanded testing capability for measuring uniaxial composite properties has been developed by Mr. Lavengood in conjunction with the Mechanics Section.

Facilities are available to all programs in the Association. Strength and modulus are measured in flexure, tension, and compression. Poisson's ratio and shear are obtained from the antielastic plate bending test. The tube torsion test for shear is currently being set-up and a cooperative study with the Mechanics Section on test evaluation has been initiated.

Use of Oriented Whiskers as Reinforcing Agents

Fabrication of whisker reinforced composites has required development of a number of special techniques. Whiskers are about two orders of magnitude smaller in diameter than conventional boron fiber, thus are truly micro-fibers. Typical dimensions are 1 x 50 microns. Dr. O. D. Deex has demonstrated excellent fiber orientation by dispersing the whiskers in a non-melting carrier polymer and wet spinning the suspension to form a strand. The whiskers become aligned during extrusion and the subsequent drawing step and are "locked" in position by coagulation of the carrier polymer. Mats can then be prepared from the strand and the carrier removed by pyrolysis. Selection of the carrier has proven to be the key to controlling fiber movement during pyrolysis, as well as spinning; and to avoiding some of the problems encountered with this approach by Wohrer, Parratt, and others. Dr. T. L. Tolbert has fabricated well oriented whisker fiber composites by laying-up whisker-filled strands in the desired orientation, pyrolyzing the carrier without disturbing whisker orientation, and impregnating the whisker mat to give a prepreg which can be shaped and molded. The technique is reproducible and amenable to scale-up. Composites of silicon carbide whiskers ($\ell/d = 50$) with flexural strengths as high as 99×10^3 psi and moduli as high as 15.4×10^6 psi have been prepared.

Studies on Composite Composition and Structure

Mr. R. M. Anderson has carried out a series of studies on composite composition and structure as a guide to processing work. A hand lay-up technique has been developed for this purpose which provides maximum control over short fiber orientation and other variables. Although somewhat time consuming, it provides a means of checking the effect of individual processing parameters, establishing property bench-marks for new materials, and obtaining property maps for the various composite systems. It has proven applicable to conventional "E" and "S" glass fibers, standard boron fiber, a special boron fiber 1.5 mils in diameter, and "Thornel" graphite fibers. Loadings as high as 80 v/o have been obtained.

Dry-Mix Molding of Short Fiber Composites

Studies involving intimate mixing of short fibers with dry, very finely divided matrix before molding have been carried out in an effort to avoid the adverse viscosity effects and fiber entanglement encountered in blending fibers with viscous matrix resins at high loadings. The study was conducted by Mr. D. A. Ludwig as an M.S. thesis problem at Washington University. It showed that fibers are at least partially protected from self-abrasion during blending by the matrix powder, that uniform blends of short fibers (below $\frac{1}{4}$") and matrix can be obtained. Although model systems were used for the bulk of the study and properties were not in the high performance range, the potential of the dry-mix approach for orthotropic composites was demonstrated. Details of this work are reported in Mr. Ludwig's thesis; copies are available on loan from Olin Library, Washington University.

Encapsulation and Flow Molding of Short Fibers

Encapsulation of short fibers has been shown to be particularly effective in overcoming processing problems and increasing fiber loadings. Follow-up of the preliminary work on encapsulation of glass fiber and flake reported by Dr. H. M. Andersen at the 1965-66 Annual Project Review has led to development of a well-defined technique for producing molding compounds of high performance fibers. Free-flowing, rice-sized aggregates of collimated fibers encapsulated with resin can now be obtained from a variety of fibers and whiskers. The granules can be compression molded or readily transfer molded. Mr. Morris has shown that encapsulated fibers are not only oriented during flow molding but also overlapped as the grains interlock during flow. Fiber efficiencies based on a rule of mixtures calculation are in the range of 70%.

Fabrication with Polyelectrolyte Resins

The polyelectrolyte resins studied by Drs. L. E. Nielsen and J. E. Fields and reported in the Chemistry and Physics Section offer unique combinations of properties which should make them suited for a variety of high performance applications. Stiffness and shear properties are outstanding, values as high as 2.7×10^6 psi for Young's modulus and 1.25×10^6 psi for shear modulus have been measured. Flexural strengths appear to range from $10-15 \times 10^3$ psi, although only a few measurements have been made. Heat distortion temperatures are well above 300 °C and calculations predict extremely low creep. Preliminary experiments indicate that sound composites can be fabricated from

the resins, that fiber-resin bonding is good, and that resultant composites are not seriously water sensitive. Work to determine the potential for these materials in practical applications is being initiated.

Summary

Overall results of fabrication work in the Project can best be reviewed in terms of the property levels of the composites which have been produced. Figures 1 and 2 compare the specific strength and modulus values obtained for the various types of composites studied. The bars represent what can be accomplished with a specific fiber or process; experimental data have been normalized at the 50 v/o loading level for comparison. It is apparent that a high percentage of the properties obtainable with continuous filaments can be achieved with short fibers. Some trade-off in properties is made in going from a careful hand lay-up of fibers to flow processing, as would be expected. The properties of the transfer molded and extruded specimens are still high enough, however, to be of very real interest and well within the high performance category. The specific properties of aluminum are shown for comparison.

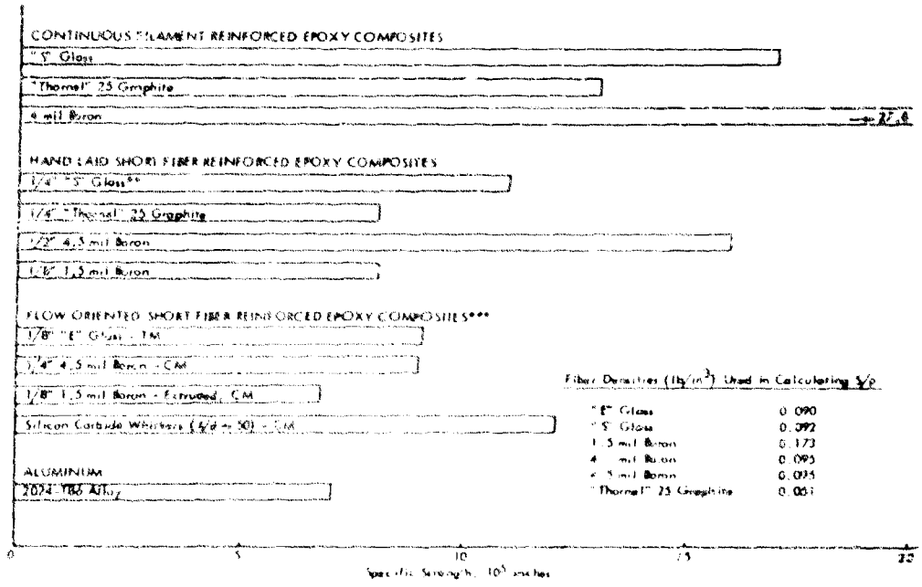

Figure 1 Specific Strengths of Composites Unidirectionally Reinforced with Short Fiber (50 v/o)*

*Experimental Data Normalized For Comparison
**Calculated Value
***Boron and Glass Fibers Encapsulated Prior to Molding; CM - compression molding, TM - transfer molding

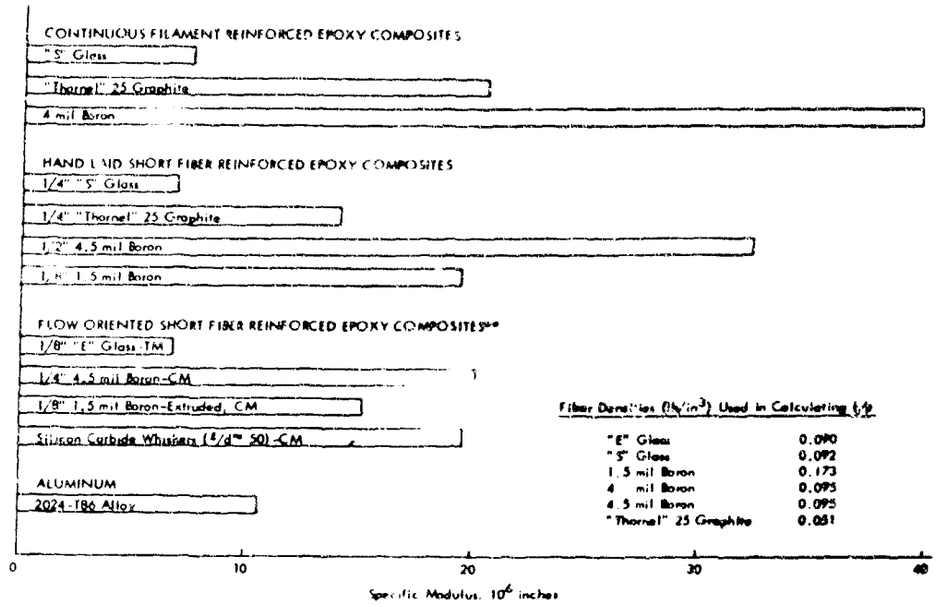

Figure 2 Specific Moduli of Composites Unidirectionally Reinforced with Short Fiber (50 v/o)*

*Experimental Data Normalized for Comparison
**Boron and Glass Fibers Encapsulated Before Molding; CM = compression molding, TM = transfer molding

Figure 3 compares the specific properties of aluminum with those of hand laid boron composites and silicon carbide whisker composites as functions of fiber loading. In both cases, fiber loadings of only 15-25% are required to reach the aluminum level and the composite curves continue upward. This is, of course, a comparison of unidirectional composite properties against isotropic metal properties. Dr. Tsai has recently shown that, at least for modulus, a more meaningful comparison is obtained using a value 1.3 times the specific properties of aluminum. Even so, the promise of short fiber boron and silicon carbide whisker composites is apparent.

Work in the Fabrication and Processing Section has progressed through all of the steps involved in getting fibers into composites - from raw material refinement to actual fabrication. The techniques, quality of material, and procedures needed for careful, systematic studies are in hand. The first exploratory phase is essentially completed and emphasis is on development and evaluation of specific fabrication and processing methods. Systems and

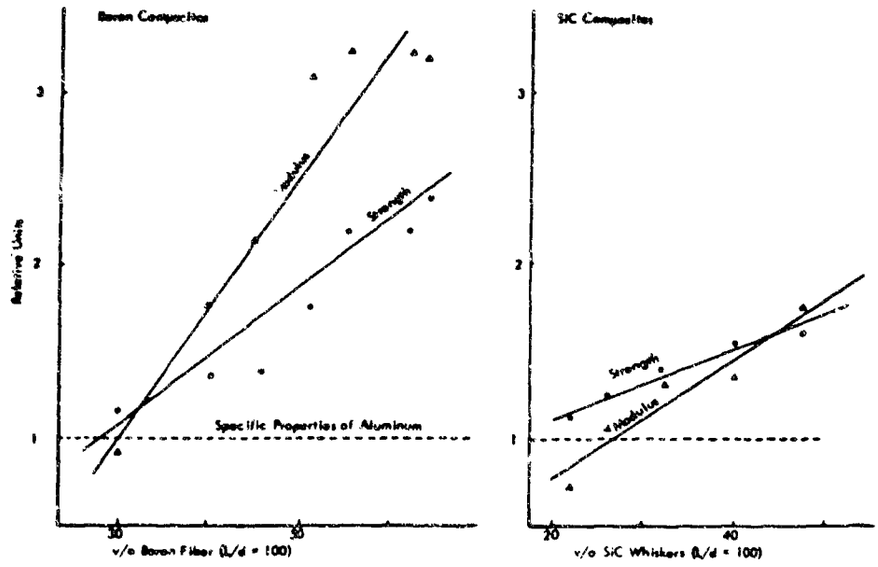

Figure 3 Comparison of Specific Properties

techniques will be selected shortly for scale-up and preparation of a variety of elemental shapes. Concurrently, new fiber and matrix systems are being evaluated and new methods for combining and processing matrix and fiber are being explored. The research program is closely coordinated with those in the Chemistry and Physics and the Mechanics Sections.

WHISKER FIBER FRACTIONATION (J. D. Fairing)

Fabrication of discontinuous fiber reinforced composites having highest performance capabilities can be achieved only by using clean fibers free of particulate matter and having an aspect ratio in excess of 50 when employed with organic matrices. Commercial whiskers with the necessary high modulus requirements have a wide range of aspect ratios and are invariably contaminated with excessive amounts of particulate matter.

A procedure was developed for upgrading the available material to produce clean, classified whiskers suitable for fabricating test specimens.

Silicon carbide whiskers, as received, contain 15 to 30 percent usable fibers, the rest being a mixture of short fibers, dust, and irregular particles ranging in size from over 1 mm to less than 0.1 micron. Figures 1 and 2 illustrate the inhomogeneity of this material. Classification is achieved by a

three step process involving (1) dispersion of the tangled mats of fibers in water, (2) removal of the short fibers, dust, and most of the particulate material by wet sieving and finally, (3) separation of the whiskers from the remaining particles by sedimentation.

Dispersion is accomplished by first wetting the fibers with ethanol and then gently stirring them into a large volume of water; typically, 5 g. of fibers are dispersed in 4 liters of water. This partially dispersed slurry is then washed repeatedly through a series of sieves of increasing fineness with openings ranging from 707 microns down to 44 microns to achieve complete dispersion and to remove the short fibers, dust, and most of the particles. The dispersion step is a critical one. It must be complete, for classification can be achieved only after the fibers have been untangled and are monodispersed.

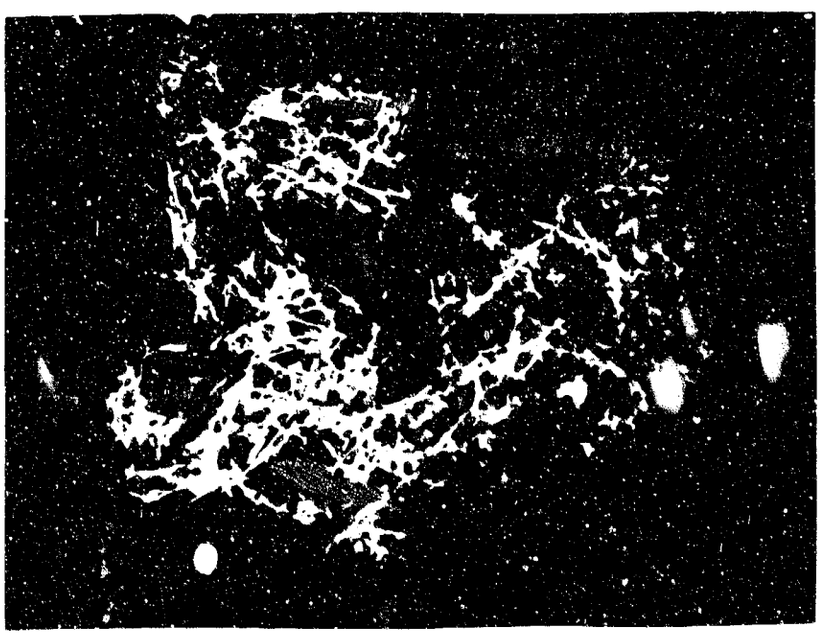

Figure 1 Silicon Carbide Whiskers "As Received" Showing Tangled Mats of Fibers of Random Length, 91X

However, it must also be gentle since the individual whiskers are fragile and readily damaged when isolated; consequently, efficient dispersion methods utilizing large energy inputs, such as ultrasonic agitation, cannot be used.

After repeated passes through the series of sieves by the use of large volumes of water, the fiber collected on sieves with 88 and 44 micron openings are uniform in length and are contaminated only with medium size particulate

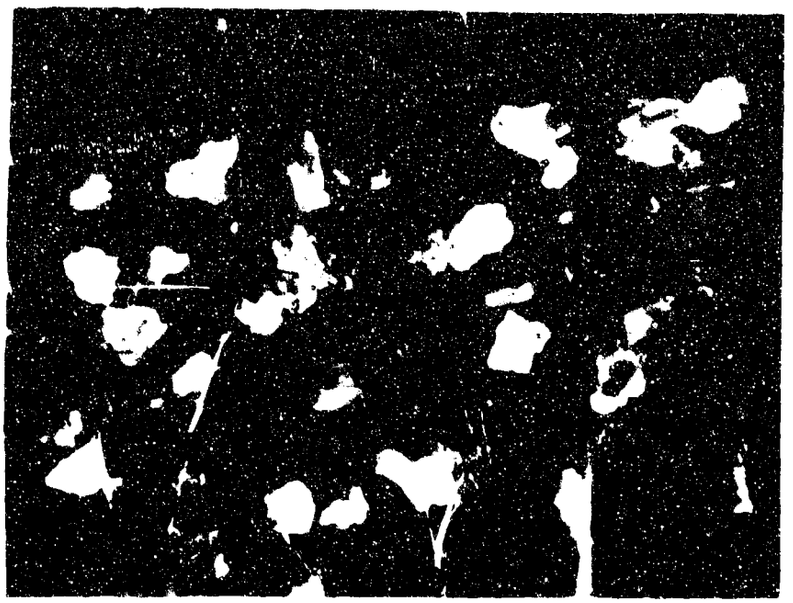

Figure 2 Silicon Carbide Whiskers "As Received" Showing Large Particulate Material, 91X.

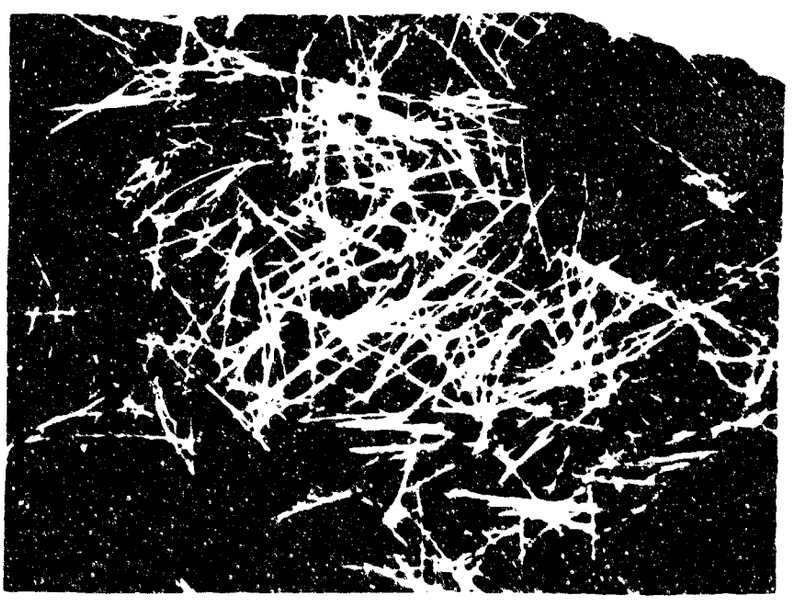

Figure 3 Classified Silicon Carbide Whiskers, 91X.

material, the short fibers and dust having been washed through and the larger contaminents isolated in the coarser sieves. The removal of these remaining particles is carried out by a sedimentation procedure in water. At the present time this step is the least efficient part of the process, and requires improvement.

Classified silicon carbide whiskers obtained by this process are shown in Figure 3. These are now being used for the fabrication of all our silicon carbide whisker composites and can be produced routinely on a laboratory scale at the rate of about 30 grams per week.

MEASUREMENT OF WHISKER ORIENTATION IN COMPOSITES BY X-RAY DIFFRACTION (R. G. Schierding)

The properties of whisker reinforced composites are directly dependent on the degree of orientation of the whiskers. Consequently, development of optimum properties requires not only a method for controlling whisker orientation but also a means for quantitatively describing it.

X-ray diffraction methods, which have long been used to measure preferred orientation in polycrystalline metals[1], have been found to be applicable to measuring whisker orientation in composites as well.

This report is divided into two parts. The first describes an x-ray photographic method which has been found to be very useful for measuring the degree of whisker orientation in highly oriented strands made by a wet spinning process. Orientation in composite sheets can also be measured with this technique provided the samples are thin enough to transmit the diffracted x-rays. The second part of this report describes a quantitative technique for measuring the degree of whisker orientation in flat composite samples. The reflection method used in this work does not require that the diffracted x-rays penetrate the sample and therefore is not restricted to thin samples. The x-ray intensity is quantitatively measured with a radiation detector and the degree of orientation is described in terms of the standard deviation of the intensity distribution.

Photographic Method

When monochromatic radiation is used to examine a specimen in a Laue camera, the result is called a pin-hole photograph[2]. The technique involves impinging a monochromatic beam of x-rays onto the composite sample. Certain crystal planes of the whiskers will make the correct Bragg angle (according

to the Bragg equation) for diffraction (reflection) of the incident be[illegible] a powder sample or a composite filled with randomly oriented whiskers, some of the whiskers will be oriented at all possible rotational positions about the axis of the incident beam. The resultant reflection will therefore have the form of a cone of diffracted x-rays, the axis of the cone coinciding with the transmitted beam. A separate cone will be formed for sets of differently spaced lattice planes[3].

When a sheet of photographic film is placed to intercept the cone of x-rays, they form an exposed circle known as the Debye ring[4]. This is shown in Figure 1. For a randomly oriented sample, continuous concentric Debye rings of constant intensity are formed on the photograph. In specimens with perfect orientation, the Debye rings are reduced to a set of intense spots symmetrically oriented about the circumference of the ring. These spots broaden peripherally as the degree of orientation decreases. The length of the arcs thus formed is a measure of the degree of orientation and the intensity along the arc is a measure of the volume fraction of material within a specified degree of orientation[2].

The composite sample is placed between the incident x-rays and a sheet of x-ray film. The sample thickness must be such as to readily transmit the diffracted x-rays. X-ray diffraction patterns were obtained in this manner using a Nonius general purpose camera and copper K-α radiation. The samples consisted of a polymeric matrix containing silicon carbide whiskers. The silicon carbide was the hexagonal high temperature polymorph (α-S_iC) of the 6H polytype[5,6,7]. Their growth axis, as determined from highly oriented samples, is perpendicular to the basal plane of the hexagon. It is this common growth axis which makes possible the measurement of preferred orientation in composites.

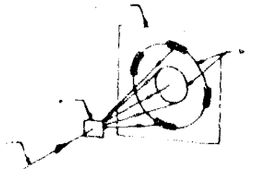

Figure 1 Transmission Pin-Hole Photographic Method for Measuring Orientation

One of the most recent methods for preparing highly oriented whisker composites is by the spinning of suspensions of whiskers in viscous polymer solutions[8]. The small orifice and following draw results in highly oriented whiskers in the polymer matrix. This "strand" can be laid-up, the polymer

burned off, and the remaining whiskers impregnated with the desired matrix material for fabrication of a finished composite. The degree of whisker orientation obtained in the spinning operation and carried through to the finished composite can be closely followed by the x-ray photograms.

The strands are approximately 0.015 inches in diameter and are easily penetrated by the copper radiation giving good distinct photograms after one to two hours exposure. The following photograms demonstrate the sensitivity of this technique. Figure 2 is a photogram of a Cupram strand and Figure 3 an acetate rayon strand, both containing silicon carbide whiskers. The

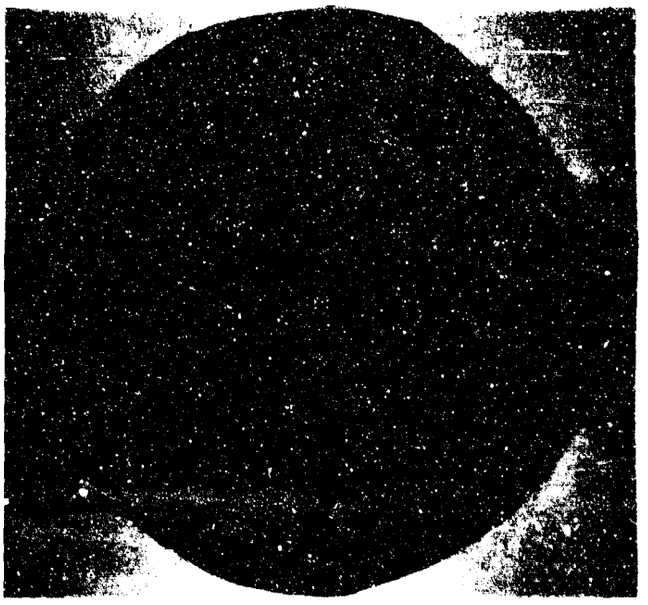

Figure 2 Photogram of a Cupram Strand Containing Silicon Carbide Whiskers

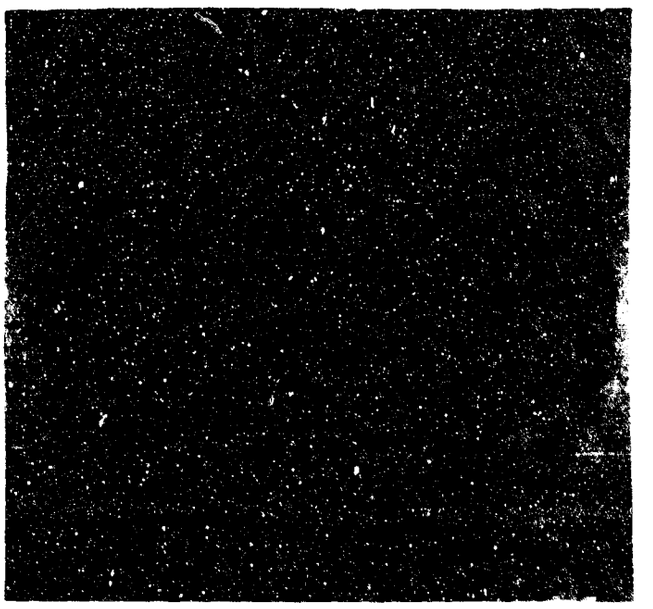

Figure 3 Photogram of an Acetate Rayon Strand Containing Silicon Carbide Whiskers

whiskers in the Cupram strand show a higher degree of orientation than the acetate strand. The length of the arcs indicates that the major portion of the whiskers are oriented within 11° of the strand axis for the Cupram and 20 for the acetate. The volume fraction represented by the intensity along the arc can be visually estimated or more accurately determined by a densitometer plot of the intensity profile. However, this is semiquantitative at best since absorption corrections cannot readily be made. Figure 4 is a photogram of a composite made from the Cupram strands.

The composite was a 1 x 1/4 x 1/64 inch sheet of epoxy filled with silicon carbide whiskers. The x-rays easily penetrated the sample. The arc lengths are much greater in the composite photogram than in that of the strand indicating that a large degree of misorientation results during the fabrication process. The broadening of the ring is probably due to increased strain in the whiskers as a result of fabrication.

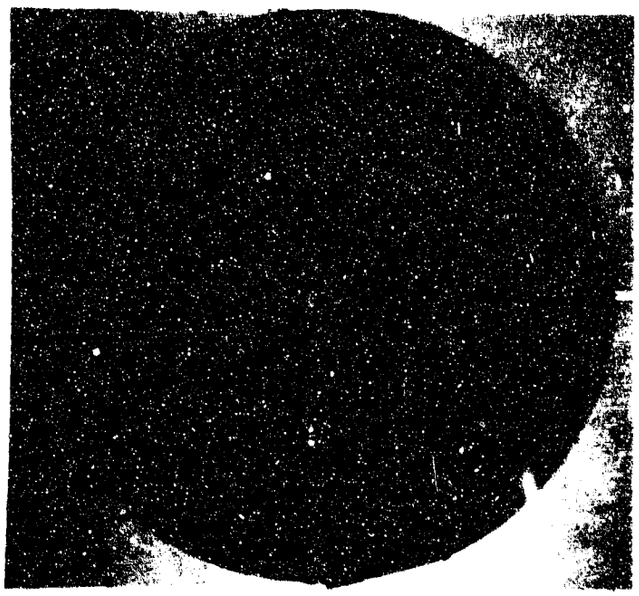

Figure 4 Photogram of an Epoxy-Silicon Carbide Composite Made From the Cupram Strands

The transmission photographic method offers an easy and rapid means of qualitatively following the degree of whisker orientation in composites. This method is limited, however, to thin samples and therefore has been used primarily to determine the orientation in the highly oriented strands produced by wet spinning. For thick composite samples or where quantitative results are required, the x-ray film must be replaced with a radiation detector. This method is described in the next section.

Quantitative Method

The measurement of preferred orientation with a radiation detector (diffractometer) provides a means of quantitatively measuring x-ray intensities. The diffractometer is set to pick up a segment of the Debye ring while the sample is slowly rotated in its own plane. The intensity profile around the Debye ring is thus quantitatively determined. This is demonstrated in Figure 5 for the transmission method.

Crystal planes are often described in terms of the normal to that plane, called a "pole", and preferred orientation is discussed in terms of pole density[1,9,10]. Imagine the sample to be at the center of a large transparent sphere. Let the poles from a given family of planes be extended from every crystallite (whisker) until they intercept the sphere. If the whiskers are oriented

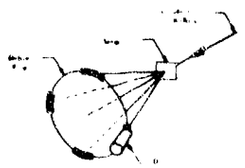

Figure 5 Transmission Method Using a Diffractometer for Measuring Orientation

randomly in the sample, the density of pole intercepts will be distributed uniformly over the entire surface of the sphere. If the whiskers have a preferred orientation however, the pole intercepts will not be uniform but will be clustered in certain areas on the sphere and absent in others depending on the degree of orientation. This pole density can be measured by rotation of the sample during irradiation. The projection of the pole distribution from the sphere onto a flat sheet of paper is called a pole figure. The pole figure is usually shown as a contour map where lines of constant x-ray intensity represent pole density.

Several authors[11,12,13,14,15,16,17,18] have described methods for determining pole densities (pole figures) with the diffractometer and one author[19] has measured the orientation of clay particles in starch coatings using the method of Field and Merchant[15]. The transmission method of Decker, Asp, and Harker[11] employs thin sheet specimens which can be rotated about two mutually perpendicular axes, one axis being normal to the plane of the sample and the other coinciding with the axis of the spectrometer. Equations are given for correcting observed counting rates for changes in absorption and scattering volume as the sample is rotated. The corrected intensities can be plotted on a polar net to give the pole figure. The transmission method is limited to samples which are thin enough to transmit the diffracted x-rays and is capable of determining pole density only in the outer portion of the pole figure, from 90° to 90° - θ (where θ is the Bragg angle). This limitation is due to the geometry of the sample and holder with respect to the detector[14].

The central portion of the pole figure is obtained by the reflection method of Schulz[13]. A flat specimen of sufficient thickness is rotated in such a manner that absorption and effective volume of scattering material remain constant. During examination, the sample is rotated about two-axes, one normal to the sample surface (O-O' in Figure 6) and the other located along the intersection of the sample and the plane of the spectrometer (X-X' in Figure 6). Rotation of the sample around the surface normal through an angle α, corresponds to scanning the circumference of the Debye ring. On a polar net, this is equivalent to measuring the pole density around one of the latitude lines of the pole

Figure 6 Reflection Method Using a Diffractometer for Measuring Orientation

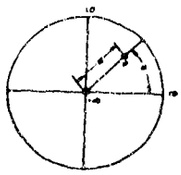

Figure 7 Pole Figure Showing the Position of the Pole P as Determined by α and Φ

figure as shown in Figure 7. Rotation around X-X', through an angle Φ, determines the pole density along a longitude line (radius of the polar net)[20]. The reflection method is limited with respect to the range of tilting angles, Φ, in which satisfactory results can be obtained. The diffracted beam intensity decreases with increasing Φ and is the result of defocusing of the diffracted beam[21]. This is discussed more fully in a later section. The reflection method is capable of providing data for constructing a complete pole figure. The outer portion of the pole figure is obtained from orthogonal surfaces of the sample constructed by sawing or grinding the sample so as to expose these surfaces[16,17]. This is destructive in the sense that the sample may no longer be suitable for mechanical or other measurements so that only the pole density out to $\Phi = 70°$ was determined in this work.

The Schulz reflection method was used to determine the orientation of silicon carbide whiskers in an epoxy matrix. A Siemens full-circle goniometer, copper K-X radiation and a crystal detector were used to obtain the data. With this instrument, the sample can be continuously and simultaneously rotated through Φ degrees of latitude and α degrees longitude at a fixed rate. The angle Φ was varied at 1° per minute while α was changed 360° every 4 minutes. In order to insure that the detector was not encountering neighboring difiraction peaks[22], the $(11\bar{2}0)$ peak of silicon carbide was chosen for study[23]. The $(11\bar{2}0)$ is a major peak, for good peak-to-noise ratio, and is sufficiently removed from neighboring peaks. Spurious signals were minimized by using pulse-height analysis to discriminate diffraction due to wavlengths longer and shorter than the copper K-X radiation. In order to achieve clear definition of the diffracted intensity distribution, the diffractometer slit system was 6 milimeters in length and 0.5 milimeters in height. The aperture slit system was 1 by 2.5 milimeters

which assured that no part of the incident beam left the sample surface during the run. For a good statistical sampling of the orientation across the sample surface, the sample holder was vacillated back and forth by ± 7.5 milimeters.

The technique is demonstrated by the following example. The composite was made with silicon carbide whiskers which had been highly oriented by the spinning process previously mentioned. The burned off whiskers were impregnated with an epoxy resin containing a curing agent and a coupling agent. The prepregged sample was then cured under 2000 psi pressure at 150 °C for 1 hour. The finished composite contained approximately 50 volume percent silicon carbide. The random sample was made with beta silicon carbide powder impregnated with epoxy. Beta silicon carbide has a major peak occurring at the same Bragg angle as the alpha form[23]. The resultant samples were 1 x 7/8 x 1/16 inch sheets. Two sheets were stacked together during irradiation in order to provide sufficient scattering volume for the diffracted x-rays[13].

The observed intensities were corrected for background by subtracting the average of the background intensity measured two degrees above and below the Bragg diffraction peak[24,25]

$$I(\Phi,\alpha) = I_{obs.}(\Phi,\alpha) - I_{bkg.}(\Phi,\alpha) \qquad (1)$$

In the Schulz reflection method, defocusing of the diffracted beam occurs as the goniometer ring is rotated from the $\Phi = 0°$ (reflecting surface vertical) to $\Phi = 90°$ (reflecting surface horizontal). This defocusing results in appreciable loss of diffracted intensity, the loss increasing with increasing Φ. This decrease can be determined experimentally however, by observing the change in diffracted intensity from a randomly oriented sample as Φ changes[26]. The data from the oriented sample are then corrected for each Φ position by a factor equivalent to the change in random intensity.

$$\text{Correction Factor} = \frac{I_R(0,\alpha)}{I_R(\Phi,\alpha)} \qquad (2)$$

$$I_c(\Phi,\alpha) = I(\Phi,\alpha) \cdot \frac{I_R(0,\alpha)}{I_R(\Phi,\alpha)} \qquad (3)$$

where

$I_{obs}(\Phi,\alpha)$ = Observed intensity from oriented sample.

$I_{Lkg}(\Phi,\alpha)$ = Background intensity from oriented sample.

$I(\Phi,\alpha)$ = Observed intensity corrected for background.

$I_R(0,\alpha)$ = Random intensity corrected for background at $\Phi = 0$.

$I_R(\Phi,\alpha)$ = Random intensity corrected for background.

$I_c(\Phi,\alpha)$ = Observed intensity corrected for background and defocusing of the beam.

The final corrected intensity, $I_c(\Phi,\alpha)$, can be normalized by dividing $I_c(\Phi,\alpha)$ by the corrected intensity at $\Phi = 0$, $I_c(0,\alpha)$.

$$I_n(\Phi,\alpha) = \frac{I_c(\Phi,\alpha)}{I_c(0,\alpha)} \times 100 \qquad (4)$$

A pole figure is not necessary if the pole density is visualized as a height above the plane of the pole figure[27]. If the pole density consists of a sharp single orientation texture, the pole distribution may take the form of a normal probability curve. The equation for the normal curve depends on two constants[28]; the arithmetic mean $\overline{X}$, and the standard deviation σ. The probability function $P(X)$ is:

$$P(X) = \frac{1}{\sigma\sqrt{2\pi}} \exp\left[-(X-\overline{X})^2/2\sigma^2\right] \quad ((-\infty < x < \infty) \qquad (5)$$

where $\overline{X} = \dfrac{\sum_{i=1}^{k} f_i \chi_i}{N}$, $\sigma = \left[\dfrac{N\sum_{i=1}^{k} f_i \chi_i^2 - (\sum_{i=1}^{k} f_i \chi_i)^2}{N}\right]^{\frac{1}{2}}$

and $N = \sum_{i=1}^{k} f_i$

χ_i = value of the class.

f_i = frequency of the class.

The probability that a whisker picked at random will be oriented within a given interval X_1 to X_2 is the area under the normal curve between these limits. This probability also represents the proportion of all the whiskers in the sample which are oriented between X_1 and X_2. The total area under the normal curve must therefore equal one.

$$\int_{-\infty}^{\infty} P(X) = 1$$

The above equation gives an indefinite integral for any real limits and therefore only approximate solutions can be obtained. Standard tables of such solutions are available[29] and the following limits and areas are sometimes sufficient to describe a given distribution.

Limits	Area or Probability
$\overline{X} - \sigma$ to $\overline{X} + \sigma$	0.6827
$\overline{X} - 2\sigma$ to $\overline{X} + 2\sigma$	0.9545
$\overline{X} - 3\sigma$ to $\overline{X} + 3\sigma$	0.9973

Thus the standard deviation, σ, gives a numerical measure of the sharpness of the pole density and the area under the normal curve gives the relative volume fraction of the whiskers within a given set of limits.

The experimental results are listed in Table I where data is given for every 5° of ϕ and for $\alpha = 0°$ and $\alpha = 90°$. This data is sufficient to demonstrate the magnitude of the results without giving data at each degree.

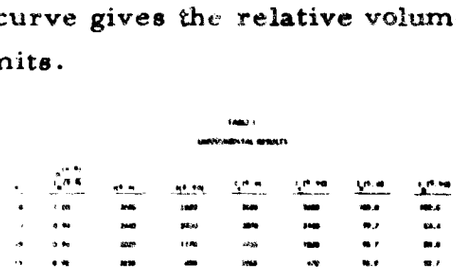

To calculate the standard deviation and arithmetic mean of the two distributions given in Table I, the number of degrees is taken as X_i and the normalized intensity as frequency, f_i. The results of this calculation are:

for $I_n(\phi, 0)$: $\sigma_1 = 35°$ and $\overline{X} = 0°$

and $I_n(\phi, 90)$: $\sigma_2 = 10°$ and $\overline{X} = 0°$.

The significance of these results can be seen in Figures 8 and 9. The sheet composite is illustrated in Figure 8 where the longitudinal, transverse, and normal directions are labeled. Since the $(11\bar{2}0)$ direction is perpendicular to the whisker axis (the (0001) direction), the distribution of $(11\bar{2}0)$ planes is a direct measure of the distribution of the whisker ends, the (0001) planes. Figure 9 shows this distribution relative to the sample directions. The whiskers are highly oriented along the longitudinal axis with respect to the normal direction and much less highly oriented with respect to the transverse direction.

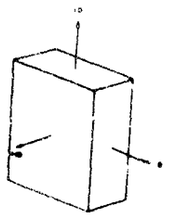

Figure 8 The Composite Coordinates Showing Normal Direction (ND), Transverse Direction (TD), and Longitudinal Direction (LD)

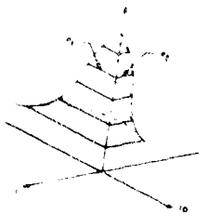

Figure 9 Pole Density Distribution with Respect to the Composite Coordinates

This result was to be expected since the sample is compressed in the normal direction during pressure molding with flow occurring in the transverse and longitudinal directions.

As the degree of orientation improves, the standard deviation along the transverse direction (σ_1) for the $(11\bar{2}0)$ planes becomes larger since the pole density is approaching rotational symmetry about the longitudinal direction. The standard deviation along the normal direction (σ_2) becomes smaller with improving orientation. Thus the distribution of the whisker ends is inversely proportional to σ_1 and directly proportional to σ_2. A single number representing both distributions would have to be some function of the ratio of σ_2 to σ_1.

$$\rho = f(\sigma_2/\sigma_1) .$$

A better solution to this problem would be to measure the $(11\bar{2}0)$ pole density around the edge of the sample, from TD to LD in Figure 9. This will involve the quantitative transmission method which is currently underway.

The above analysis of the experimental data depends on the assumption that the pole density distribution follows the normal curve. Figure 10 shows a plot of Ln I_n (Φ) versus Φ^2. The solid lines represent theoretical normal distribution obtained by inserting the experimental standard deviations and arithmetic means into Equation 5. The circled data points are the experimental intensities from Table I. The data follows the normal curve initially but shows increasing deviation with increasing Φ. This deviation may result from the defocusing discussed earlier. The intensity decreases with increasing Φ so that finally at $\Phi = 70°$ the correction for defocusing results in a 100 percent increase in the measured intensity. The precision of the data will, therefore, decrease proportionally. The deviation from normality, however, should not detract from the usefulness of the results since it is the sensitivity of the method for measuring small deviations in whisker orientation which is important.

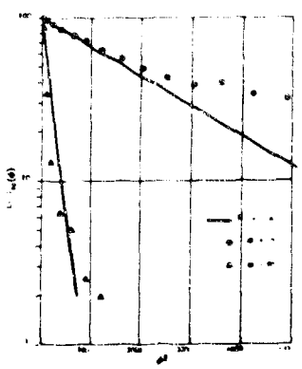

Figure 10 Theoretical and Experimental Data for Ln I_n (Φ) versus Φ^2 for $\alpha = 0°$ and 90°

The relative error in the counting rate of the measured x-ray intensity varies from about 3% at $\Phi = 0°$ to about 6% at $\Phi = 70°$, at the 95% confidence level. The increasing error with increasing Φ is due to the decreasing x-ray intensity resulting from defocusing. The precision can be increased by longer counting times. The full-circle goniometer can be accurately read to ± 1/4°.

X-ray diffraction has been shown to offer a quantitative means of measuring the degree of orientation in whisker filled polymer composites. By treating the measured x-ray intensities as a normal distribution, the standard deviation becomes a measure of the degree of orientation. The precision of the measurements indicates that small deviations in orientation should be detectable.

The reflection method offers the advantage over the transmission method in that it does not require thin samples and it is not necessary to make corrections for absorption and volume of scattering material. The method should be applicable to any composite containing a crystalline filler exhibiting a certain degree of orientation in the crystallites. The measurements and calculations are readily amenable to computer techniques[24] which eliminate tedious hand calculations.

References

1. Barrett, C. S. Structure of Metals, 2nd Edition, McGraw-Hill Book Co., Inc., New York (1952).

2. Cullity, B. D. Elements of X-ray Diffraction, Addison-Wesley Publishing Co., Inc., Reading, Mass. (1956).

3. Henry, N. F. M., H. Lipson, and W. A. Wooster. The Interpretation of X-ray Diffraction Photographs, 2nd Edition, MacMillan and Co., Ltd., London, England (1960).

4. Klug, H. P. and L. E. Alexander. X-ray Diffraction Procedures, John Wiley and Sons, Inc., New York (1954).

5. O'Connor, J. R. and J. Smiltens. Silicon Carbide, Pergamon Press, New York (1960).

6. Knippenberg, W. F. Philips Research Reports, 18, #3, 161 (June 1963).

7. Ramsdell, L. S. Studies on Silicon Carbide, American Mineralogist, 32, 64 (1947).

8. Wohrer, L. C., F. Frechetti, and J. Economy. "Fiberization of Whiskers," Presented at the Am. Chem. Soc. Meeting, New York, Sept. 12, 1966.

9. Geisler, A. H. Crystal Orientation and Pole Figures Determination, Modern Research Techniques in Physical Metallurgy, Am. Soc. of Metals Cleveland, Ohio (1953).

10. ASTM, Specification, E81-63, 151 (1963).

11. Decker, B. F., E. T. Asp, and D. Harker. "Preferred orientation determination using a Geiger counter x-ray diffraction goniometer," J. Appl. Phys., 19, 388-392 (April 1948).

12. Norton, J. T. "A technique for quantitative determination of texture of sheet metals," J. Appl. Phys., 19, 1176 (1948).

13. Schulz. L. G. "A direct method of determining preferred orientation of a flat reflection sample using a Geiger counter x-ray spectrometer," J. Appl. Phys., 20, 1030 (1949).

14. Schulz, L. G. "Determination of preferred orientation in flat transmission samples using a Geiger counter x-ray spectrometer," J. Appl. Phye., 20, 1033-36 (1949).

15. Field, M. and M. E. Merchant. "Reflection method of determining preferred orientation on the Geiger-counter spectrometer," 20, 741 (1949).

16. Mueller, M. H. and H. W. Knott. "Quantitative pole figures for sheet materials by the reflection technique," Rev. Sci. Instr., 25, #11, 1115 (1954).

17. Lopata, S. L. and E. B. Kula. "A reflection method for pole figure determination," Trans. AIME, 224, 865 (1962).

18. Cullity, B. D. and A. Freda. "Quantitative method for the determination of fiber texture," J. Appl. Phys., 29, #1, 25 (1958).

19. Kraske, D. J. "Methods for the analysis of the physical structure of clay-starch coating films," Tappi, 43, #1, 73 (1960).

20. Chernock, W. P. and P. A. Beck. "An automatic x-ray reflection specimen holder for the quantitative determination of preferred orientation," Rev. Sci. Instr., 24, #10, 925 (1953).

21. Chernock, W. P. and P. A. Beck. "Analysis of certain errors in x-ray reflection method for the quantitative determination of preferred orientation," J. Appl. Phys., 23, #3, 1341 (1952).

22. Geisler, A. H. "Spurious areas in pole figures," J. Appl. Phys., 25, #10, 1245 (1954).

23. Thibault, N. W. "Morphological and structural crystallography and optical properties of silicon carbide," The Am. Mineralogist, 29, 249 (1944).

24. Holland, J. R. "The use of computer techniques to plot pole figures," Adv. X-ray Analysis, 4, 74 (1961).

25. Holland, J. R. "Quantitative determinations and descriptions of preferred orientation," Adv. X-ray Analysis, 7, 86 (1964).

26. Fuller, M. L. and G. Vaux. "Modification of the Schulz technique for the x-ray determination of preferred orientation in rolled metal," J. Metals, 5, 1038 (1953).

27. Dunn, C. G. "The analysis of quantitative pole figure data," J. Appl. Phys., 25, 233 (Feb. 1954).

28. Burr, I. W. Engineering Statistics and Quality Control, McGraw (1953).

29. Handbook of Chemistry and Physics, 45th Ed. (1964).

SPIN ORIENTATION OF WHISKER FIBERS (O. D. Deex)

Single-crystal whisker fibers probably represent the ultimate in properties obtainable in a fiber reinforcement for use in composites. Materials such as SiC, Si_3N_4 and Al_2O_3 are reported[1] to have moduli in excess of 50 x 10^6 psi and tensile strengths of 2-3 x 10^6 psi. Utilization of these properties however, requires among other things, that the whisker fiber be oriented. Orientation permits development of composite strength in the desired direction and also allows close packing of the whiskers so that high volume loading can be achieved.

One means of orienting micron size whiskers is by spinning them into an organic fiber. The flow forces at the spinneret and the draw given the fiber align the whiskers along the fiber axis. The fiber forming matrix can then be burned off and the resulting whisker strands impregnated with the desired thermoset or metal matrix.

Workers at Carborundum Company have reported[2] the use of poly(acrylonitrile) copolymers, poly(ethylene-maleic anhydride) and nylon 66 to orient SiC whiskers. Filaments containing 10 volume percent SiC in the poly(acrylonitrile) copolymer system are commercially available[3]. These filaments show very good orientation by x-ray measurements, but burning off the matrix resin without destroying the orientation is very difficult. Even thin "mats" made from these strands tend to curl when ignited.

Workers in Great Britain have also reported[4] success in orienting Si_3N_4 whiskers, but no details have yet been published nor are their strands available.

Since our interest in whiskers lies in their performance in composites, we have developed several fiber spinning systems which can be readily used in the laboratory, are amenable to a variety of whisker materials, and allow burn-off (even in relatively thick sections) without loss of whisker orientation. These are described below. The properties of composites made from the oriented whiskers are described in another paper[5].

General Considerations

To be suitable for whisker orientation, the temporary matrix polymer must have a number of attributes. These include:

1. The polymer must be a good fiber or film former. This implies a high molecular weight, linear polymer preferably soluble in a readily available, non-toxic solvent. A long list of such materials is available from any good text on man-made fibers.
2. The temporary matrix polymer must be capable of being wet spun from fairly dilute solution, preferably under 10%. The surface area

to volume ratio of most whisker fibers is such that 2.0-2.5 volume % is the maximum that can be handled in the spinning solution. (Actually, the aspect ratio as well as the surface area influences the concentration. As the aspect ratio goes up, the concentration of whiskers must be decreased.) Thus at 2 vol. % whiskers in the spinning solution, 10% polymer will give a fiber containing 20 vol. % whiskers, 5% gives 40 vol. %, etc. Melt spinning is, of course, very poor (100% polymer). Dry spinning generally requires concentrated polymer solutions (~25%) and is difficult on a laboratory scale.

3. The filled fiber must have sufficient strength as it emerges from the bath to allow draw, windup and handling. Although most of the whisker orientation probably occurs at the spinneret, drawing the fiber further increases orientation. Obviously a very weak fiber is difficult to wind up and does not lend itself readily to the direct formation of flat tapes or mats.
4. The spinning solution (polymer + solvent) must be capable of dispersing the whiskers. Rigid, fibrous particles have a great tendency to form aggregates or clumps. These can be broken up with a high shear stirrer (e.g. a blender) but will reform unless the spinning solution has some dispersing ability.
5. The spinning solution must also have sufficient viscosity to pull the whiskers through the spinneret and prevent the formation of aggregates which "filter" the solution. In general, it has been found that the viscosity rather than the ability to form fibers limits the lower concentrations that can be used with most polymers.
6. The dry, whisker filled fiber must be flexible enough to be unwound from the takeup drum, straightened, formed into mats, wound on a mandrel, shipped, etc. While any fiber containing 10 vol. % or more whiskers will be brittle, the ability of certain matrix polymers to be plasticized temporarily with water enhances their utility a great deal.
7. The temporary matrix must burn off without disturbing the orientation of the whiskers and without leaving a residue. Materials which char and burn without melting (e.g. cellulose) are ideal. However, resins which char very close to their melting point are also useable by preheating before actual burn off.

A number of temporary matrix polymers have been used and are listed below, together with brief comments. Preparation and use of the more successful polymers are described in detail.

Methyl cellulose (Dow Methocel MC-4000 cps and 90 HG-4000 cps) -- poor wet and dry strengths, extremely sensitive to water.

Carboxymethyl cellulose (Hercules CMC types 7H and 7M) -- poor fiber formers, disperse whiskers well.

Poly (ammonium isobutylene maleamate) (Monsanto experimental sample) -- weak fiber, difficult to coagulate.

Poly (vinyl alcohol) (duPont Elvanol 72-60) -- good fibers but difficult to remove the $(NH_4)_2SO_4$ left from the coagulating bath. Very brittle unless plasticized. Does not disperse whiskers unless CMC, $Na_4P_2O_7$ or sodium lauryl sulfate is added.

Alginic acid (Kelco Superloid) -- very poor wet strength, difficult to handle. Excellent whisker disperser.

Cuprammonium rayon (laboratory preparation, see below) -- gives good fiber with adequate wet and dry strength. Requires dispersing aid such as $Na_4P_2O_7$ (best) or sodium lauryl sulfate.

Cellulose acetate (Eastman types 400-25, 394-45 and 394-60) -- gives a porous, weak fiber when wet spun from most solvents, however, disperses whiskers well and is easy to handle. With methyl acetate as the solvent, the fiber is sticky and can be used to make mats or tapes directly on the takeup drum. Plasticizes well with water.

Cellulose Triacetate (Eastman Cat 2314) -- gives best fiber, strong enough to be wound onto mandrels and handled. Requires careful burn off.

Of these materials, the rayon and the two cellulose acetates appear to be most suitable for whisker orientation.

Experimental

All reagents, solvents, etc. except where specifically noted to the contrary are reagent or laboratory grade, used as supplied by the larger supply houses.

SiC whiskers, purchased from Carborundum Company, were used for all of this work. As received, the SiC contains about 70% particulate matter and very short fibers. The particulate matter is removed by a flotation method and the fibers classified by wet screening. The largest of the classified material, which comprises 10-20% of the starting material, has a number average diameter of 1.25μ and a number average length of 70μ; a nominal aspect ratio of 56:1.

Since the lengths and diameters were measured separately, the true aspect ratio and aspect ratio distribution are not known.

Removal of the fine particulate matter from the SiC results in a tendency for the remaining long fibers to form aggregates or clumps when suspended in a liquid medium. (This has been observed with other rigid fibers as well.) The larger of these aggregates will block the spinneret; the smaller ones cause the fiber to be "knotty" and poorly oriented. About the only effective means of dispersing these aggregates is a high speed stirrer. A Blendor run at medium speed works well. Good results have also been obtained with a modified tissue grinder (0.820" rotor in a 0.890" tube). Some whisker damage results from the use of such vigorous treatment but this is unavoidable since milder agitation (viz. gentle stirring, tumbling, shaking) does not disperse the whiskers.

The design of the spinneret or orifice is quite important. The square-edged spinneret, (i.e., a hole drilled in a flat plate or cup) normally used for fiber spinning, blocks readily and cannot be used. Instead the orifice must be in the form of a venturi with curved inner walls. The orifices used for this work were drawn from glass tubing with an original inside diameter of 0.087". Normal tip inside diameter is 0.030", although a range from 0.020" to 0.040" has been used.

The spinning set up is quite conventional and is similar to that described in standard texts[6]. A 50 ml B-D disposable syringe is filled with the spinning solution and the glass orifice attached with a piece of polyethylene tubing. The syringe is placed vertically in a Model 255-1 Sage syringe driver and the tip of the orifice lowered until it touches the spin bath. The bath is 36" long x 2" deep x 3" wide. The fiber, as it emerges from the orifice is led under a polyethylene-coated hook near the bottom of the bath, through the bath to another hook at the far end, up over a fluorocarbon rod and then to the guide and takeup drum. Both the takeup drum and the guide are run with variable speed motors. Normally the solution is expelled from the syringe at 3 ml/min., the guide moves 0.4"/min. and the fiber is taken up at 45'/min.

The cuprammonium-cellulose solution is made as follows:[7,8,9,10] To 22.5g $CuSO_4$ (anhy) in a 250 ml beaker is added 100 ml H_2O. When the $CuSO_4$ has dissolved, 80 ml 15N NH_4OH and enough H_2O to make 200 ml total solution is added. In a 100 ml beaker, 11.25g NaOH is dissolved in enough H_2O to make 80 ml solution. Both solutions are cooled to 0.4°C. Then the $CuSO_4$ solution

is poured into a pre-cooled (ice) 1 qt. glass Blendor jar and the beaker rinsed with two 5 ml portions of H_2O. The stirrer is started and the NaOH solution is added and its beaker rinsed with two 5 ml portions of H_2O. To the resulting cold, deep purple, 300 ml solution of cuprammonium hydroxide is added 13.0g absorbent cotton (cellulose). The stirrer is adjusted to give maximum stirring with minimum air entrapment. The cotton is added in small pieces as rapidly as possible. The resulting viscous solution is then stirred vigorously until it warms to 20°C, cooled, restirred etc., for about 2 hours, or until it is smooth and all the cellulose has dissolved. The solution may be stored under N_2 in the dark at 15°C for up to 6 weeks.

This solution is used to spin oriented whiskers as follows: Thirty ml of the 4% stock solution and 0.1g $Na_4P_2O_7 \cdot 10\ H_2O$ are placed in a 50 ml Blender jar and thoroughly mixed. Then 2.0g classified SiC whiskers are added to the solution in small portions, with stirring to wet and disperse them. Since air is entrapped with the fluffy SiC, it is necessary to stop the stirrer and "burp" the solution frequently. When the SiC is reasonably well dispersed, 10 ml 4.5N NH_4OH is added and the solution is sucked into a 50 ml disposable syringe, the air bubble worked out and the syringe capped. A partial vacuum is created by withdrawing the plunger part way and the solution is degassed by vibrating and tapping the syringe. When degassed, the syringe is fitted with a 0.040-0.050" glass orifice and placed in a syringe driver. The solution is spun into 2N NaOH. The takeup drum is run at a speed that just causes the fiber to lift off the bottom of the bath. At the end of the run, the loose ends are taped to the drum and the fiber is washed for 15 minutes in warm (35-40°C), running tap water. During this process the fiber shrinks to about half its original diameter. Next the fiber is washed for 15 minutes in 1N H_2SO_4 and finally for 30-45 minutes in warm running water. When dry (overnight in air) the yield is usually 3g fiber containing 40 vol. % SiC (62 wt. %).

The cellulose acetate spin solution is made as follows when using the 394-45 (39.4% acetyl, 45 sec. ASTM visc) or 400-25 (40.0% acetyl, 25 sec ASTM visc) cellulose acetate, which are available in powder form: To 50 ml methyl ethyl ketone in the 50 ml Blender is added 2.5g classified SiC. The mixture is stirred to wet and disperse the whiskers and with continued stirring, 4.0g cellulose acetate powder (Eastman 400-25 or 394-45) is added.

The mixture is stirred until the cellulose acetate is dissolved and the whiskers thoroughly dispersed. The solution is then sucked into a 50 ml disposable syringe, degassed (as described above) and spun into Stoddard solvent through a 0.020-0.030" glass orifice. The takeup rate is adjusted to just raise the fiber off the bottom of the bath. After drying over night a yield of a 5.5 fiber containing 20 vol. % SiC (38 wt. %) is obtained.

For the preparation of flat composites, the whisker strands are most conveniently handled as flat tapes or mats one or two fibers deep and 1-6" wide. As the cupram and acetate fiber are relatively weak and brittle, this is best done by soaking the drum of fiber in distilled water for 5-10 minutes, laying it on a flat glass plate and cutting off the fibers so they can be rolled out on the plate. The fibers are then combed with a wire or small spatula until they are parallel and painted with a 3-4% solution of poly(vinyl alcohol) to glue them together. When dry, the mat can be cut into pieces of the desired size and shape.

If single fibers are not desired, tapes may be made directly on the takeup drum by spinning the high molecular weight cellulose acetate (Eastman 394-60) from methyl acetate. Since the 394-60 acetate is in flake form and does not dissolve rapidly it is made up as a 10% solution in methyl acetate before use. The spinning solution is made up as follows: Two grams of classified SiC is placed in a stoppered 125 ml bottle and 10 ml acetone added. After brief shaking, the SiC forms into granules. These are added in small portions to 30 ml 10% 394-60 cellulose acetate in methyl acetate in the 50 ml Blender, using the stirring and burping techniques previously described. When the solution is thoroughly mixed and smooth, it is sucked into a syringe and spun into Stoddard solvent. The travel of the guide is adjusted so that each turn of fiber on the drum touches the next. Since the fiber is sticky as it emerges from the bath, a continuous tape is formed. At the end of the run it is cut off the drum, moistened with water and allowed to dry between two flat glass plates. The tape contains 21 vol. % SiC.

Cellulose triacetate (Eastman Cat 2314) is spun exactly as described above except that chloroform is used for the solvent and 50 ml of a 13.3% solution is used with 2.5g classified SiC. The fiber, which is not sticky, contains 20 vol. % SiC. Since the fiber is quite strong and reasonably flexible when wet with water, it can be unwound from the drum and rewound on a mandrel to give mats of any

desired shape or size. If the fiber is wound evenly, flat tapes can be made quickly by pushing moistened fibers together on the takeup drum, painting with poly(vinyl alcohol) solution, cutting and flattening.

All of these resins can be burned off of the oriented SiC whisker without disturbing the orientation. The rayon can be burned off directly at 600 °C. Cellulose acetate burns off well at 600 °C, although a slow rise (1-2 hours) from 250 °C to 600 °C appears to give better results. Cellulose triacetate must be charred at 325-350 °C for an hour before complete burn off at 600 °C.

Discussion

Cuprammonium rayon is normally spun from an 8% solution into hot running water. At 3%, coagulation in water is poor and acid coagulation gives a weak fiber, so sodium hydroxide solution is used. The sodium pyrophosphate is needed to keep the whiskers dispersed. Sodium lauryl sulfate (at the same concentration) also works well but forms foam which makes degassing very difficult. Whisker loading to 50 vol. % is possible but the 40 vol. % used gives a better fiber.

Although it was not tried in the course of this work, viscose rayon should give results comparable to cuprammonium rayon. Viscose is difficult to prepare reproducibly on a small scale, but is very amenable to filling and variations in draw cross-section, etc.

Cellulose acetate is normally dry spun from a 25% acetone solution. A large number of solvent-non solvent systems were investigated to develop a suitable one for wet spinning a 10% solution. Even the best of these, methyl ethyl ketone into Stoddard solvent, gives a weak, brittle, porous fiber with a flat corss-section. Nevertheless, the whisker filled strand is strong enough to allow handling and, plasticized with water, can be shaped and made into mats. The three different grades of cellulose acetate used all give about equal results.

Cellulose triacetate is normally dry spun in a manner similar to that used for the acetate. Unlike acetate, however, it can be readily wet spun from 10% chloroform or methylene chloride solution to give a dense transparent fiber of flat cross-section. Thus the whisker-filled strands exhibit good strength. Although less sensitive to water than cupram or acetate, SiC-filled triacetate becomes sufficiently pliable when wet to allow sharp bends without breaking.

X-ray diffraction pictures of the cupram, acetate and triacetate SiC-filled strands are shown in Figures 1, 2 and 3. All show good orientation. Although the cupram fiber is somewhat better than the acetates, composites made from

whiskers oriented in the different polymers are comparable. Evidently, the slight differences is l[illegible] in the manipulations required to make the test sample.

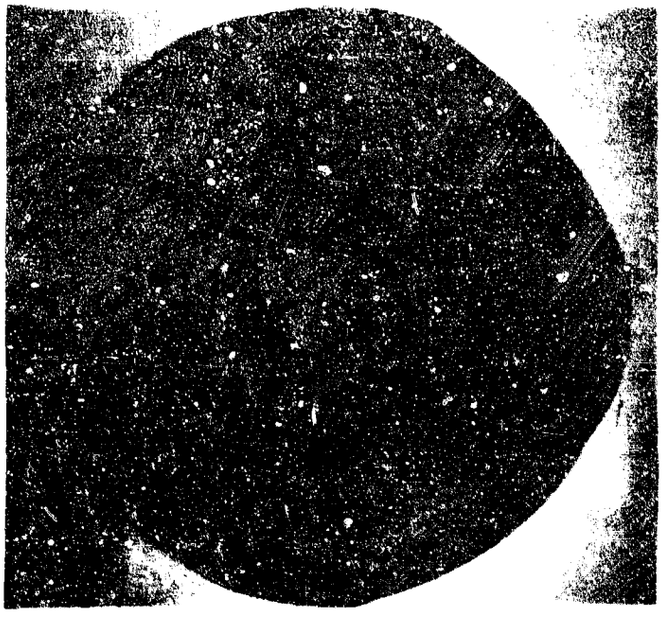

Figure 1 Cupram - SiC Filled Strand

Figure 2 Acetate - SiC Filled Strand

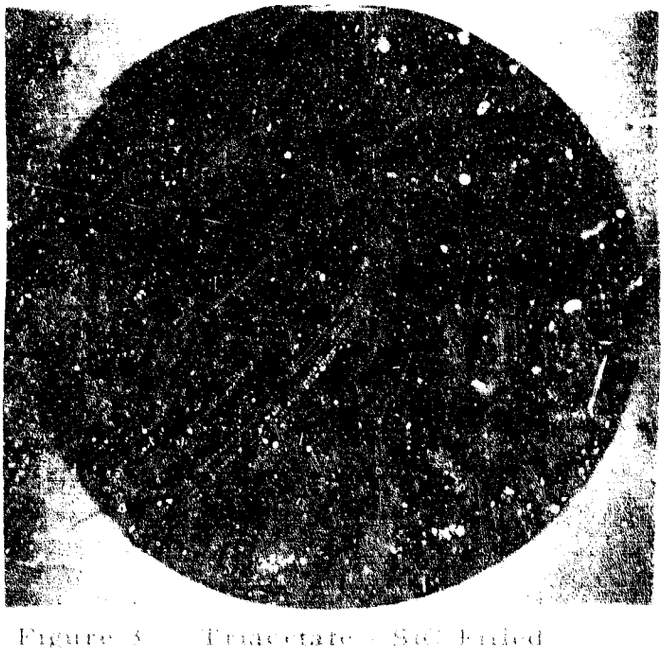

Figure 3 Triacetate - SiC Filled Strand

Obviously, much remains to be done to quantify and refine the system. Orifice design, the effect of varying extrusion rate and draw, and the influence of stirring on whisker damage and dispersion are among the more important variables that have not, as yet, been completely investigated. Equally important is the study of whisker fibers other than SiC, preferably ones with aspect ratios of 100 or 200 to 1.

While the temporary matrix method is a tedious, commercially expensive way of utilizing whisker fibers, it is a relatively quick and simple system for evaluating their potential in the laboratory.

References

1. Sutton, W. H. Astronautics and Aeronautics, p. 46 (August 1966).

2. Wohrer, L. C. and J. Economy. "Single crystal fiber reinforcements," (paper presented at the November 1966 SAMPE Meeting).

3. Carborundum Company, Bulletin No. 202, "Silicon carbide whisker filaments."

4. Parratt, N. J., Chem. Eng. Prog., 62 # 61 (March 1966).

5. Tolbert, T. L. This report p. 228.

6. Sorenson, W. and T. W. Campbell. Preparation Methods of Polymer Chemistry, p. 30 (Interscience, N. Y., 1961).

7. Moncrieff, R. W. Artificial Fibers, pp. 127-132 (Wiley, N.Y., 1950).

8. U. S. 2,336,481 (CA 38, 3127^2).

9. U S. 2,247,120 (1937).

10. Browning, B. L., et al. Tappi, 37, 273 (1954).

FABRICATION OF WHISKER COMPOSITES (T. L. Tolbert)

Whiskers are among the most promising of all short fibers for reinforcement of structural composites. Unfortunately, they also present some of the greatest challenges from the standpoint of composite fabrication. The problems in preparing directionally reinforced whisker composites are such that the extent to which whisker properties can be practically utilized has not even been fully determined. Consequently, the primary objective of fabrication work in this area is to evaluate the practical importance of whiskers as reinforcing agents.

It is aimed at developing laboratory methods for preparing whisker reinforced composites and at comparing whisker reinforcement with that given by other types of short fibers. Additional goals are to evaluate whisker processing variables in terms of composite performance and to define process and handling requirements for practical, larger scale use of whiskers in composites.

Silicon carbide whiskers purchased from the Carborundum Company have been used almost exclusively in these studies. Although the "as received" material contains a great deal of particulate matter and many of the whiskers are covered with overgrowth, this is the only whisker material available at a price which permits use in quantity. Techniques have been worked out for cleaning and sorting the whiskers and for unidirectionally aligning them in strands of carrier polymer; these are described elsewhere. The classification procedure yields two fractions of reasonably good quality whiskers comprising a total of about 30% of the starting material, in addition to a small amount of relatively long fibers. Only these fractions have been used for fabrication studies. Fibers in the preferred fraction have a number average diameter of 1.25μ and a number average length of 70μ (ℓ/d of 56); those in the other are shorter and vary more in size ($\ell/d < 50$, probably 20-30).

Essentially the same procedure has been used to incorporate whiskers in composites for all levels of loading and patterns of orientation. It involves two steps, (1) preparation of a mat of whiskers oriented as desired in the final composite and (2) addition of a resin solution to yield a prepreg which can be shaped and molded. Mats for randomly reinforced composites are prepared by dry pressing classified whiskers under 50-100 psi pressure; enough entanglement results to give the mat reasonable integrity. Mats for directionally reinforced composites are prepared by hand laying whisker-filled strand (produced by wet spinning) in the desired pattern and removing the carrier polymer by pyrolysis. The resultant mat is quite fragile but has enough green strength to permit weighing and careful cutting and handling. Prepregging consists of impregnating the whisker mat with a dilute solution of resin, catalyst and coupling agent, evaporating the solvent, and "B staging" the resin under controlled conditions. The prepreg has the consistency of damp, lightweight cardboard and can be readily shaped and molded. Molding conditions range from 100-190°C and 500-3500 psi depending on the nature of the resin, the extent of "B staging" and the final whisker loading desired.

Loading levels, fiber orientation, and properties of composites prepared in this way can be predicted and reproduced. The composites exhibit flexural strengths and moduli as high as 99 x 10^3 psi and 15.4 x 10^6 psi, respectively, (48 v/o loading), thus easily qualify as high performance materials. Figure 1 shows the levels and rate of increase of flexural strength and modulus with fiber loading; Figure 2 compares specific properties as a function of loading. The magnitude of these values is particularly significant in light of the fact that

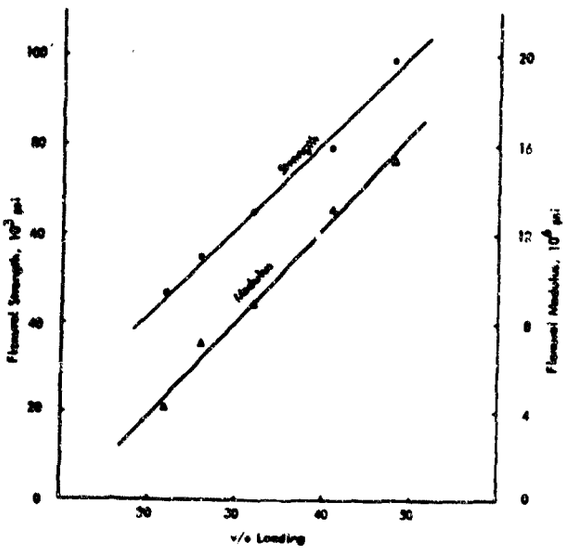

Figure 1 Properties of SiC Composites

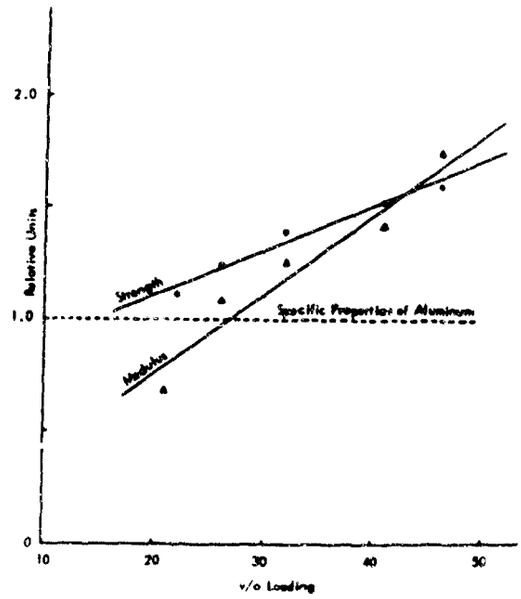

Figure 2 Comparison of Specific Properties of SiC Composites with Those of Aluminum

aspect ratios of the whiskers in the composites average no higher than 50 (nominal aspect ratios before spinning are only 50-60).

The property levels which have been obtained for silicon carbide composites are quite encouraging. However, to be of practical significance and justify the cost and labor involved, even on a laboratory scale, whisker reinforcement must offer properties not obtainable with other fibers. The main advantage in using whisker fibers should lie in their extremely high strength, if it can be translated into composite strength. The results shown in Table I indicate that this is the case. The flexural strengths and moduli of compression molded, unidirectionally reinforced composites of silicon carbide whiskers and of boron fiber are compared at similar fiber loading levels and aspect ratios.

The modulus of the whisker composite is equivalent to those of the boron-reinforced materials, as the rule of mixtures would predict, but flexural strength is 35% higher.

TABLE I

COMPARISON OF COMPOSITE* PROPERTIES

Fiber (ℓ/d)	Fiber Loading v/o	Flexural Strength x 10^3 psi	Flexural Modulus x 10^6psi	Specific Strength x 10^6 in	Specific Modulus x 10^6 in
SiC Whiskers (50-60)	48	99	15.4	1.23	192
1/4" Hand Laid 4 mil Boron (62.5)	48**	65	14.8	0.91	212
1/4" Encapsulated 4 mil Boron (62.5)	47	56	12.8	0.83	190
1/8" Encapsulated 1.5 mil Boron (83)	46	66	14.9	0.64	144

*Unidirectionally reinforced epoxy composites prepared under similar conditions by compression molding.

**Data calculated for 48 v/o loading from the highest results obtained for 1/4" boron; the actual sample contained 70 v/o fiber and exhibited a flexural strength and modulus of 94.6 x 10^3 psi and 21.7 x 10^6 psi, respectively.

Control permitted by this method of fabrication makes it possible to evaluate whisker handling and processing variables in terms of composite properties. Table II compares composites prepared from different types of whisker-filled strand and presents some preliminary data on the effect of ignition rate and whisker aspect ratio on composite properties. The variation in properties as a function of strand composition and ignition rate has been varified by x-ray diffraction measurements* as due to differences in fiber orientation.

Much remains to be done before the practical importance of whiskers as reinforcing agents can be fully assessed even on a laboratory scale. However,

---

*Using techniques developed by R. G. Schierding.

TABLE II

EFFECT OF PROCESSING VARIABLES ON COMPOSITE PROPERTIES

Carrier Polymer in Strand	Whisker Loading v/o	Flexural Strength 10^3 psi	Flexural Modulus 10^6 psi
Cellulose Acetate	47.8	92.6	13.5
Cellulose Triacetate	47.9	98.5	13.1
Cuprammonium Rayon*	48.0	90.0	13.1
Polyvinyl Alcohol**	48.0	80.5	13.3

Each composite was prepared from the same grade of silicon carbide whiskers (ℓ/d 50-60) and under conditions found to yield best whisker orientation and highest composite properties from that type strand.

*Sample had only one molded edge. Property values projected from a sample which contained 40.6 v/o whiskers; original values were 76 x 10^3 psi flexural strength and 11.1 x 10^6 psi flexural modulus.

**Property values projected from a sample which contained 45 v/o whiskers; original values were 75 x 10^3 psi flexural strength and 12.5 x 10^6 psi flexural modulus.

Ignition Rate of Strand			
Gradual Char	48.0	64.3	10.7
Rapid Ignition	48.5	56	9.3

Acetate strand containing silicon carbide whiskers, $\ell/d < 50$. Heating conditions: gradual char, temperature gradually raised from 25° to 600° over a four hour period, sample held at 600°C for 15 minutes; rapid ignition, sample placed in oven at 600°C and held at 600-650°C for 30 minutes.

Whisker Aspect Ratio			
ℓ/d = 50-60	47.9	98.5	13.1
ℓ/d < 50	48.0	53.4	13.4

Composites prepared from cellulose triacetate strand.

several conclusions can be drawn from the work to date.

1. High performance composites can be prepared by reinforcing epoxy resins with whisker fibers, even those having an aspect ratio as low as 50.
2. The strength of silicon carbide whisker reinforced epoxy resins is significantly higher than obtainable with boron fiber of the same ℓ/d. Moduli are of the same order.
3. The fabrication technique in use is adequate for determining the effect of parameters such as aspect ratio and orientation on properties and for evaluating the strand produced by various spinning systems.
4. The current method of fabrication may not be practical for larger scale studies. A simpler procedure which avoids handling polymer-free oriented whiskers is needed. Ideally, a prepregged sheet or rod should be obtained directly from the extrusion or spinning system and molded directly.

Experimental

The following procedure is typical of that used to prepare specimens measuring 4" x 1/4" x 1/32": Package whisker-filled cellulose triacetate strand obtained by wet spinning* into mats by bonding 4" lengths of parallel strands together, 1-5 layers deep, with a dilute solution of a non-melting polymer such as polyvinyl alcohol. Pyrolyze the mat by placing it on a quartz plate in an oven held at 325-350°, leaving it there for 45 minutes and then transferring it on the plate to another oven held at 600 °C for 20 minutes. Weigh the polymer-free mat of oriented whiskers which results and split off the amount needed for the composite, 0.3-0.9 grams depending on the loading desired, along strand lines. Compact the whiskers to be used to the approximate dimensions of the mold, taking care not to disturb orientation. Prepreg the mat with a predetermined amount of resin solution by carefully and uniformly adding it dropwise over the mat surface using a syringe fitted with a 22 or smaller gauge needle; the mat will darken but otherwise should not change significantly in appearance. The resin solution should consist of approximately 10 grams of Epon 815, 2 grams (20 phr) of curing agent Z, 0.3 grams of amino silane A-1100 finish and 100 grams of dichloromethane. Allow the impregnated mat to dry in the air for 15 minutes before lightly "B staging" it in an oven under house vacuum at 40-45 °C for 30 minutes. The prepreg which results should look and feel like damp cardboard, but will break and

---

*Using techniques developed by O. D. Deex

crumble if severely bent or rubbed. Place it in a conventional compression mold under 2000-2500 psi pressure, holding it at 100 °C for 15 minutes and then at 195 °C for 1 hour. Bumping the sample two or three times as soon as the whole mold is hot is advisable for samples containing more than 40 v/o whiskers. Post cure the sample for 4-5 hours at 150 ° for improved results.

The sample can be tested in tension by molding glass tape reinforced epoxy tabs on the ends or in flexure using a microflexural jig with the span set for a span-to-depth ratio of from 20-1 to 25-1. Tensile strengths have been found to range from 55-60% of flexural strength for these specimens; tensile and flexural moduli are equivalent. Whisker loading is most easily determined gravimetrically; a 20 minute exposure at 600 °C is sufficient to burn off the polymer. For most purposes density can be simply calculated from the loading measurement.

COMPOSITION VARIABLES AFFECTING SHORT FIBER COMPOSITE PROPERTIES

(R. M. Anderson)

A hand lay-up procedure which permits control over fiber length, orientation, and loading has been developed for fabricating composites from discontinuous boron fibers. The technique has been used to establish experimentally the relationship of fiber variables to the flexural strength and modulus properties of short fiber-reinforced composites. Graphs are presented.

Preliminary data is also presented for composites reinforced with short graphite fiber. These composites were prepared by hand lay-up or by extruding bundles of prepregged roving and compression molding the extrudate.

It is well documented that both strength and modulus of fibrous reinforced composites are highly dependent on fiber loading levels and fiber orientation. However, quantitative information is available only for continuous fiber composites (i.e., where fiber length is the same as that of the test coupon).

The equation relating volume fraction of unidirectional fibers and composite modulus is quite familiar:

$$E_c = \phi_f E_f + \phi_m E_m$$

where E = Young's modulus

ϕ = Volume fraction

c, f, m = Subscripts referring to composite, fibers, and matrix.

In practice, the first term on the right hand side of the equation dominates and decides the composite modulus. Normally, ϕ_f is in the range of 0.4 to 0.8 and $\frac{E_f}{E_m}$ ranges 20 to 100; at a minimum the first term accounts for about 93% of composite modulus (i.e., using $\phi_f = 0.4$, $E_f = 10 \times 10^6$ psi, and $E_m = 500,000$ psi, typical of a moderately loaded fiber glass/epoxy composite).

Theoretically, the equation is applicable to all purely unidirectional composites reinforced with continuous fibers. It must be modified for any departure from unidirectionality, however. The literature teaches that, on the average, randomly oriented fibers impart only 20% of their potential modulus to the composite as compared to nearly 100% for unidirectional fibers.

As mentioned above, published quantitative studies of fiber orientation and loading parameters have been largely restricted to continuous fiber composites. A major objective of our work was to develop similar quantitative data for short fiber composites. Such information would provide: (a) a test of theoretical calculations and (b) a property map showing the potential of discontinuous fiber composites.

To accomplish these goals it was necessary to develop a fabrication technique which would give control of fiber orientation. Hand lay-up was the technique chosen. It provides maximum flexibility and control of several individual parameters. The essential steps of the procedure developed are:

1. Prealignment of the short fibers in a vibrating "V" shaped trough.
2. Placement of the fibers in a cavity mold with a width ≤ fiber lengths, care being taken that fiber ends overlap in adjacent rows.
3. Addition of the matrix resin and "working" it into fibers with a flat ended spatula until good fiber orientation is achieved.
4. Curing under heat and pressure.

The process is time consuming, but it provides the essential characteristics of near perfect fiber orientation. Photomicrographs have demonstrated that a high degree of fiber orientation is obtained by this method for short boron fibers.

Using this technique, a series of composites was prepared using short boron fibers in an epoxy matrix. The principal variable was fiber length (1/8", 1/4", 1/2", 1", and continuous fibers were used). Since these fibers were 5 mils in diameter, the corresponding aspect ratios (ℓ/d) were 25, 50, 100, 200 and ∞, as indicated in the figures. Flexural strengths varied over this range from

73,000 to 280,000 psi and moduli from 22 x 10^6 to 41 x 10^6 psi; an aspect ratio of 200 gave about 70% of the strength and over 80% of the modulus obtainable with continuous filament. Similar results were obtained using a special grade of boron fiber (1.3 mil diameter) and prepregged "S" glass fiber. The small diameter of the glass fibers (0.4 mil) did not permit them to be processed using the vibrating technique, so a special hand lay-up technique using short pieces of prepreg tape was developed. A "brick-lap" construction was used. Strengths and modulus data are given in Figure 1 through 4. Figures 1 and 2 show the variation of modulus and strength of short fiber boron composites with fiber aspect ratio. Another way of considering the data is shown in Figures 3 and 4 where fiber efficiences are plotted versus aspect ratio of the fibers.

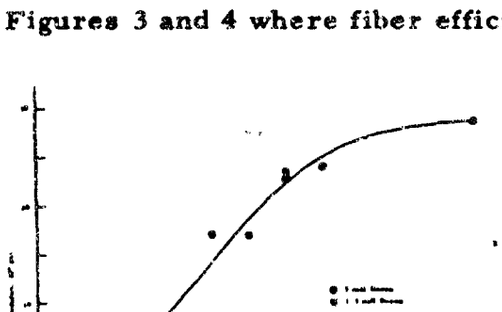

Figure 1 Effect of Aspect Ratio on Composite Modulus

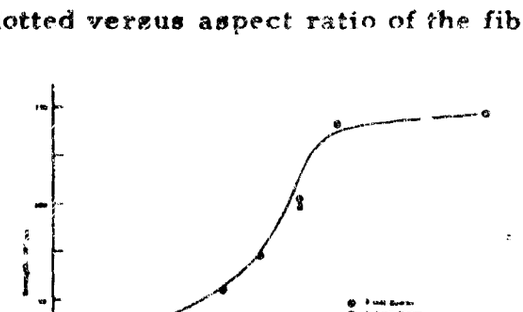

Figure 2 Effect of Aspect Ratio on Composite Strength

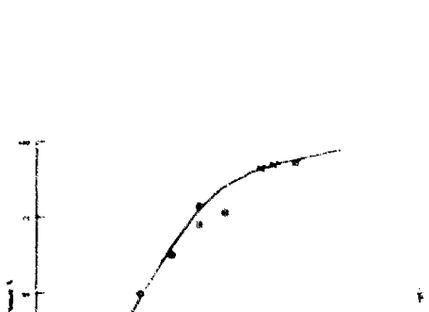

Figure 3 Effect of Fiber Aspect Ratio on Fiber Efficiency (Modulus)

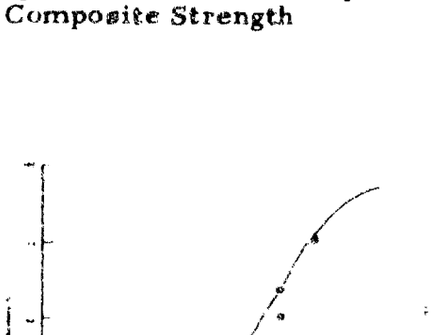

Figure 4 Effect of Fiber Aspect Ratio on Fiber Efficiency (Strength)

In Figure 3, modulus data, efficiency is calculated as:

$$\text{Efficiency} = \frac{\text{measured modulus}}{\text{theoretical modulus}}$$

Theoretical modulus is calculated from the rule of mixtures equation. In Figure 4, strength data, efficiency calculations were based on data obtained for continuous fibers:

$$\text{Efficiency} = \frac{\text{measured strength}}{\text{strength of continuous fiber composite}}$$

In all cases results were normalized to 55% fibers before being plotted.

Preliminary results have also been obtained using short graphite fibers. "Thornel" 25, a continuous graphite yarn from Union Carbide made up to 10μ diameter filaments, was cut to desired lengths for the study. Since small diameter filaments cannot be oriented by the vibrational technique, three alternative fabrication techniques were used. In these: (1) yarn was vacuum impregnated with "A" stage epoxy while in a cavity mold (2) chopped "B" staged yarn was laid up by hand using procedures developed for boron and (3) prepregged yarn was extruded and the extrudate compression molded. Data is summarized in Table I and the fabrication technique (1, 2 or 3 from above) indicated. The volume percent fiber reported for the composites was calculated using the density of the carbon filaments and nitrogen content of the composite from Kjeldahl analyses.

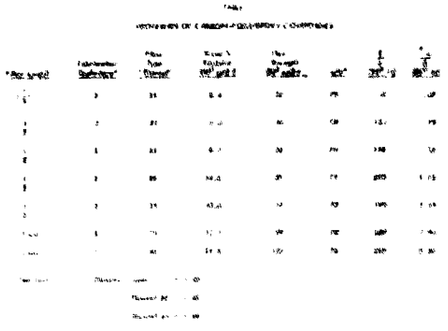

Conclusions

1. High performance composites can be prepared from short boron fibers; absolute and specific strengths and moduli significantly exceed those of aluminum.
2. Fiber aspect ratio (ℓ/d) is a much more pertinent fiber characteristic than fiber length for predicting composite strength and modulus.
3. Fiber aspect ratios of about 100 to 200 are required to achieve fiber efficiencies of 70% and above.

In the future these studies will be extended to cover additional variations in fiber modulus, matrix modulus, fiber orientation, volume fraction loading, coupler studies and water soaking, and test temperature.

DYNAMIC FATIGUE RESISTANCE OF FIBROUS REINFORCED PLASTIC COMPOSITES (R. M. Anderson)

In many applications, fatigue performance of composite materials is of equal importance, sometimes even of greater importance, than other physical properties. Accordingly, fatigue studies were started early in the fabrication program. The information is needed to guide fabrication work since good dynamic as well as good static properties must be built into the composite.

During the last year investigations have been directed toward identifying and quantifying major factors controlling fatigue of composite materials. These studies have led to the first reported parametric equation for fatigue performance of composite materials. It defines the quantitative contribution of several of the composite constituent properties in the fatigue phenomena.

$$F.L. \propto \frac{E_M \, \epsilon_{M_{ult}} \int_{T_1}^{T_2} G_M \, dT}{\sigma^B}$$

where

E_M = matrix modulus

$\epsilon_{M_{ult}}$ = ultimate elongation

$\int_{T_1}^{T_2} G_M \, dT$ = an integral of the shear modulus of the matrix resin from cure temperature to test temperature.

σ = maximum cyclic shear stress on the NOL ring under test.

B = the slope of the line where log F. L. is plotted versus log.

F. L. = fatigue life; or number of elapsed cycles where sample deformation has increased 30% where operating fatigue under constant load conditions.

In its current form the equation is, of course, restricted to simple filament wound structures and to the specific test conditions under which it was developed;

i. e., (1) the testing mode described in previous reports (2) the use of chemical coupling agents, and (3) testing temperatures from 25°C down to -196°C.

Studies not previously reported show that (1) testing speeds from 100 to 400 cycles per minute do not significantly affect the fatigue performance and (2) nor does surface machining of the NOL rings. In addition it has been shown that the chosen failure criteria in these tests (i. e., cycles where a 30% increase in deformation occurs) gives comparable quantitative composite damage whether starting at low or high stress levels for the fatigue test. In current studies the influence of reinforcement concentration is being defined. At this time however, it can be stated that this factor does influence fatigue life and therefore will constitute a new parameter to be added to the fatigue life equations. Qualitatively speaking, increases in volume fraction loading of the glass reinforcement give an increase in fatigue life of the composite.

A new fatigue apparatus has been designed and is now under construction. It will provide a new dimension to the fatigue studies. The apparatus will accommodate two specimen shapes, (1) a hollow tube tested in shear and (2) a rectangular cross section beam tested in three point flexural fatigue. These capabilities will provide for studying important additional factors in the fatigue studies.

Future plans consist of (1) testing of hollow tubes from which engineering data can be expected, (2) testing in flexural fatigue mode which will permit greater stresses to be applied to the fibrous reinforcement, and (3) to conduct corresponding studies where short fibers represent the reinforcing phase of the composite.

FIBER ENCAPSULATION AND FLOW ORIENTATION (H. M. Andersen and D. C. Morris)

A method has been developed for encapsulating chopped boron fibers in epoxy resin to give a prepreg molding compound in which each fiber is imbedded and collimated in the resin. Flow-molding of the granules gives specimens having high-performance properties. The method is also applicable to other fibers.

Fabrication of high performance composites from discontinuous fibers presents a number of special problems. Most arise from the nature of the fibers which must be used. In addition to being very small and very stiff, they must be incorporated at high loadings, thoroughly mixed into and wetted by the resin matrix, and

oriented to take advantage of their properties. The fibers are highly susceptible to damage during mixing and in any subsequent forming operation, especially if melt flow is involved. These and related problems have hindered the development of processing techniques for short, high performance fibers.

Ideally, the fibers should be incorporated into molding compounds processible by conventional techniques - extrusion or transfer molding. Granular prepregs of this type would permit the preparation of complex shapes by much more efficient and effective methods than the laborious techniques now used. Some glass reinforced molding compounds now available represent a step in this direction but generally are deficient in flow and do not yield the modulus required of high performance composites.

Our work has been aimed at developing molding compounds which overcome the processing problems and permit fabrication of complex shapes reinforced with short, high performance fibers. To this end, our work has concentrated on incorporation of chopped boron fibers in epoxy resins. Glass fibers and several other materials have also been used. The work is divided into two phases: (1) The preparation of the molding compound itself (encapsulation) and (2) The forming processes.

Experimental

The molding compound is prepared by a process referred to in the Project as encapsulation. This consists of the following steps:

1. The fibers are slurried in an aqueous solution of an emulsifying agent along with any additional component such as interstitial fillers. In some cases the emulsifying agent can be omitted.
2. Coupling agent is added and the slurry heated to 70 °C.
3. The required amount of resin is heated to the same temperature and added to the slurry with stirring.
4. The hardener is added and stirring is continued at 70 ° for 30 minutes. The choice of time and temperature is arbitrary; it has merely been found to produce a B-stage satisfactory for our purposes.
5. The mixture is rapidly cooled, the water decanted, the product washed with cold water, and air-dried.

The granular product obtained from the above process has a specialized structure worth noting. Starting with loose pre-cut fibers, granules are obtained in which individual fibers are uniformly imbedded in epoxy resin in a collimated,

parallel array. Grain length is roughly one to two times the original fiber length; grain diameter is roughly half the fiber length. Grain shape may vary from slim and pointed through elongated ellipsoids to nearly perfect right cylinders or skewed cylinders. The interstitial space between fibers may be filled with clear resin or with a mixture of resin and interstitial agent (finely divided solid). A mixture of fibers such as glass and boron can be used. Some examples are shown in Figures 1 to 8.

We have employed three methods for forming specimens:

1. Transfer molding.
2. Extrusion, followed by compression molding of the strand.
3. Compression molding of the grains directly.

Transfer molding and extrusion are highly preferred. Both produce good fiber orientation and overlap and therefore yield improved properties. Transfer molding has the advantage that a finished article is produced in one operation. We have not as yet determined the degree to which fiber orientation can be produced and controlled in other than a long narrow cross-section. Transfer molding has been restricted to small (2½") tensile bars; good fiber orientation was obtained in the gage section. Thus far, the extruded strands have been too irregular to test per se, but can be compression molded to give excellent specimens.

The present extrusion equipment is primitive. It consists of a heavy-walled steel cylinder fitted with an aluminum piston. The orifice is screwed into the side of the cylinder near the bottom. The assembly is placed in a hydraulic press to apply force to the piston. Heat is supplied by the platens and by steam tracing on the orifice.

This design results in two major problems. One, the pressure is difficult to control with the press now in use and results in uneven extrusion rates. Second, the extruded strand comes out horizontally; with no take-up mechanism, it is difficult to control straightness, continuity, and draw-down. A vertical, in-line extruder is being built which is expected to alleviate these problems. Orifice geometry will require major attention.

Results

We have found that for circular orifices significant orientation parallel to the flow axis will occur with volume loadings of 30 v/o and greater as long as the orifice diameter is about equal to or smaller than the length of the fibers.

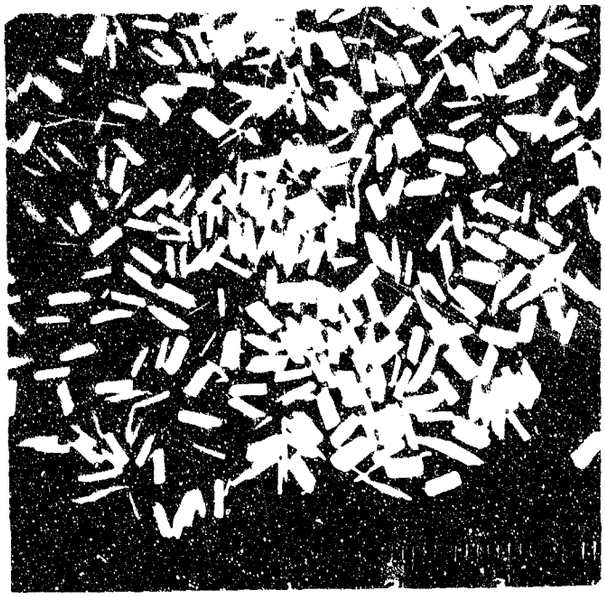

Figure 1. E-218
40 v/o glass, 1/8" chopped roving

Figure 2. E-229
30 v/o glass, 1/8" roving
5 v/o Attapulgus Clay

Figure 3. E-230
30 v/o glass, 1/8" roving
10 v/o Attapulgus Clay

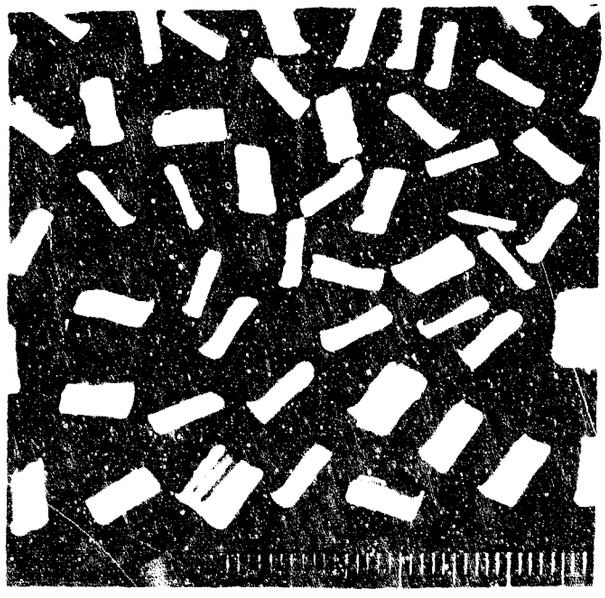

Figure 4. E-231
30 v/o glass, 1/4" roving
10 v/o Attapulgus Clay

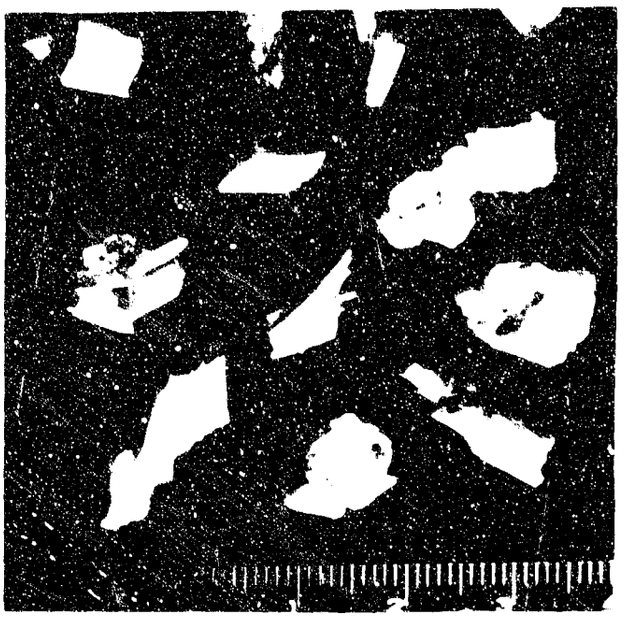

Figure 5. E-232
30 v/o glass, 1/4" roving
5 v/o Attapulgus Clay

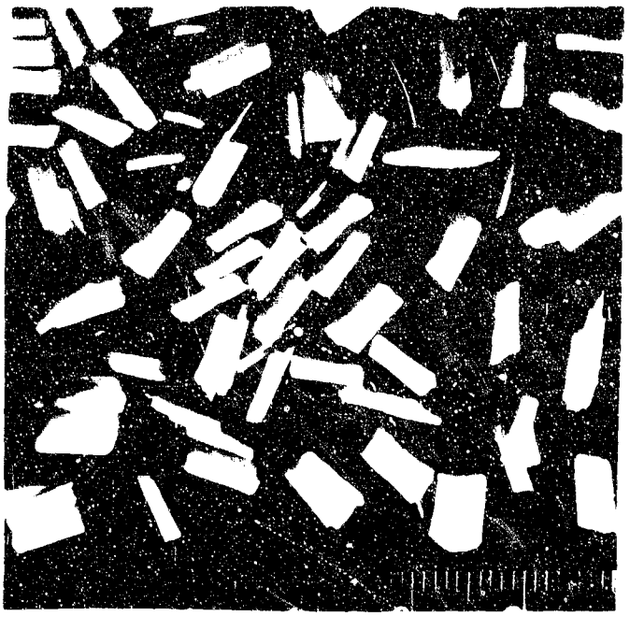

Figure 6. E-242
40 v/o glass, 1/4" chopped roving

Figure 7. E-244
30 v/o Boron-W, 1/8" x 1.3 mil
10 v/o Attapulgus Clay

Figure 8. E-246
30 v/o Boron-W, 1/4" x 4 mil
10 v/o Attapulgus Clay

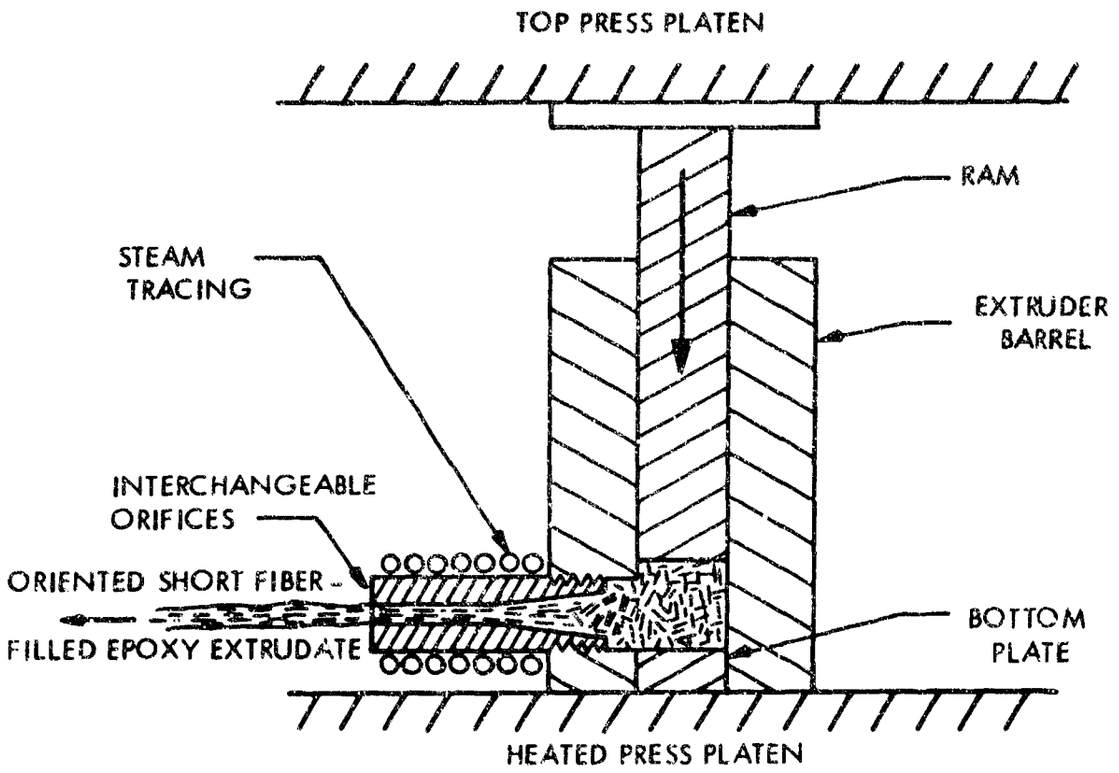

Figure 9 Fiber Filled Thermoset Extruder

At present, alignment of fibers is based only on visual observation and microphotographs of strand left in the orifice after extrusion; no actual measurements have been made. However, orientation must be reasonably good since high efficiencies of 60-70% are obtained in translating fiber moduli to composite moduli. This is also an indication that compression molding of the strands does not disrupt fiber alignment. Strengths are also high.

The best properties obtained for each of several composites are given in the Property Summary Table. The column headed "Formed By" refers to the method used to make the specimen. Sample E-252, shown on the next-to-the-last line in the Table, illustrates that the objectives of the study can be met:

1. It contained a high-modulus fiber at a loading high enough to be effective.
2. It was easily extrudable and extrusion produced orientation without excessive fiber breakage. The extruded strand was readily compression molded to give test specimens.
3. Properties are in the high performance range.

Epoxy Encapsulated Fibers

Property Summary

Reinforcement	Vol. %	Flex. Str. psi x 10^3	Flex. Mod. psi x 10^6	Formed By	E-Ident.
Glass:					
1/32" Milled Fiber	40	20.4	1.5	Transfer	124
1/8" Milled Flake	33	17.1	2.1	Transfer	110
1/8" Chopped Strand	40	65.3	2.2	Transfer	206
1/8" Chopped Strand	40	55.5	2.0	Transfer	218
1/8" Chopped Strand	40	67.0	2.9	Extr. + Comp.	218
1/8" Chopped Strand	45	60.4	2.1	Transfer	224
1/8" Chopped Strand	45	71.0	3.3	Extr. + Comp.	224
1/4" Chopped Strand	40	67.5	2.0	Transfer	242
1/4" Chopped Strand	40	71.0	2.9	Extr. + Comp.	242
Whiskers:					
Si_3N_4, 50-200μ	20	23.8	3.0	Compression	158
SiC (90% Particulate)	30	29.3	1.8	Transfer	147
Asbestos: (Refined)					
Chrysotile	40	19.2	2.0	Transfer	131
Crocidolite	40	30.6	1.8	Transfer	217
Crocidolite	40	--	2.9	Compression (1)	217
Boron:					
1/4" x 4 mil	47	56	12.8	Compression (1)	196
1/8" x 1.3 mil	46	66	14.9	Compression (1)	226
1/8" x 1.3 mil (2)	35	60	11.9	Extr. + Comp.	227
1/8" x 1.3 mil	50	75	16.7	Extr. + Comp.	252
1/8" x 1.3 mil (2)	35	40	6.0	Ribbon-Extr. + Comp.	244

(1) Oriented by hand lay-up
(2) Plus 12 v/o attapulgus clay

To our knowledge this is the first experimental verification that automated forming processes - extrusion and perhaps transfer molding - can be adapted to chopped boron composites. It is particularly significant that these results were obtained with "thin", 1.3 mil, boron fiber. This material is more flexible and has a small enough diameter that aspect ratio does not have to be seriously sacrificed in chopping to a processible range. Four mil boron fiber in $\frac{1}{4}$" and $\frac{1}{8}$" lengths has also been successfully encapsulated, but preliminary extrusions have caused excessive fiber breakage.

Discussion

The exploratory nature of the program has precluded any systematic variable study or mechanism study. However, based on spot observations and intuition, the following is what is thought to happen:

The oil phase, consisting of hardener dissolved in resin, is in the emulsion state initially. As the resin crosslinks, its modulus gradually increases, the emulsion becomes unstable, and the particles tend to coalesce. The coalescing resin is attracted to and wets out the fiber; this process appears to be aided by a cationic finish on the glass or the use of a cationic emulsifier. As the resin-coated fibers collide, they stick together. Surface tension of the resin then causes crossed fibers to straighten out into a parallel array - minimizing the total resin-water interface. This has actually been observed under the microscope. In favorable cases, longitudinal motion of the fibers also occurs, giving grains with "squared-off" ends, rather than long grains with over-lapping fibers. At present, this requires the presence of a suitable anti-clumping or interstitial agent. Cure,"B-staging", is now continued to the point where the grains are no longer tacky enough to stick together when cool. In the absence of an interstitial agent, the grains may continue to grow indefinitely, resulting in a massive clump.

Squared-off grains are preferred for handling characteristics. However, to produce the fiber overlapping necessary for good strength and modulus in the composite they require shear during the forming operation. This is provided by extrusion or transfer molding. "Pointy" grains have overlapping fibers, and therefore compression molding may better suffice for them. Some compromise between "squared-off" and "pointy" is probably desirable.

An important development in the study is recognition of the role of interstitial agents in granule formation. They make practicable the use of the longer fibers

required for best properties. If none is used, the longer fibers (1/8" and up) tend to form very large grains (1 to 3") or clumps. These large aggregates are unmanageable for extrusion or transfer molding, and can be compression molded only with difficulty. Addition of interstitial agents causes the longer fibers to be encapsulated in bundles of dimensions roughly the lengths of the fibers used. As described above, the grain shape may vary from pointed grains to right cylinders, depending on the fibers and the interstitial agent.

We have done essentially no work on the mechanism of grain formation, with or without interstitial agents. We assume that surface tension, electrical, and rheological forces may all be involved. Now that some results have been obtained, such studies are justified and needed.

A potential problem in the process is water retention by the grains, causing porosity when moldings are made directly from them without any pre-heating. Extrusion appears to drive off this water as no difficulties are encountered in subsequent molding operations. Probably the usual radio-frequency pre-heating would also serve this purpose. The problem does not appear severe, but a means to pre-dry the grains is desirable.

Transfer molding of boron composites has met only limited success so far. Good fills have been obtained, but fiber breakage has been excessive. Additional work using molds and gates better suited to this very stiff fiber may cure the problem. Our transfer molding capability is being expanded to permit varying both product rheology and the molding operation. If successful, the formation of complex shapes by this route would be most attractive. The glass composites transfer-mold readily.

Extrusion offers an alternate route to complex shapes containing oriented fibers. The extruded strand can be warmed, shaped to the approximate contour desired, and placed in an appropriate compression mold. Heat and pressure then result in forming the article in which the fiber orientation has been largely determined by the placement of the strand.

Fiber orientation in the strand is achieved by extrusion using an orifice with the correct exit diameter. The remaining problems are essentially to find the combination of inlet profiles, temperature profiles and extrusion pressure, which for a given molding compound will give a strand with the desired compactness, B-staging, and minimum fiber damage.

As previously mentioned, an in-line, vertical extruder is being constructed which will be in operation by the time this report is published. It will allow a more thorough study of the numerous parameters involved in melt flow fiber orientation. Besides alleviating previously mentioned problems of pressure control and horizontal output inherent with the present apparatus, the new equipment will allow control of temperature profiles and provide a symmetrical flow pattern. The symmetrical flow pattern should enable extrusion at lower pressures, thus reducing fiber breakage and permitting extrusion of compounds with higher volume loadings of fibers.

At present, extrusion is generally limited to circular cross sections. An extrusion of a boron composite through a ribbon orifice ($\frac{1}{8}$" x 0.060") resulted in inferior fiber orientation. Additional work on orifice geometry and other factors will be necessary to produce highly oriented rectangular cross sections.

Both transfer molding and extrusion have the essential virtue that fiber orientation and overlap are accomplished mechanically rather than by a manual process.

Overall, the encapsulation technique makes three contributions to the fabrication effort in the ARPA Project:

1. It permits the preparation of extrudable oriented prepregs from fibers which are not readily pre-pregged in continuous, multifilament form. Boron filament is the prime example.
2. It permits the easy preparation of ternary (or higher) composites. These may be two macro-fibers, such as boron plus glass, or a macro-fiber plus an interstitial reinforcement, such as glass plus whiskers.
3. It provides a method for prepregging loose fiber. This permits use of whiskers and may present some advantage for fibers which can be pre-pregged before cutting, such as glass roving. In the latter case, bare roving is easier to cut to short lengths than is pre-pregged roving; and our encapsulated glass tends to have a lower bulk factor than any chopped pre-pregged roving which we have seen.

Conclusions

1. Short fibers, including boron, can be encapsulated in epoxy resin in a collimated grain form.
2. Solid phases, in addition to the macro-fiber and resin, may be incorporated in the composite grains.

3. Such grains containing short boron fibers can be extruded and molded by conventional techniques to yield oriented specimens having high performance properties.
4. The process is adaptable to using a number of reinforcing materials.

ABSTRACT (Continued)

In Fabrication and Processing, techniques were developed for whisker fiber classification; strands of well-oriented whisker fibers made and fabricated into high performance composites; x-ray diffraction techniques applied to measuring fiber orientation, property maps developed for short fiber composites; short boron fibers encapsulated to make a pre-preg molding compound in bead form; fiber-matrix dry mix molding explored; and data obtained relating matrix properties to fatigue characteristics.

In education, a graduate program in materials science was put into effect by the university; two one-semester seminar courses conducted for the Association students and scientists; and a summer workshop in mechanics organized.

In communication, the second annual symposium on high performance composites was held; publication of a new journal, Journal of Composite Materials, begun; and five papers published.

Security Classification

DOCUMENT CONTROL DATA - R & D

(Security classification of title, body of abstract and indexing annotation must be entered when the overall report is classified)

1. ORIGINATING ACTIVITY (Corporate author)	2a. REPORT SECURITY CLASSIFICATION
Monsanto Research Corporation 800 N. Lindbergh Blvd. St. Louis, Missouri 63166	Unclassified 2b. GROUP

3. REPORT TITLE

MONSANTO/WASHINGTON UNIVERSITY ARPA ASSOCIATION
SECOND ANNUAL PROJECT REVIEW AND TECHNICAL REPORT

4. DESCRIPTIVE NOTES (Type of report and inclusive dates)

Annual 1 May 1966 - 30 April 1967

5. AUTHOR(S) (First name, middle initial, last name)

John D. Calfee

6. REPORT DATE	7a. TOTAL NO. OF PAGES	7b. NO. OF REFS
12 July 1967	249	180

8a. CONTRACT OR GRANT NO	9a. ORIGINATOR'S REPORT NUMBER(S)
N0014-67-C-0218 b. PROJECT NO	HPC 67-28
c.	9b. OTHER REPORT NO(S) (Any other numbers that may be assigned this report)
d.	

10. DISTRIBUTION STATEMENT

Distribution of this document is unlimited.

11. SUPPLEMENTARY NOTES	12. SPONSORING MILITARY ACTIVITY
	Office of Naval Research Washington, D. C. 20360

13. ABSTRACT

The purpose of the Monsanto/Washington University ARPA program, "High Performance Composites," is to demonstrate through accomplishments in research, education, and communication that university-industry coupling is an effective system for doing advanced materials research. This report is an accounting for the second year of the project.

In Mechanics, the finite-element method was used to calculate the longitudinal stiffness of short fiber composites; the instability of parallel edge cracks determined from the energy concept and the strength and inherent crack size obtained from the stability calculations; Young's modulus calculated for randomly oriented fibrous composites; a mathematical approach proposed for calculating stress fields around interior cracks; and invariant properties of a laminated composite derived from the transformation equations of the anisotropic moduli.

In the Physics and Chemistry Section, the electron scanning microscope provided insight into fracture mechanics; composites were improved by incorporating a flexible layer around the fiber; polyacrylic acid reacted with ZnO to produce a high modulus, temperature-resistant matrix; data obtained indicating silane couplers decrease water diffusion at the interface, a decrease in fracture toughness associated with a change in crack propagation mechanism; and the viscosity of aggregate suspensions described by the Mooney equation.

(continued on separate page)

DD FORM 1473 (PAGE 1)

Security Classification

Security Classification

14. KEY WORDS	LINK A		LINK B		LINK C	
	ROLE	WT	ROLE	WT	ROLE	WT
composites						
mechanics						
stress						
cracks						
interfaces						
diffusion						
mechanical properties						
interlayers						
polyelectrolytes						
fabrication						
test specimens						
casting						
molding						
epoxy resins						
boron						
glass fibers						
discontinuous fibers						
silicon carbide						
filaments						
whiskers						
encapsulation						
prepregs						
orientation						
fatigue						
matrices						
Materials Research Laboratory						
Washington University						
impregnation						

DD FORM 1473